To the Graduate Council:

I am submitting herewith a dissertation written by Mahendrakumar C. Joshi entitled "Acoustic Investigation of Upper Surface Blown Flaps." I recommend that it be accepted in partial fulfillment of the requirements for the degree of Doctor of Philosophy, with a major in Mechanical Engineering.

James R. Maus

James R. Maus, Major Professor

We have read this dissertation
and recommend its acceptance:

Grant I. Pattison

William A Dunnill

Walter Frost

Accepted for the Council:

L Evans Roth

Vice Chancellor
Graduate Studies and Research

Thesis
776
J675
cop. 2

ACOUSTIC INVESTIGATION OF UPPER SURFACE BLOWN FLAPS

A Dissertation

Presented for the

Doctor of Philosophy

Degree

The University of Tennessee, Knoxville

Mahendrakumar C. Joshi

March 1977

1315206

ACKNOWLEDGMENTS

The author wishes to express his gratitude to his advisor, Dr. James R. Maus for his guidance and support of this dissertation. Appreciation is expressed to Dr. Grant T. Patterson for his contributions to this study and to Dr. William A. Dunnill, Dr. J. M. Wu and Dr. Walter Frost for their review of the present work.

He is grateful to Dr. B. H. Goethert for giving him the opportunity to associate with the Aeroacoustics Research Group. Appreciation is due to Mr. J. R. Goodman for his assistance in the experiments and to Mrs. Vicki Perry for her excellent typing of this manuscript.

The author is indebted to his mother and brothers for their sacrifices and encouragement.

This research was supported by the Federal Aviation Administration under contract DOT-FA72WA-3053.

ABSTRACT

The acoustic characteristics of upper surface blown flaps were investigated experimentally. The blown flap was modeled by a slot nozzle exhausting over a plane flap and measurements were made in the free field and in a reverberation room. Flap length, flap deflection angle, nozzle aspect ratio and the jet exit Mach number were among the parameters that were varied. Shadowgraphic stills and movies were obtained for flow visualization and limited turbulence measurements were made using hot film anemometry. Flap surface pressure fluctuations were spectrum analyzed and cross-correlated with the far-field sound.

Measurements in the free and reverberant fields showed the sound output of a slot jet to be less than that of an equivalent area circular jet exhausting at the same mean velocity. In addition, the sideline plane of the slot jet was identified to be quieter than the flyover plane. For jet flaps the non-dimensional flap length (= flap length/ nozzle height) was shown to be the most important geometric parameter affecting the sound field. The sound output of jet flaps increases with increasing flap length, upto δ_F nearly equal to ten. With further increase in flap length the sound output decreases so that for all jet exit Mach numbers the sound output is maximum when $\delta_F \approx 10$. This characteristic of the sound output of jet flaps brings

out the importance of the location of the flap trailing edge relative to the termination of the jet potential core. Measured OASPL directivities, sound spectra and sound power data have been attributed to the combined effects of jet noise, edge noise, secondary mixing region noise, scrubbing noise and the shielding by the flap surface. Cross-correlations of the surface pressure fluctuations with the far-field sound showed the flap trailing edge to be a major noise source region, but the dominant noise mechanisms depend on the flap length.

At high jet exit Mach numbers flaps with δ_F around ten generate high intensity tones. Shadowgraphic pictures showed the presence of vortical structures in the secondary mixing region and a flapping motion of the jet potential core above the flap surface. This instability of the jet is thought to be triggered by the edge noise field of the flap which has maximum radiation in the upstream direction. The tone could be eliminated by modifications of the geometry that altered the flow structure in the primary mixing region or reduced the edge effect.

TABLE OF CONTENTS

CHAPTER		PAGE
1.	INTRODUCTION.	1
2.	EXPERIMENTAL FACILITIES AND PROCEDURE	9
3.	NOISE CHARACTERISTICS OF SLOT JETS.	22
4.	ACOUSTIC MEASUREMENTS ON JET FLAPS.	43
	Free Field Measurements.	43
	OASPL directivities and sound pressure spectra in flyover plane	43
	OASPL directivities and sound pressure spectra in sideline plane.	85
	OASPL directivities and sound pressure spectra in YZ plane.	92
	Reverberant Field Measurements	99
	Discussion of Results.	113
5.	PRESSURE CORRELATIONS AND TONE CHARACTERISTICS.	142
6.	SUMMARY AND CONCLUSIONS	179
LIST OF REFERENCES		184
APPENDIX		189
VITA		195

LIST OF FIGURES

FIGURE		PAGE
1.1.	Upper surface blowing high lift devices.	2
1.2.	Slot nozzle and straight flap geometry	7
2.1.	The free field test facility	10
2.2.	Coordinate axes for the jet flap system in the free field.	13
2.3.	Instrumentation for acoustic measurements in the free field and reverberation room	15
2.4.	Test set up for pressure correlations.	16
2.5.	Test set up for fluid dynamic measurements . . .	19
2.6.	Test set up for shadowgraphic observations . . .	20
3.1.	Theoretical jet noise directivity.	25
3.2.	Comparison of measured OASPL directivities of slot nozzle with theory	26
3.3.	OASPL directivities in XZ and XY planes for slot nozzle.	28
3.4.	Sound pressure spectra in XZ and XY planes for the 13.85 aspect ratio slot jet	31
3.5.	Sound pressure spectra of 13.85 aspect ratio slot jet.	35
3.6.	Sound power level versus jet velocity for circular and slot nozzles	37
3.7.	OASPL directivities of slot jet at different aspect ratios	39
3.8.	Power density spectra for circular and slot jets	41

FIGURE PAGE

4.1. OASPL directivities in XZ plane of 13.85 aspect ratio slot-nozzle and flaps 44

4.2. Sound pressure spectra at θ = 30°, 60° and 90° for δ_F = 7.12 flap. 47

4.3. Sound pressure spectra for flaps on 13.85 aspect ratio slot nozzle. 48

4.4. Sound pressure spectra for δ_F = 7.12 and 12.5 flaps 50

4.5. Sound pressure spectra at θ = ±30° for flaps on 13.85 aspect ratio slot jet 52

4.6. OASPL directivities in XZ plane of 13.85 aspect ratio slot nozzle and flaps at M = 0.7. . . . 55

4.7. OASPL directivities in XZ plane for flaps on 27 aspect ratio slot nozzle at M = 0.7 56

4.8. OASPL directivities in XZ plane for flaps on 27 aspect ratio nozzle at M = 0.9. 58

4.9. Sound pressure spectra at θ = 90° for flaps on the 27 aspect ratio slot nozzle. 60

4.10. Sound pressure spectra at θ = 30° for δ_F = 18 flap. 61

4.11. OASPL directivities in XZ plane for flaps on 54.1 aspect ratio slot nozzle at M = 0.7. . . 63

4.12. OASPL directivities in XZ plane for flaps on the 54.1 aspect ratio slot nozzle at M = 0.9. . . 64

FIGURE PAGE

4.13. Sound pressure spectra at θ = 90° for flaps on 54.1 aspect ratio slot nozzle. 67

4.14. Sound pressure spectra at θ = ±30° for flaps on the 54.1 aspect ratio slot nozzle 69

4.15. Sound pressure spectra at θ = ±30° for flaps on the 54.1 aspect ratio slot jet. 72

4.16. OASPL directivities in XZ plane for long flaps . 75

4.17. Sound pressure spectra at θ = -30° for long flaps 76

4.18. Sound pressure spectra for long flaps. 77

4.19. Shielding effect of long flaps 80

4.20. OASPL directivities in XZ plane for deflected flaps 83

4.21. Sound pressure spectra for δ_F = 7.12 flap at various deflections 86

4.22. OASPL directivities of flaps in XY plane 88

4.23. Sideline noise reduction of a long flap. 93

4.24. Sound spectra in XY and XZ planes for δ_F = 25.5 flap. 94

4.25. OASPL directivities in YZ plane for jet flaps. . 97

4.26. Sound pressure spectra at ψ = 0° and 90° for δ_F = 9.9 flap 100

4.27. Sound power output variation with flap length. . 101

4.28. Power density spectra for the 54.1 aspect ratio slot jet and flaps. 103

FIGURE PAGE

4.29. Jet velocity dependence of the sound power of jet flaps. 107

4.30. Power density spectra of slot jet and flaps at different jet exit Mach numbers. 110

4.31. Power density spectra for deflected flaps . . . 114

4.32. Edge geometry of Ffowcs Williams and Hall [8] and Hayden [31]. 117

4.33. Slot nozzle with flap flow field nomenclature . 122

4.34. Spark shadowgraphs of jet flaps on the 27 aspect ratio slot jet at M = 0.9 125

5.1. Surface pressure autocorrelations for $\delta_F = 18$. 145

5.2. Surface pressure spectra for $\delta_F = 18$. 146

5.3. Cross-correlations of surface pressures with far-field sound. 148

5.4. Correlation zero crossing delay time variation with surface microphone position 150

5.5. Cross-correlation of surface pressures with far field sound in 6300 Hz one-third octave band 152

5.6. Cross-correlations between flap surface pressures. 154

5.7. Surface pressure spectra for $\delta_F = 9.9$ 156

5.8. Surface pressure spectra at x/h = 6.3 157

5.9. Geometry for hot wire measurements. 159

5.10. Turbulence spectrum in the secondary mixing region - one slot height downstream of flap trailing edge. 160

FIGURE PAGE

5.11. Sound power spectra corresponding to the shadowgraphs of Figure 4.34 (page 125). . . . 162

5.12. Tone alleviation by trip wire. 166

5.13. Tone alleviation with roughening 168

5.14 Shadowgraphs of the δ_F = 9.9 jet flap at M = 0.9 170

5.15. Shadowgraphs of the δ_F = 9.9 jet flap with rough nozzle and acoustic excitation by a reflector plate 173

5.16. Porous flap geometry and spectral comparison with non-porous flap. 176

5.17. Unsteady nature of the tone. 178

LIST OF SYMBOLS

a_o	Ambient speed of sound
d	Jet diameter
dB	Decibel (relative to 2×10^{-5} Newton/m^2 or 10^{-12} watt/m^2)
D (θ)	Directivity function
f	Frequency
f_c	One third octave band center frequency
h	Nozzle height
Hz	Hertz
I	Intensity
k	Acoustic wave number
kHz	Kilo hertz
ℓ	Characteristic length scale
ℓ_F	Flap length
m	Turbulence Mach number
M	Jet exit Mach number
M_c	Convection Mach number
OASPL	Overall sound pressure level
p	Pressure (acoustic or hydrodynamic)
p_{ij}	Compressive stress tensor
p_s	Fluctuating surface pressure
P_i	Surface dipole strength
PWL	Sound power level

r	Distance of a far-field point from the nozzle
$\bar{r}_o$	Distance of the center of an eddy from the edge of a half plane
$R_{11}(\tau)$	Surface pressure autocorrelation function
$R_{12}(\tau)$	Far field pressure autocorrelation function
$R_{12_{max}}$	Maximum value of cross-correlation function
S	Surface of integration
t	Time
$\hat{t}$	Retarded time
T_{ij}	Lighthill stress tensor
T_R	Reverberation time
u_i	Velocity component in direction x_i
U	Jet exit velocity
U_c	Convection velocity
V	Volume of integration or reverberation room
w	Nozzle width
W	Sound power
w_c	Wetted span
x	Distance downstream of nozzle exit
x_1	Distance to the trailing edge
X,Y,Z	Coordinate axes

Greek Symbols

δ	Boundary layer thickness
δ_F	Non-dimensional flap length (= ℓ_F/h)
δ_{ij}	Kronecker delta

θ	Angle from jet axis in XZ plane
θ'	Angle defined in Figure 4.32
θ_F	Flap deflection angle
Λ	Nozzle aspect ratio (= w/h)
μ	Coefficient of viscosity
ρ	Local density
ρ'	Fluctuating density in the acoustic field
ρ_o	Ambient density
$\rho_{12_{max}}$	Maximum correlation coefficient (= $R_{12_{max}} / \sqrt{R_{11}(0)\ R_{22}(0)}$)
τ	Delay time
τ_o	Zero crossing time of the cross correlation function
ϕ	Angle from jet axis in XY plane
ϕ'	Angle defined in Figure 4.32
ψ	Angle in YZ plane

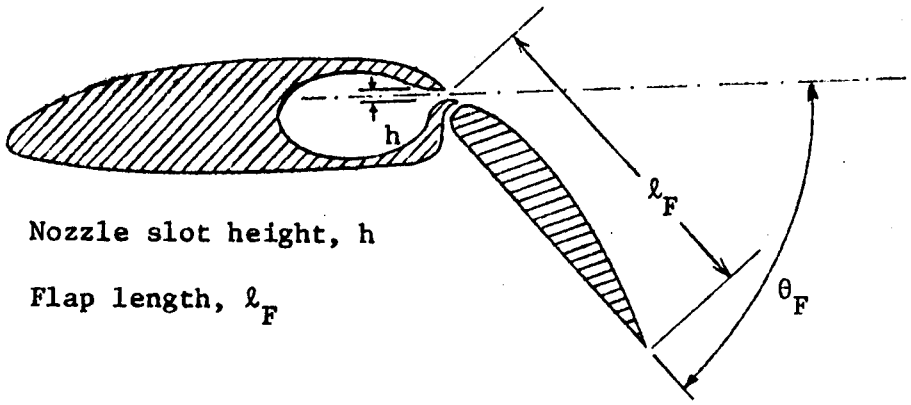
CHAPTER 1

INTRODUCTION

The growing concern for the quality of our environment calls for considerable emphasis on the noise reduction of Short Take Off and Landing (STOL) aircraft that will operate in the proximity of residential and commercial areas. STOL capability requires a considerable increase in the installed engine thrust in order to provide the needed lift augmentation. In addition, the high lift system used on these aircraft may introduce powerful new sources of surface interaction noise. These two factors make the design of STOL aircraft with low noise levels a challenging task.

Various types of flap devices are being considered for lift augmentation. The jet blown flap (Figure 1.1) is one promising contender. It is essentially a high energy jet from a slot nozzle blowing tangentially to the flap surface. Bypass air of the turbofan engine is usually ducted to the wing to supply the slot nozzle. Working on the same principle is the engine over the wing scheme shown in the bottom in Figure 1.1. This scheme, however, eliminates the complexity of ducting required in the jet blown flap scheme by blowing the engine exhaust over the wing. In both these upper surface blowing (USB) concepts

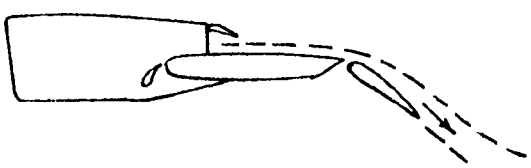
(a) Internally blown jet flap



Nozzle slot height, h

Flap length, ℓ_F

(b) Engine over the wing



Upper surface blown jet flap (USB)

Figure 1.1. Upper surface blowing high lift devices.

it is the Coanda turning of the jet by the flap surface that produces increased circulation and lift augmentation.

The USB concept is acoustically attractive since for most directions below the wing the jet and engine internal noise can be expected to be at least partly shielded by the wing. However recent tests by Dorsch et al [1] on jet blown flaps (called "jet flaps" hereafter) have shown that the interaction of the jet flow and the wing and flap surfaces create new noise sources. Extrapolation of the data to representative full scale STOL flap system showed that with a quiet engine the flap noise can be a major contribution to the total aircraft noise. The airframe noise of which the flap noise is a major part has been identified by Gibson [2] as the "ultimate noise barrier". Flap noise suppression techniques thus need to be developed to beat this barrier.

Upper surface blowing has generally been modeled by a high aspect ratio[1] slot nozzle exhausting over a flat or curved plate. Maglieri and Hubbard [3] conducted measurements in the free field of model jet flaps that used a slot nozzle of aspect ratio 200 and flaps with nondimensional lengths[2] δ_F = 20, 72 and 190. The jet exhaust Mach

---

[1]aspect ratio = slot width/slot height

[2]non dimensional flap length (δ_F) = flap length/ nozzle height

number was 0.96. With the shortest flap only an increase in noise was observed with only minor changes in the directional radiation characteristics. The longest flap (δ_F = 190), however, considerably reduced the sound radiation below the flap. Coles [4] used a model with an aspect ratio of 100 and nondimensional flap length equal to 20. At a jet Mach number of 0.9 he observed reduced sound levels below the flap. The high aspect ratio slot nozzles used in these investigations might be a good model for the internally blown jet flaps. The engine over the wing concept is, however, likely to use nozzles with smaller aspect ratios.

Grosche [5] , with the intention of investigating the feasibility of shielding the jet noise by means of large surfaces mounted at varying distances below the jet, made measurements in the far field of a slot jet of aspect ratio 23 with shield plates of various lengths. In the limiting case of the distance between the jet and the shield plate approaching zero, this configuration models a jet flap. Grosche's major findings were that the flap causes additional noise which has greater radiation in the plane normal to the flap surface and increases in strength with decreasing flap length. The nondimensional flap length in this experiment varied from δ_F = 25 to 100. The sound intensity was found to vary as the fifth power of jet exit velocity.

In an effort to locate the noise sources in the flow Grosche [5] used a spherical reflector to create an image of a small volume of the turbulent source and measured the acoustic intensity of the image source by a microphone. By focusing the reflector on the source from different directions and repeating this for several source volumes along the flow he found that a considerable portion of the total acoustic power is radiated by a region at or behind the flap trailing edge. Hayden [6] has shown that the directional radiation characteristic of a jet flap in a plane normal to the flap surface is similar to that of a point dipole source located immediately behind and diffracted by the flap trailing edge. Schrecker [7] made measurements in the flow field of jet flaps with δ_F = 5.6, 9 and 15.4. His measurements showed the turbulence in the shear layer that develops behind the flap trailing edge to be very intense. It was concluded that this shear layer is a region of high acoustic emission. Both Schrecker and Hayden's measurements were made with the jet exhausting at low subsonic Mach numbers ($M < 0.4$). Recently Ffowcs Williams and Hall [8] obtained a theoretical solution of the sound field generated by turbulence in the vicinity of an edge which showed that the edge serves to amplify the sound generation ability of a turbulent eddy.

Experiments to date have thus recognized that the interaction of the jet flow with flap surface causes the

jet flap, in general, to be noisier than the basic jet. For the aircraft designer, the effect of various geometrical and flow parameters on the sound generation and radiation from the jet flap device is of greater interest. It is, therefore, the purpose of this thesis to carry out a systematic investigation of the acoustic characteristics of the jet flap system. Besides providing a large data base which can be used to formulate noise prediction schemes, such an investigation will also improve our understanding about the existence of various noise mechanisms which could lead to successful noise suppression schemes.

To retain simplicity the flap system was modeled by a slot nozzle exhausting over a straight flap that was attached to the nozzle at its exit (Figure 1.2). Flap length (ℓ_F), nozzle aspect ratio (Λ = w/h) and jet exit Mach number are among the parameters that were varied. The nozzle exit area was kept constant at that of an equivalent circular nozzle 3 cm in diameter. The aspect ratios of the nozzles were 13.85, 27.0 and 54.1. Flap length was varied to cover a wide range of δ_F (= ℓ_F/h) - from 2.85 to 132. A matrix of all the slot nozzle and flap dimensions is given in Table 1.1. The jet exit Mach number was varied from 0.5 to 0.9. These models were tested in the acoustics test facility described in the next chapter. Some results of this investigation have been reported in References 9 and 10.

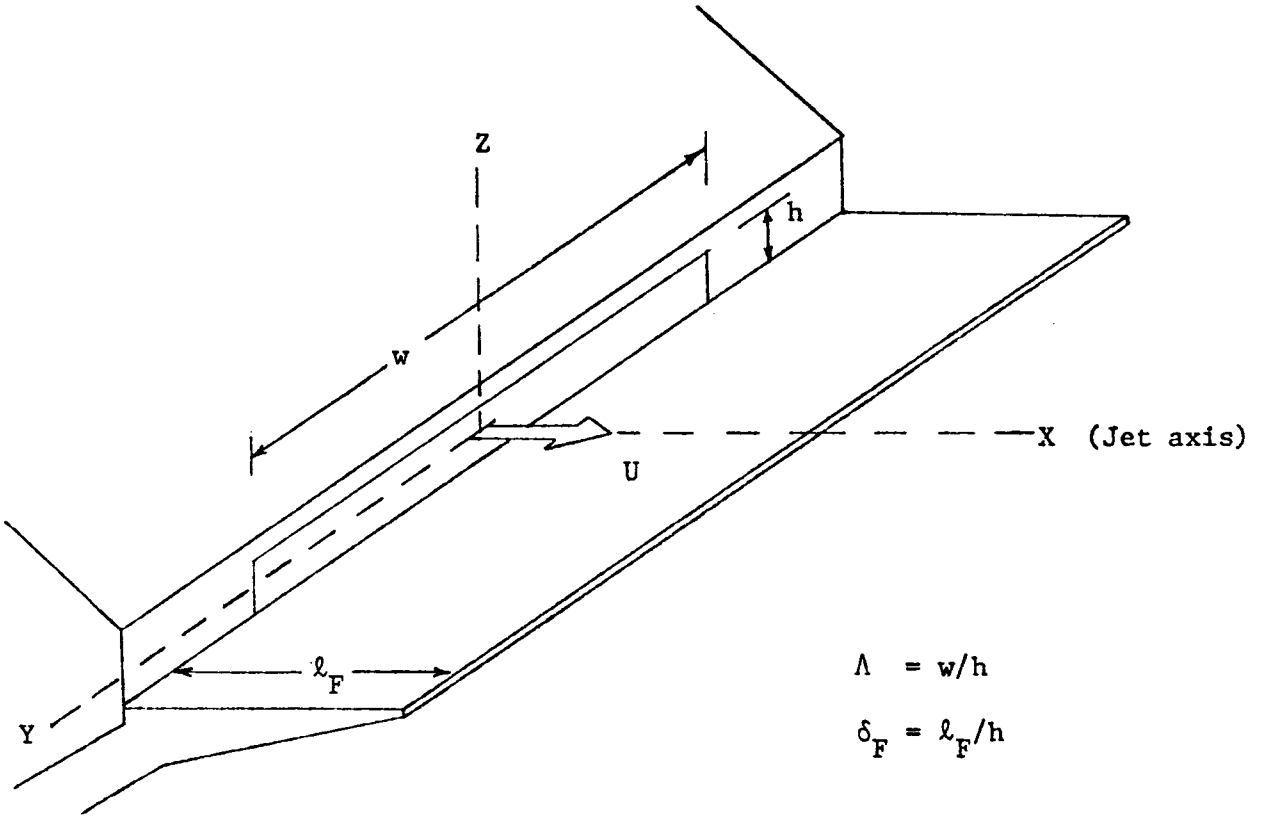


Figure 1.2. Slot nozzle and straight flap geometry.

TABLE 1.1

NOZZLE AND STRAIGHT FLAP CONFIGURATIONS

Nozzle Area = 7.07 cm^2

Diameter of Equivalent Circular Nozzle = 3 cm

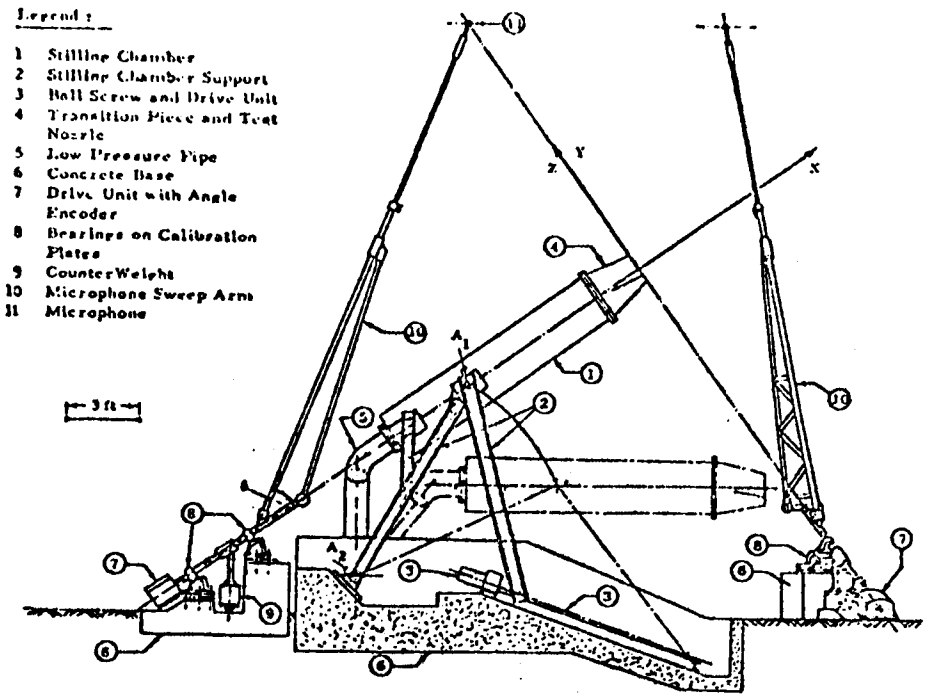
Nozzle	$\Lambda = \frac{w}{h}$	13.85	27.0	54.1
	h (cm)	0.714	0.512	0.361
Flap ℓ_F (cm)		δ_F		
0.0		0.0	0.0	0.0
2.03		2.85	3.96	5.63
3.50		4.91	6.83	9.72
5.08		7.12	9.90	14.10
9.21		12.50	18.00	25.50
18.42			36.00	51.00
30.48				84.50
47.63				132.00

CHAPTER 2

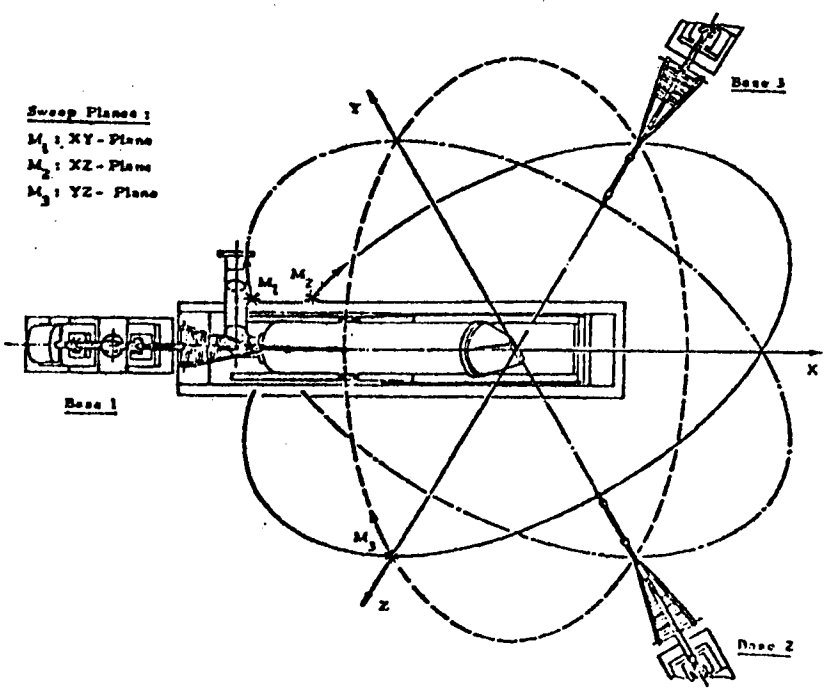
EXPERIMENTAL FACILITIES AND PROCEDURE

This investigation was carried out in the UTSI aeroacoustics test facility which consists of an air supply system, three test stands and associated acoustic and turbulence instrumentation. The outdoor free field facility, the reverberation room and indoor fluid dynamic facility constitute the test stands.

The free field test stand (Figure 2.1) is the major component of the facility. It permits acoustic measurements in three orthogonal planes centered about the model (simultaneously, if so desired). Such capability is essential in studying the noise characteristics of rotationally asymmetric nozzles. In order to minimize reflections from the ground the stilling chamber is inclined at an angle of 35° to the ground. With such an arrangement, the test nozzle when mounted on to the stilling chamber, is approximately four meters above the ground. Three motorized arms are mounted to bases that are 120° apart on the ground with one base directly behind the chamber. The axes of the arms form a mutually perpendicular system of axes with one axis along the flow centerline. Rotation of these arms about their axes then causes the microphones mounted at the



(a) Side view



(b) Top view

Figure 2.1. The free field test facility.

tip of the arms to sweep in three perpendicular planes. The arms are generally rotated at a slow speed to obtain directivity measurements and spectral data are obtained when the arm is stationary. The sweep radius (i.e., the distance of the microphone from the nozzle) can be varied. Sweep radius of 4 meters was used for the directivity and spectral measurements reported in this dissertation. The free field test stand has the capability of exhausting at Mach numbers up to M = 1 from nozzles up to 30 cm in diameter at stagnation temperatures up to 800° K. Other features of this facility and the air supply system have been described in detail by Dunnill [11] and Borchers [12].

The reverberation room is made of heavy plywood and is 2.4 m long, 2.1 m wide and 2 m high with a corresponding volume of about 10 cubic meters. The jet from the test nozzle attached to the stilling chamber, 24 cm in diameter, exhausts in the length direction of the room and is ducted out of the room from a 20 cm hole in the opposite wall. The lower cut off frequency of the room is approximately 500 Hz. Nozzles up to 5 cm in diameter have been tested in this facility at M $\approx$ 1. The indoor test stand has the same flow capability as the reverberation room test stand but is primarily used to make fluid dynamic measurements and flow visualization experiments.

All three test stands were used in the present investigation of jet flap models. In the free field OASPL directivities were obtained in all the three planes- the flyover or XZ plane, the sideline on XY plane and the nozzle exit or YZ plane (Figure 2.2) - for jet exit Mach number M = 0.9 and 0.7. In addition, spectral data were recorded at M = 0.9 at the following locations: $\theta = \pm 30°$, $\pm 60°$ and $\pm 90°$ in XZ plane, $\phi = \pm 30°$, $\pm 60°$ and $\pm 90°$ in XY plane and $\psi = 0°$, $\pm 30°$, $\pm 60°$ and $\pm 90°$ in YZ plane.

The sound power output of jet flaps was obtained from measurements in the reverberation room. Since the sound field in the reverberation room is diffuse, the mean square acoustic pressure, $\overline{p^2}$ as measured by a microphone placed in the room is related to the sound power output, W of the noise source in the room by the formula given by Kinsler and Frey [13].

$$W = \frac{13 \cdot 9V}{\rho_o a_o} \frac{\overline{p^2}}{T_R}$$

where $\overline{p^2}$ is in Newtons/m^2, V is the volume of the room in cubic meters and T_R is the reverberation time in seconds. ρ_o and a_o are the ambient density and speed of sound. The reverberation time (T_R) is a measure of the sound absorption characteristic of the room and is defined as the time required for a sound to decay by 60 dB. This time depends on the frequency of the sound and was

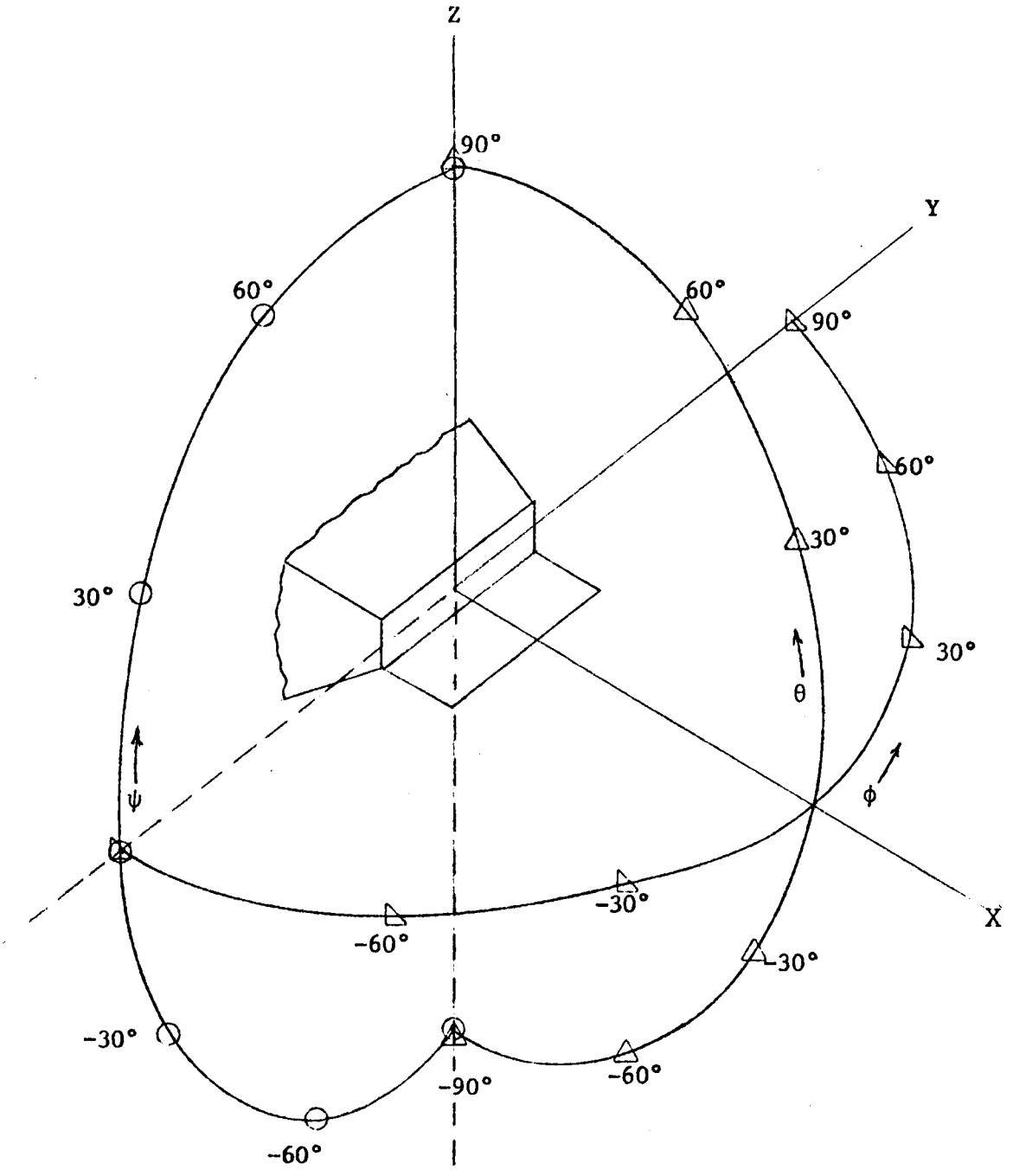


Figure 2.2. Coordinate axes for the jet flap system in the free field.

determined by standard methods [14] for all one third octave bands. The measured times, T_R (f_c) and the mean square acoustic pressures $\overline{p^2(f_c)}$ in different one third octave bands were used in the above formula to determine the sound power level, PWL and the power density spectrum, G (f_c) which is the sound power output per unit frequency.

Figure 2.3 represents in a block diagram the acoustic instrumentation used in both free field and reverberation room tests. It consists of a 0.64 cm B & K Type 4136 condenser microphone with a Type 2615 preamplifier, B & K Type 2112 one third octave Audio Frequency Spectrometer and B & K Type 2305 level recorder. The system was used in duplicate as a check on the diffuse nature of the sound field in the reverberation room and to make measurements in two different planes in free field tests. Microphones were located away from both the wall and the jet in reverberation tests and were mounted on the sweep arms during free field tests. The analyzer and recorder were calibrated before each test using a General Radio Sound Level Calibrator Type 1562-A.

Flap surface pressure measurements and pressure correlations were performed in the free field and the associated instrumentation is represented in Figure 2.4. Condenser microphones (0.64 cm size) were used to monitor both the pressure fluctuations on the flap surface and the far field sound. For ease of mounting, flaps used in this phase of the investigation were made of plexiglass but were

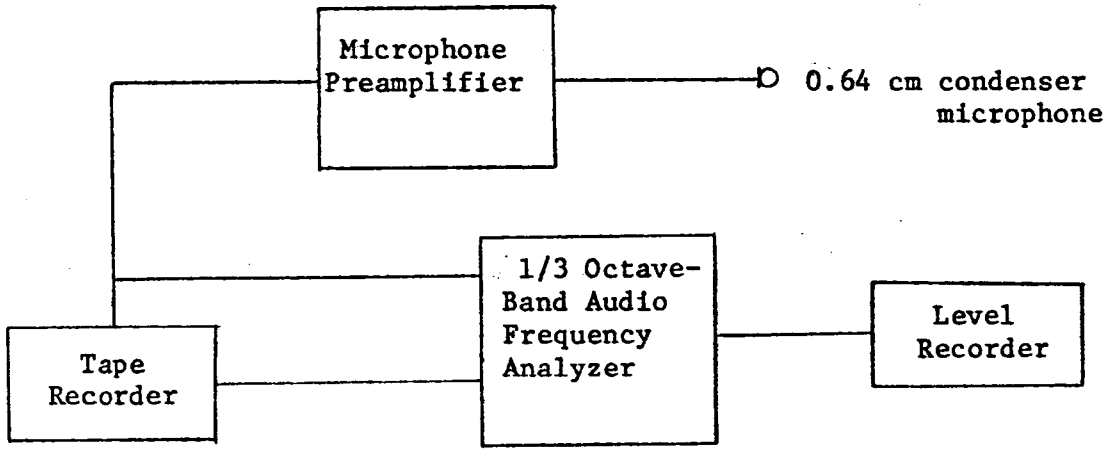


Figure 2.3. Instrumentation for acoustic measurements in the free field and reverberation room.

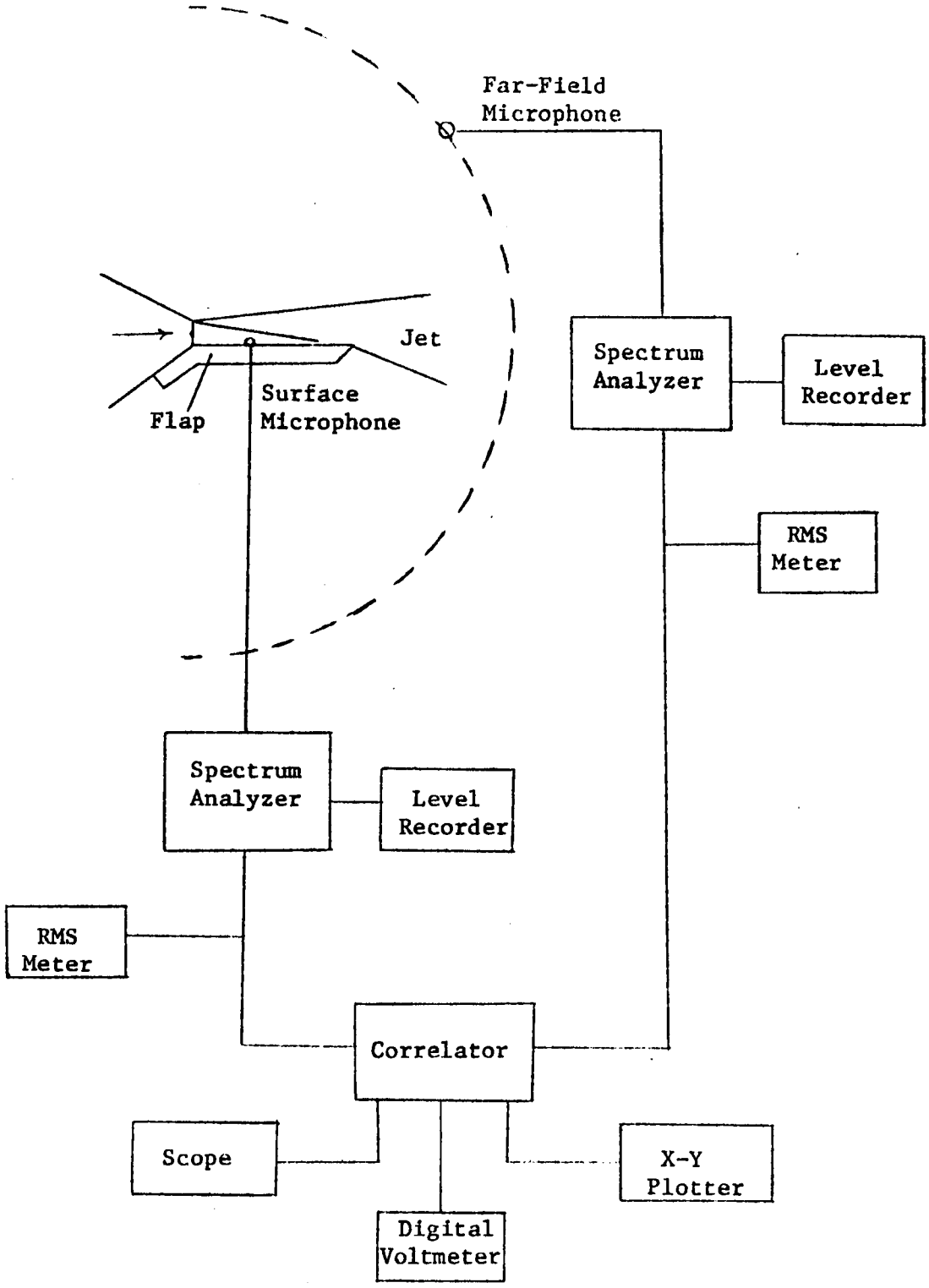


Figure 2.4. Test set up for pressure correlations.

otherwide identical to the aluminum flaps used in acoustic and flow measurements. Microphones were inserted into the flap surface from the underside and the microphone diagragm was set flush with the flap surface. They were positioned along the mid span line at three locations x/h = 6.3, 9.4 and 17.5 where x is the distance of the center of the microphone from the nozzle exit. These positions were chosen so as to be able to monitor surface pressure fluctuations from under the potential core, at the core termination and at the flap trailing edge for the jet flap with $\delta_F = 18$. Signals from the surface and far field microphones were fed to identical spectrum analyzers and level recorders for spectral recording. Broad-band or one third octave filtered signals from the analyzers can be fed to the input channels of a Honeywell Saicor Model SAI-42A Correlation and Probability Analyzer for autocorrelation of individual pressure signals or cross correlation between the two. This correlator determines the correlation function simultaneously at 100 incremental lag points and can display the function of an oscilloscope or a X-Y recorder. Incremental lag or time delay values ranging from 0.5 μsec to 1 sec are available although real time computation is possible for incremental values equal to greater than 50 μsec. An incremental time delay of 10 μsec was typically used here. The far field microphone was about 2 meters from the nozzle and correlations were performed for a jet Mach number of 0.9.

The indoor test stand was used to make turbulence measurements and for shadowgraphic observations. The set up for turbulence measurements (Figure 2.5) consists of a single hot film probe and a DISA constant temperature anemometer system. The correlator and spectrum analyzers were again used to obtain auto-correlation of the fluctuating velocity and the spectrum of turbulence. Figure 2.6 shows the set up for shadowgraphic observations. For still shadowgraphs a spark light source was placed on one side of the nozzle exit (about a meter away) and a film holder with a Kodak Royal Pan 4141 film was placed in line with the light source and the jet on the other side (about 25 cm from the jet). The spark source used was a discharging capacitor type source with a high voltage power supply to charge the capacitors. The intensity of the light was high and the duration short resulting in sharp pictures of the flow field. The shadowgraphs were printed on Kodak Kodabromide high contrast paper.

The set up for shadowgraphic movies (Figure 2.6) had a constant point light source (S) placed at the focus of mirror (M_1) to obtain a parallel beam of reflected rays which pass normally through the air jet issuing out of the nozzle. This beam is collected by mirror (M_2) and reflected towards a Fastax camera placed beyond the focal point of M_2. The camera is essentially a rotating prism camera and has a

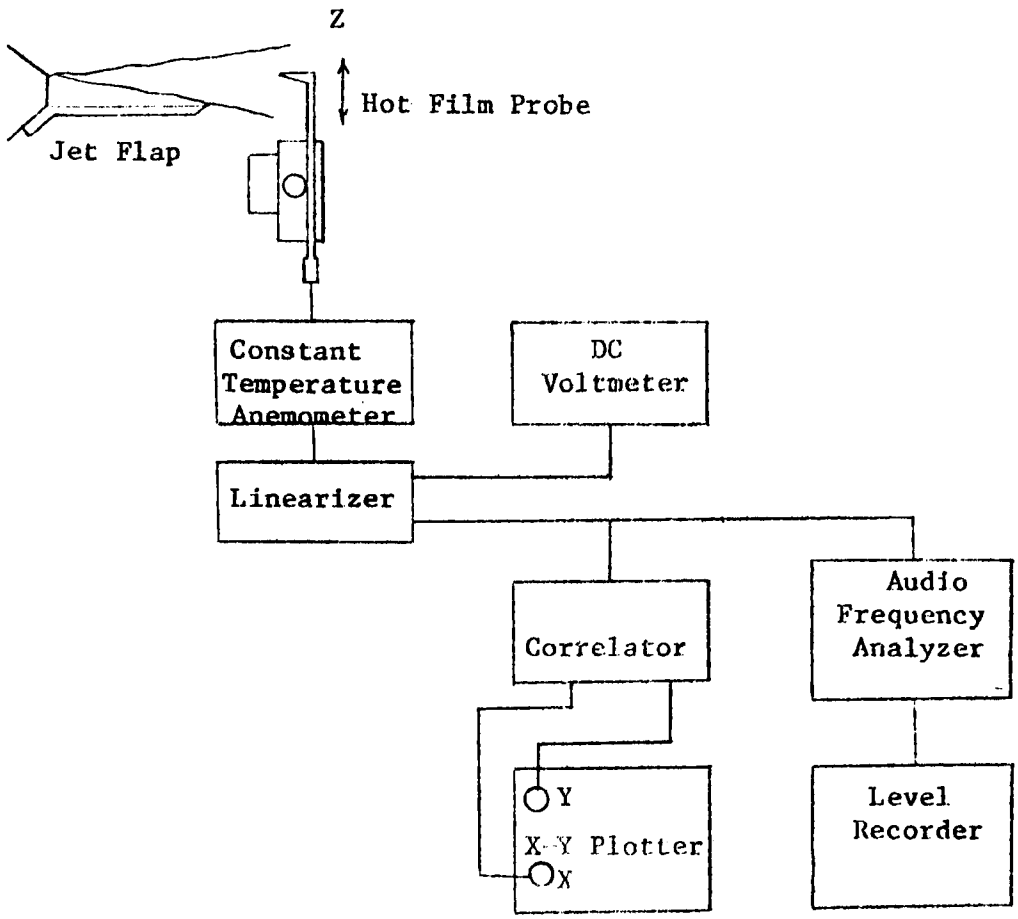
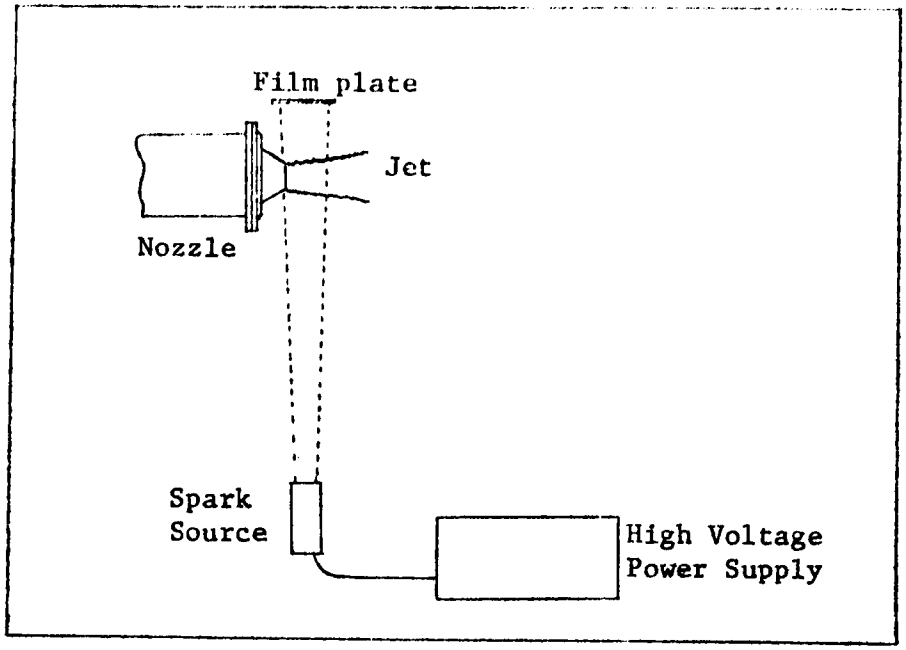
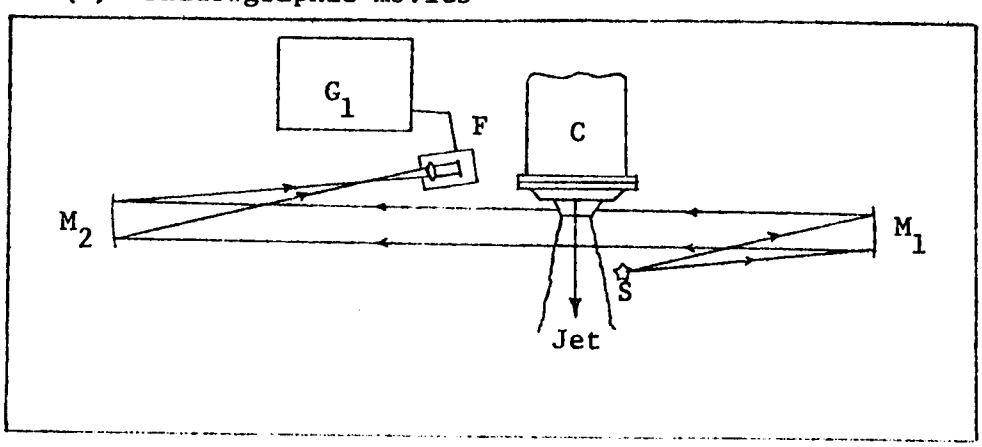


Figure 2.5. Test set up for fluid dynamic measurements.

(a) Still shadowgraphs



(b) Shadowgraphic movies



S: Constant light source
M_1,M_2: Mirrors
F: Fastex movie camera
G: Goose control unit
C: Stilling chamber

Figure 2.6. Test set up for shadowgraphic observations.

high framing rate which can be varied by changing the voltage on the Goose control unit of the camera. A framing rate of 3500 frames per second was typically used.

CHAPTER 3

NOISE CHARACTERISTICS OF SLOT JETS

Having chosen to model the jet flap by a slot nozzle exhausting over an attached flap, it is necessary to know the noise characteristics of the basic slot nozzle jet (without the flap) in order to evaluate the noise shielding ability of the flap. It is the purpose of this chapter to make observations regarding the noise characteristics of slot jets based on acoustic measurements made according to the procedures outlined in Chapter 2 and compare them with the predictions of jet noise theory.

The most successful theory of aerodynamic noise is due to Lighthill [15] . He showed by a simple but ingenious rearrangement of the continuity and momentum equations governing the flow that the noise radiated by the flow is that which would be produced by a static distribution of acoustic quadrupoles whose instantaneous strength per unit volume is T_{ij}. The rearranged equation yielded a retarded potential type solution for the radiation field density fluctuations. Dimensional analysis of this solution showed the acoustic power output of the flow to increase like the eighth power of a typical velocity in the flow. Ffowcs Williams [16] correctly accounted for the convection of sources in the flow and obtained for the far-field

acoustic intensity, a variation according to

$$\frac{\rho^2 U^8 d^2}{\rho_o a_o^5 R^2} \quad \frac{D(\theta)}{(1 - M_c \cos\theta)^5}$$

where ρ is the density of the flowing fluid, U the flow velocity, d a characteristic flow dimension, ρ_o and a_o the density and speed of sound in the external fluid, R the distance from the flow to the observer and θ the angle between the direction of sound emission and the downstream flow axis. The function $D(\theta)$ is the directivity of the unconvected quadrupole distribution and M_c equals U_c/a_o where U_c is the speed of convection of the quadrupoles. For unheated subsonic jets, the jet density, ρ, may be taken to be equal to the ambient density, ρ_o, and following Davies, Fisher and Barratt [17] the source convection velocity, U_c, can be taken to be 0.65 times the jet velocity. Furthermore by an examination of the overall intensity patterns at low jet velocities Lush [18] has shown the absence of any predominant quadrupole orientation so that $D(\theta)$ is approximately equal to unity. The expression for the far field intensity then reduces to

$$I \sim \frac{\rho_o U^8 d^2}{a_o^5 R^2} \quad \frac{1}{(1 - 0.65\, M \cos\theta)^5}$$

where $M = U/a_o$

The theoretical sound intensity of a jet calculated using the above formula is plotted in Figure 3.1 for jet Mach numbers of 0.5, 0.7, 0.8 and 0.9. A comparison of the measured directivities for the 13.85 aspect ratio slot nozzle with the theoretical directivity is given in Figure 3.2. The theoretical directivities have been adjusted vertically to "best fit" the data. Note in this figure that the agreement of the measurements with the theory is fairly good at M = 0.5. However, the convective amplification, as measured by the difference between the maximum intensity level in the plane and the level at $\theta = 90°$ (or $\phi = 90°$), is considerably overestimated by theory at higher jet velocities. The agreement between theory and measurements in XY plane is not as good as for XZ plane. The measured directivities peak around 30° as opposed to the peak in the 0° direction as predicted by the convected quadrupole model. This is due to the refraction of sound away from the flow direction by the jet.

Comparison of the directivities in the XZ and XY planes of slot jets (Figure 3.3) identifies the XY plane as the quieter plane of the slot jet. Lower noise levels are particularly evident in a small sector near the jet axis ($\theta = \phi = 20°$ to 50°). The lower sideline noise levels of the slot jet makes it an attractive choice for aircraft applications. Crighton [19] has shown that for an elliptic incompressible jet, modes representing sideways oscillations

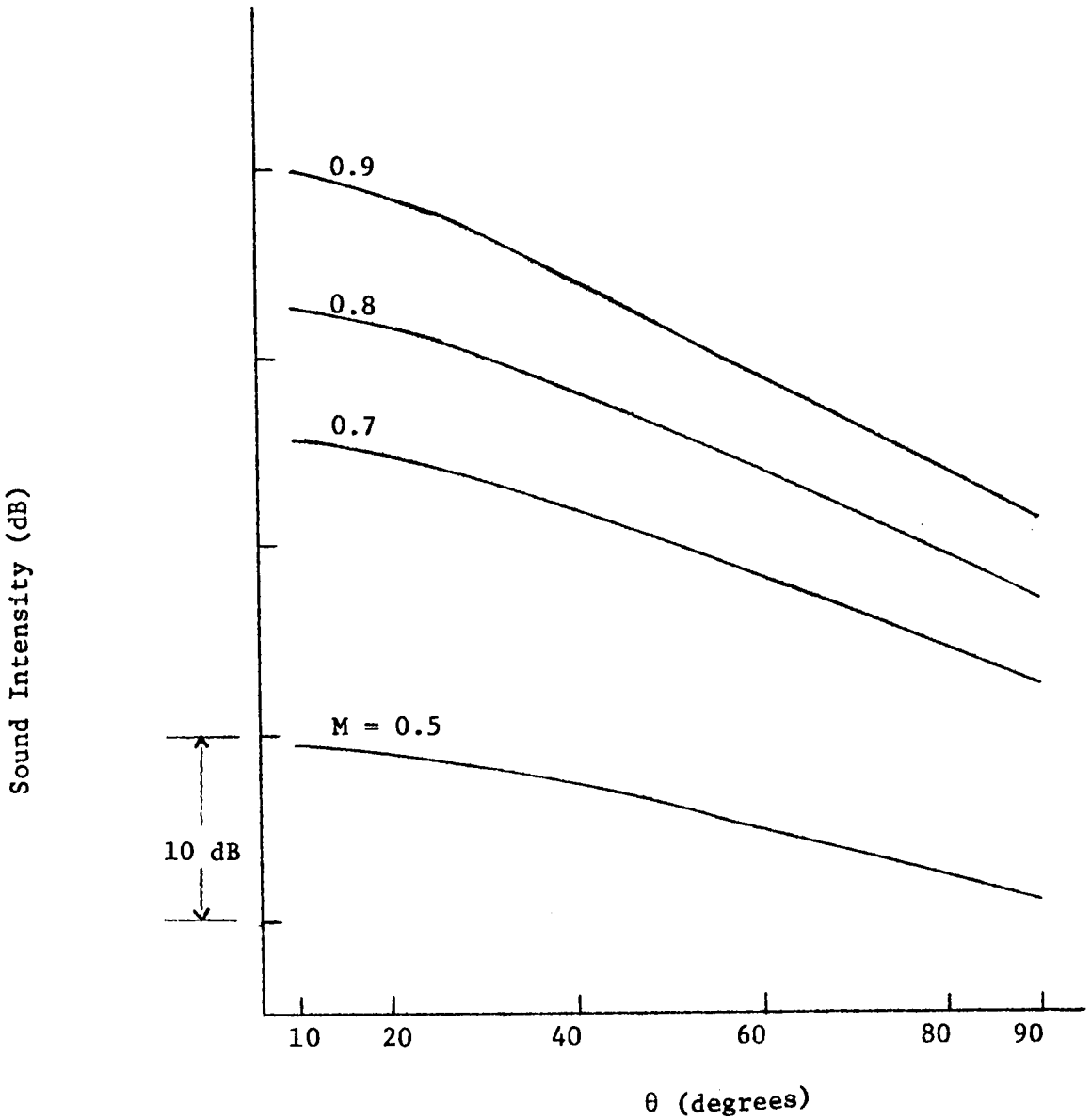


Figure 3.1. Theoretical jet noise directivity.

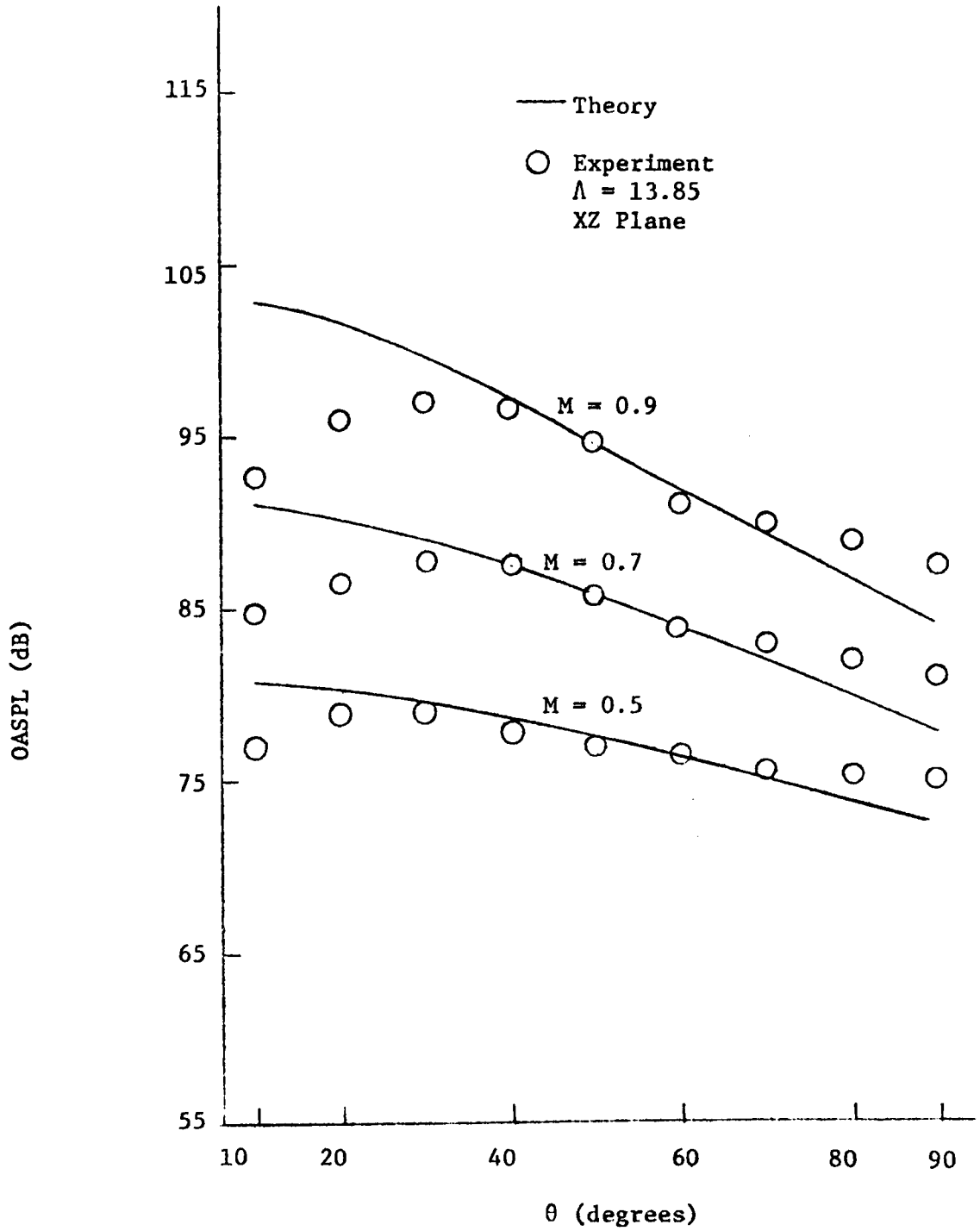


Figure 3.2. Comparison of measured OASPL directivities of slot nozzle with theory.

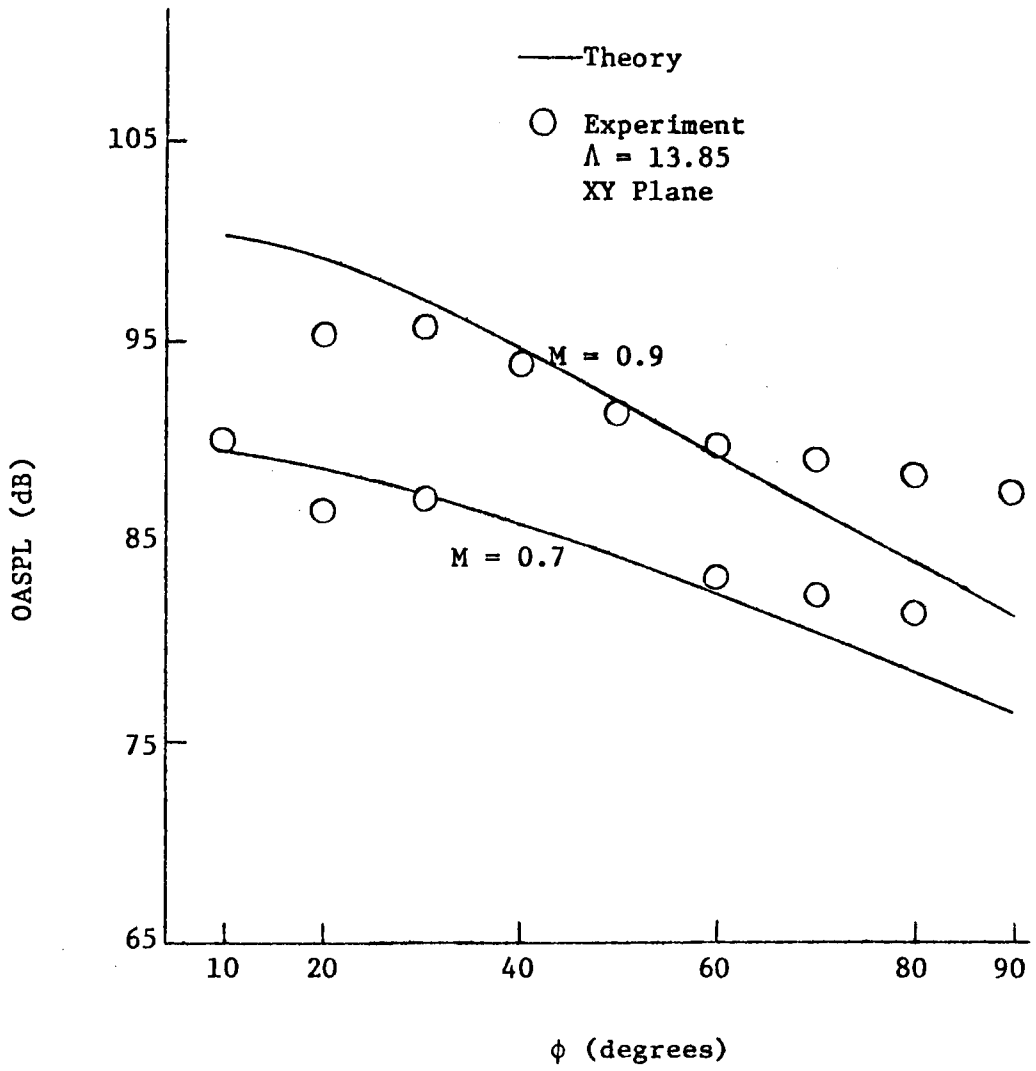


Figure 3.2. continued.

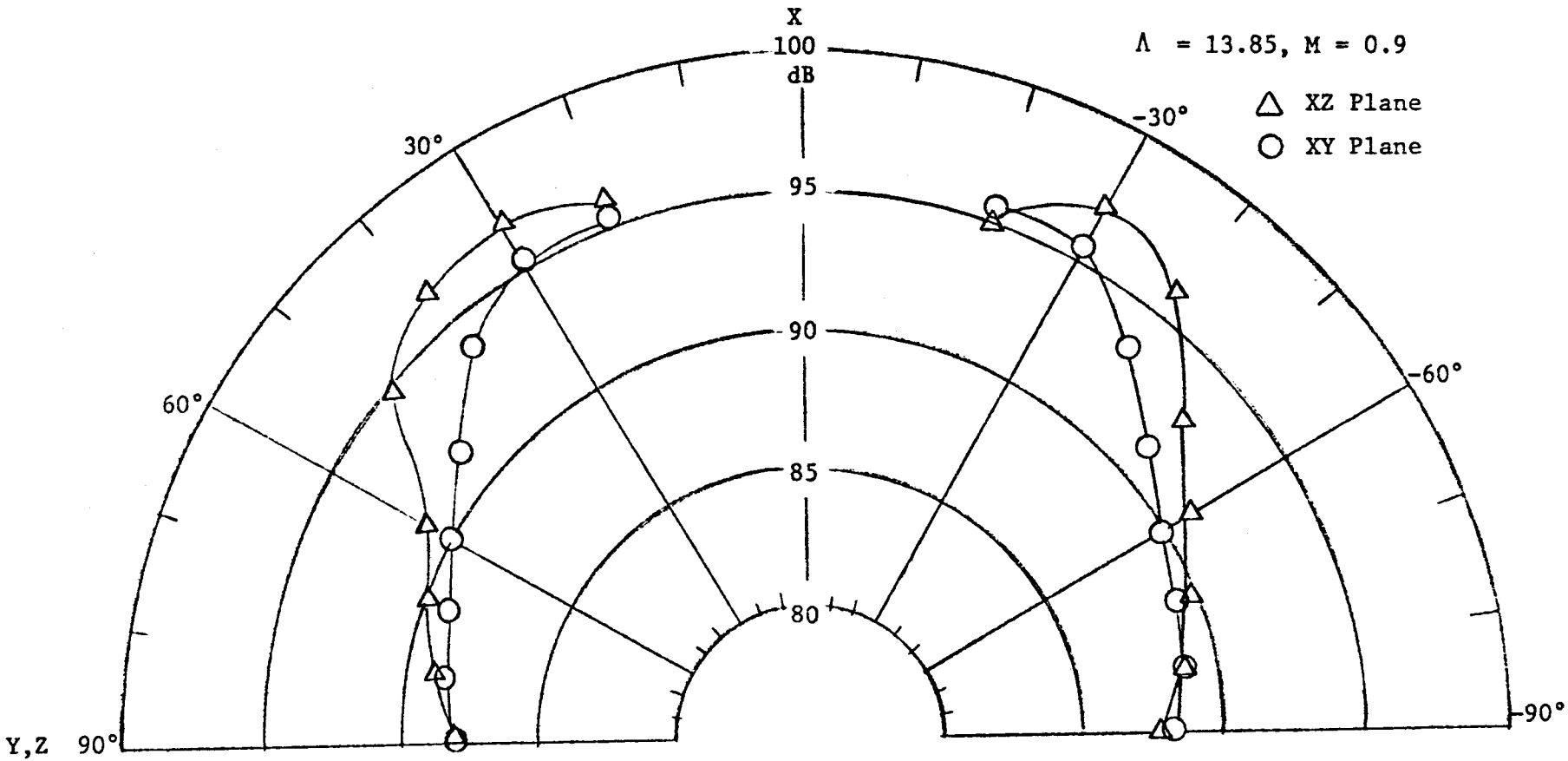


Figure 3.3. OASPL directivities in XZ and XY planes for slot nozzle.

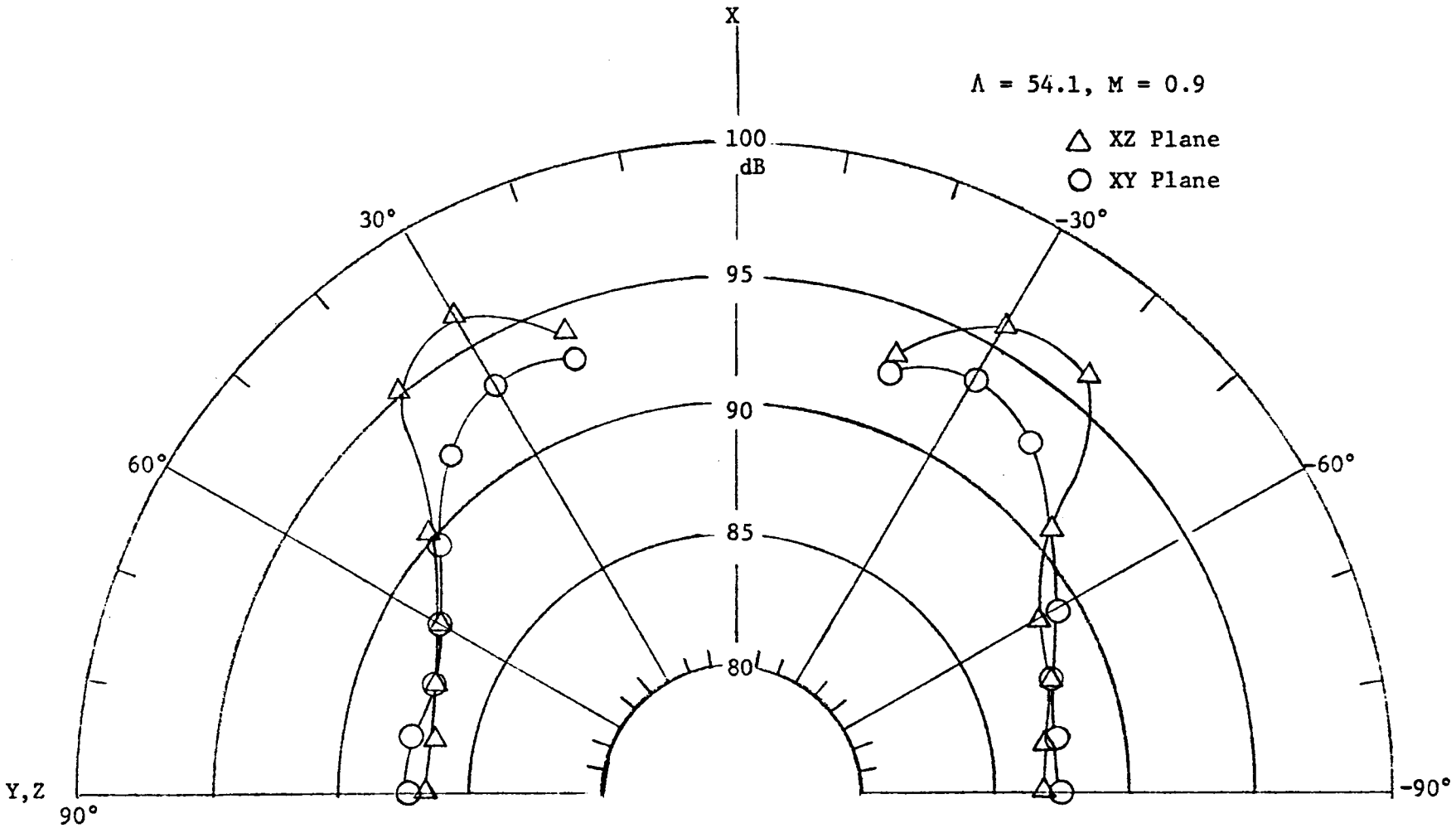


Figure 3.3. continued.

parallel to the major axis (Y axis) have small growth rate while those representing a flapping motion parallel to the minor axis (Z axis) have large growth rate. The greater stability of the jet along the major axis might be responsible for the reduced noise levels in the XY plane. Balsa [20], however, has shown that a plausible explanation for the appearance of the quiet and noisy planes is the shielding of noise by the jet flow. Since shielding is more effective at high frequencies, the reduced levels of high frequency components in XY plane shown in the spectra of Figure 3.4 indicates the possible presence of fluid shielding effect. Furthermore the sound waves of a source radiating in the direction of $\phi = 30°$ have to travel through a longer stretch of jet flow than those radiating in the $\phi = 90°$ direction and are, therefore, likely to experience a greater shielding effect. This is so observed in the spectra of Figure 3.4- the reduction in the intensity levels of high frequency components in XY plane compared to their levels in the XZ plane is considerably larger at $\phi = 30°$ than at $\phi = 90°$. Fluid shielding (also referred to as shrouding effect of jet flow or interaction between sound and jet flow) has increasingly been recognized as an important effect in the sound produced by air jets. By incorporation of the mean flow shrouding effects on the radiation of convected quadrupoles, Mani [21] has predicted directional distributions of sound intensity of jets that agree very well with

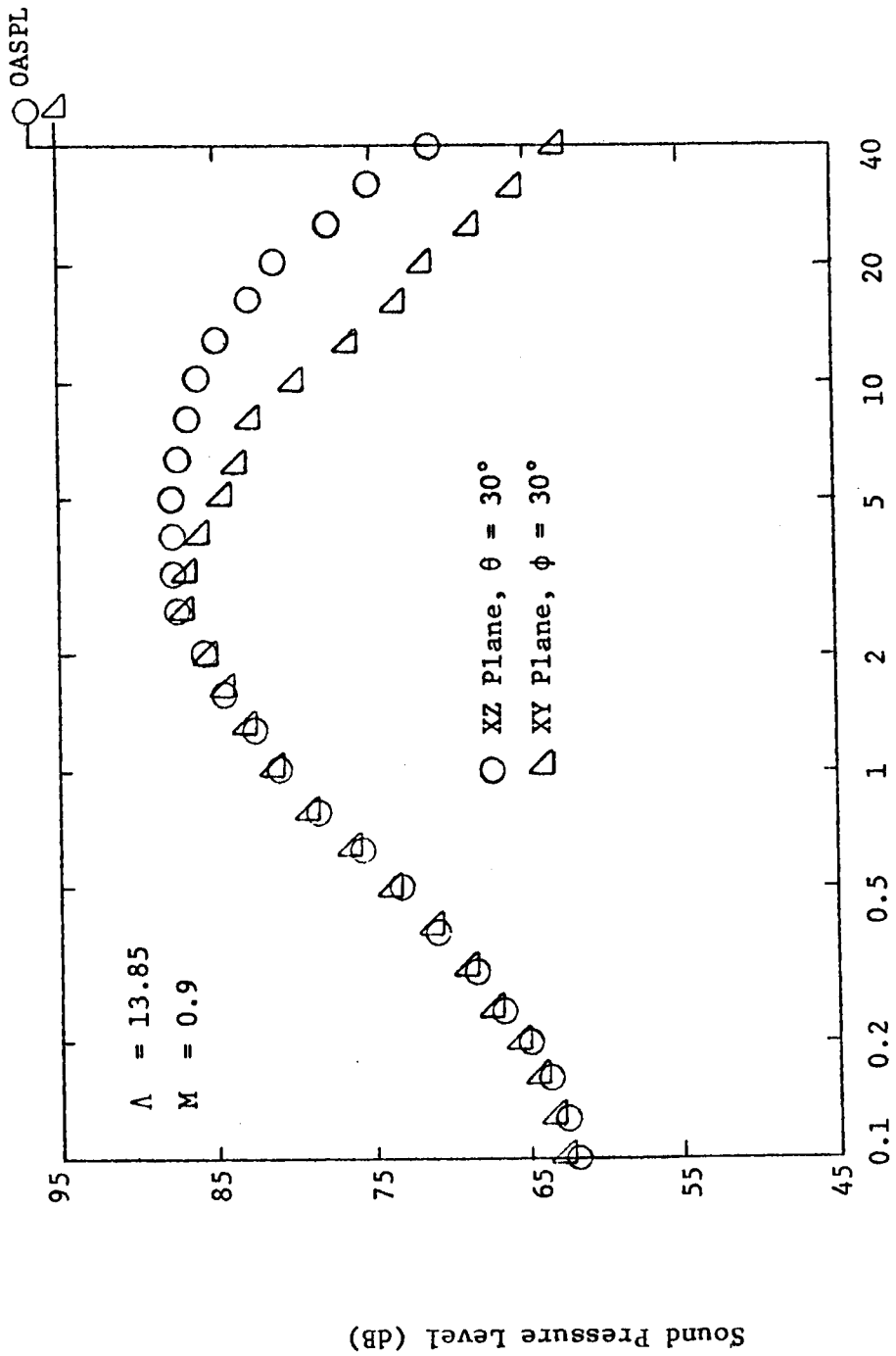


Figure 3.4. Sound pressure spectra in XZ and XY planes for the 13.85 aspect ratio slot jet.

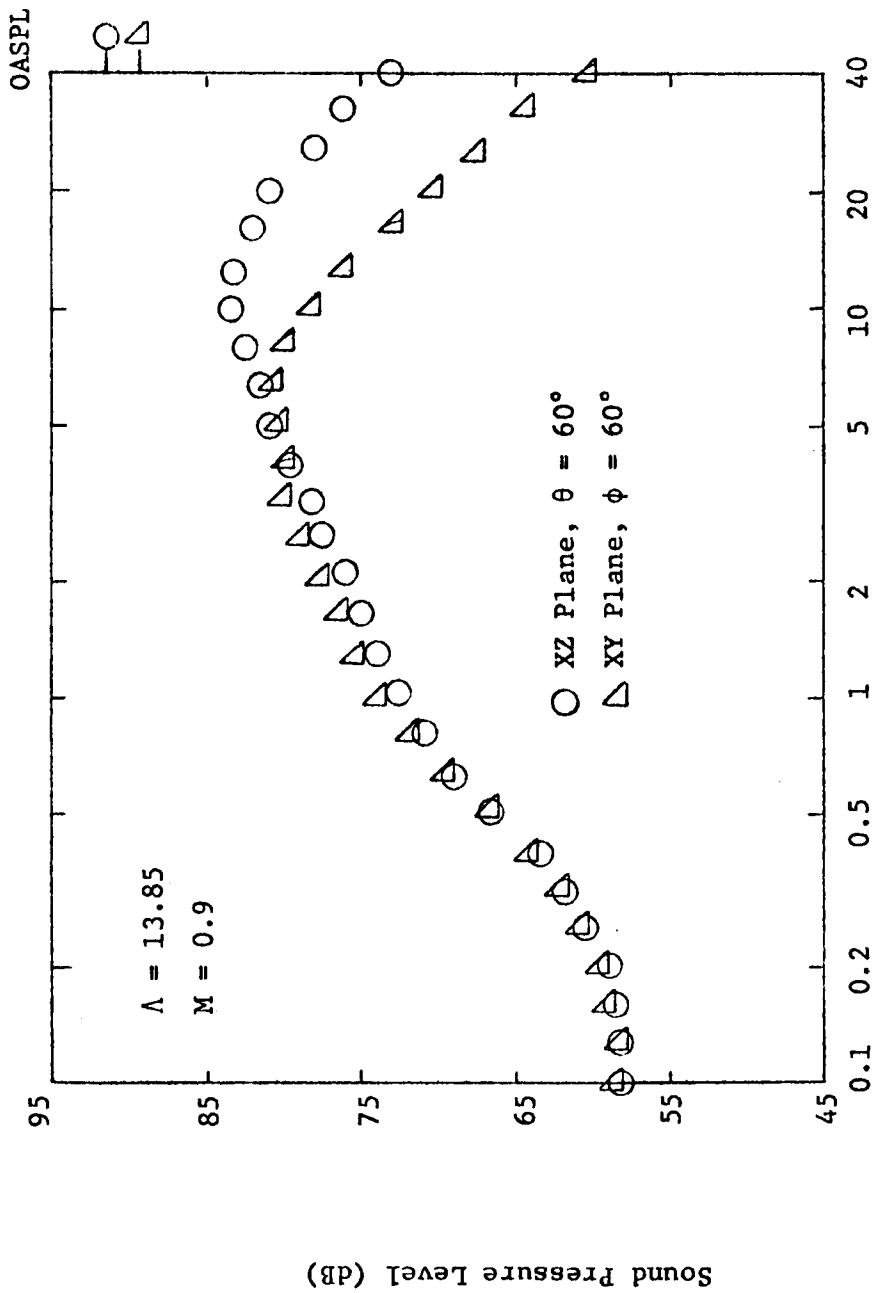


Figure 3.4., continued.

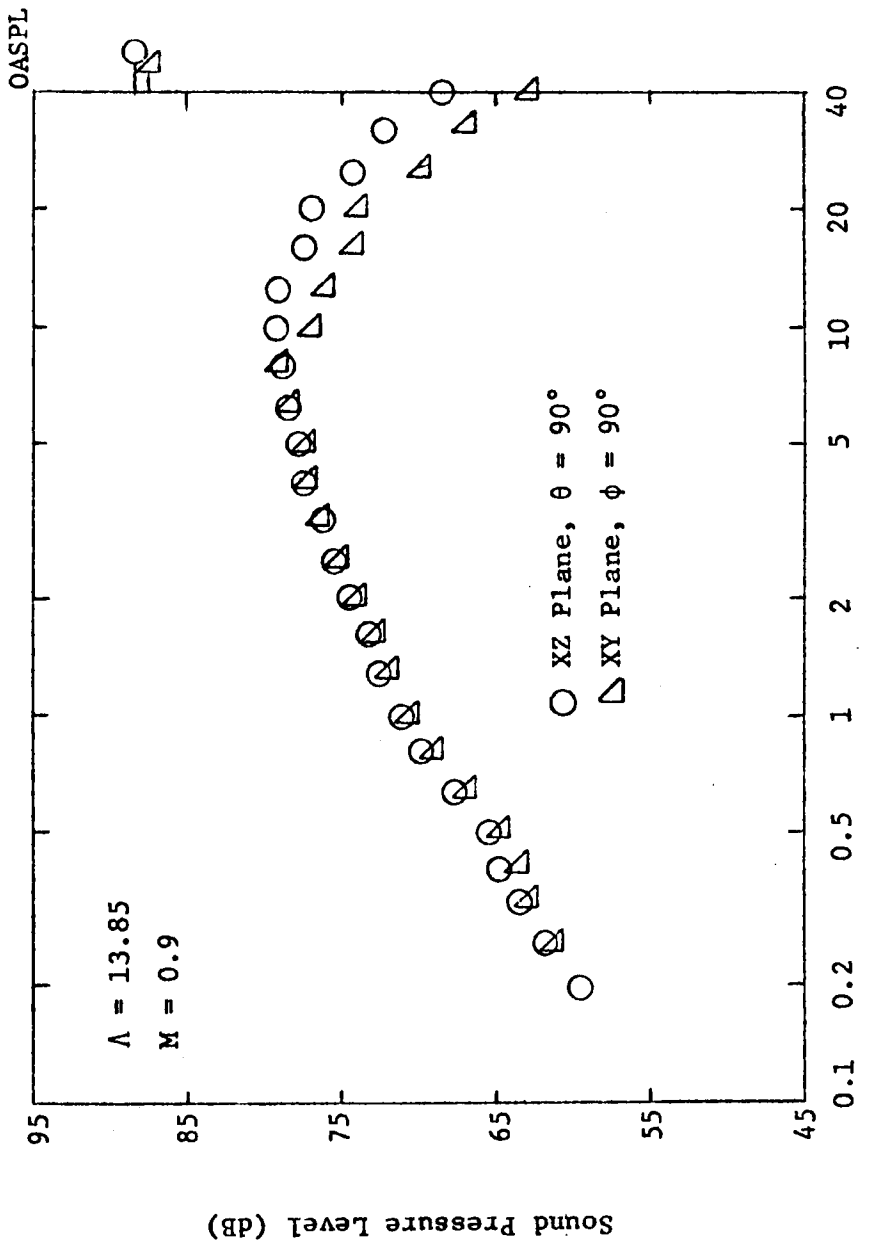


Figure 3.4. continued.

measurements. This suggests that the overestimation by Lighthill's theory of the convective amplification of high velocity jets (shown in Figure 3.2) is due to the neglect of shrouding effect of the jet. It should be noted that fluid shielding is different from refraction. Refraction causes a directional redistribution in the sound energy radiation by keeping the integrated sound energy constant, whereas shielding causes a reduction in the radiated power.

The directional preference of certain frequency components is evident in Figure 3.5 which compares the sound pressure spectra of the 13.85 aspect ratio slot jet in 30°, 60° and 90° directions. While high frequency components radiate almost uniformly in all the directions, the low frequency components clearly dominate the sound radiated in directions close to the jet axis (30°). Ribner [22] has shown that the basic directivity of a jet is composed of self noise (from turbulence alone) which is high pitched and non directional and shear noise (due to mean flow-turbulence interaction) which is low pitched and dominates in the fore and aft direction.

Compared to a circular jet of equivalent area, the slot jet has higher perimeter and therefore mixes more rapidly with the surrounding fluid causing reduced length of the potential core. If this is believed to be the reason for the reduced sound power level of the slot jet (as shown in Figure 3.6) then the noise reduction should

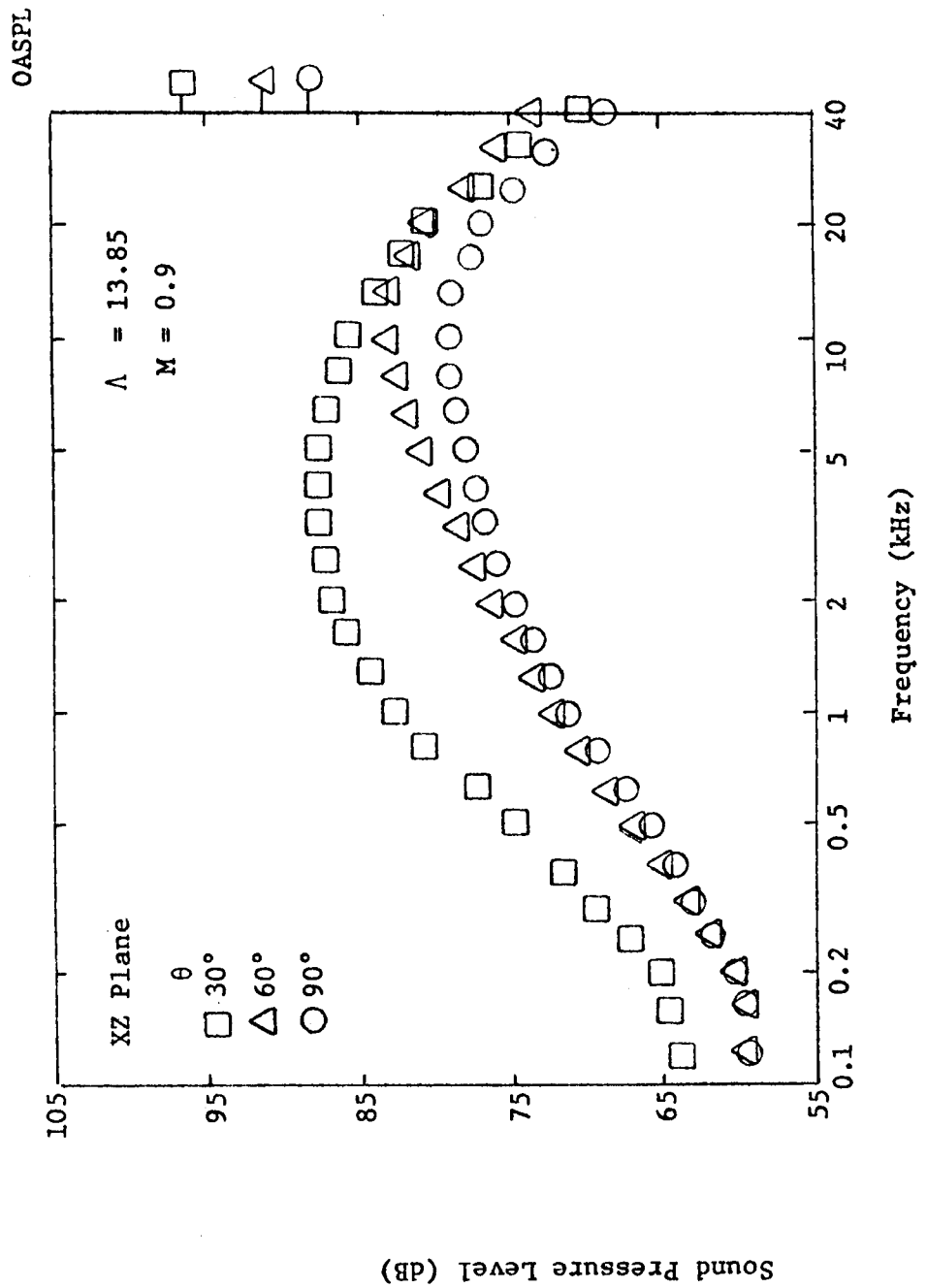


Figure 3.5. Sound pressure spectra of 13.85 aspect ratio slot jet.

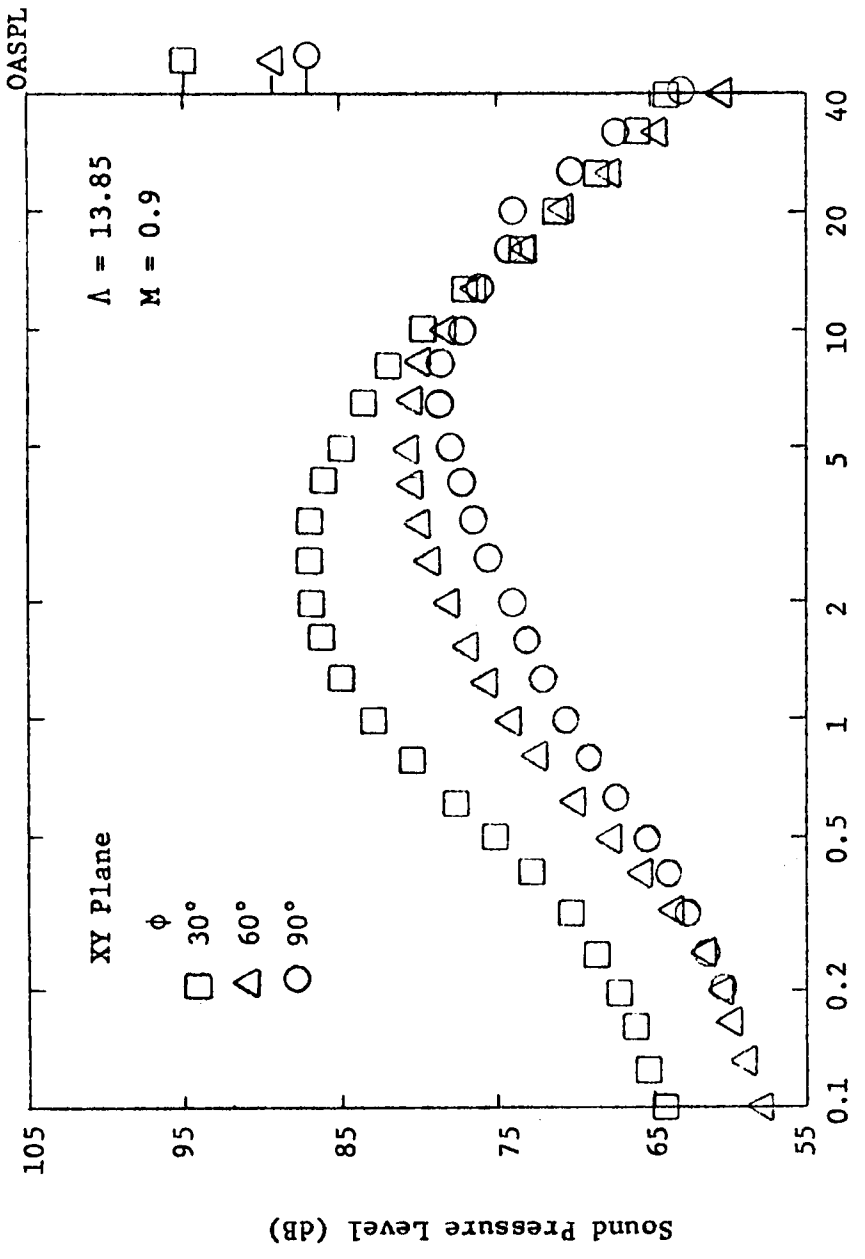


Figure 3.5. continued.

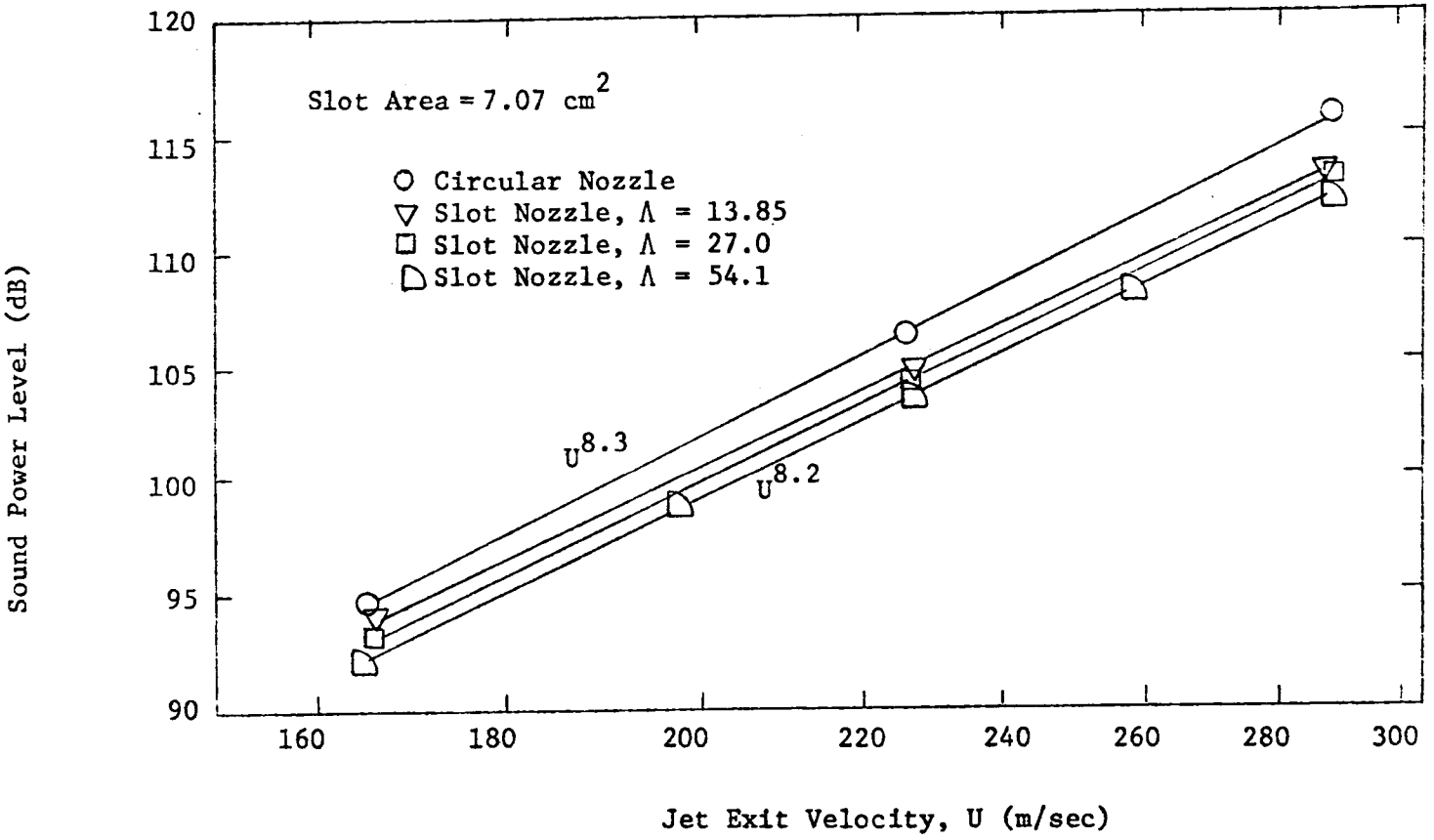


Figure 3.6. Sound power level versus jet velocity for circular and slot nozzles.

improve with increasing aspect ratio of the slot jet and should be observed in both XY and XZ planes. Figure 3.6 shows that while the 13.85 aspect ratio slot jet is about 2 dB quieter than the circular jet, increasing the aspect ratio to 54.1 produces an additional sound power reduction of only 1 dB. Reduced intensity levels for the higher aspect ratio nozzle are observed in both XZ and XY planes as shown in Figure 3.7. Assuming that the similarity of flow in a two dimensional jet is the same as that found in a circular turbulent jet, Coles [23] deduced that the quadrupole sound emitted by a high aspect ratio slot jet is only half (i.e. 3 dB lower than) that emitted by an equivalent area circular jet. In light of this observation additional attenuation due to increase in aspect ratio above 54.1 is very unlikely. The reduction in sound power of the 13.85 aspect ratio slot jet relative to the equivalent circular jet and the additional reduction obtained by increasing the aspect ratio to 54.1 is seen in Figure 3.8 to be due to reductions in the low and mid-frequency components ($f < 10$ kHz). Reduction of slot height, subsequent shortening of the potential core and a general reduction in the mixing region width causes a reduction in turbulence scale and since low frequency noise is associated with large scale turbulence it can be expected to decrease. However Lighthill [24] has shown that high frequency sound is emitted from the initial mixing region of the jet and has

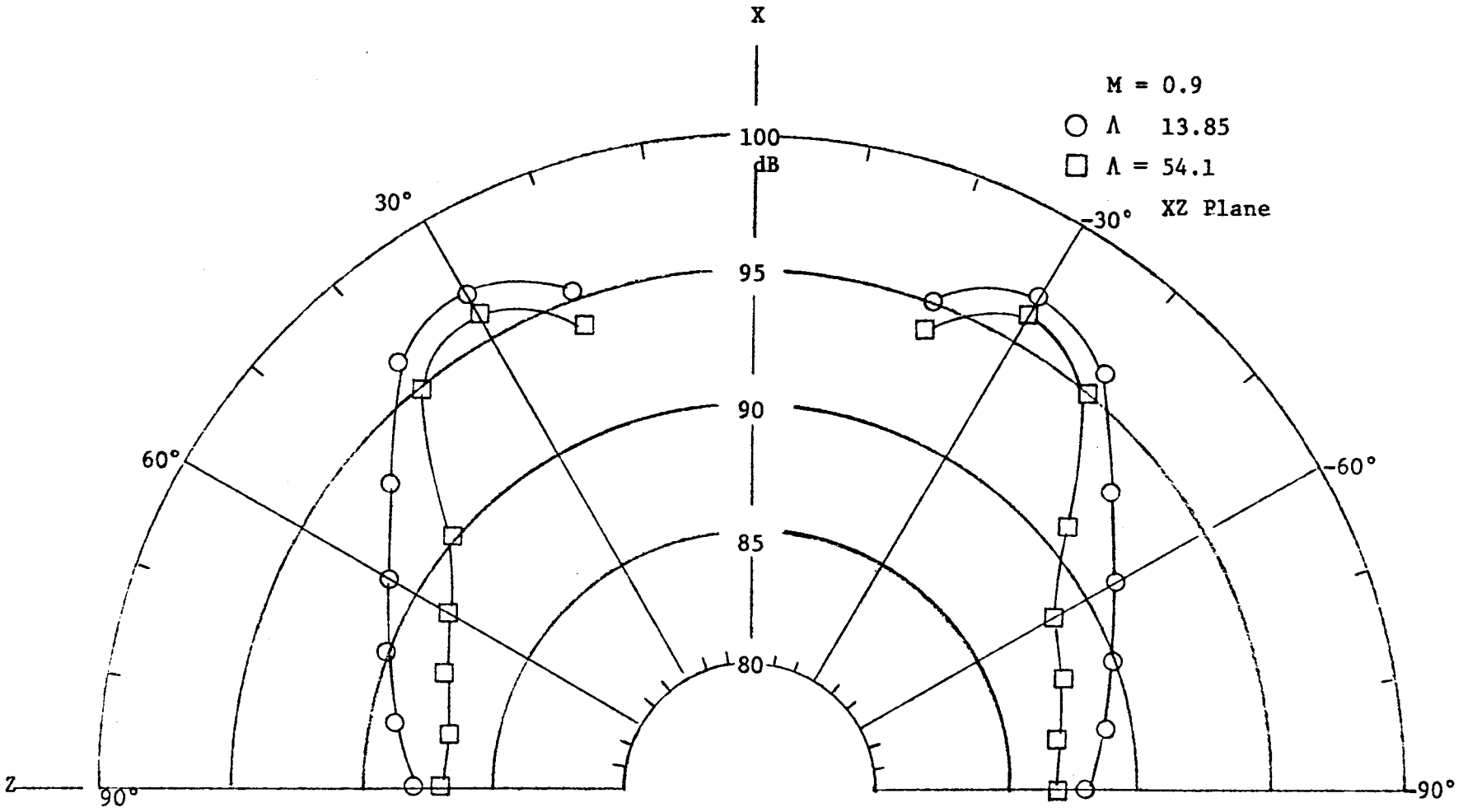


Figure 3.7. OASPL directivities of slot jet at different aspect ratios.

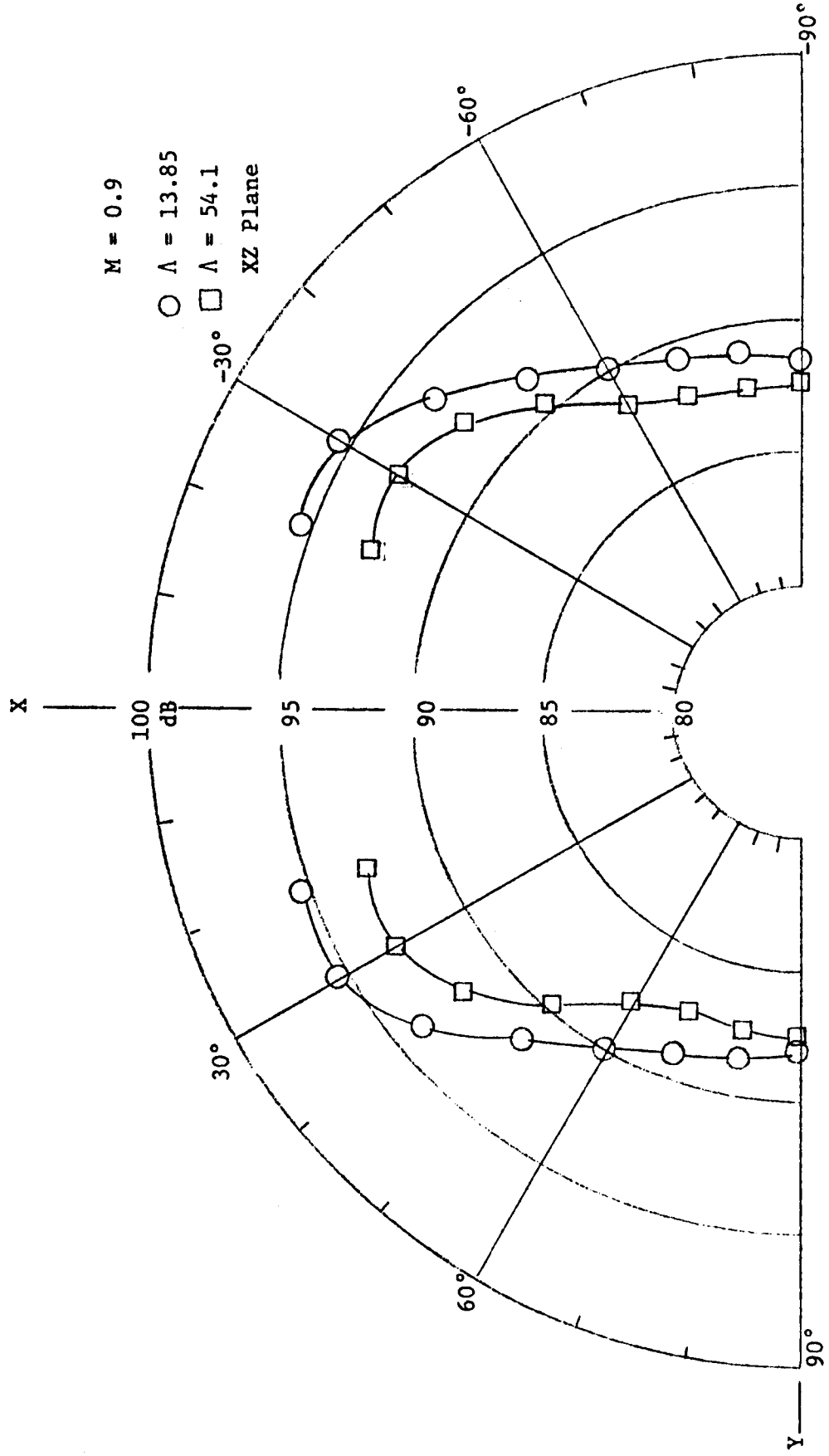


Figure 3.7. continued.

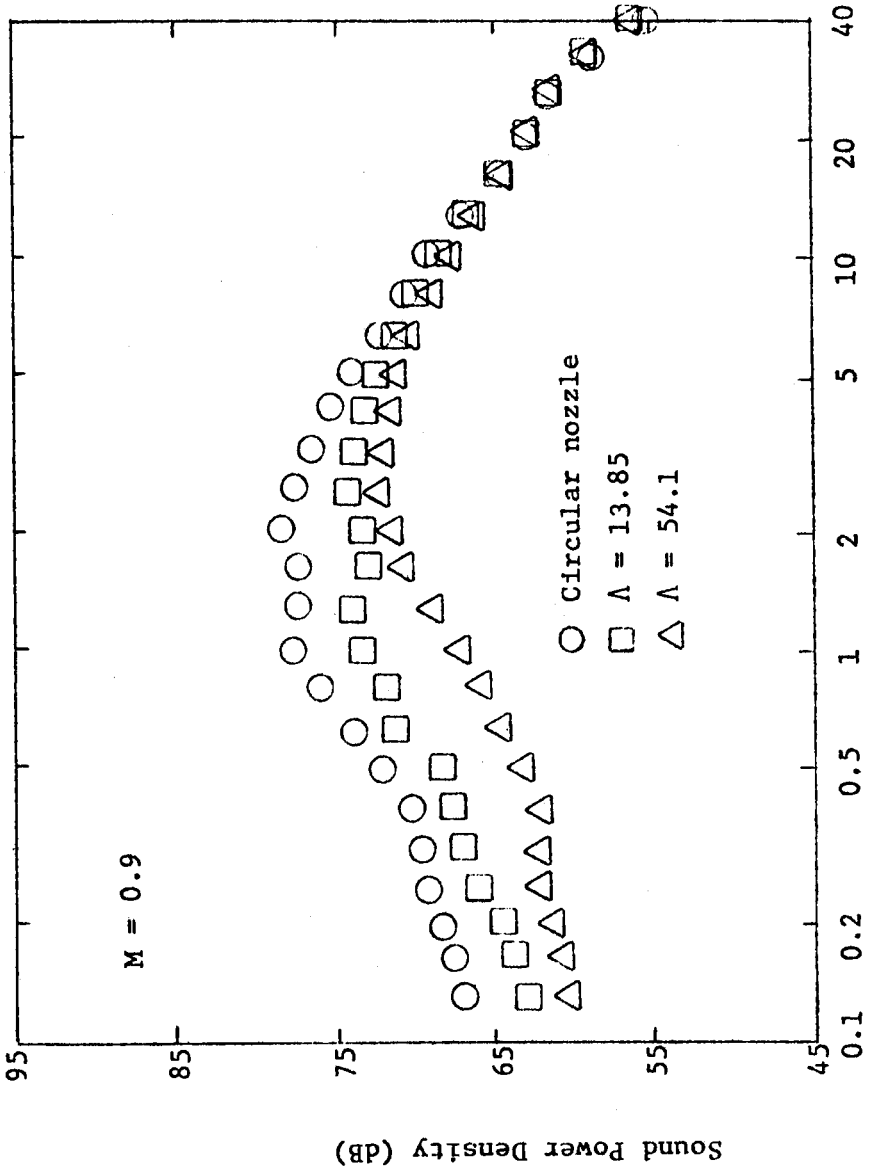


Figure 3.8. Power density spectra for circular and slot jets.

a spectral density that varies as $1/(\text{frequency})^2$. Low frequency noise, on the other hand, comes from sections of the jet that are further downstream of the potential core and has a spectral density that varies as frequency to the second or fourth power. Observe in Figure 3.8 that for both the circular and slot nozzles the power spectral density at high frequencies decays at approximately 6 dB/ octave which corresponds to a $1/(\text{frequency})^2$ variation but at low frequencies it rises 6 dB per octave for the circular jet and 4 to 5 dB per octave for the slot jets. This behaviour then suggests that the difference in the total intensity levels of the circular and slot jets is due to the difference in contribution from regions of jet that are downstream of the potential core.

Another point that should be noted in the comparison of the characteristics of slot and circular jets is the near eighth power variation with jet velocity (as predicted by Lighthill) for both. The eighth power law for circular jets has been borne out very well in experimental investigations. For slot jets, however, results have varied with investigators. Variations from U^6 to U^9 have been observed. The most likely reason for this difference is as suggested by Kouts and Yu [25], the presence of lip noise which is a dipole source caused by a fluctuating force and has a U^6 variation. Furthermore, the slot nozzle geometry would seem to favor the existence of lip dipole source as compared to the circular geometry.

CHAPTER 4

ACOUSTIC MEASUREMENTS ON JET FLAPS

This chapter reports acoustic measurements on the jet flap models. Determination of noise characteristics of jet flaps being the main thrust of this investigation, measurements are reported in detail to bring out the effect of geometrical parameters like flap length, flap deflection angle and flow parameters like the jet exit velocity on the directional radiation characteristics, total sound power output and the spectral content of the radiated sound. Discussion of results in light of the presence of possible noise mechanisms is included at the end of the chapter.

A. FREE FIELD MEASUREMENTS

OASPL DIRECTIVITIES AND SOUND PRESSURE SPECTRA IN FLYOVER PLANE

The OASPL directivities in the flyover plane for the 13.85 aspect ratio slot jet and jet flaps of various flap lengths at M = 0.9 are presented in Figure 4.1. It is evident that the effect of addition of the shortest flap to the slot nozzle is to increase the noise level in all directions in the plane. The noise levels are further

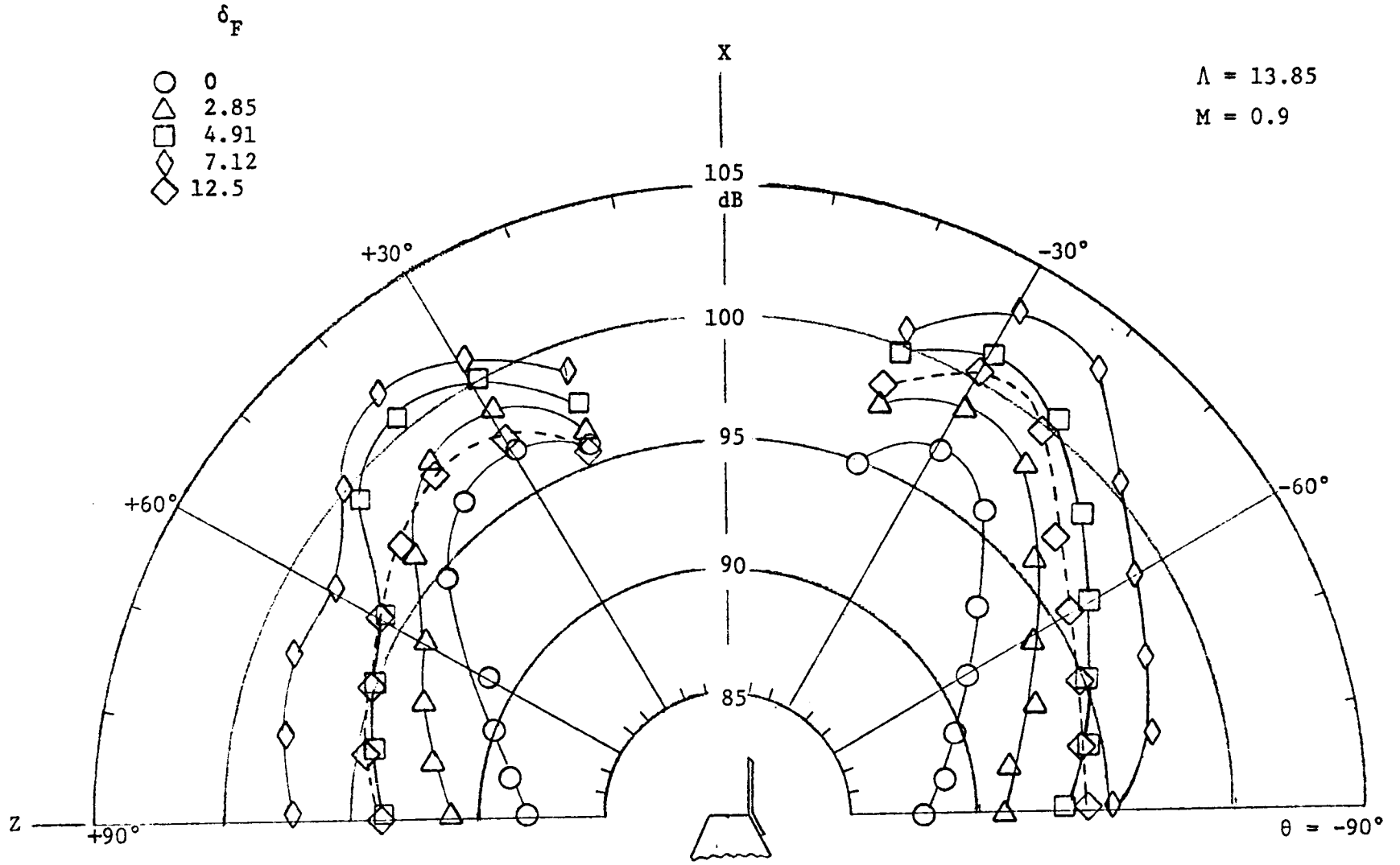


Figure 4.1. OASPL directivities in XZ plane of 13.85 aspect ratio slot-nozzle and flaps.

increased with increase in the flap length up to $\delta_F = 7.12$. However, increases in flap length beyond $\delta_F = 7.12$ causes reduction in noise levels in all directions. The directivities of the slot jet and the shortest jet flap ($\delta_F = 2.85$) peak around $\theta = 30°$ while those of the longer jet flaps peak around $\theta = 35°$ to $40°$. It is important to notice that relative to the OASPL directivity of the slot jet the augmented noise level of the jet flap is most pronounced at $\theta = 90°$. For the jet flap with $\delta_F = 7.12$, for example, the sound pressure level at $\theta = 90°$ is 10 dB higher than that of the slot jet compared to the 4 dB difference in the slot jet and jet flap sound levels in $\theta = 30°$ direction. This results in a smaller convective lobe for the jet flaps. Thus the convective amplification, measured as the difference in sound pressure level in $\theta = 90°$ direction and the maximum sound pressure level in the plane (which occurs around $\theta = 30°$ to $40°$ as mentioned above), is 4.5 dB for the jet flap with $\delta_F = 7.12$ whereas its value for the slot jet is 8.7 dB.

The directivity for the slot jet is symmetric about the X axis as would be expected. In the case of jet flaps, however, slightly higher sound pressure levels are seen on the underside of the flap in directions closer to the jet axis (i.e., $\theta < 50°$). For example, for the jet flap with $\delta_F = 7.12$, the overall sound pressure level in $\theta = -30°$ direction is about 1.5 dB higher than that in $\theta = +30°$ direction.

Some spectral data taken in the XZ plane are presented in Figures 4.2 through 4.5. Sound pressure spectra in θ = 30°, 60° and 90° directions as shown in Figure 4.2 for the jet flap with δ_F = 7.12 are typical of all the jet flaps whose directivities appear in Figure 4.1. The directional preferences of certain frequency components are identical in the slot jet and jet flap cases. This can be seen by comparing Figure 4.2 with Figure 3.5 (page 35). While the high frequency components radiate uniformly in all directions in the plane, the low frequency components have preferential radiation in directions closer to the jet axis ($\theta \sim 30°$).

Figure 4.3 shows that the increase in sound pressure level with the addition of a flap to the slot jet and with increasing flap length is due to increase in frequency components around the peak spectrum frequency. This is true for both θ = 90° and θ = 30° directions. The increases are however higher in the θ = 90° directions. The sound spectrum of the jet flap with δ_F = 7.12 in the θ = 90° direction shows a discrete frequency component at 5000 Hz which is about 4 dB above the "smooth" spectrum level. The discrete frequency component disappears if the flap length is increased to δ_F = 12.5. This can be seen in Figure 4.4 which also shows that the reduction in overall sound pressure level of the jet flap when the flap length is increased from δ_F = 7.12 to δ_F = 12.5 is again due to

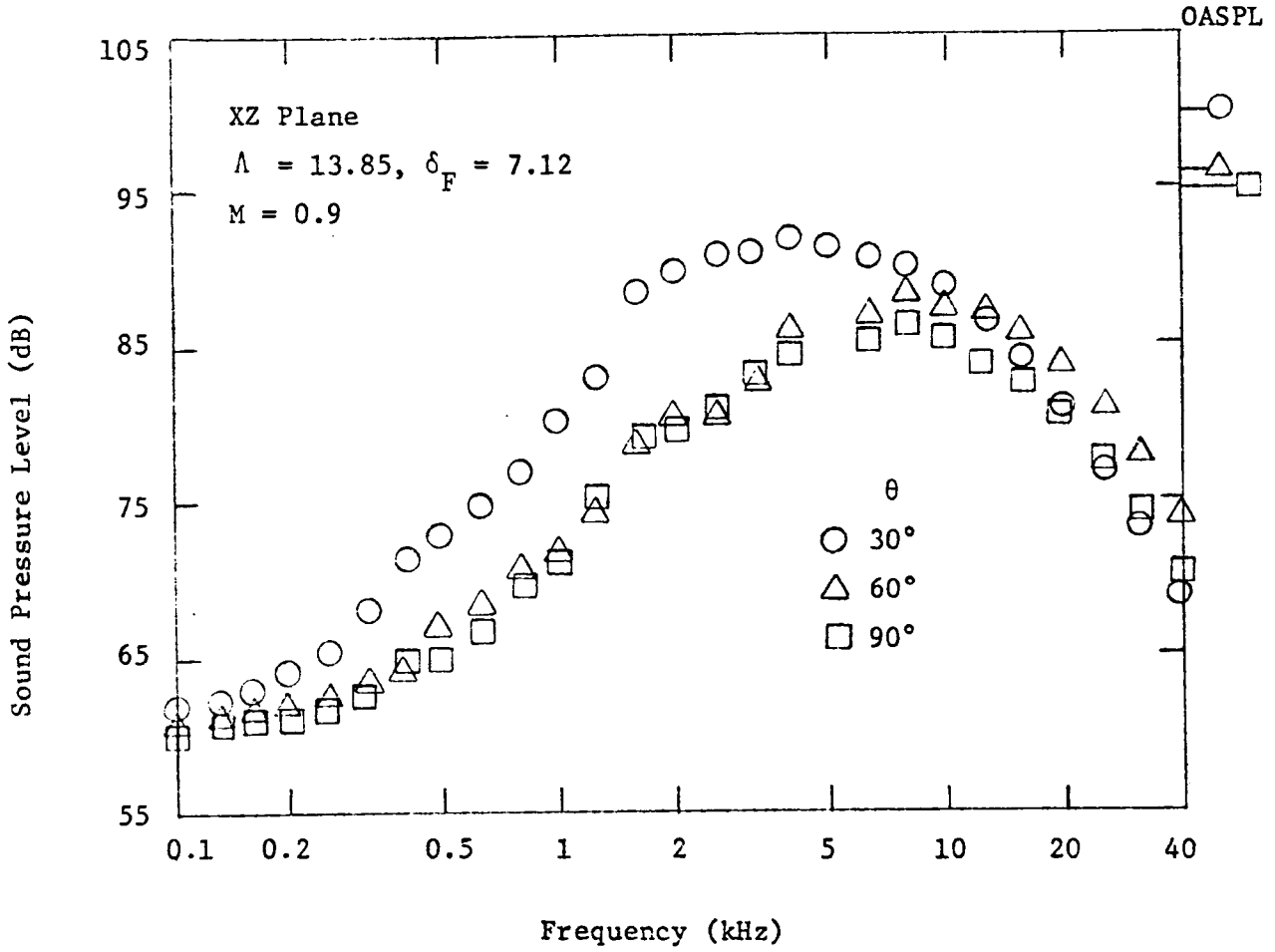


Figure 4.2. Sound pressure spectra at θ = 30°, 60° and 90° for δ_F = 7.12 flap.

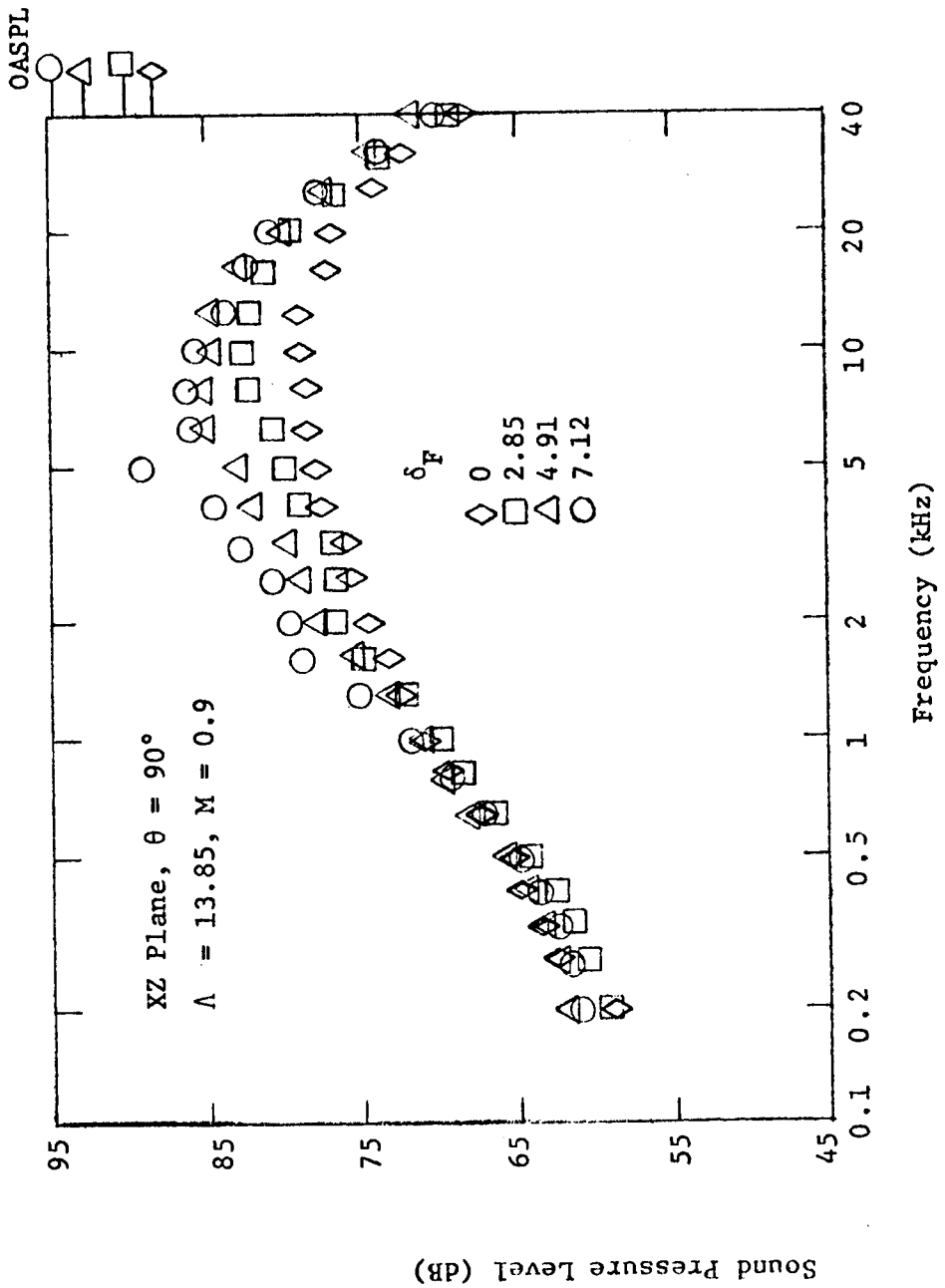


Figure 4.3. Sound pressure spectra for flaps on 13.85 aspect ratio slot nozzle.

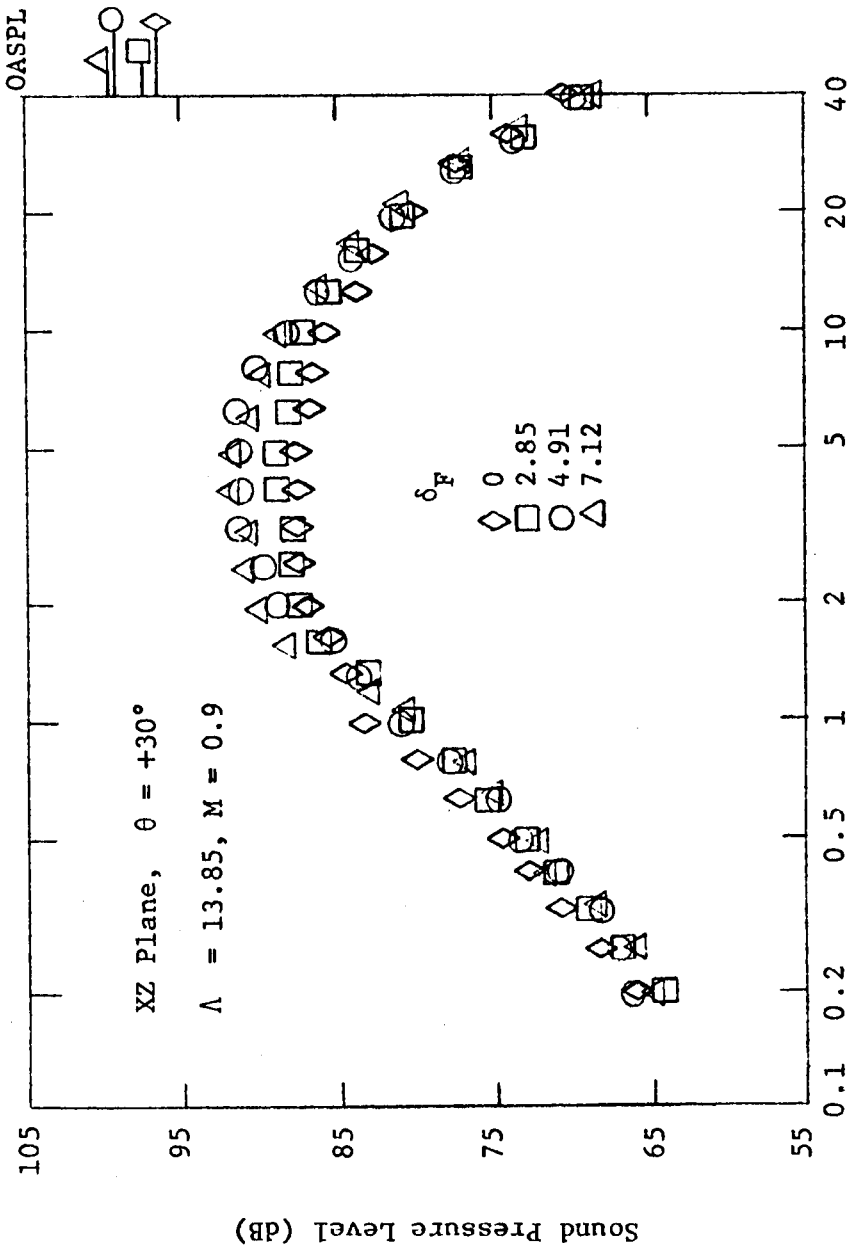


Figure 4.3 continued.

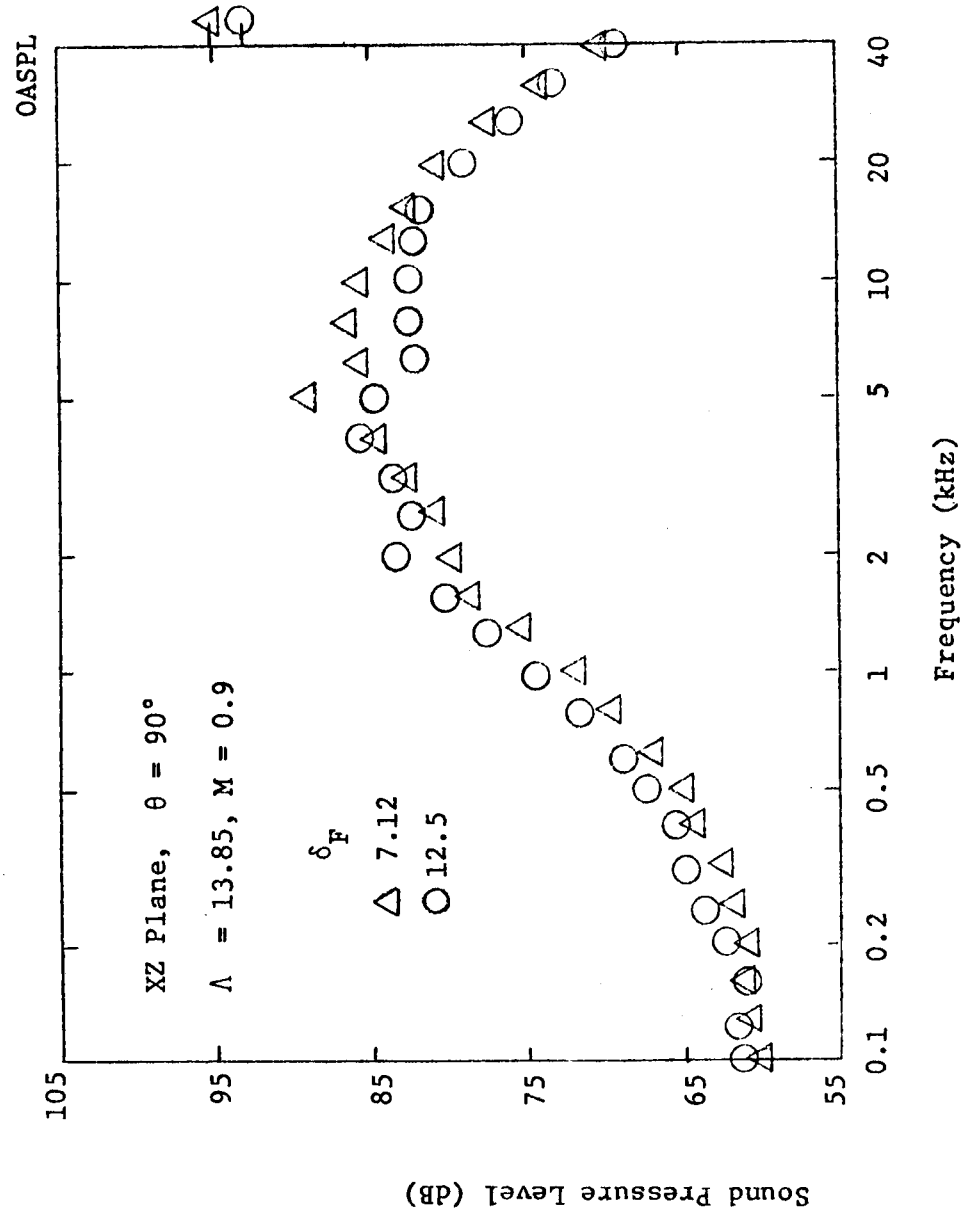


Figure 4.4. Sound pressure spectra for δ_F = 7.12 and 12.5 flaps.

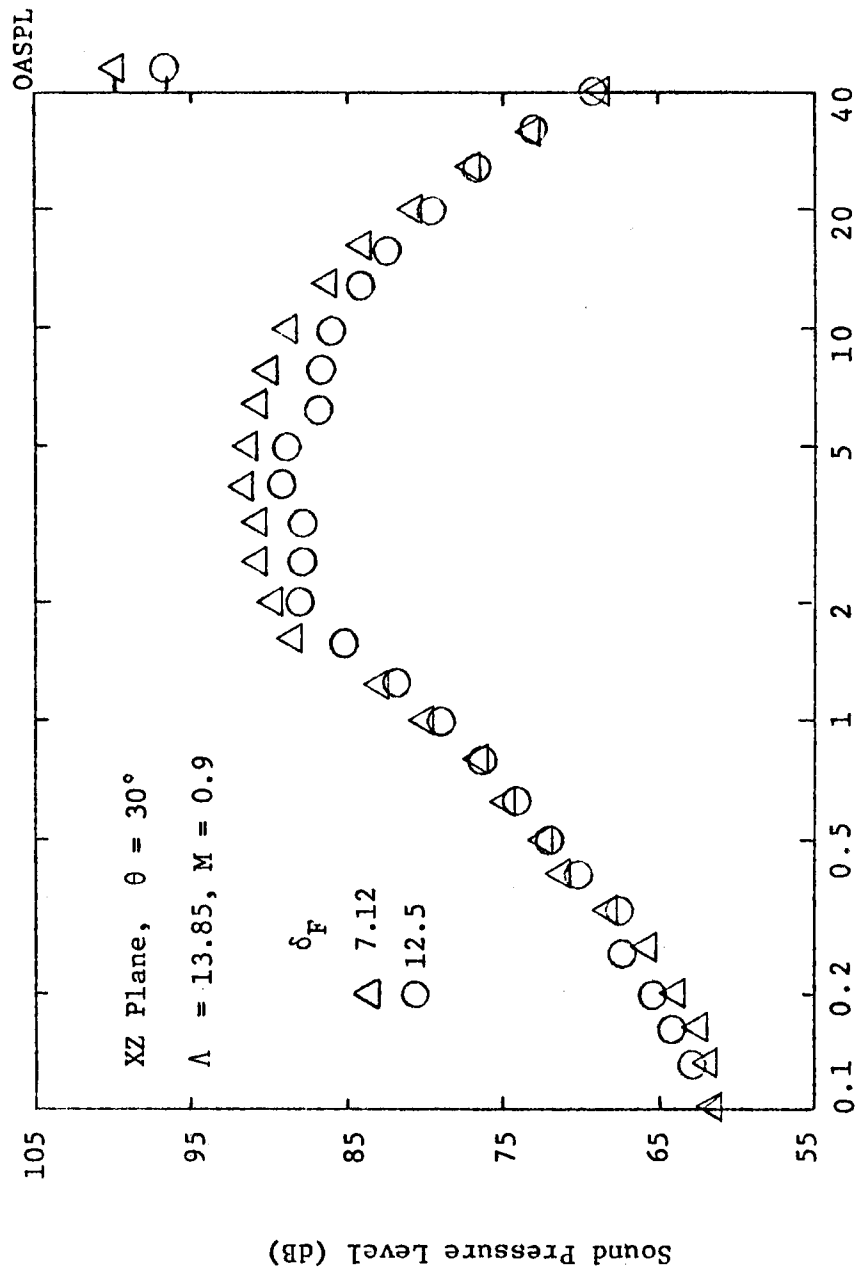


Figure 4.4. continued.

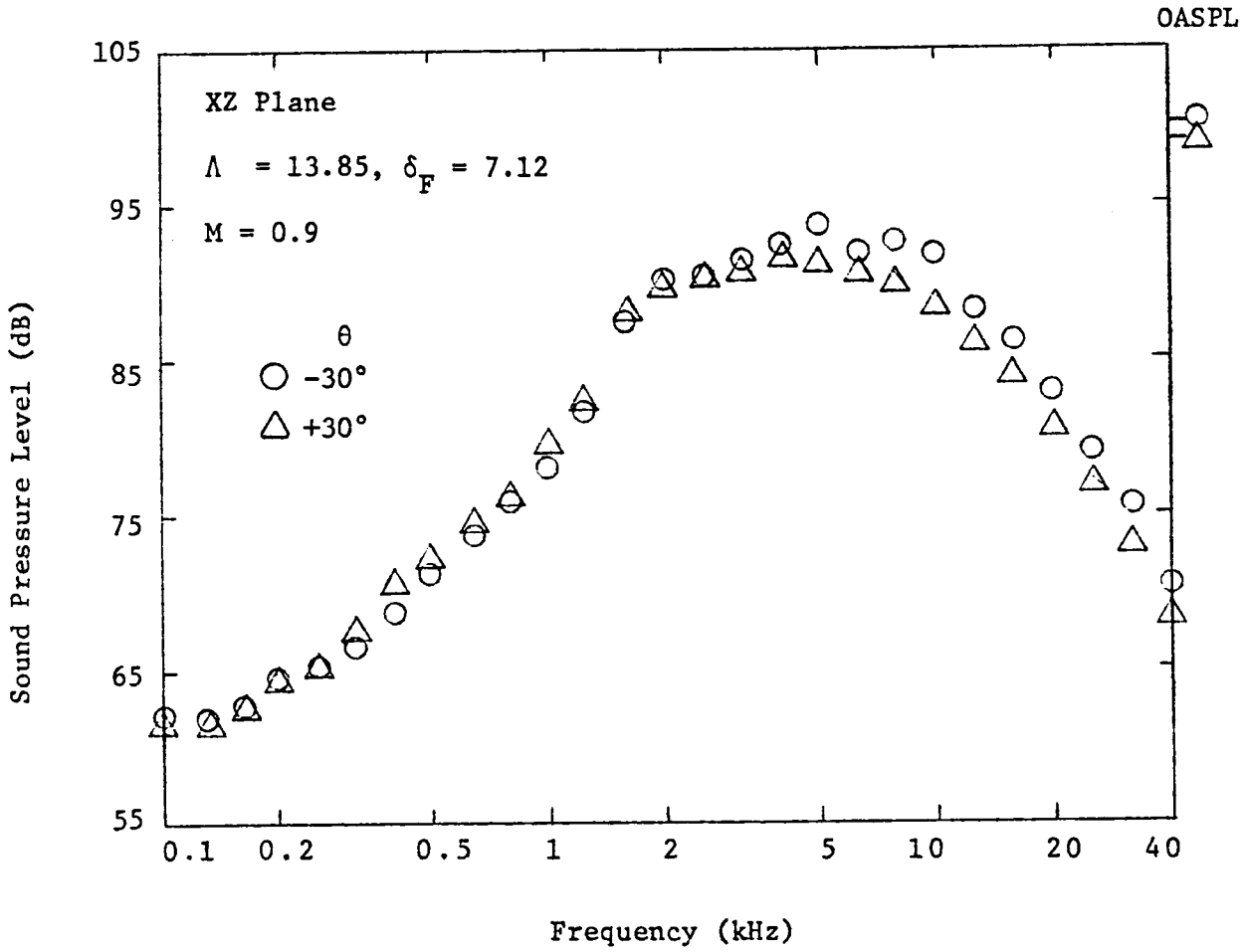


Figure 4.5. Sound pressure spectra at θ = ±30° for flaps on 13.85 aspect ratio slot jet.

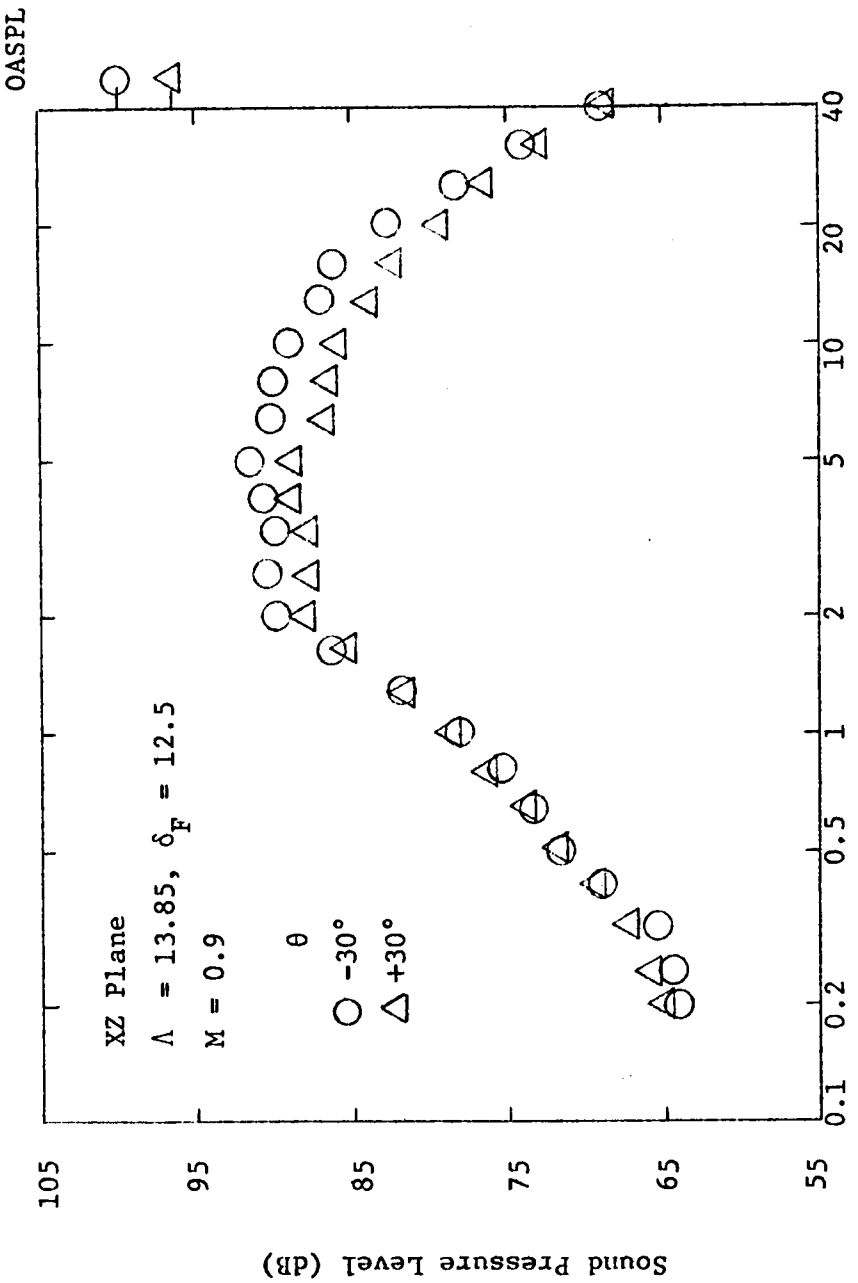


Figure 4.5. continued.

decrease in frequency components around the spectrum peak frequency in both $\theta = 90°$ and $\theta = 30°$ directions. Higher sound levels on the underside of the flap for jet flaps are seen in Figure 4.5 to be due to increased high frequency component ($f > 2000$ Hz) contribution to the underside of the flap (i.e. -30° direction in Figure 4.5). This increase is greater for the jet flap with $\delta_F = 12.5$ than for $\delta_F = 7.12$. Finally the OASPL directivities of the slot jet and jet flaps of various length at $M = 0.7$ have, as can be observed in Figure 4.6, gross similarities with the corresponding directivities at $M = 0.9$.

OASPL directivities in the XZ plane with the jet exhausting at $M = 0.7$ for the slot jet from the 27 aspect ratio slot nozzle and for jet flaps of various lengths are depicted in Figure 4.7. Addition of the shortest flap to the slot jet again causes an increase in sound levels throughout the plane. The OASPLs increase with increasing flap length until a flap length of $\delta_F = 9.9$ is reached. This increase in sound pressure level is again highest in the $\theta = 90°$ direction. Increasing the flap length beyond $\delta_F = 9.9$ produces reduced sound pressure levels in the entire plane. Jet flaps with $\delta_F = 9.9$ and 18 radiate more sound in -30° direction than they do in the +30° direction. The longest flap used with this slot jet had a flap length $\delta_F = 36$. For this jet flap the sound radiation is almost uniform in all directions with a

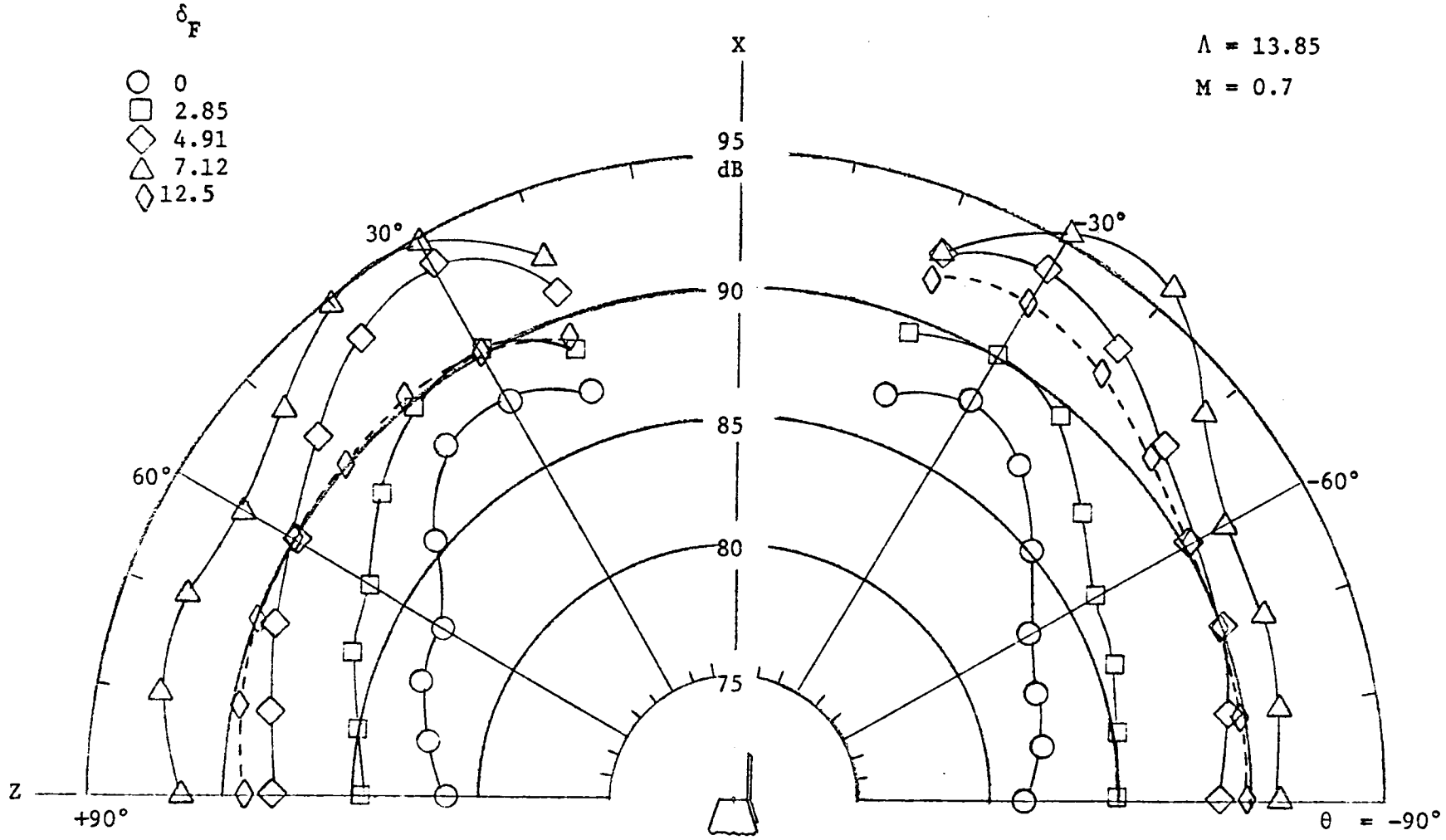


Figure 4.6. OASPL directivities in XZ plane of 13.85 aspect ratio slot nozzle and flaps at M = 0.7.

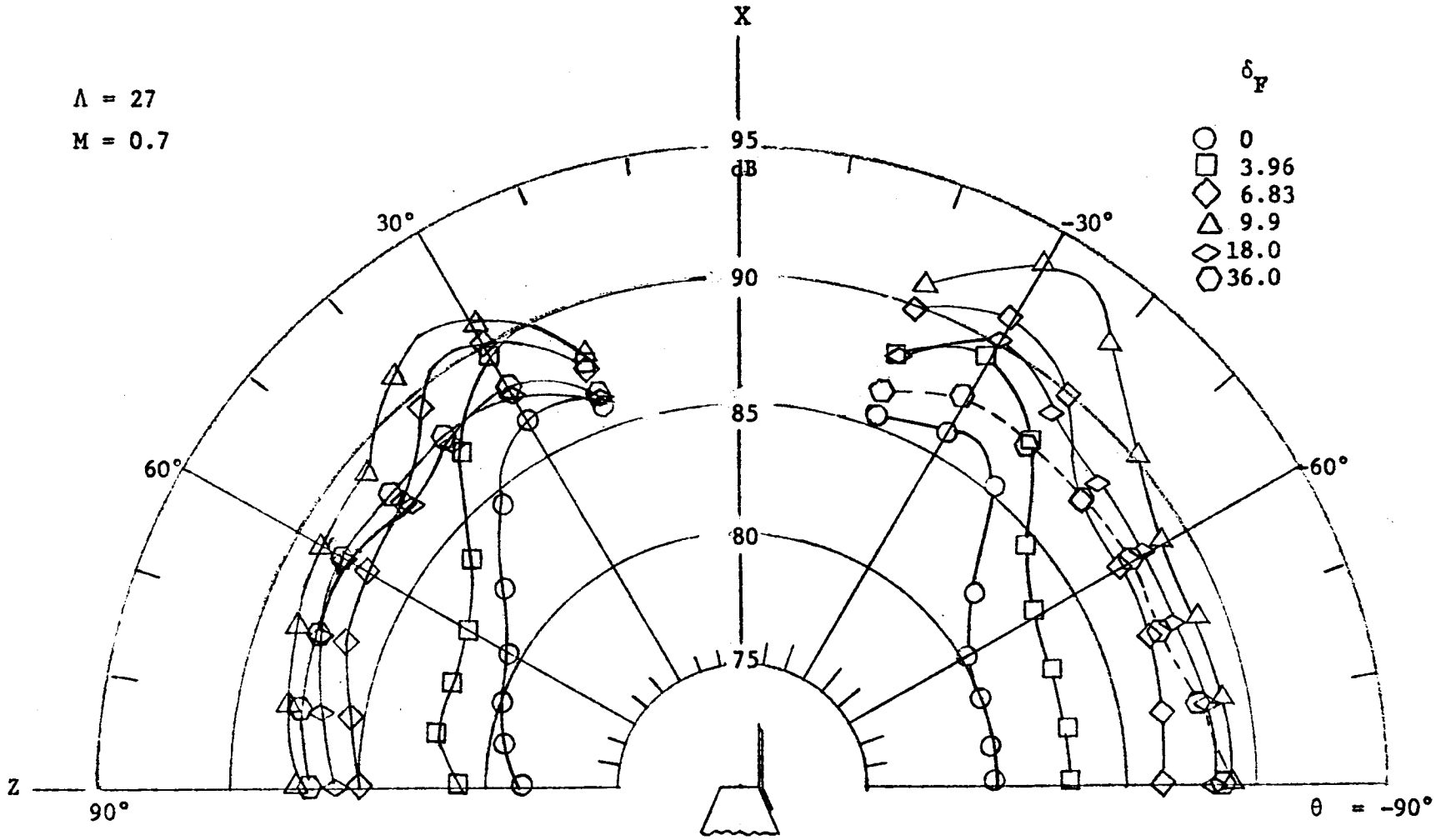


Figure 4.7. OASPL directivities in XZ plane for flaps on 27 aspect ratio slot nozzle at M = 0.7.

clear absence of the convective lobe. Observations recorded in this paragraph on the OASPL directivities of jet flaps with the 27 aspect ratio slot jet show the radiation characteristics of these jet flaps to be similar to those of the 13.85 aspect ratio slot jet and flaps.

Additional acoustic characteristics of jet flaps are revealed in Figure 4.8 which shows the OASPL directivities of the 27 aspect ratio slot jet and jet flaps for jet exit Mach number of 0.9. The most important feature to be observed in this figure is the tremendous increase in the sound pressure levels in all directions when the flap length is increased from $\delta_F = 3.96$ to $\delta_F = 6.83$. While addition of the flap with $\delta_F = 3.96$ to the slot jet causes a maximum OASPL increase of 3 dB, the effect of increasing the flap length to $\delta_F = 6.83$ is to increase the sound level throughout the plane by about 12 dB. Increasing the flap length further to $\delta_F = 9.9$ produces a change in the directivity and increased sound pressure levels in certain directions. The double lobed directivity for $\delta_F = 9.9$ on the underside of the flap is evident. Increase in flap length beyond $\delta_F = 9.9$ causes reduction in the noise level as is apparent from the OASPL values for $\delta_F = 18$ and 36. Again the maximum sound pressure level radiated below the flap is slightly higher than that radiated above the flap for $\delta_F = 6.83$, 9.9 and 18. It is interesting to note that for the longest flap, $\delta_F = 36$,

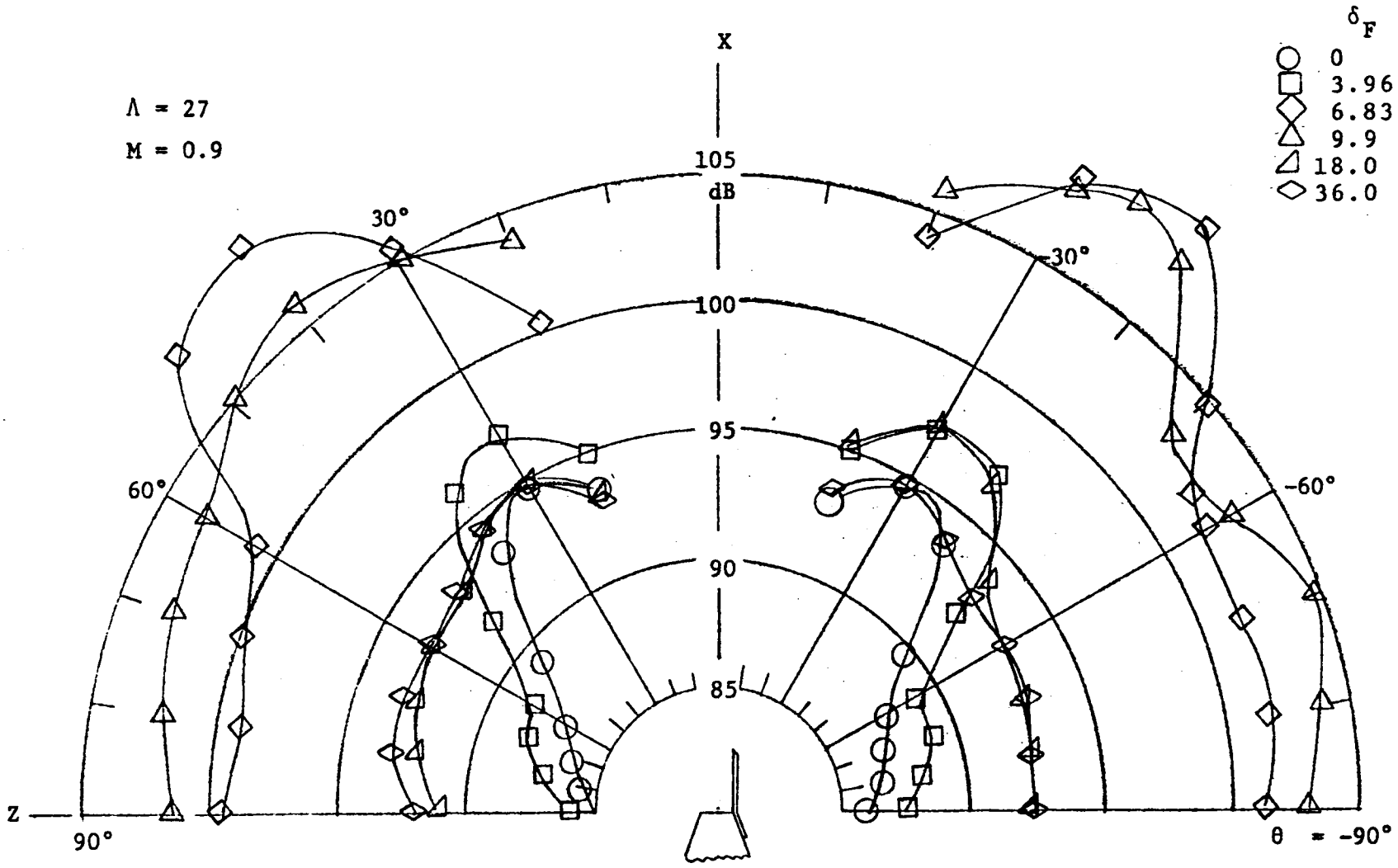


Figure 4.8. OASPL directivities in XZ plane for flaps on 27 aspect ratio nozzle at M = 0.9.

the OASPL values in the convective lobe (θ = ±20° to ±40°) are nearly equal to those of the slot jet without flap. This jet flap furthermore radiates almost equally in both +30° and -30° directions.

Spectral data in XZ plane for the 27 aspect ratio slot jet and jet flaps are given in Figures 4.9 and 4.10. In θ = 90° direction, the addition of flap with δ_F = 3.96 produces increased contribution only from sound components with frequencies near the spectrum peak frequency. This was observed (Figure 4.3, page 48) in the case of 13.85 aspect ratio slot jet and jet flaps also. However, when the flap length is increased to δ_F = 6.83 a large increase in the high frequency components (f > 2000 Hz) is observed. In addition to this increase very loud "whistle" tones were generated which could be seen as discrete frequency components in 6300 Hz and 12,500 Hz one-third octave bands. For the jet flap with δ_F = 9.9 the sound pressure levels are further increased at all frequencies. In addition, a discrete frequency tone is now generated in the 3150 Hz one-third octave band. It should be noted that the center frequencies of the one third octave bands in which discrete frequency tones occur are harmonically related. The effect of increasing the flap length from δ_F = 9.9 to δ_F = 18 is to reduce the high frequency components that were increased when the flap length was increased from δ_F = 3.96 to δ_F = 9.9 and to eliminate the tones.

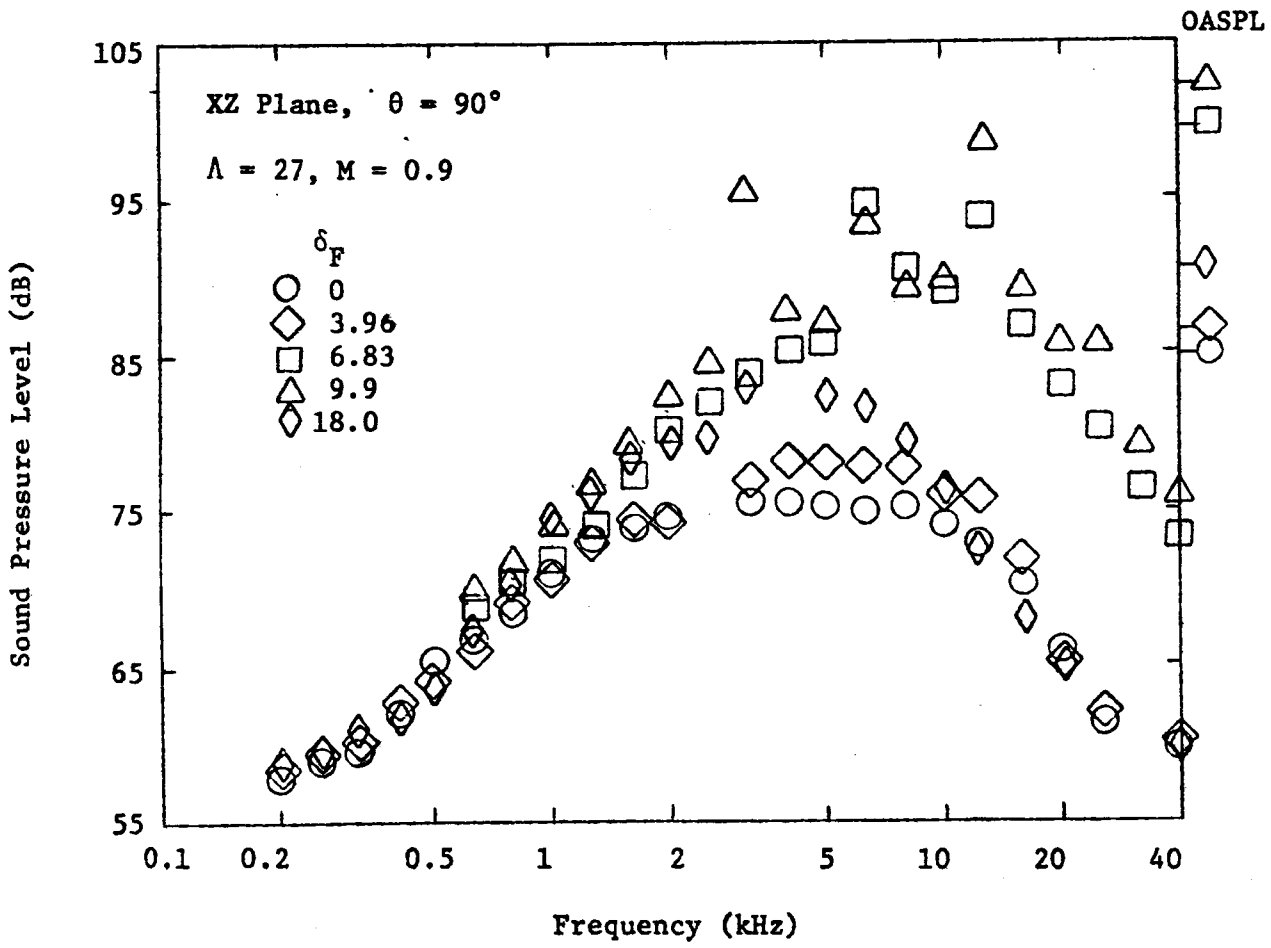


Figure 4.9. Sound pressure spectra at θ = 90° for flaps on the 27 aspect ratio slot nozzle.

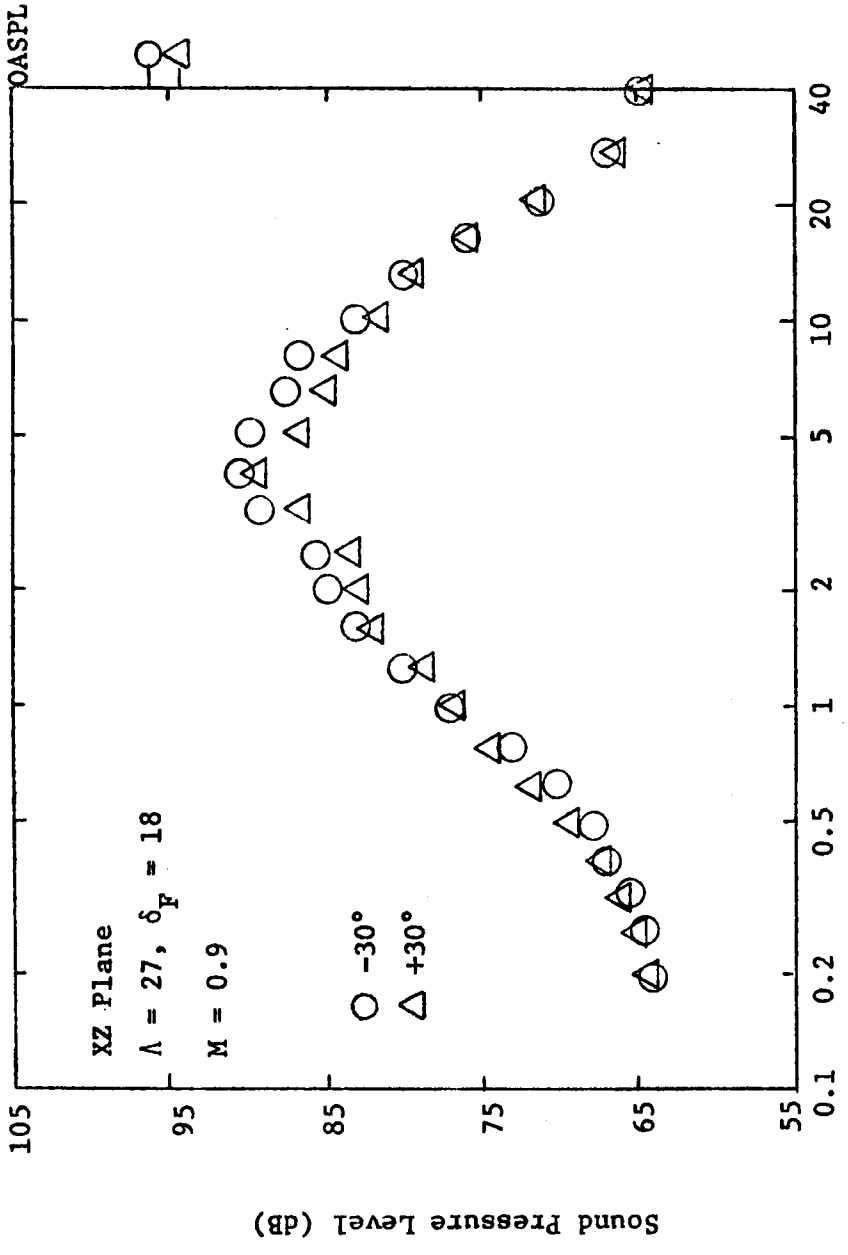


Figure 4.10. Sound Pressure Spectra at θ = 30° for δ_F = 18 flap.

In $\theta = 90°$ direction the higher noise level of the $\delta_F = 18$ jet flap relative to the slot jet is due only to frequency components near the peak frequency.

For the jet flap with $\delta_F = 18$ the higher noise radiation in the -30° direction, compared to the radiation in +30° direction, can be seen in Figure 4.10 to be due to increased contribution from components near the spectrum peak frequency.

Figure 4.11 depicts the OASPL directivities in XZ plane for the 54.1 aspect ratio slot jet exhausting at a Mach number of 0.7 and for jet flaps of various lengths. The radiational characteristics of these jet flaps are generally similar to the characteristics of jet flaps with the 13.85 and 27 aspect ratio slot jets. Increasing flap lengths cause increased sound radiation in all directions until a flap length $\delta_F = 9.72$ is reached. Noise levels begin to decrease with further increase in flap length. Higher radiation on the underside of the flap is evident for jet flaps with $\delta_F = 9.72$, 14.1 and 25.5. Interestingly, the jet flap with $\delta_F = 51$ radiates less sound than the slot jet in the convective lobe directions (i.e. $\theta \sim 20°$ to 40°). For this jet flap, the sound radiation in -30° direction is less than the radiation in +30° direction.

The characteristics mentioned above are generally preserved and slightly amplified when the jet exit Mach number is increased to 0.9. This is evident in Figure 4.12.

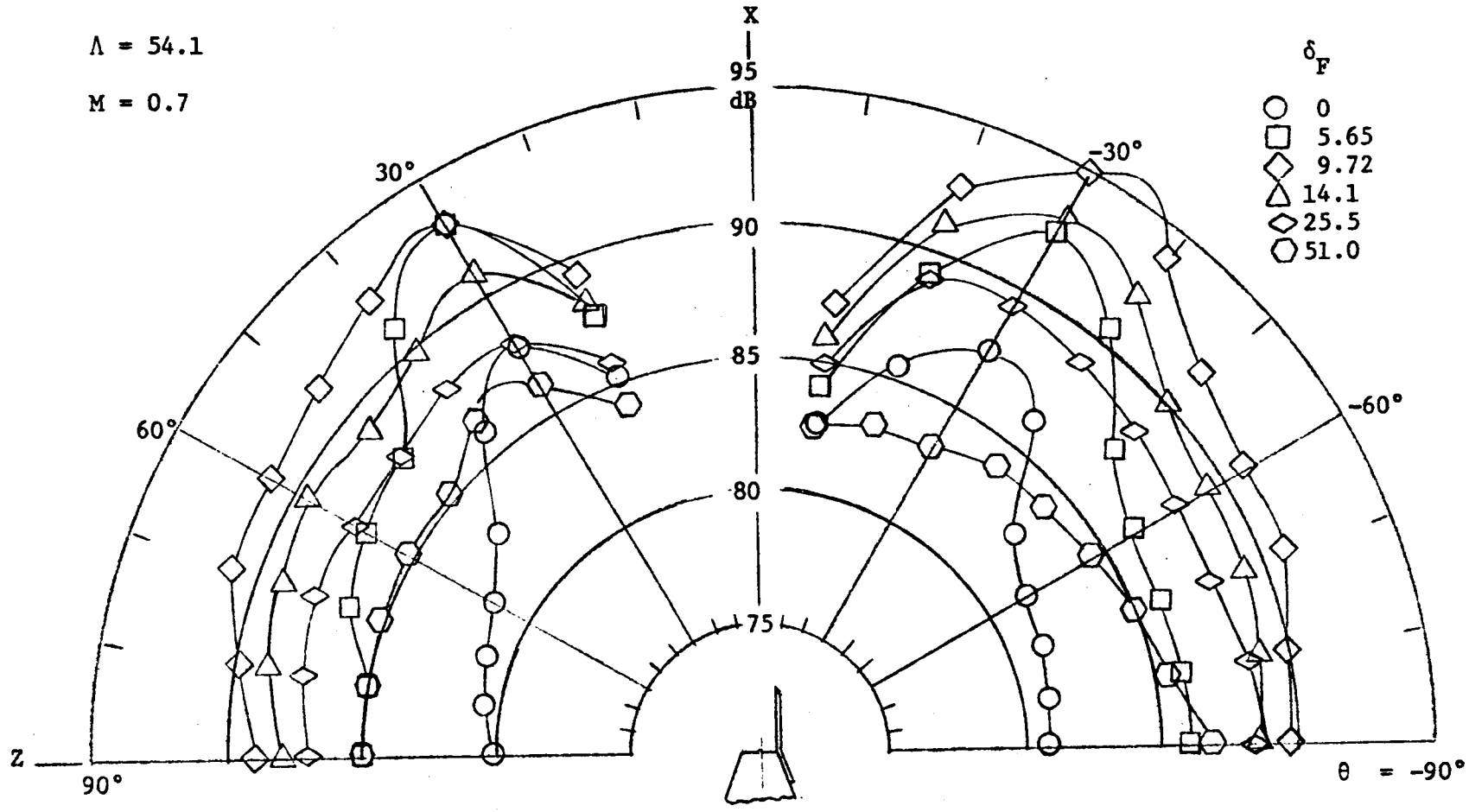


Figure 4.11. OASPL directivities in XZ plane for flaps on 54.1 aspect ratio slot nozzle at M = 0.7.

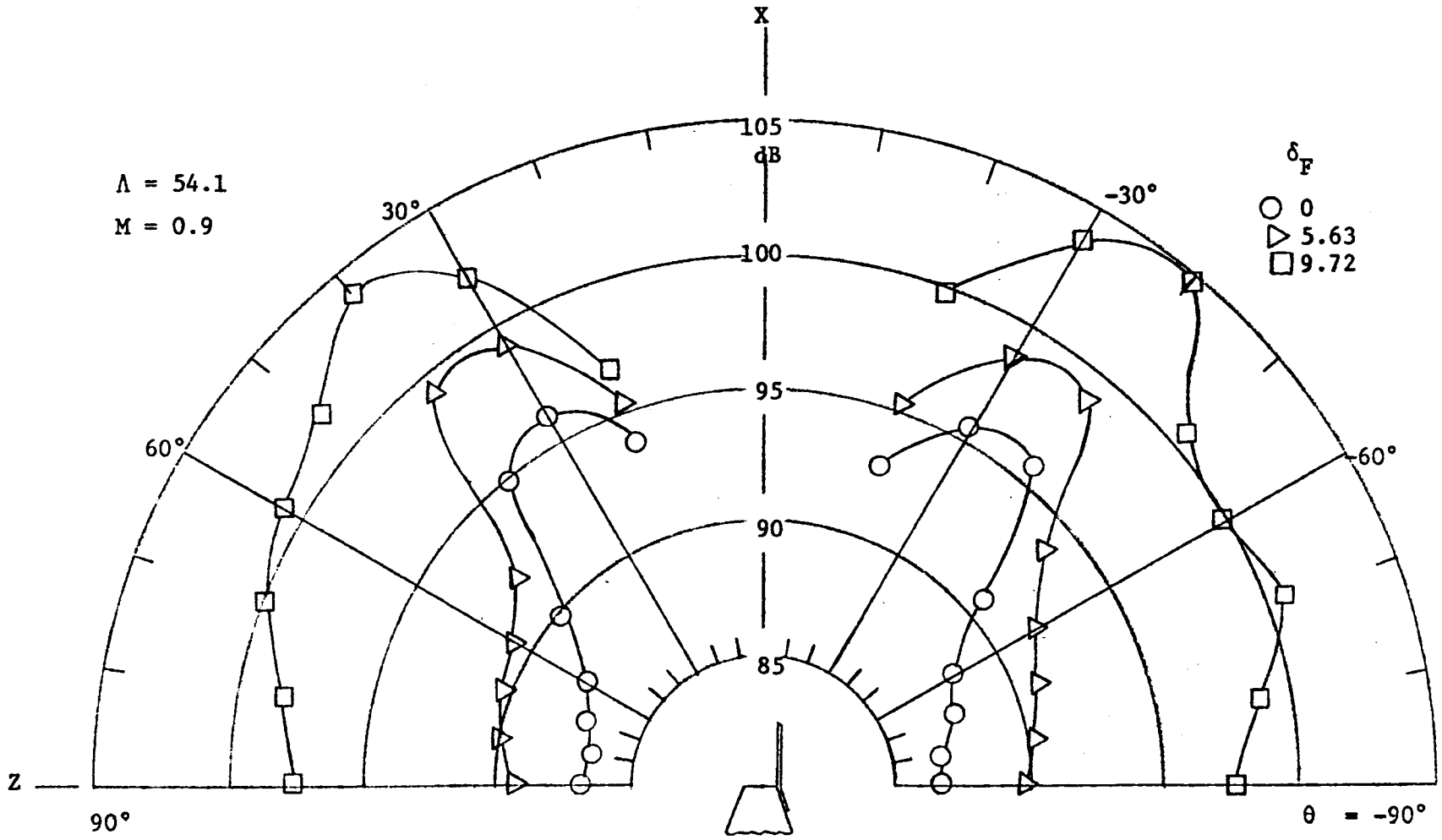


Figure 4.12. OASPL directivities in XZ plane for flaps on the 54.1 aspect ratio slot nozzle at M = 0.9.

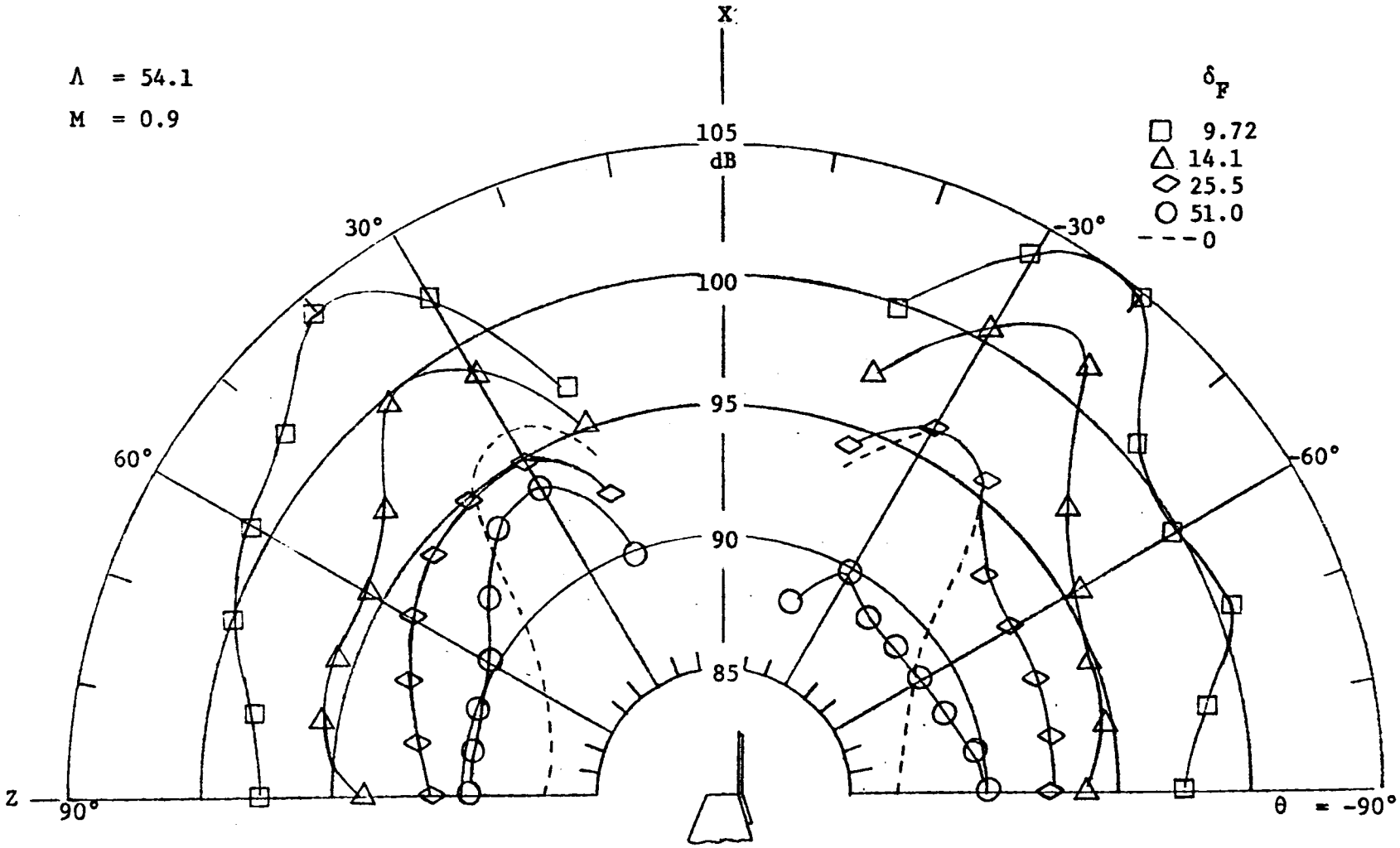


Figure 4.12. continued.

The jet flap with δ_F = 9.72 has a double lobed directivity on the underside of the flap with peaks at -40° and -70°. This was also observed for the jet flap with δ_F = 9.9 on the 27 aspect ratio slot nozzle (Figure 4.8, page 58). The reduction in the convective lobe directions for δ_F = 51 is enhanced at M = 0.9. This reduction (6 dB at -30°) is more below the flap than above it.

In θ = +90° direction, the increase in sound pressure level with increasing flap length is seen in Figure 4.13 to be due to increased contribution from high frequency components (f > 2000 Hz). The jet flap with δ_F = 9.72 generates a discrete frequency tone at 10,000 Hz. The sound level decreases upon increasing the flap length to δ_F = 14.1 through reductions again in the high frequency components. The tone is also eliminated by the increased flap length. These features are observed in θ = 30° direction also, as can be noted in Figure 4.14. The second part of Figure 4.13 shows that at θ = 90° the effect of changing flap length from δ_F = 14.1 to δ_F = 25.5 and further to δ_F = 51 is to reduce the high frequency components and increase the low frequency components, thereby shifting the spectrum peak to lower frequencies. In θ = 30° direction, however, increase in flap length from δ_F = 14.1 to 25.5 causes reduction in mid frequency components without increasing the low frequency components. Further increase in flap length to δ_F = 51 produces little

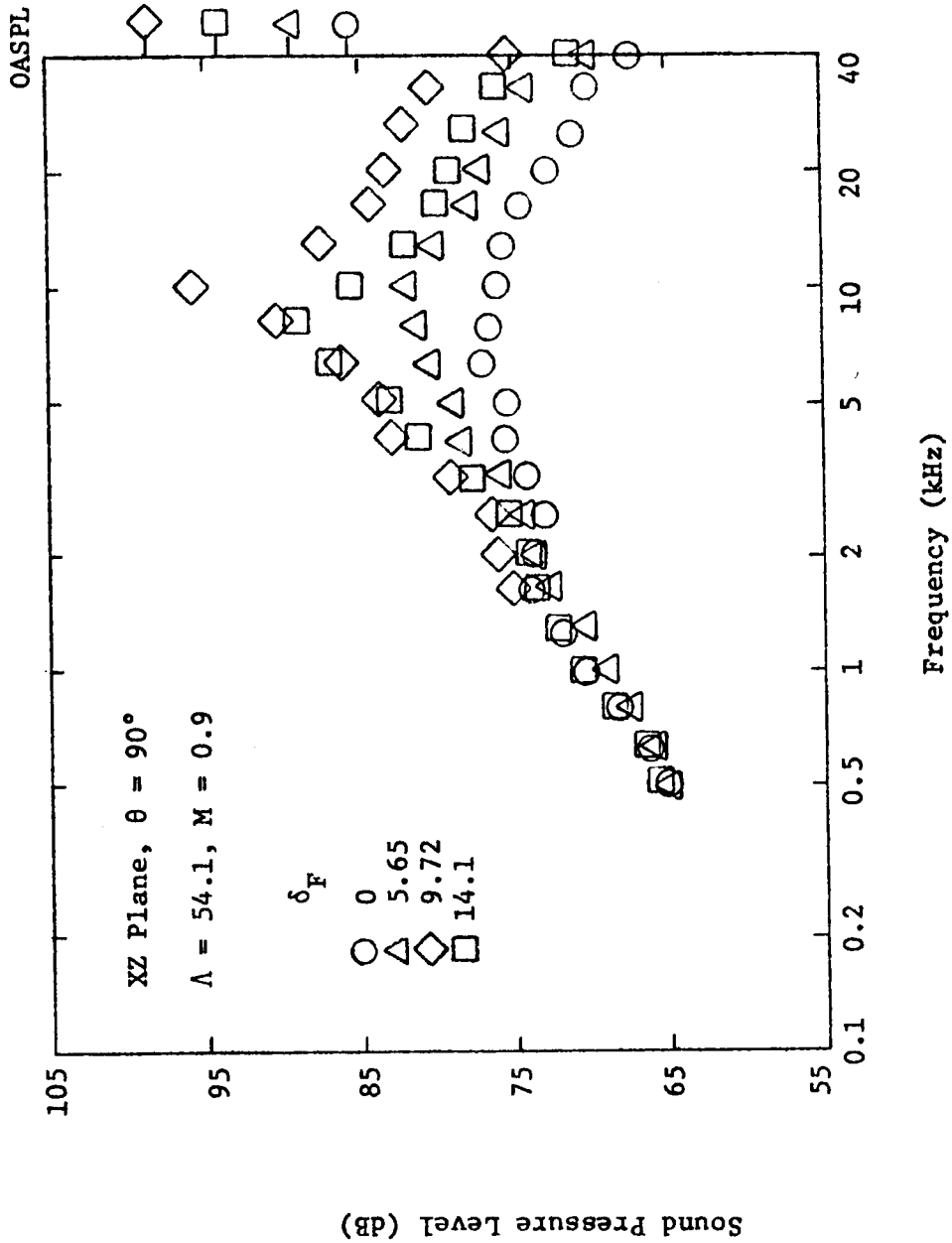


Figure 4.13. Sound pressure spectra at θ = 90° for flaps on 54.1 aspect ratio slot nozzle.

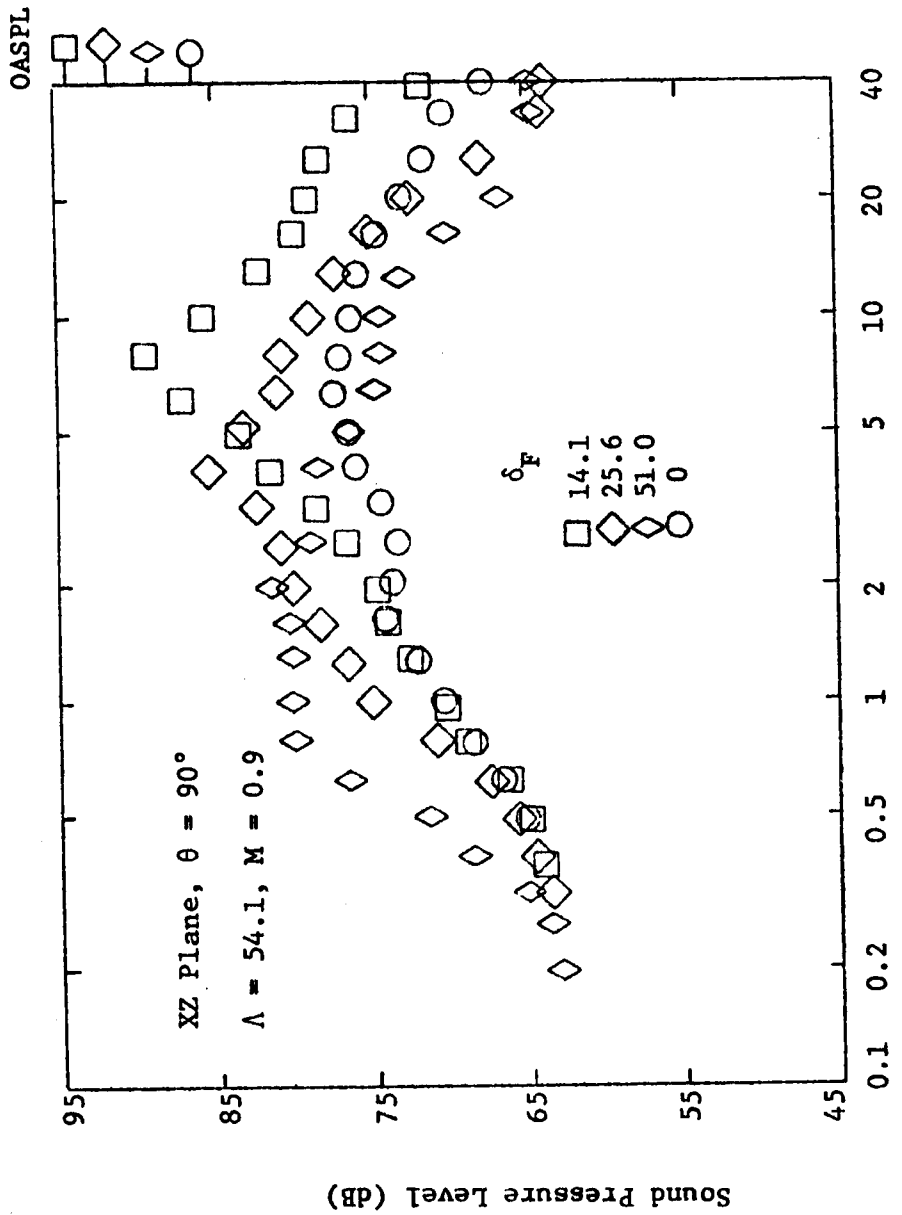


Figure 4.13. continued.

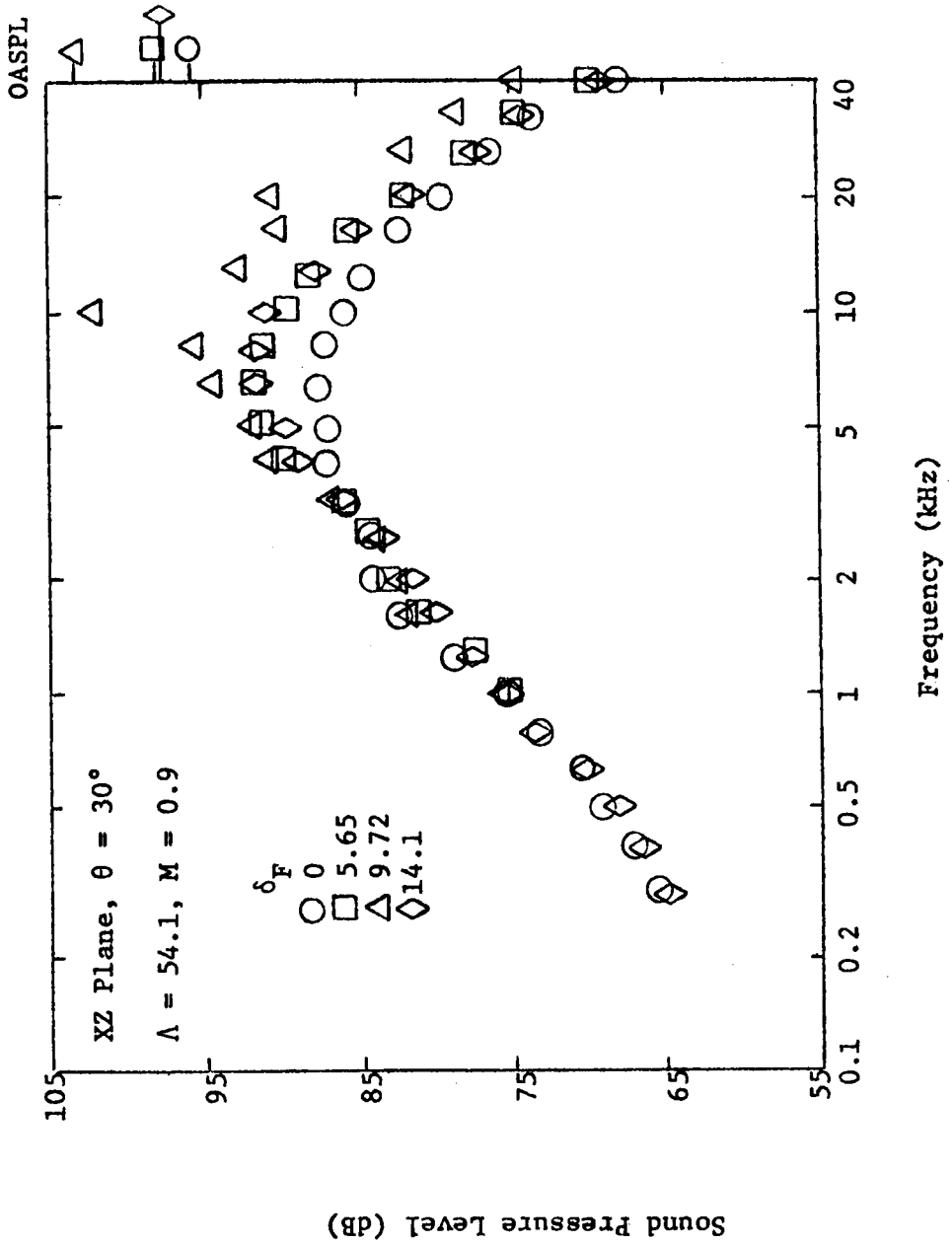


Figure 4.14. Sound pressure spectra at θ = +30° for flaps on the 54.1 aspect ratio slot nozzle.

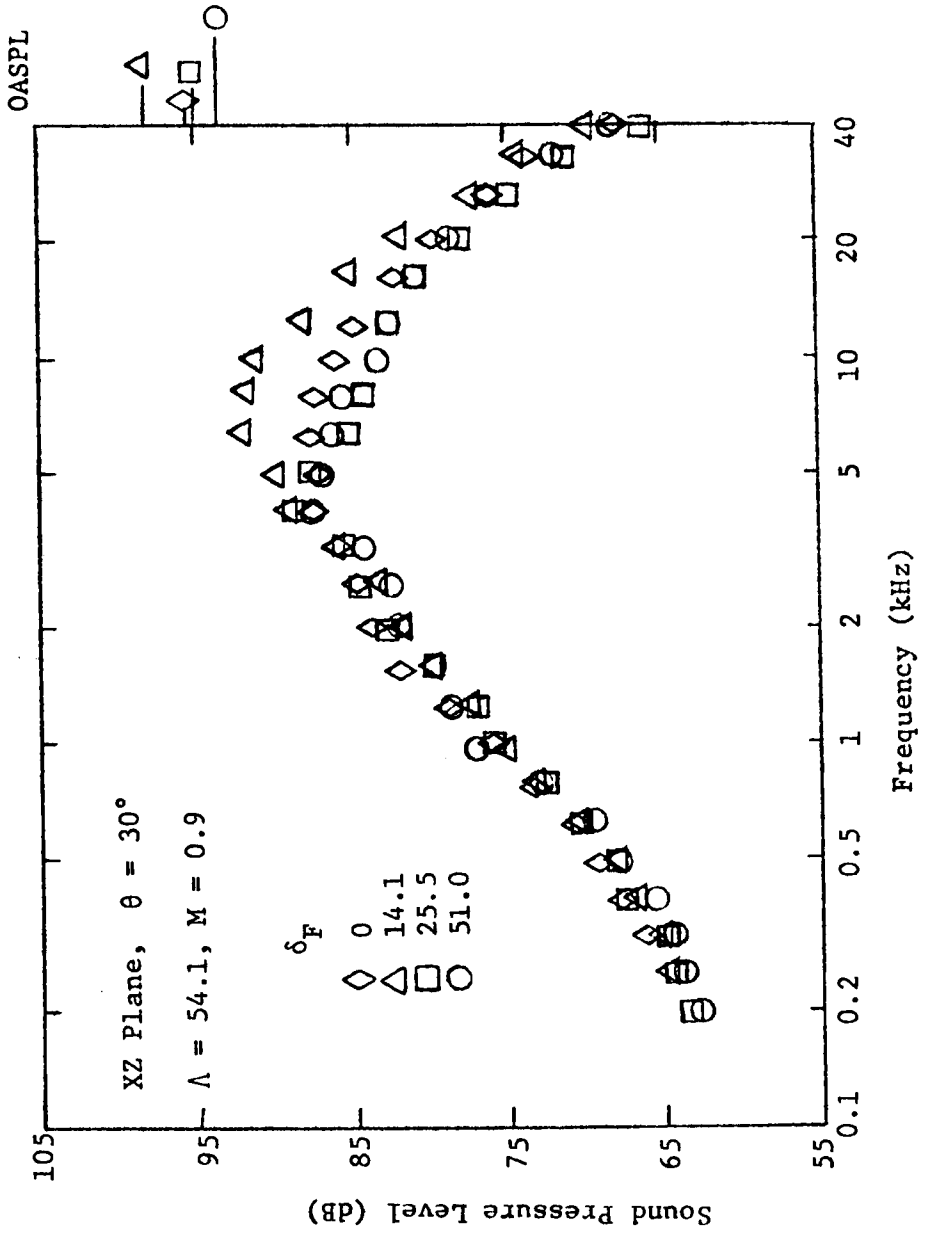


Figure 4.14. continued.

change so that the decrease in peak frequency with increased flap length is slower at 30° than at 90°.

The greater sound radiation in $\theta = -30°$ direction compared to that in $\theta = +30°$ direction is due to increased contribution from high frequency components ($f > 3000$ Hz) for the $\delta_F = 14.1$ jet flap (Figure 4.15). For the jet flap with $\delta_F = 25.5$ this reduction is due to mid frequency components ($1000 < f < 10{,}000$ Hz). Components above 2000 Hz are, however, responsible for the OASPL reduction at $\theta = -30°$ compared to that at $\theta = +30°$ for the jet flap with $\delta_F = 51$ as is evident in the last part of Figure 4.15.

Figure 4.16 brings out the effect of increasing the flap length beyond $\delta_F = 51$ on the OASPL directivity in XZ plane. The effect on overall levels of sound radiated above the flap is weak but OASPLs on the flap underside, especially in directions $\theta < -60°$, are considerably reduced. The longest flap with $\delta_F = 132$ produced a 9 dB reduction in OASPL in -30° direction. These reductions can be seen in Figure 4.17 to be due to large decrease in high frequency noise ($f > 2000$ Hz). Increased flap length at the same time produces low frequency noise, causing the peak frequency of the sound pressure spectrum to shift to lower frequencies. Figure 4.18 reflects the latter effect for the sound radiated in +90° direction. The peak frequency of the sound and its level

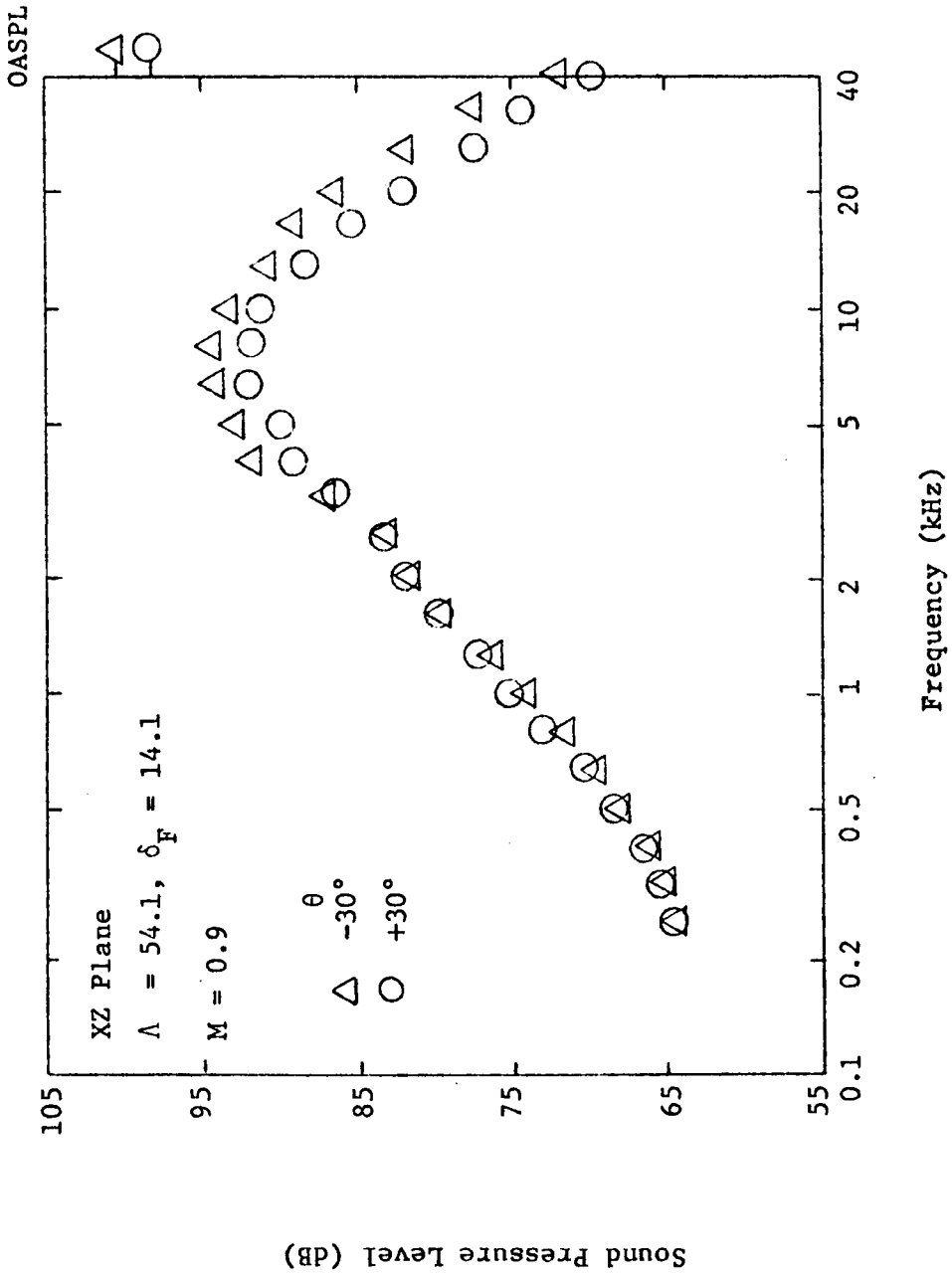


Figure 4.15. Sound pressure spectra at θ = ±30° for flaps on the 54.1 aspect ratio slot jet.

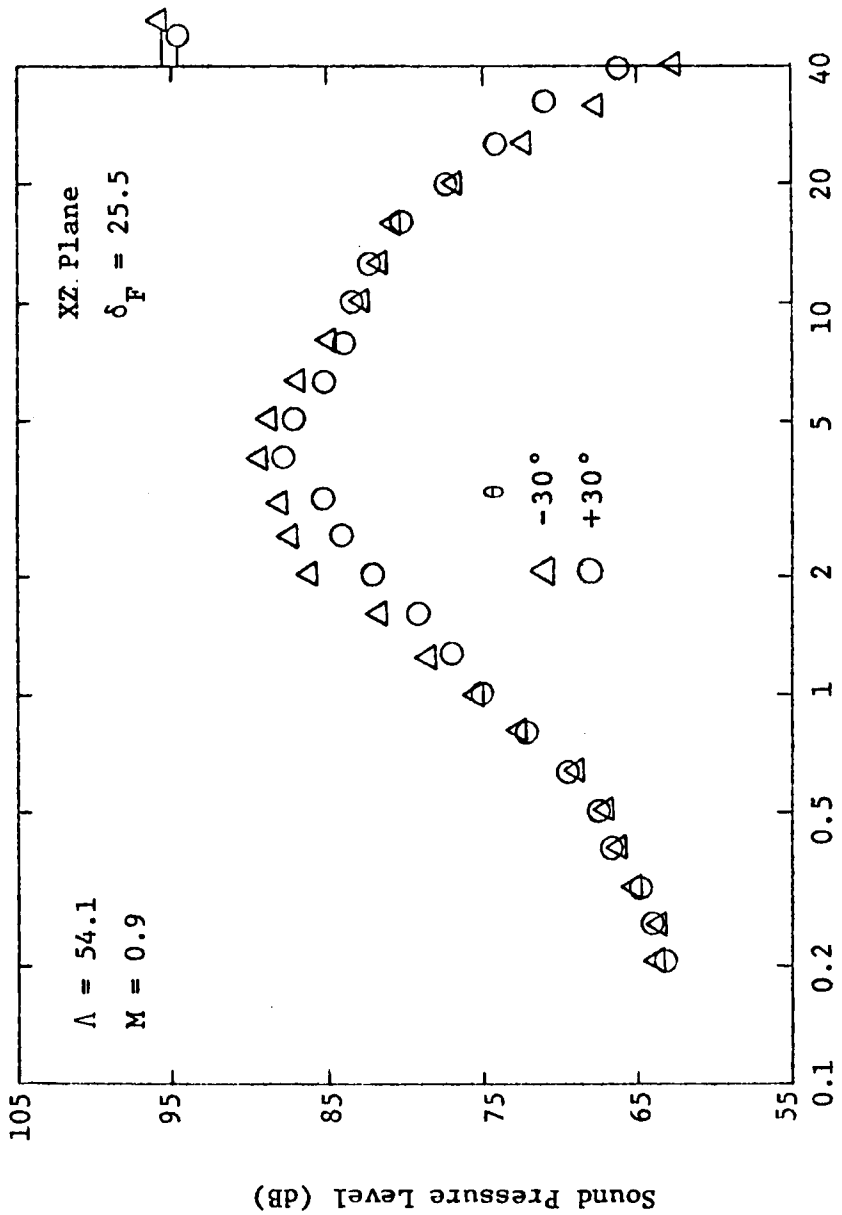


Figure 4.15. continued.

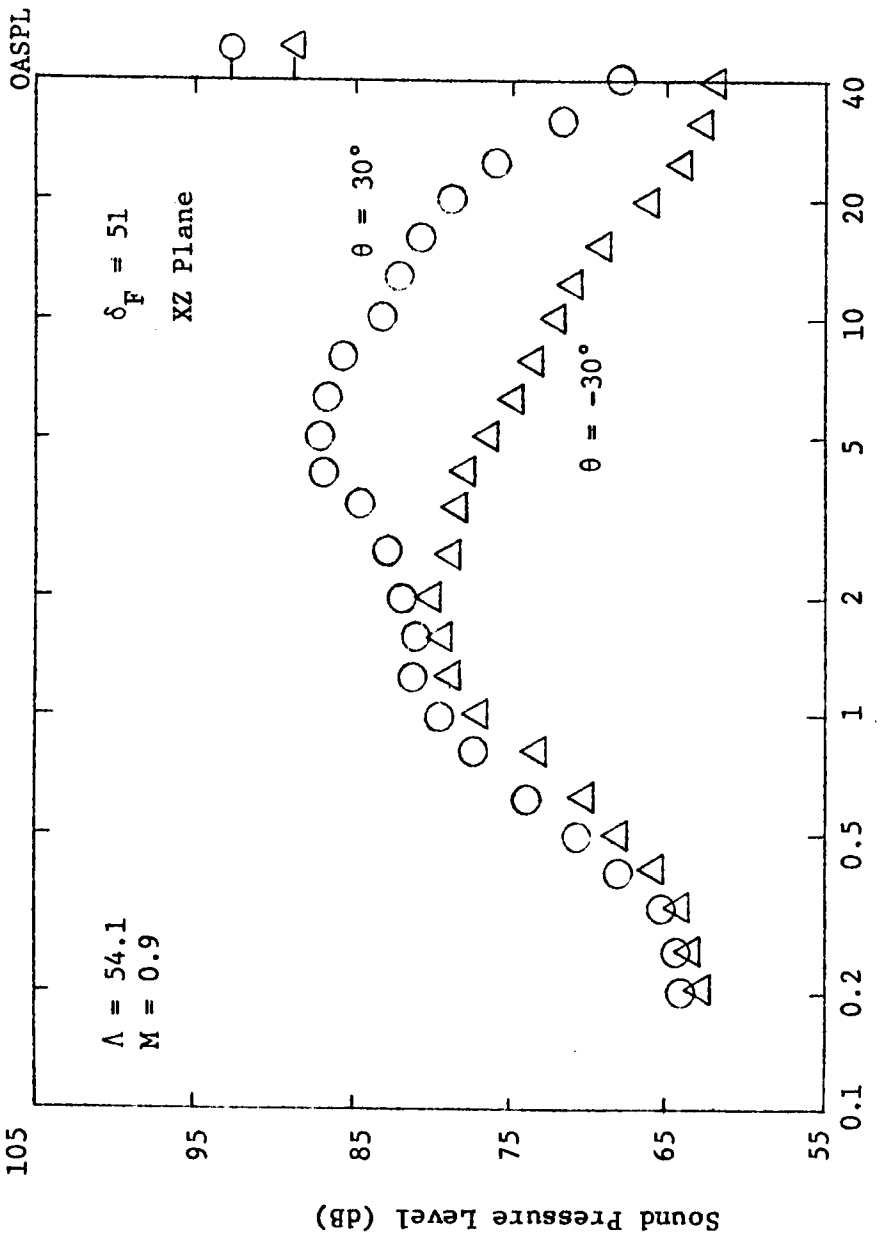


Figure 4.15. continued.

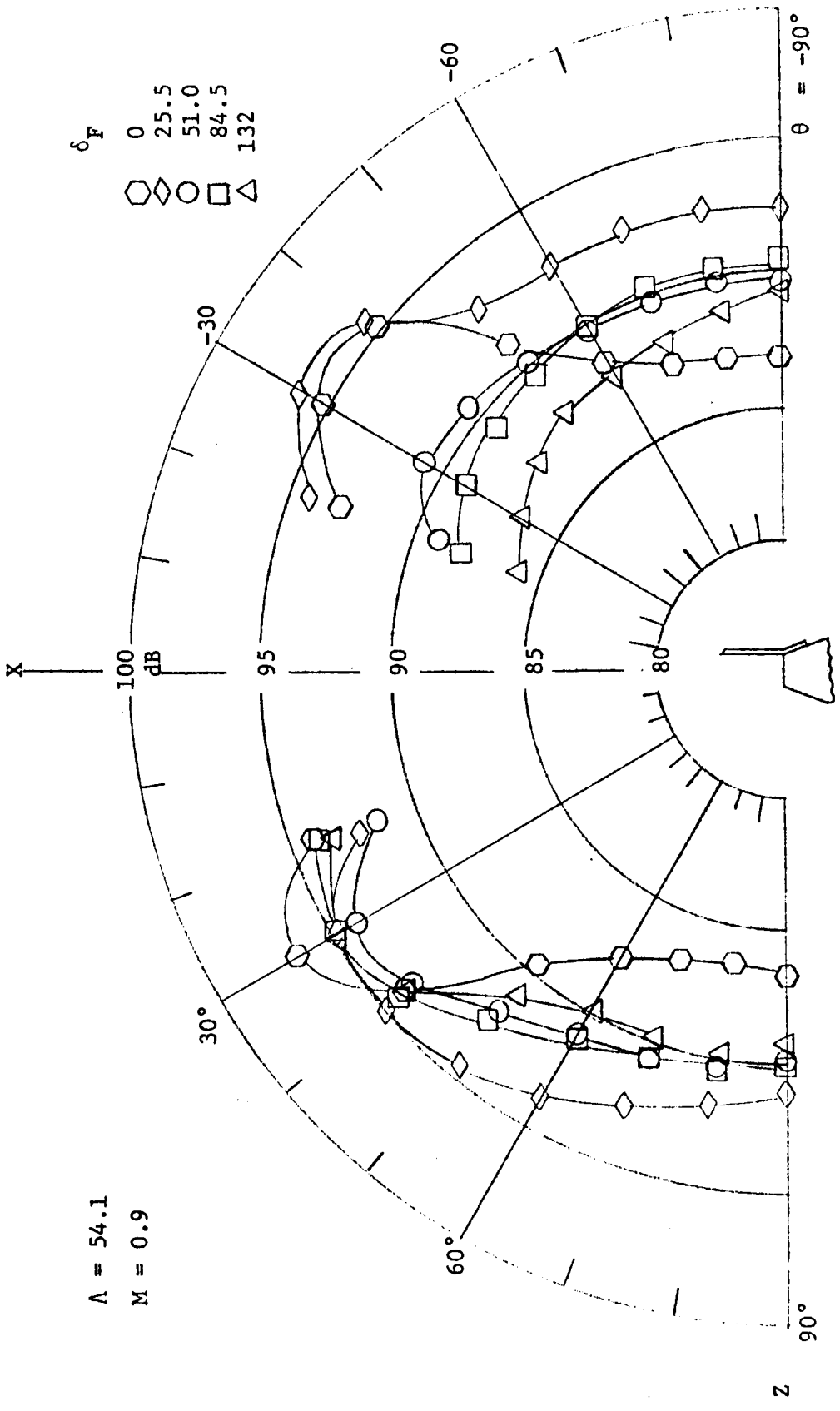


Figure 4.16. OASPL directivities in XZ plane for long flaps.

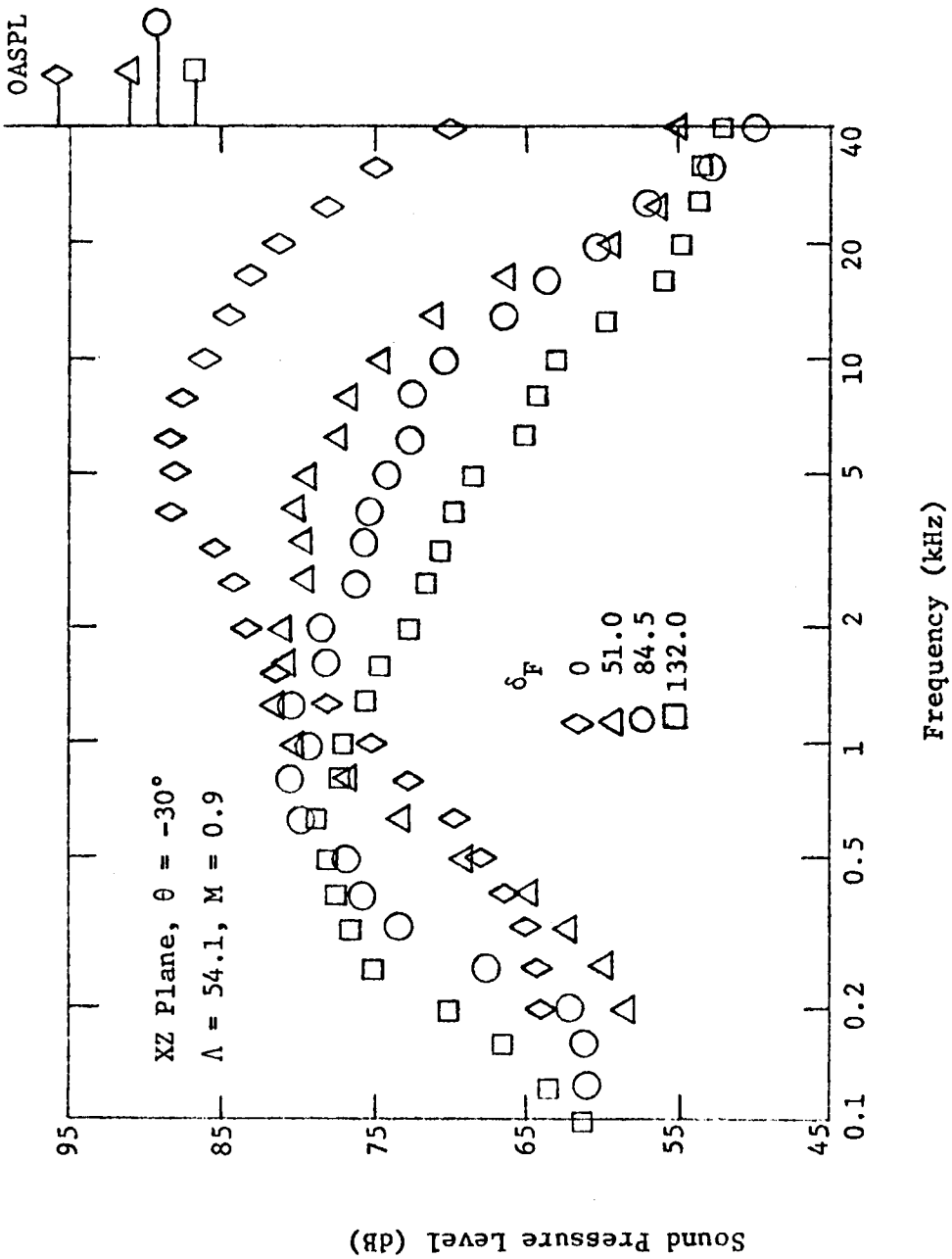


Figure 4.17. Sound pressure spectra at θ = -30° for long flaps.

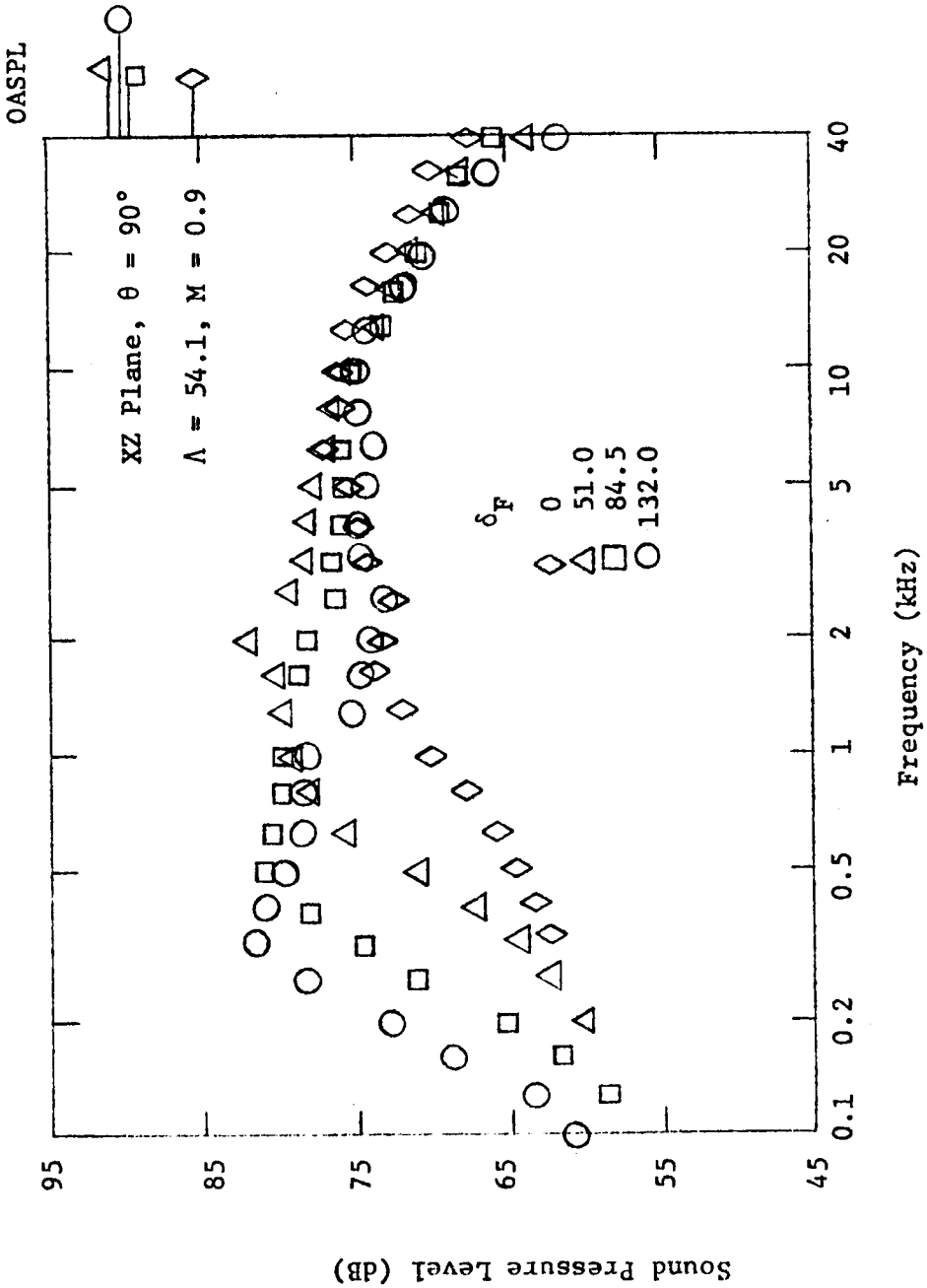


Figure 4.18. Sound pressure spectra for long flaps.

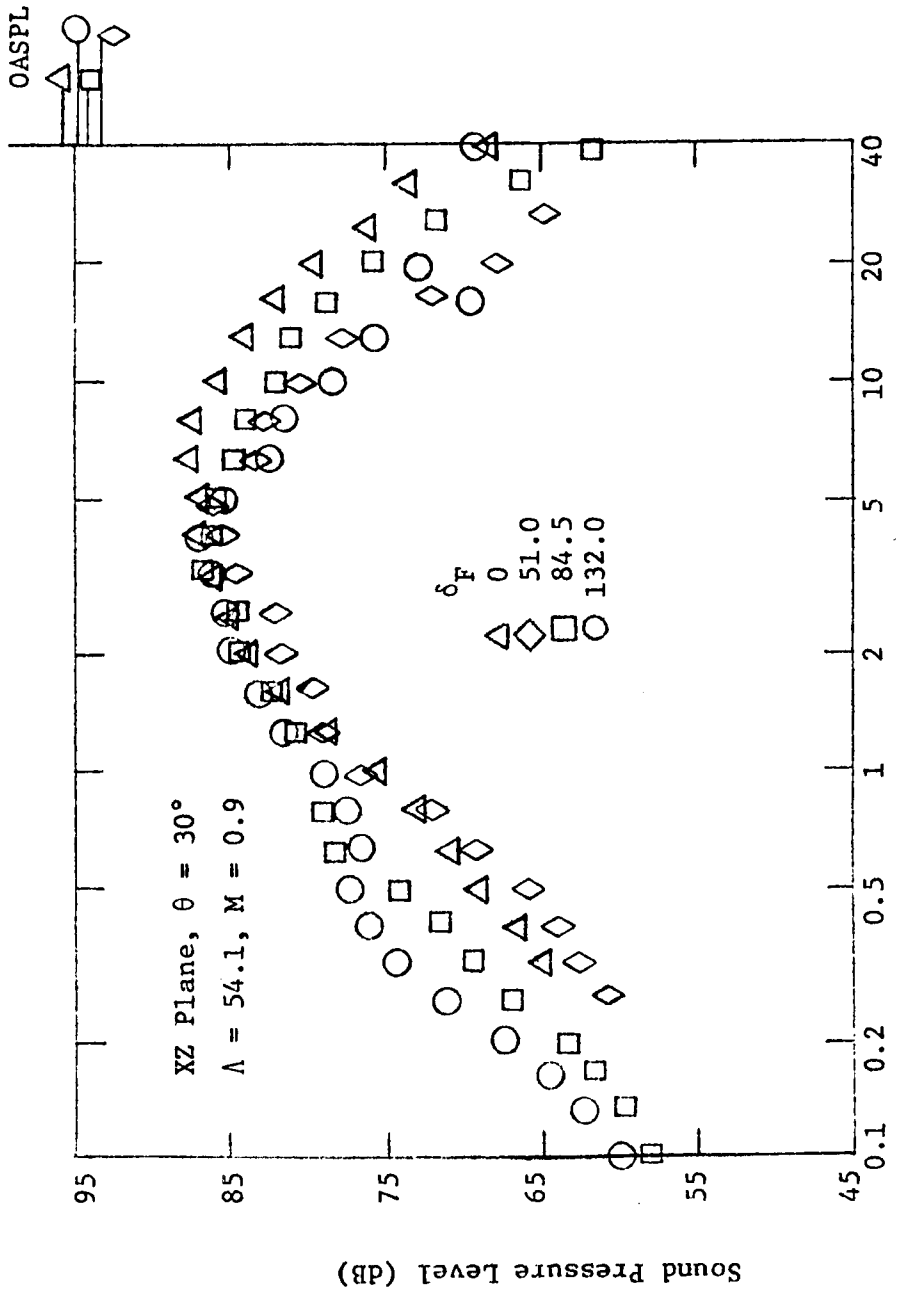


Figure 4.18. continued.

in $\theta = +30°$ direction is, however, insensitive to the change in flap length as is evident from the second part of Figure 4.18. Thus the difference between OASPL at $\theta = +30°$ and $\theta = -30°$ for long flaps is due to reduced contribution to the -30° direction from high frequency components (f > 2000 Hz). This difference increases with increasing flap length. The high frequency reduction on the flap underside is also present in $\theta = 60°$ and 90° directions as shown in Figure 4.19. However, in these directions, the spectral peak being at low frequencies, no reduction in the peak frequency sound level is achieved so that the OASPL value below the flap is not reduced much.

The effect of flap deflection (away from the jet) on the OASPL directivity in the flyover plane is shown in Figure 4.20 for the 5.08 cm long flap on 13.85 and 54.1 aspect ratio slot nozzles. The general effect is to reduce the sound levels in the plane and cause a rotation of the directivity. Rotation of directivity is especially evident in the occurrence in the plane of the peak OASPL. For example, the jet flap with $\delta_F = 14.1$ and no deflection has a peak in the directivity polar at about +40°. The polar peak shifts to about +37° when the flap is deflected down by 3° and to about +30° when the flap deflection is increased to 10°. Similar rotation of directivity is also seen in the case of jet flap with $\delta_F = 7.12$ on the

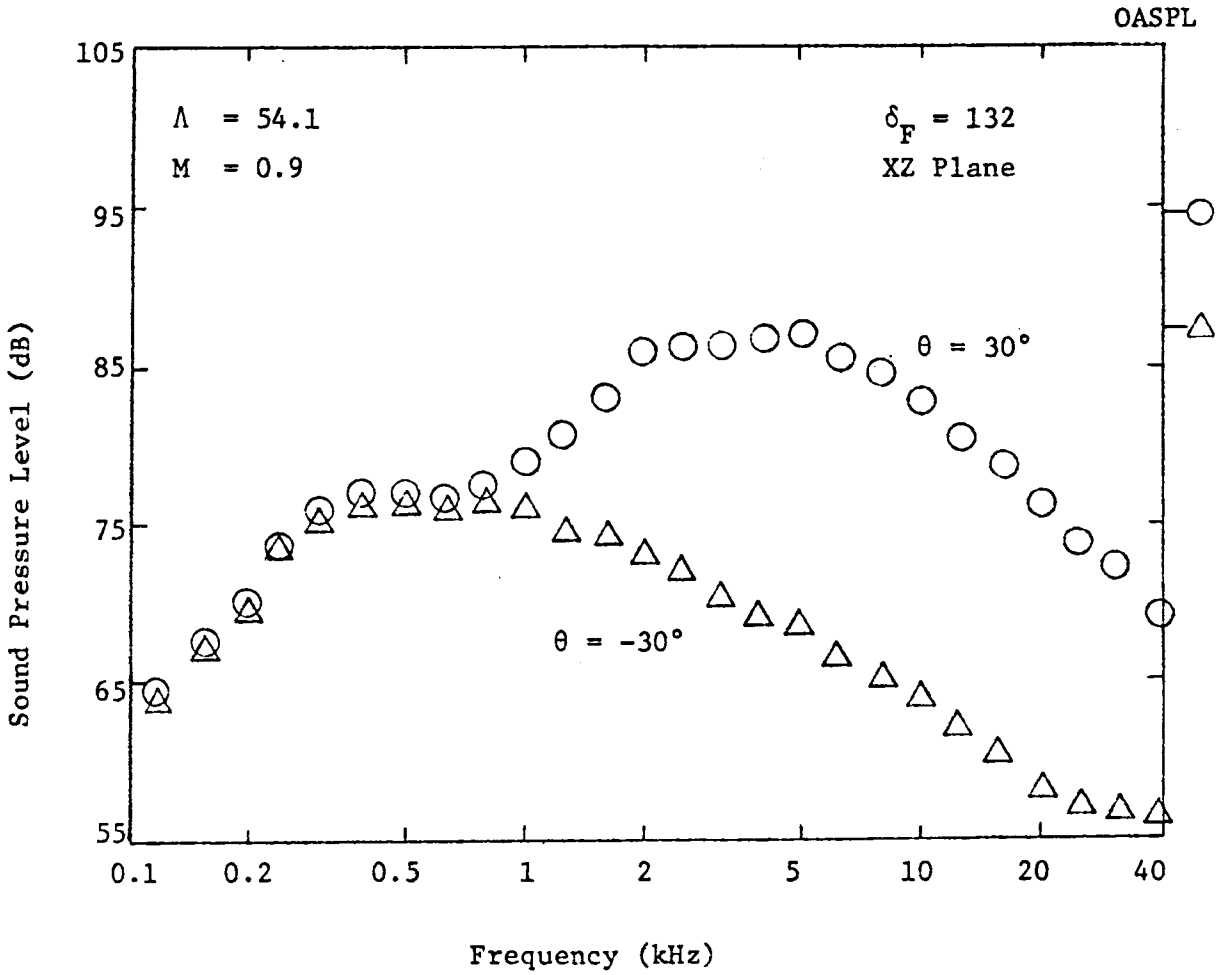


Figure 4.19. Shielding effect of long flaps.

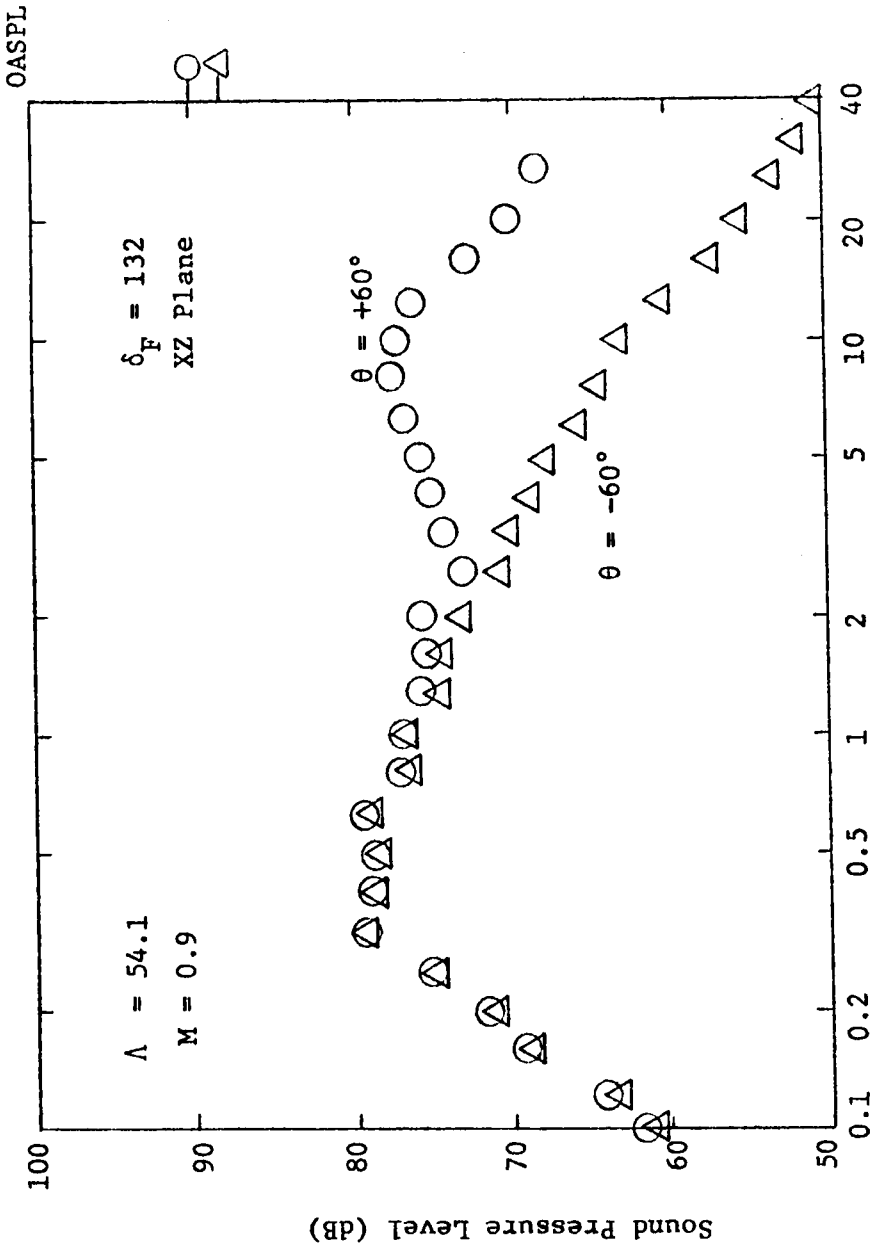


Figure 4.19. continued.

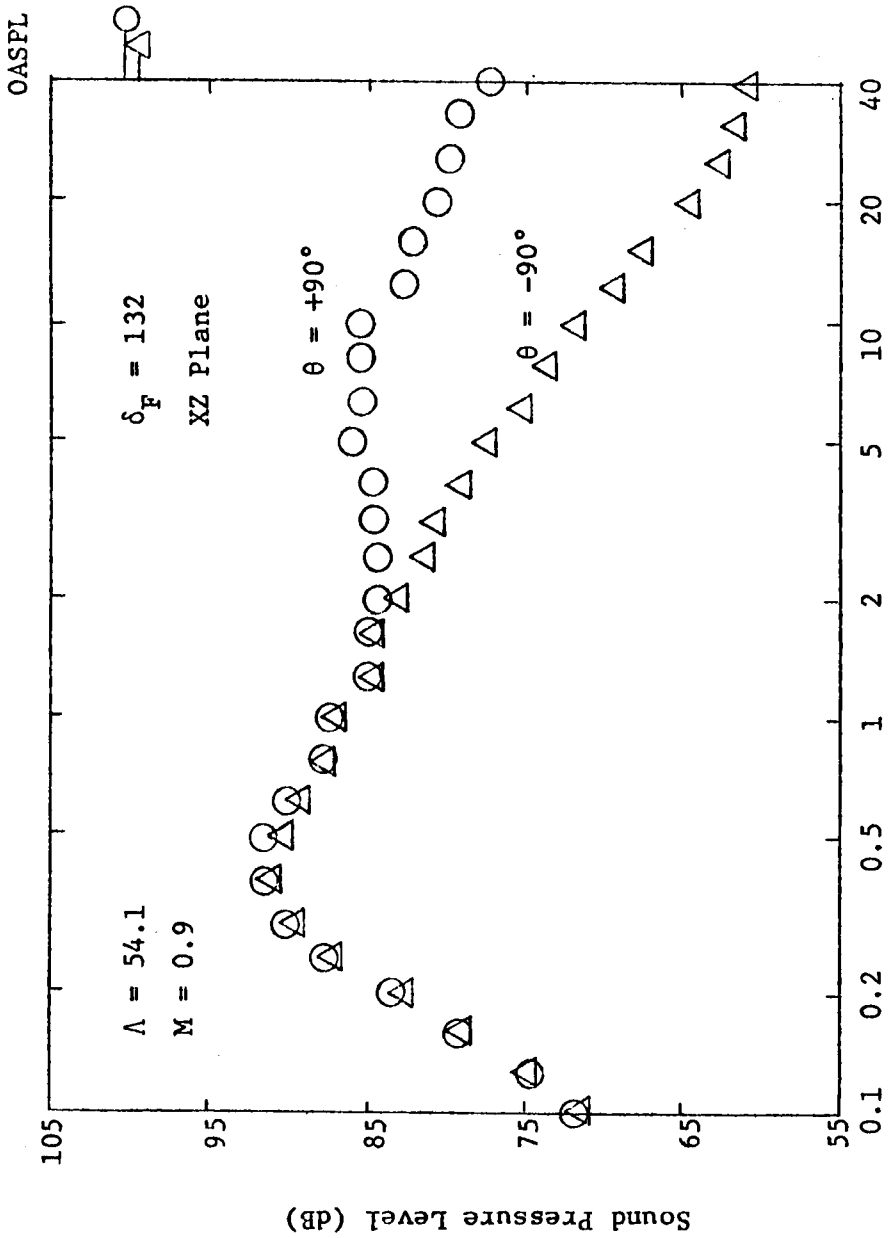


Figure 4.19. continued.

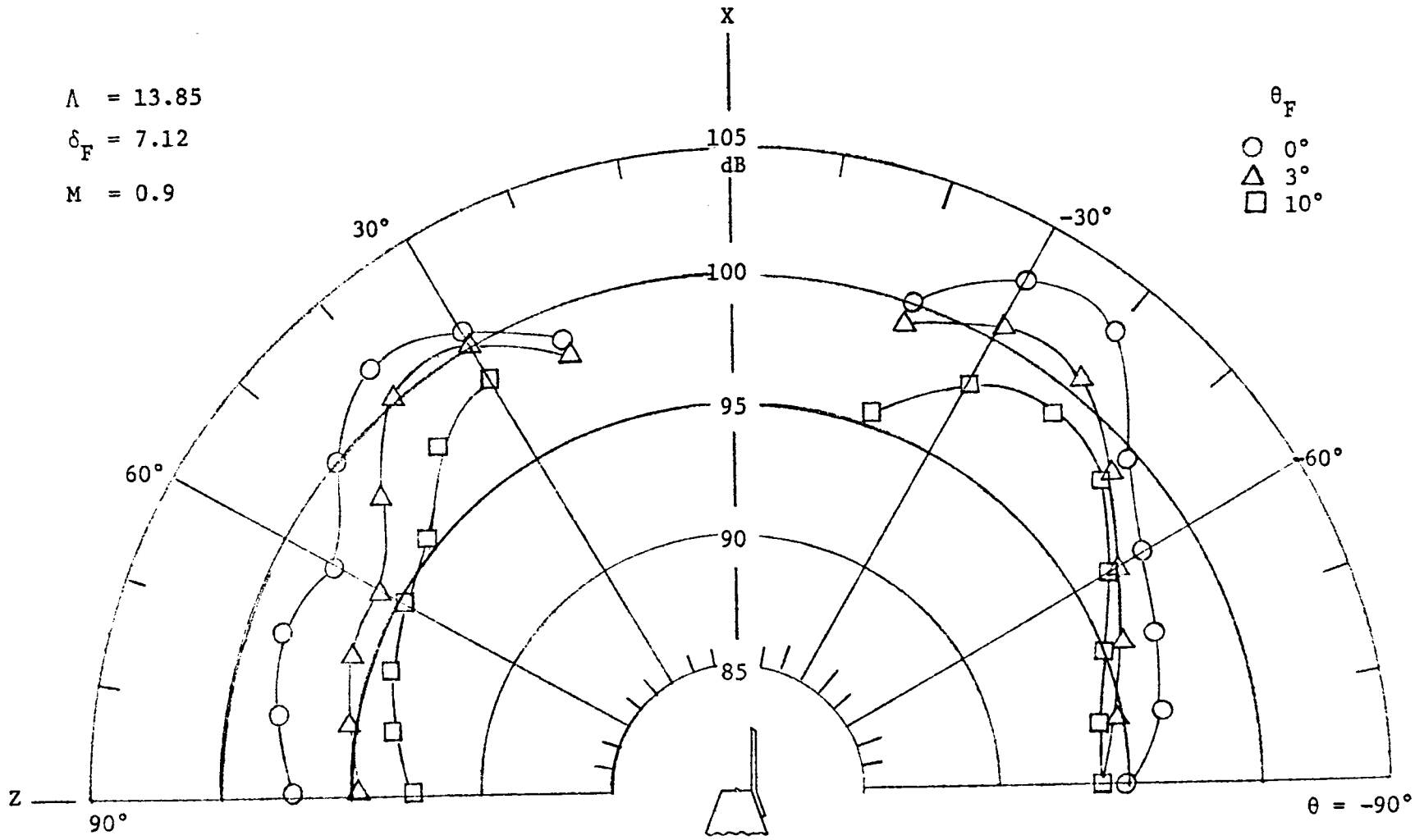


Figure 4.20. OASPL directivities in XZ plane for deflected flaps.

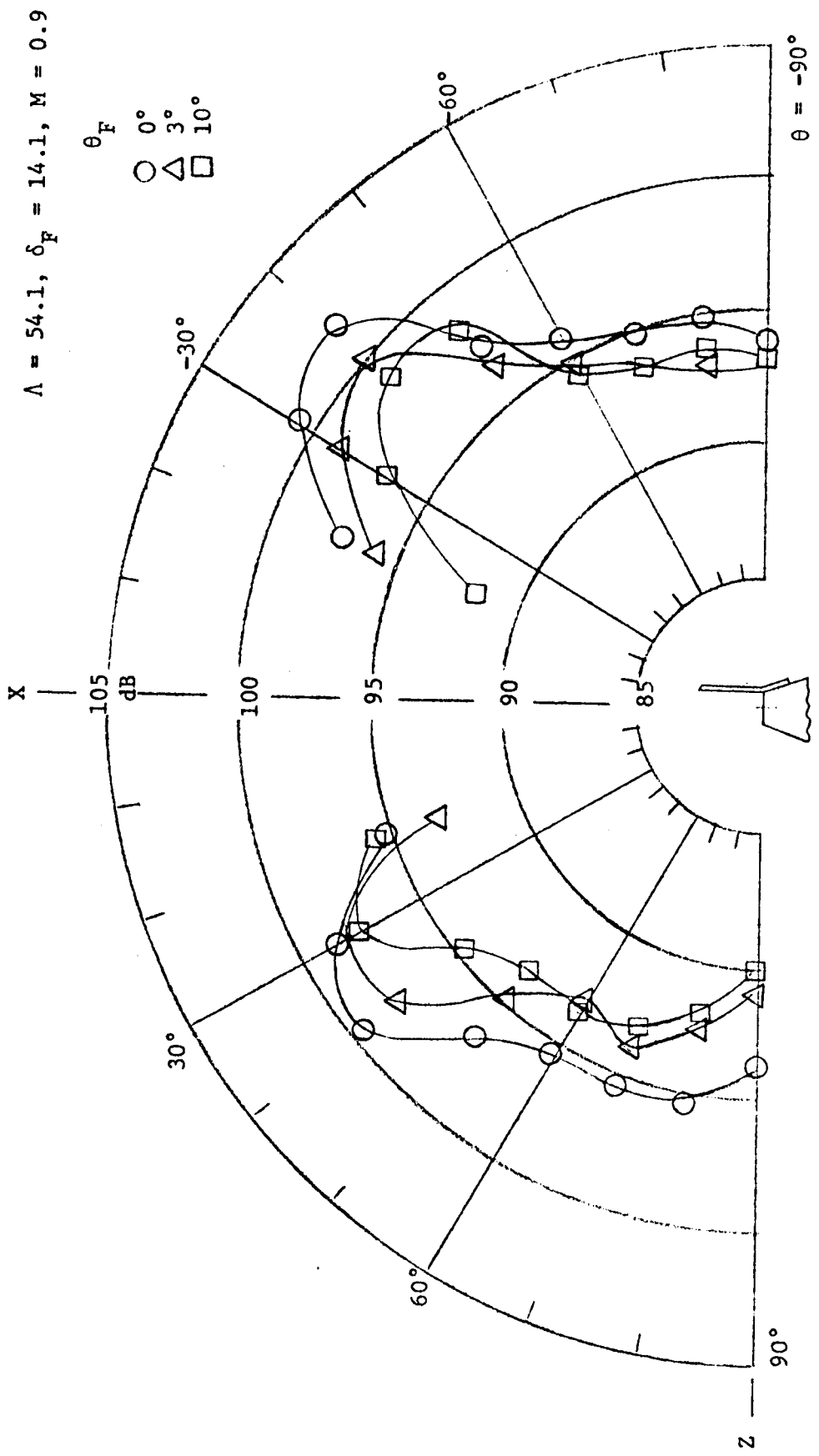


Figure 4.20. continued.

13.85 aspect ratio slot jet. The reduction in sound level due to flap deflection results from reduction in high frequency components as can be observed in Figure 4.21. Flap deflection of 10° also eliminates the discrete frequency tone at 5000 Hz that was present in the far field sound radiation in $\theta = 90°$ direction for the jet flap with $\delta_F = 7.12$.

OASPL DIRECTIVITIES AND SOUND PRESSURE SPECTRA IN SIDELINE PLANE

Overall sound pressure level data in the sideline (XY) plane for the three slot jets and jet flaps of various flap lengths are presented in Figure 4.22. Symmetry of the flow geometry in the XY plane about the X axis led to symmetric directivity patterns. OASPL measurements in one quadrant of the plane only are shown. The effect of increasing flap length is to increase the OASPL in the plane until a flap length that produced maximum sound levels in the flyover (XZ) plane is reached. Further increase in flap length caused only reduction in the sound pressure levels in the XY plane. There are, however, three major differences in the effects of flap length on the OASPL distributions in the XZ and XY planes. First, the increase in sound levels in XY plane is much smaller than the increase in XZ plane for a given flap length. Second, the increase in OASPL in XZ plane due to a flap is

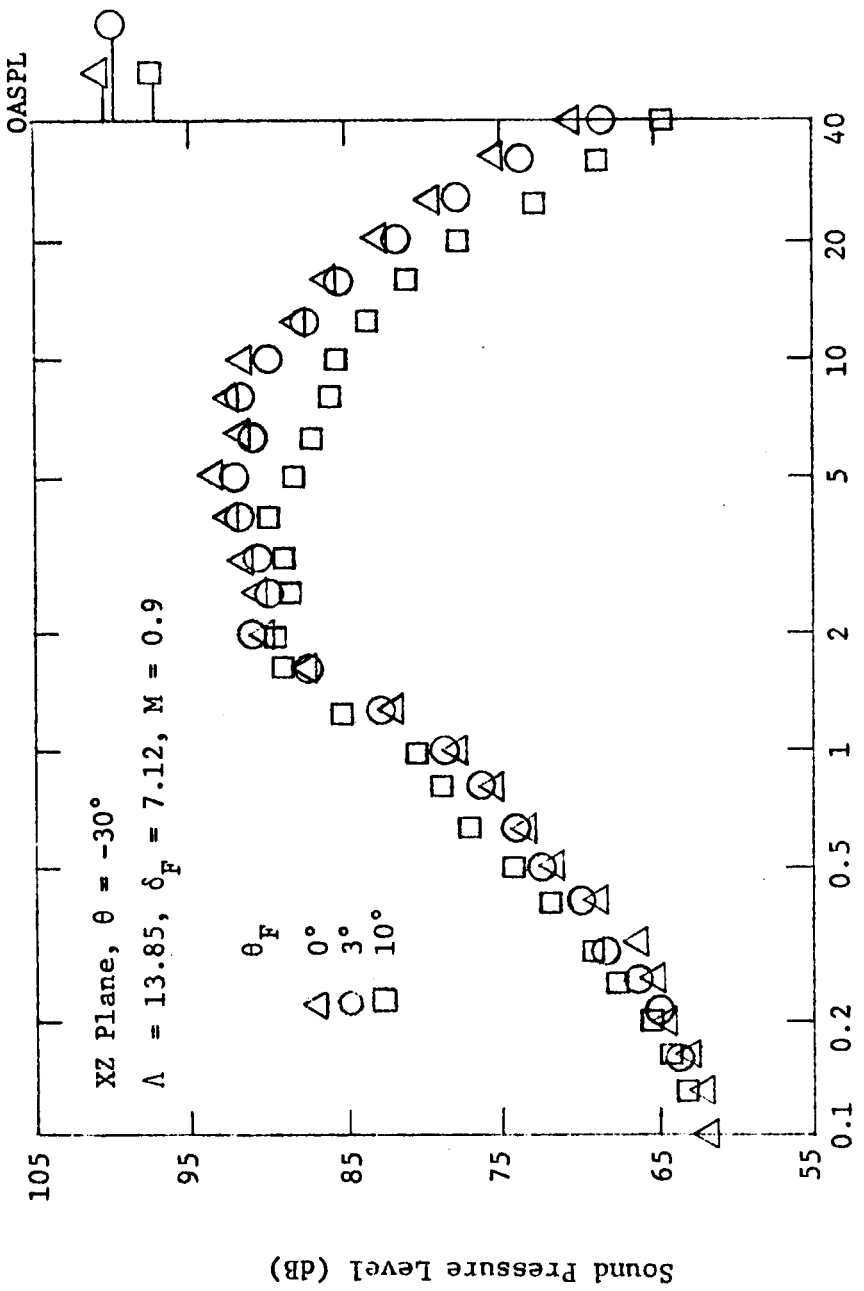


Figure 4.21. Sound pressure spectra for δ_F = 7.12 flap at various deflections.

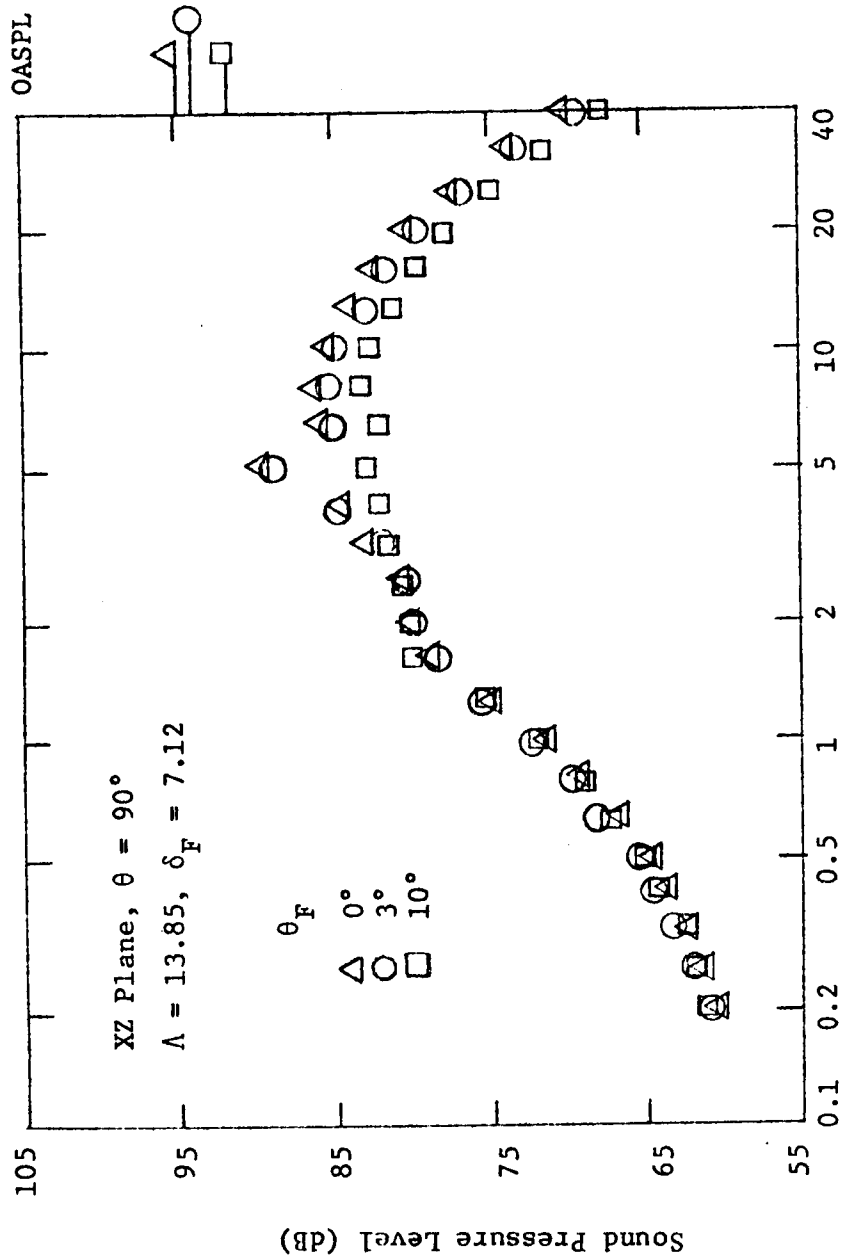


Figure 4.21. continued.

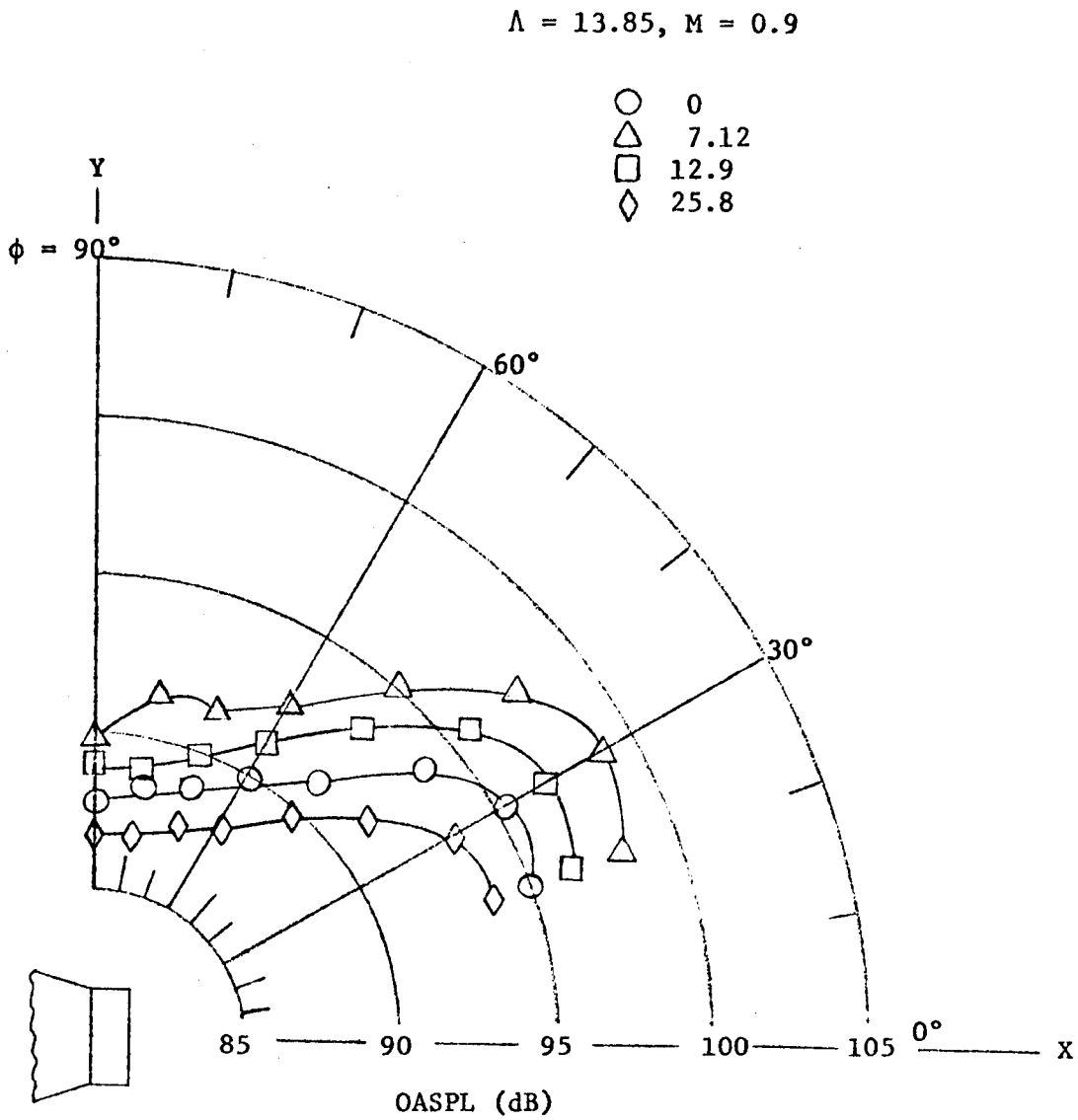


Figure 4.22. OASPL directivities of flaps in XY plane.

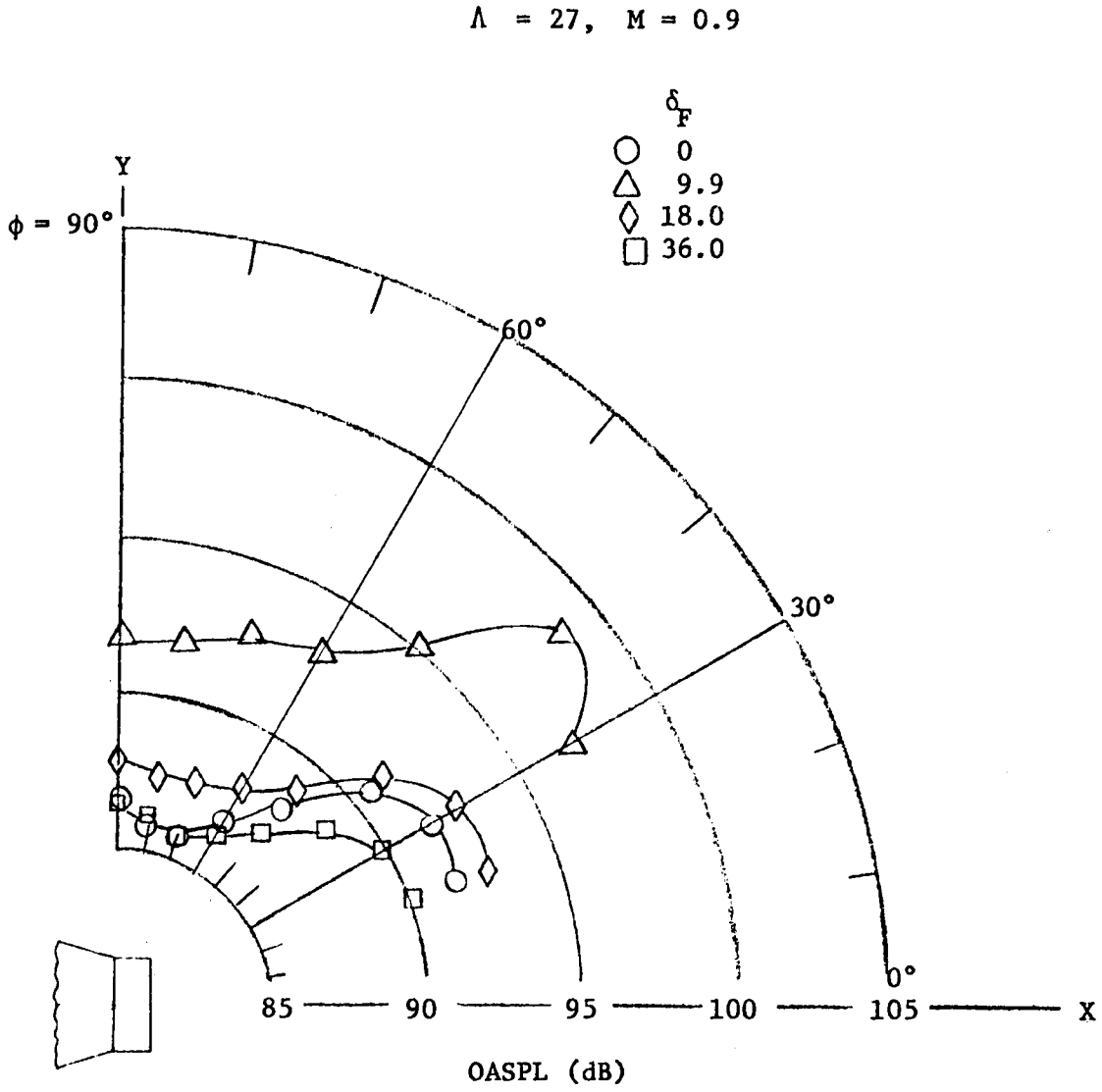


Figure 4.22. continued.

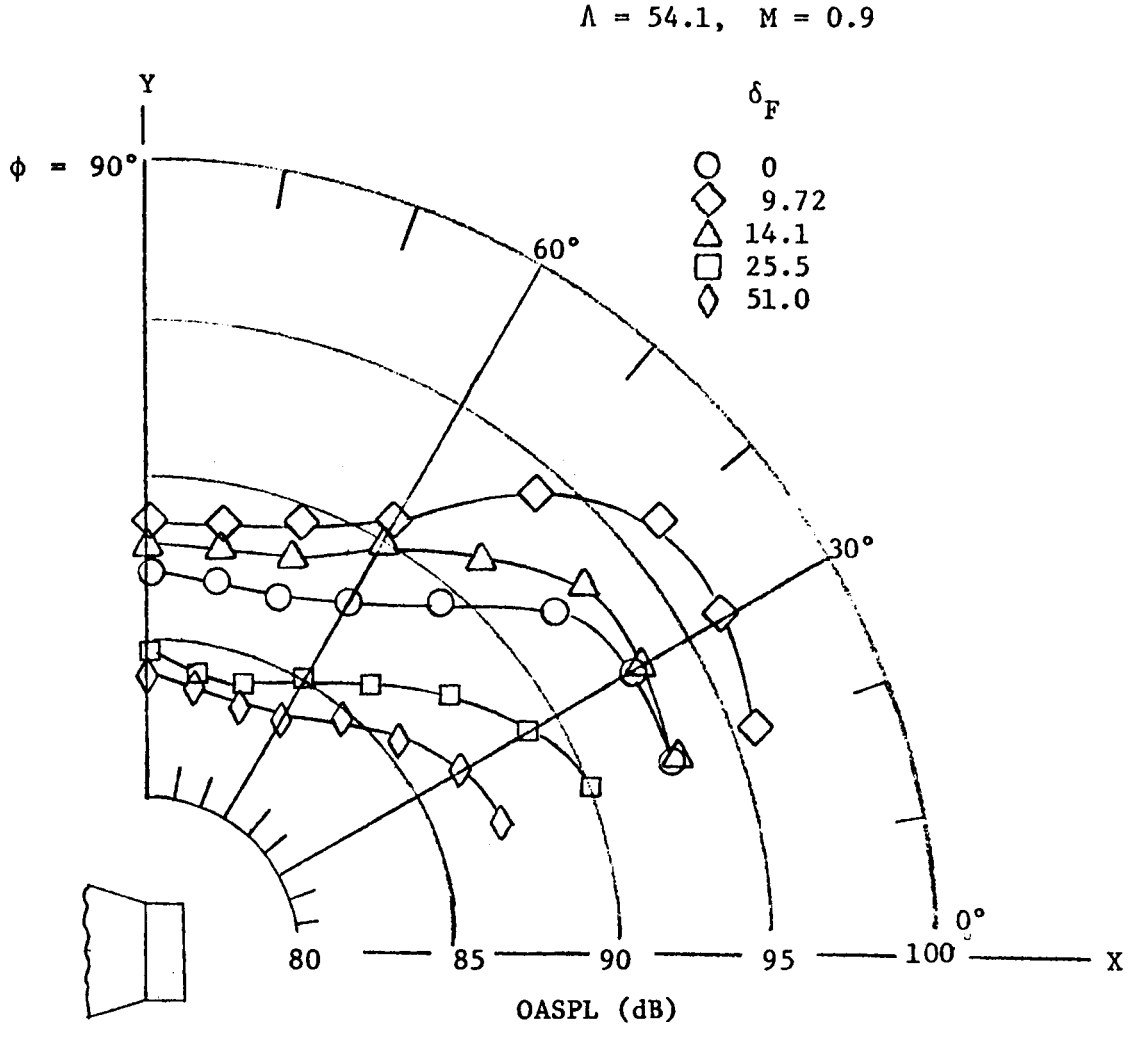


Figure 4.22. continued.

considerably larger at 90° to the flow axis than in the peak radiation direction ($\theta \sim 30°$ to 40°). In XY plane, however, OASPL increase due to a flap is slightly larger in the peak radiation direction than in $\phi = 90°$ direction. Finally, jet flaps with $\delta_F = 25$ or more produce sound levels in entire XY plane that are less than those produced by corresponding slot jets without flap. In XZ plane these long flaps are capable of reducing the sound level to values less than those of the slot jets only in the sector $\theta < -50°$ on the underside of the flap. These differences become apparent when the directivities of Figure 4.22 are compared with those in Figures 4.1, 4.8, and 4.12 (pages 44, 58 and 64 respectively). With the 13.85 aspect ratio slot jet, for example, the flap with $\delta_F = 7.12$ increases the OASPL by 10 dB and 5 dB in $\theta = +90°$ and +30° directions (in XZ plane) respectively but only by 2 dB and 4 dB respectively in $\phi = 90°$ and 30° directions (in XY plane). The OASPL of the jet flap with $\delta_F = 25.8$ is lower than the slot jet OASPL by more than 2 dB in $\phi = 30°$ direction and by 1 dB in $\phi = 90°$ direction. Higher reductions in OASPL in XY plane are achieved by further increase in δ_F. This is evident in the XY directivity patterns for the 54.1 aspect ratio slot jet and jet flaps.

That the reduced OASPL of long flaps is due to decrease in the levels of mid and high frequency components

is obvious from Figure 4.23. This spectral comparison is typical of all directions in the XY plane. Figure 4.24 shows spectra at 90°, 60° and 30° to the flow axis in the XY and XZ planes. These figures represent comparison of sound pressure spectra at flyover and sideline points in the nozzle exit plane and two parallel planes further downstream. The 90° comparison shows a low and mid frequency reduction in XY plane, the 30° comparison shows a mid and high frequency reduction and the 60° comparison shows a broad-band reduction.

OASPL DIRECTIVITIES AND SOUND PRESSURE SPECTRA IN YZ PLANE

Figure 4.25 shows the OASPL directivity in the nozzle exit plane for slot jets of aspect ratios 27 and 54.1 and jet flaps of various lengths. The slot jets without the flap have fairly symmetric directivities, and so does the shortest jet flap. However, when the flap length is increased to $\delta_F = 9.9$ sound pressure levels increase by 17 dB in the normal direction ($\psi = 90°$) above the flap but by 2.5 dB only in the sideline direction ($\psi = 0°$) with intermediate increases in other directions. In addition to the peak level in the 90° direction a relative peak appears in the directivity in $\psi = +60°$ direction. This observation is important since for the jet flap with $\delta_F = 9.72$ on the 54.1 aspect ratio slot nozzle

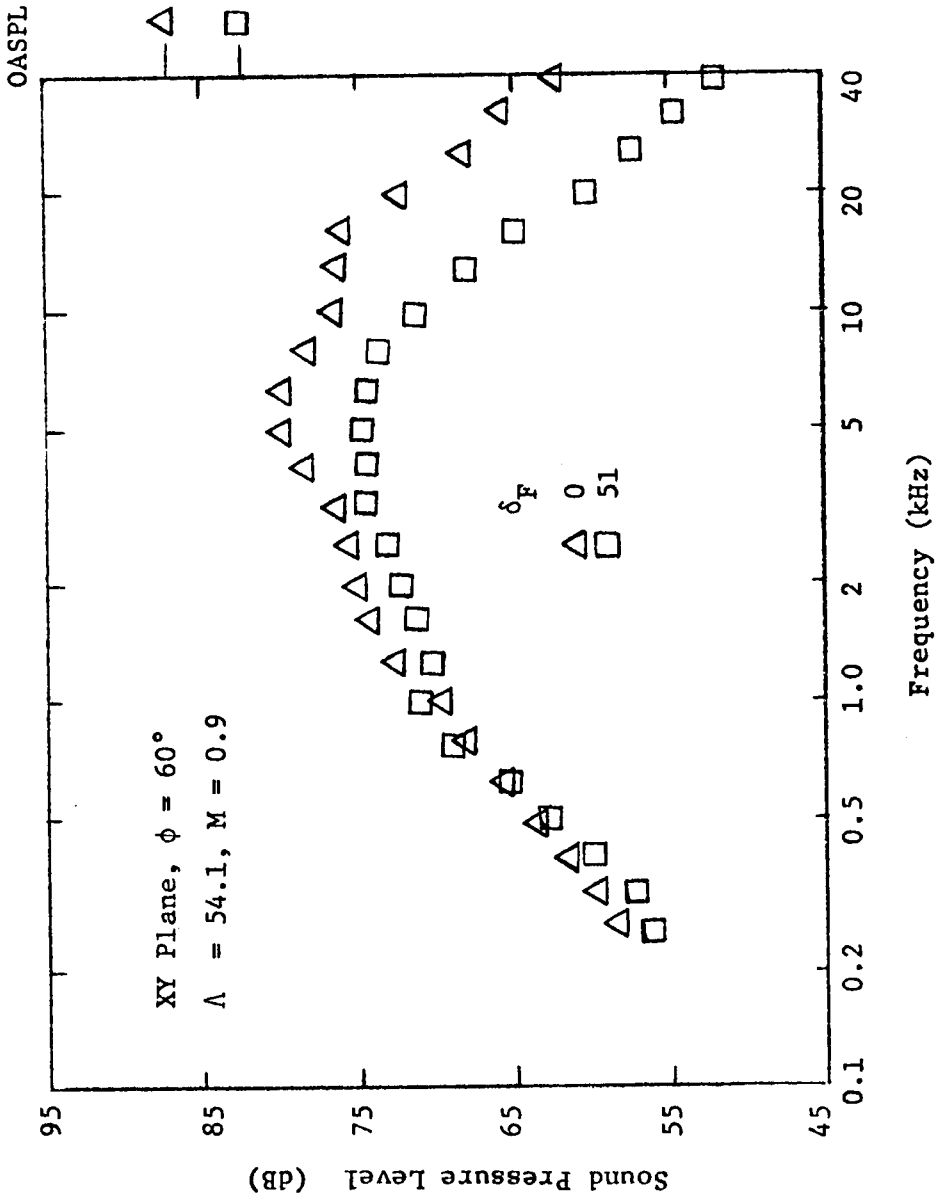


Figure 4.23. Sideline noise reduction of a long flap.

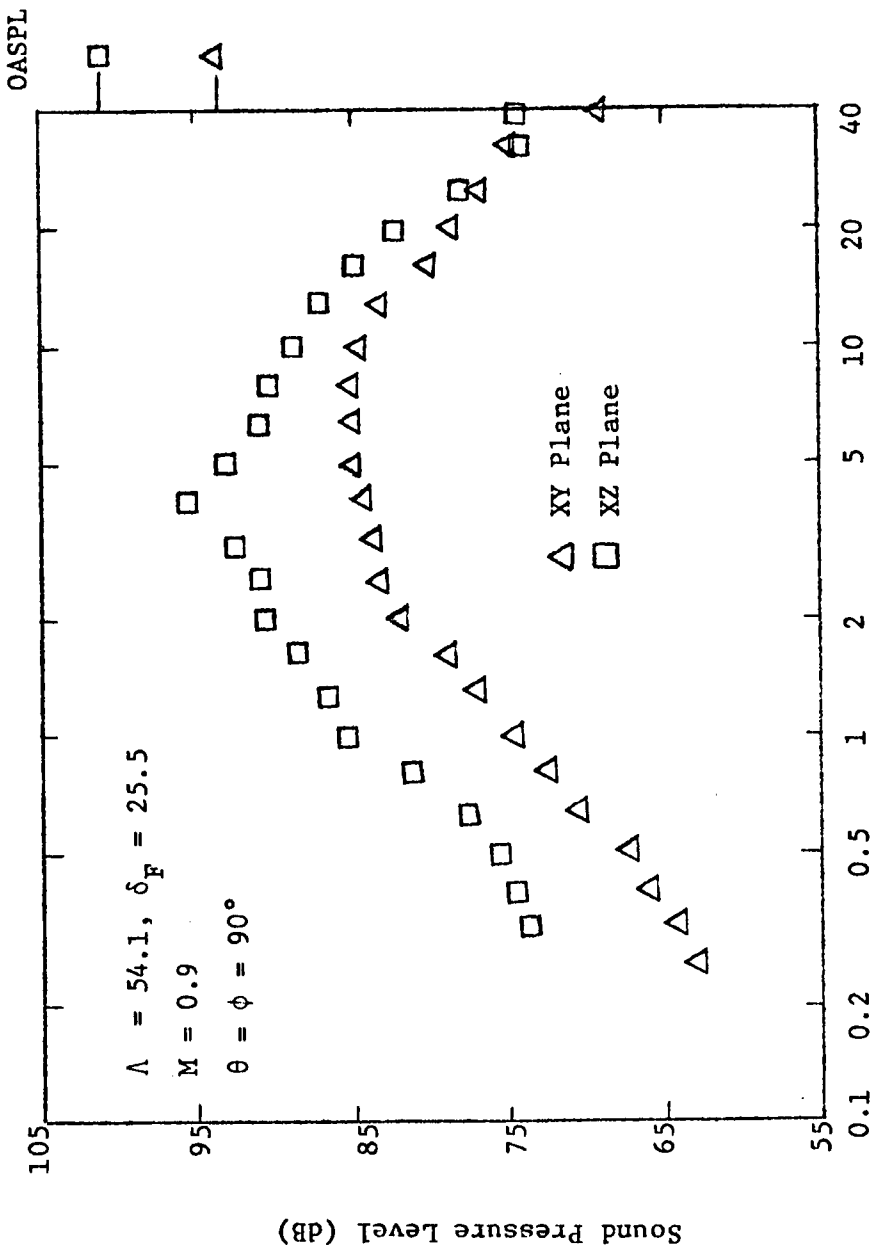


Figure 4.24. Sound spectra in XY and XZ planes for δ_F = 25.5 flap.

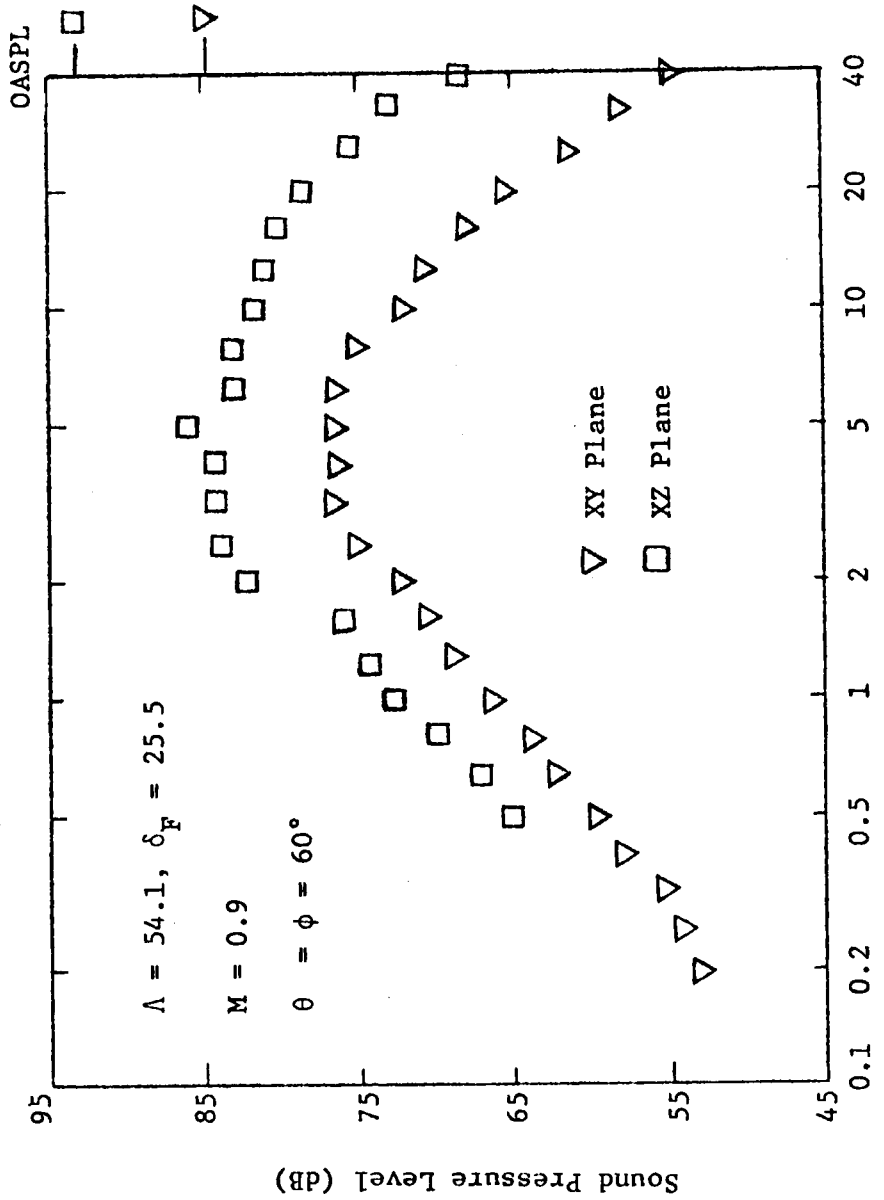


Figure 4.24. continued.

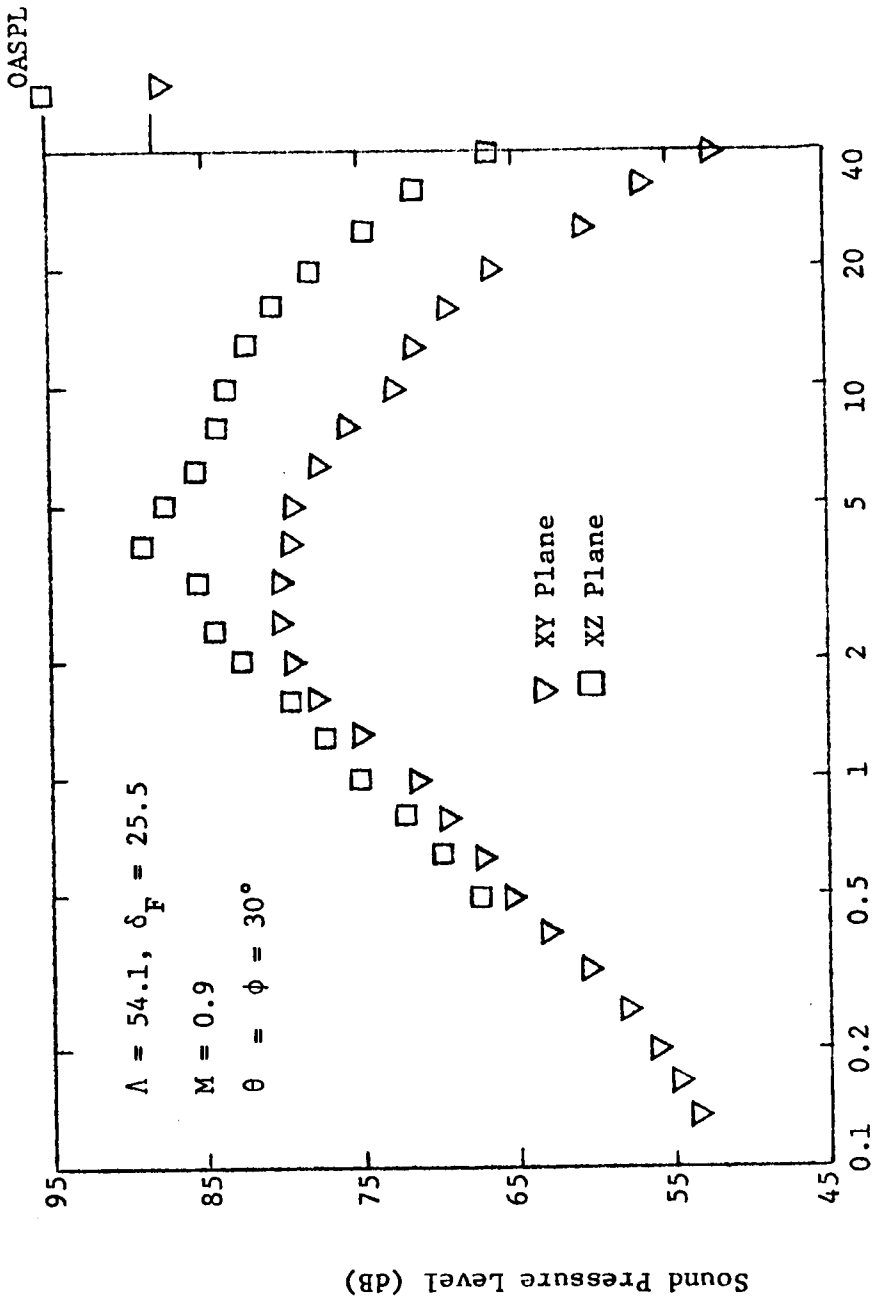


Figure 4.24. continued.

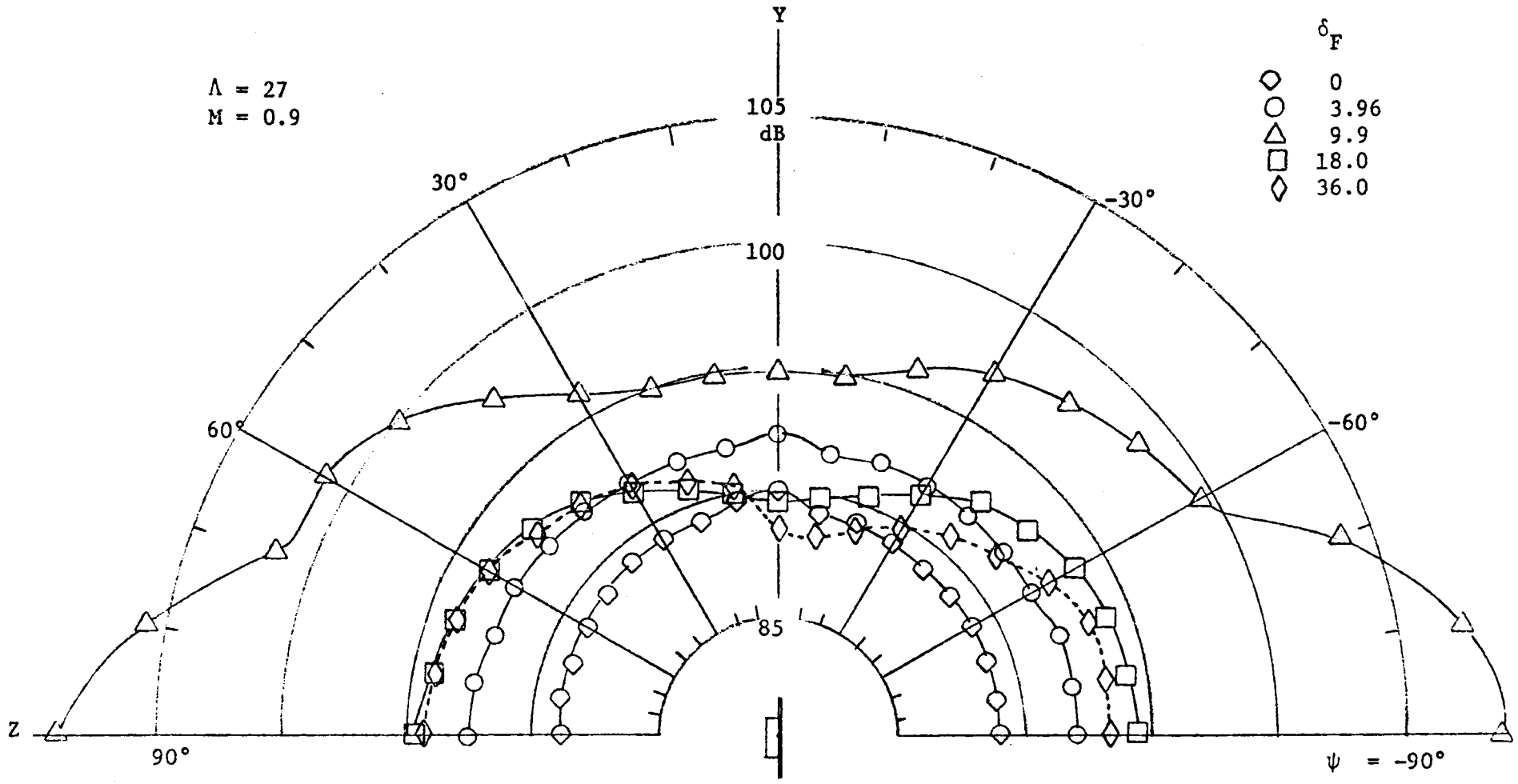


Figure 4.25. OASPL directivities in YZ plane for jet flaps.

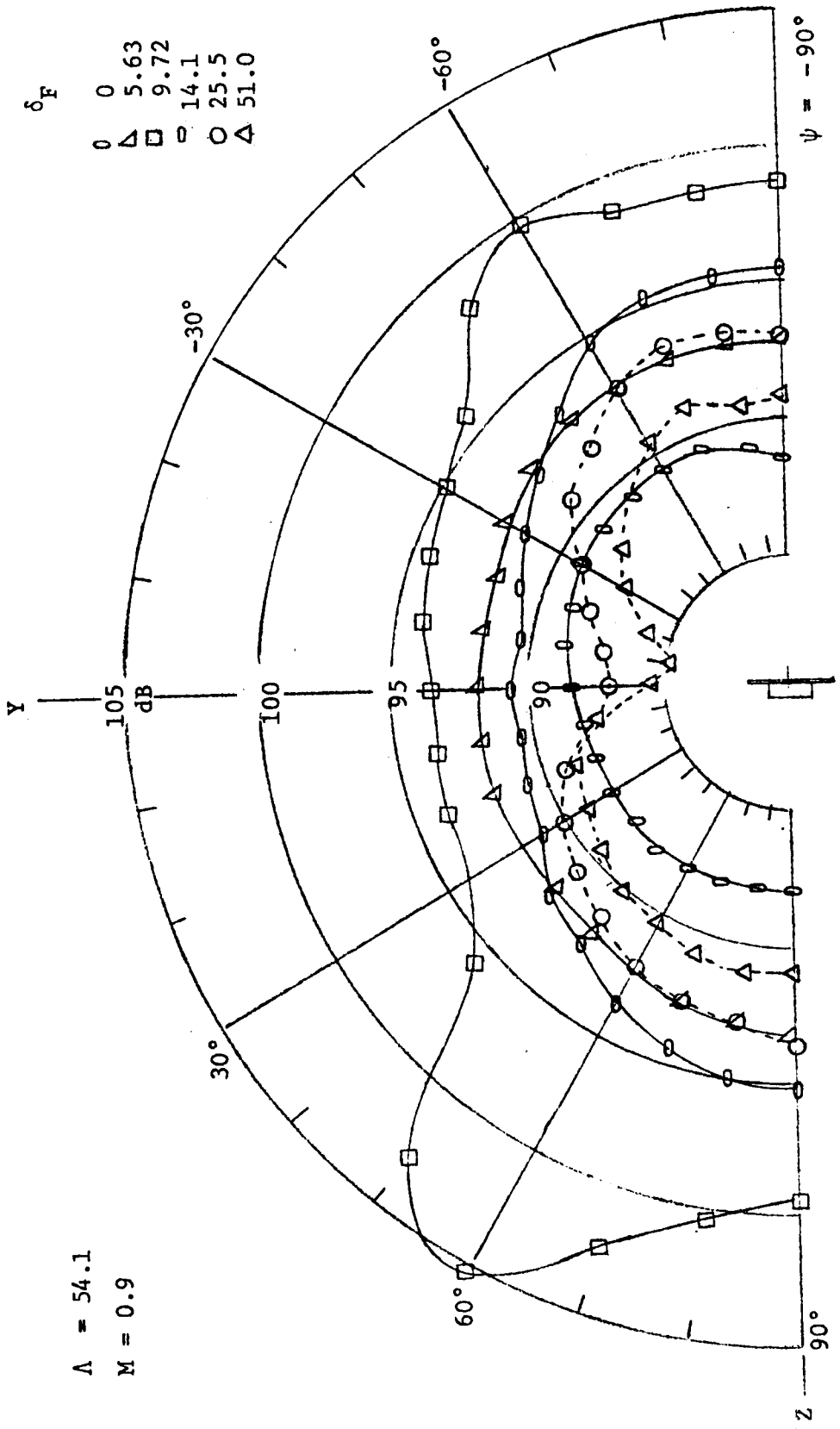


Figure 4.25. continued.

the peak of the OASPL directivity occurs in $\psi = 60°$ direction as seen in the second part of Figure 4.25. With further increase in flap length the sound levels decrease throughout the plane, although the directivity patterns remain flat in the sideline directions and elongated normal to the flap surface. Directivities for $\delta_F = 18$ with the 27 aspect ratio slot nozzle and for $\delta_F = 14.1$ with the 54.1 aspect ratio slot nozzle are examples of such shape. Longer flaps ($\delta_F = 25.5$ and 51) have still lower sound levels with slightly greater reduction under the flap than above it. The directivities have a shape like the figure eight, due to the necking of the directivity patterns in the sideline directions. The almost elliptic directivity for $\delta_F = 9.9$ is due to the preferred directional radiation of the discrete frequency tones in one third octave band with center frequencies equal to 6300 Hz, 12,500 Hz and 20,000 Hz as can be seen in Figure 4.26. For the jet flap with $\delta_F = 9.72$ on the 54.1 aspect ratio slot nozzle the discrete frequency tone occurred at 10,000 Hz and had preferential maximum radiation in $\psi = 60°$ direction.

B. REVERBERANT FIELD MEASUREMENTS

Sound power levels of slot jets and jet flaps were measured in a reverberation room as described in Chapter 2. Figure 4.27 shows the variation in the sound power level of

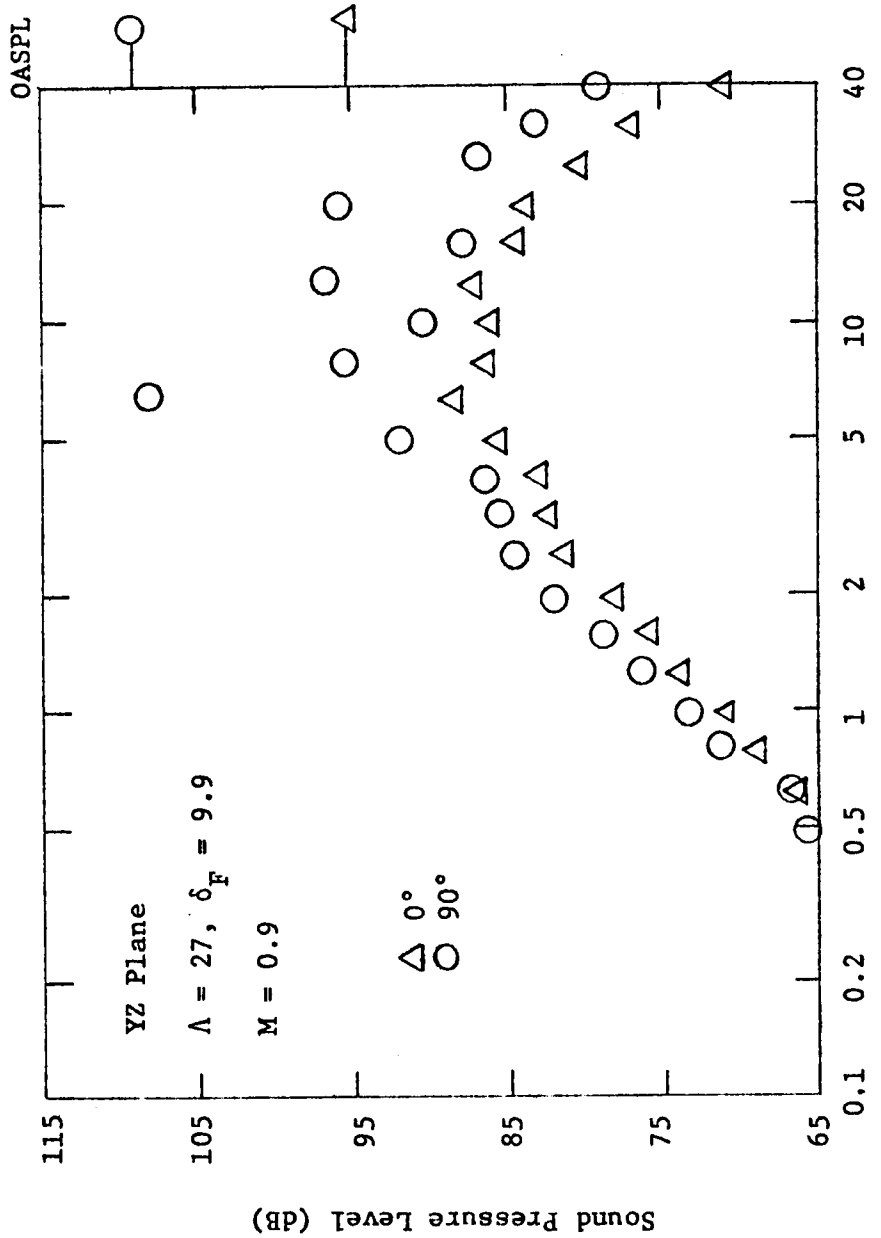


Figure 4.26. Sound pressure spectra at ψ = 0° and 90° for δ_F = 9.9 flap.

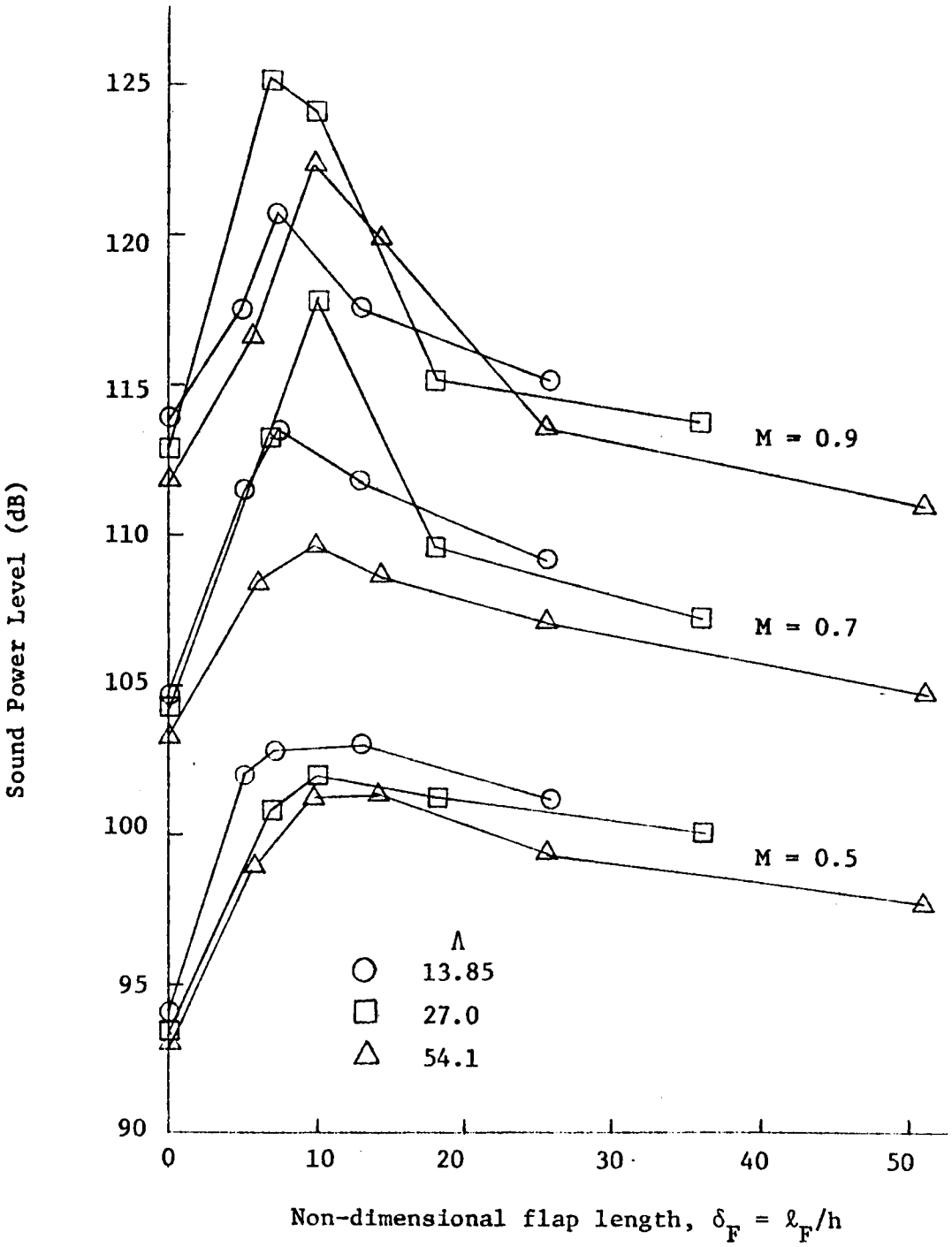


Figure 4.27. Sound power output variation with flap length.

jet flap due to changes in flap length for 13.85, 27 and 54.1 aspect ratio slot jets exhausting at Mach numbers 0.5, 0.7 and 0.9. At all Mach numbers the sound power output of a slot jet is seen to increase due to the addition of flap, continue to increase with increasing flap length, reach a maximum for flap lengths from δ_F = 7 to 10, and to decrease at a slower rate with further increase in flap length. The sound power output of a jet flap can thus be higher than that of the slot jet by as much as 6 to 13 dB. Such a large increase is a result of the discrete frequency tones generated by jet flaps at higher jet exit Mach numbers. This can be noticed in the power density spectra of Figure 4.28. The sound power output of jet flaps has a well behaved variation with flap length and this variation (Figure 4.27) is similar for all the three slot nozzles at low jet Mach numbers ($M \sim 0.5$) - the curves for Λ = 27 and 54.1 showing relative to the sound levels of jet flaps on Λ = 13.85 an almost constant reduction of 1 and 2 dB respectively for all values of δ_F. At higher Mach numbers, when discrete frequency tones are generated, the three curves have fairly similar characteristics but the sound powers for a given δ_F with different nozzles are not simply related except at very small and very large values of δ_F. It should be noted that except for the flaps generating the tones, the sound power output of a jet flap relative to that

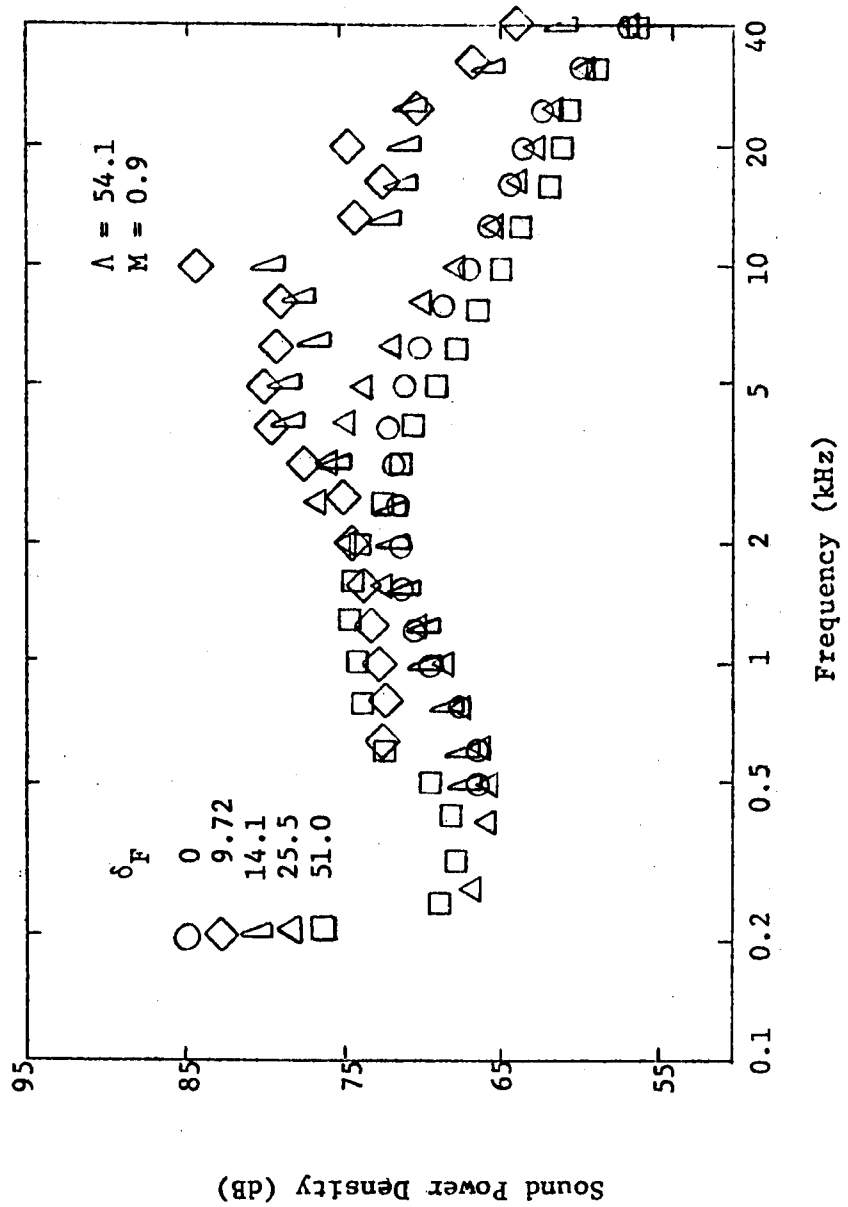


Figure 4.28. Power density spectra for the 54.1 aspect ratio slot jet and flaps.

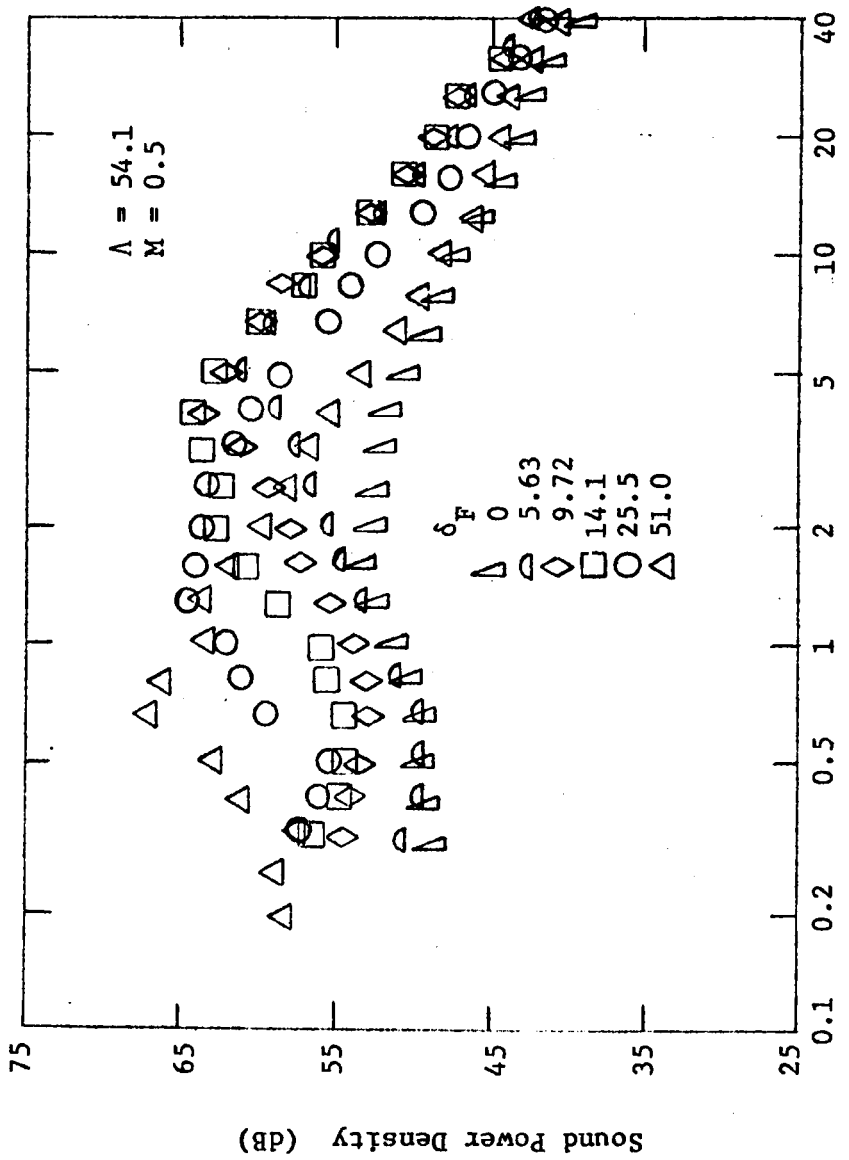


Figure 4.28. continued.

of the slot jet alone is higher at lower Mach numbers suggesting the surface generated noise of the flap to be dominant at low Mach numbers.

The effect of flap length on the power spectral density of jet flaps is shown in Figure 4.28. At low jet Mach numbers ($M \sim 0.5$) the sound power density spectrum of the slot jet has a broad-band character. The shortest jet flap has the effect of increasing the acoustic energy in the high frequencies ($f > 2000$ Hz) thereby causing a shift in peak frequency from 2000 Hz to 5000 Hz. Increasing the flap length from $\delta_F = 5.63$ to 9.72 and to 14.1 results in an increase in contribution to the sound power from low frequency ($f < 4000$ Hz) components with no change in the high frequency components. It takes longer flaps (for example, $\delta_F = 25.5$ and 51) to reduce the high frequency acoustic output. However, they generate considerably more low frequency noise than shorter flaps. This results in very low peak frequencies for long flaps. The spectrum of $\delta_F = 51$ peaks, for example, at 630 Hz compared to the 5000 Hz peak frequency for $\delta_F = 5.63$.

At higher jet Mach numbers ($M \sim 0.9$) the changes in sound power density spectrum due to changes in flap length are essentially the same as mentioned above for $M = 0.5$. Certain jet flap configurations, however, generate discrete frequency tones at high jet Mach numbers.

Again, the high frequency acoustic energy for longer flaps is either equal to or less than that of the slot jet without the flap.

Sound power measurements were carried out for all jet flaps over a range of jet exit Mach numbers. These data for jet flaps on the 27 and 54.1 aspect ratio slot jets are presented in Figure 4.29. Over the entire jet Mach number range ($M < 0.9$) the jet flaps generate more acoustic power than the slot jets without the flap. Also indicated in the figure are the jet velocity power law variations of the measured sound power levels of all jet flap configurations. In the case of the 27 aspect ratio slot jet, the slot jet without the flap has a near eighth power variation with velocity and the longer flaps ($\delta_F = 18$ and 36) have a near sixth power variation, thus making them considerably noisier than the slot jet at lower jet Mach numbers. At $M = 0.9$, the jet flap with $\delta_F = 36$ is only one dB louder than the slot jet. When the flap length is $\delta_F = 9.9$, the sound power output of the jet flap does increase as the sixth power of jet velocity at low jet Mach numbers. However, when the jet Mach number is increased from $M = 0.6$ to $M = 0.7$ the sound power level goes up by 11 dB. Beyond $M = 0.7$ the near sixth power variation is again observed. For $\delta_F = 6.85$ also the near sixth power law velocity variation occurs at low jet Mach numbers. Increasing the jet Mach number

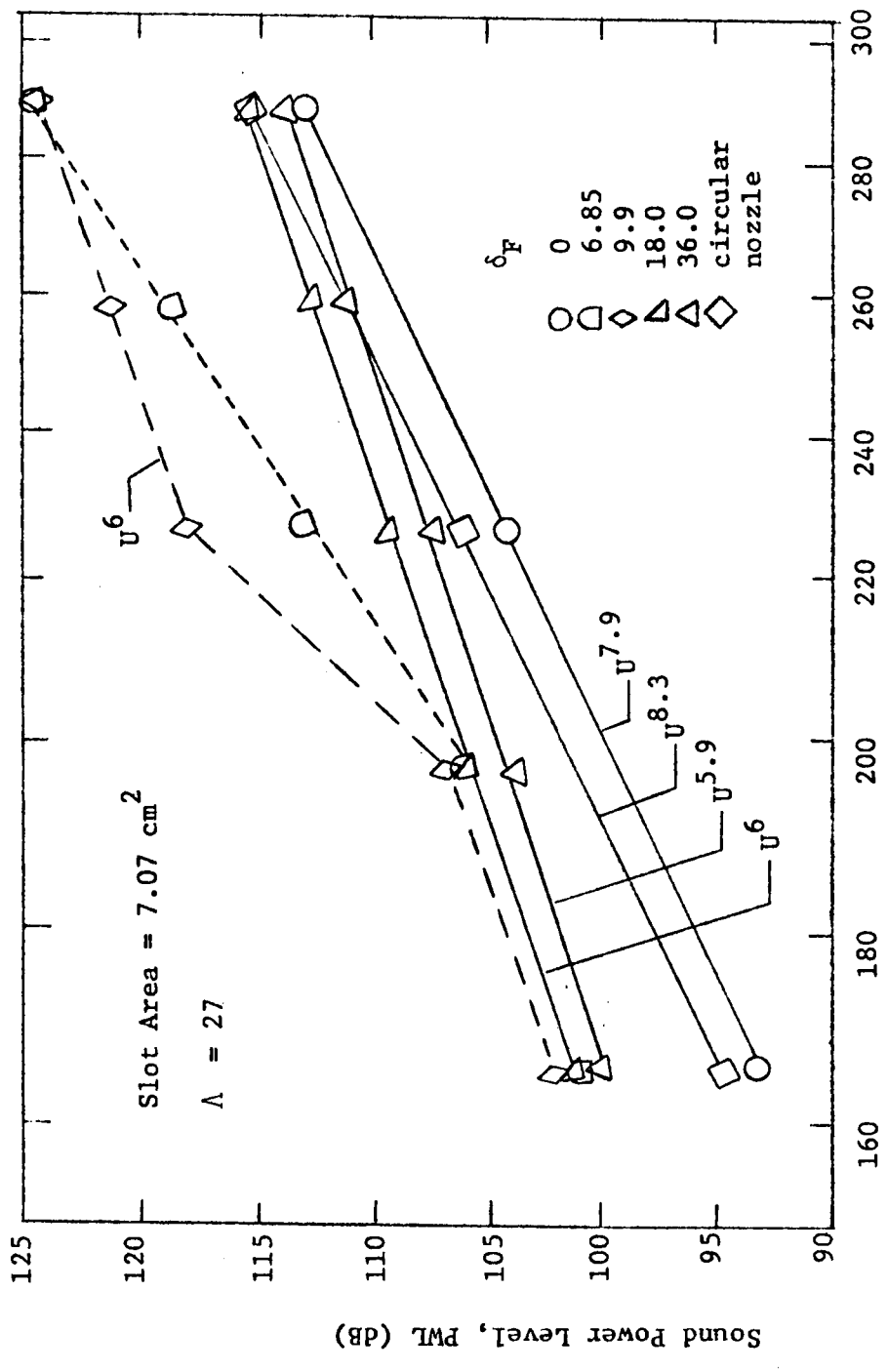


Figure 4.29. Jet velocity dependence of the sound power of jet flaps.

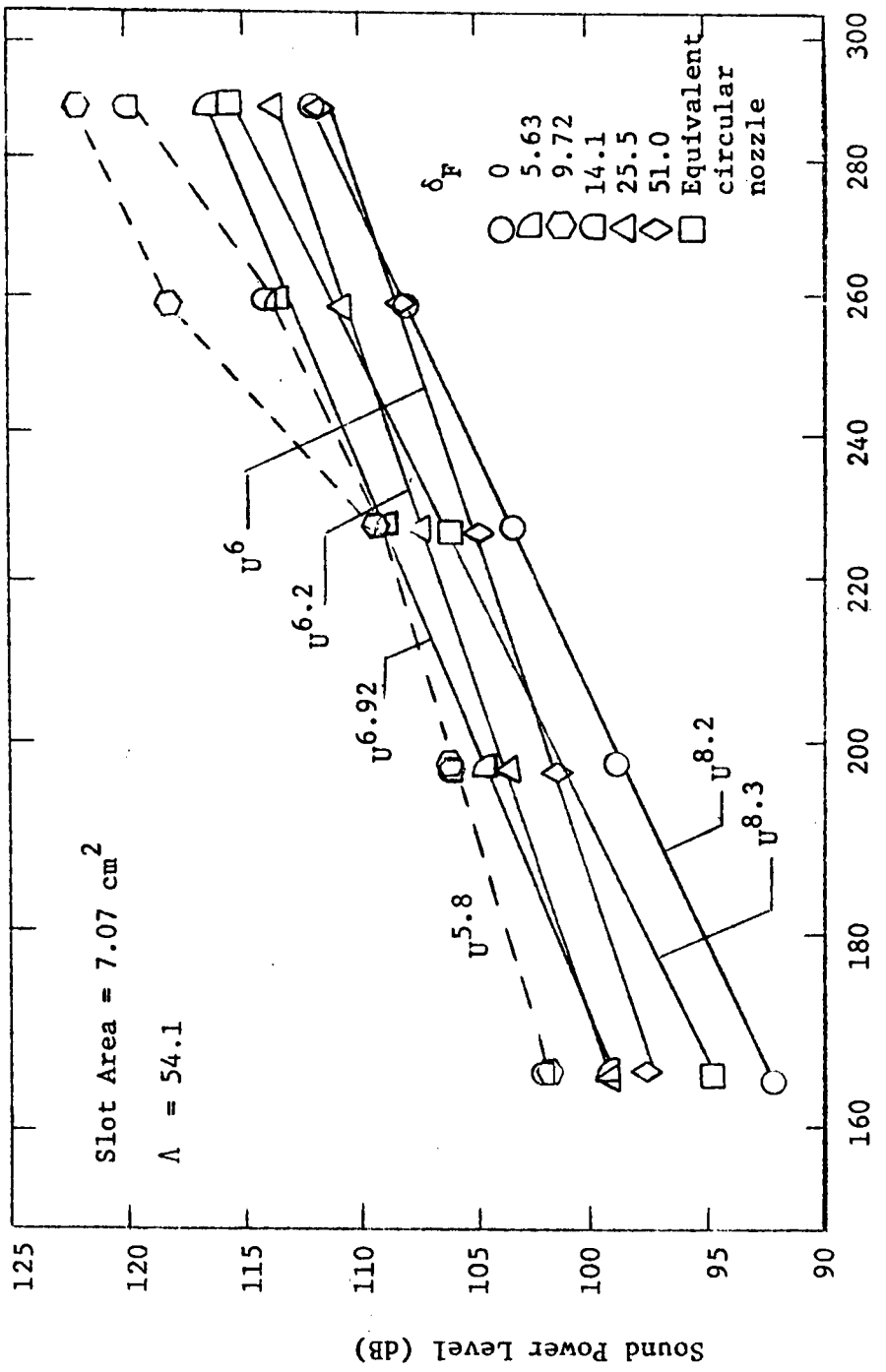


Figure 4.29. continued.

beyond 0.6 causes the sound power to rise at almost double this rate. Thus for δ_F = 6.85 and 9.9, the jet flap sound power level is considerably higher than the slot jet sound power level, even at higher Mach numbers. The jet flap with δ_F = 9.9 generates the maximum sound power at all Mach numbers less than 0.9.

Essentially similar characteristics are observed in the data on jet flaps with 54.1 aspect ratio slot jet. Sound power levels are maximum for δ_F = 9.72 but the sudden jump in level occurs at M = 0.8 (instead of M = 0.7 as for δ_F = 9.9 jet flap on 27 aspect ratio slot nozzle) and produces a lower increase in the sound power level. An interesting observation is the near seventh power velocity variation for the sound power output of jet flap with δ_F = 5.63. The longest jet flap (δ_F = 51) has the same sound power level as the slot jet at M = 0.9.

Jet Mach number effect on the sound spectral density of various jet flaps is pictured in Figure 4.30. For the slot jet without the flap spectral density increases almost uniformly over the entire frequency spectrum with increasing Mach number. The frequency at which the spectrum density function peaks (i.e. the peak frequency) also increases with jet Mach number. For the shortest jet flap (δ_F = 5.63) the spectral density does increase with jet Mach number but the peak frequency changes very little. Longer flaps (e.g. δ_F = 25.5) show greater increases at

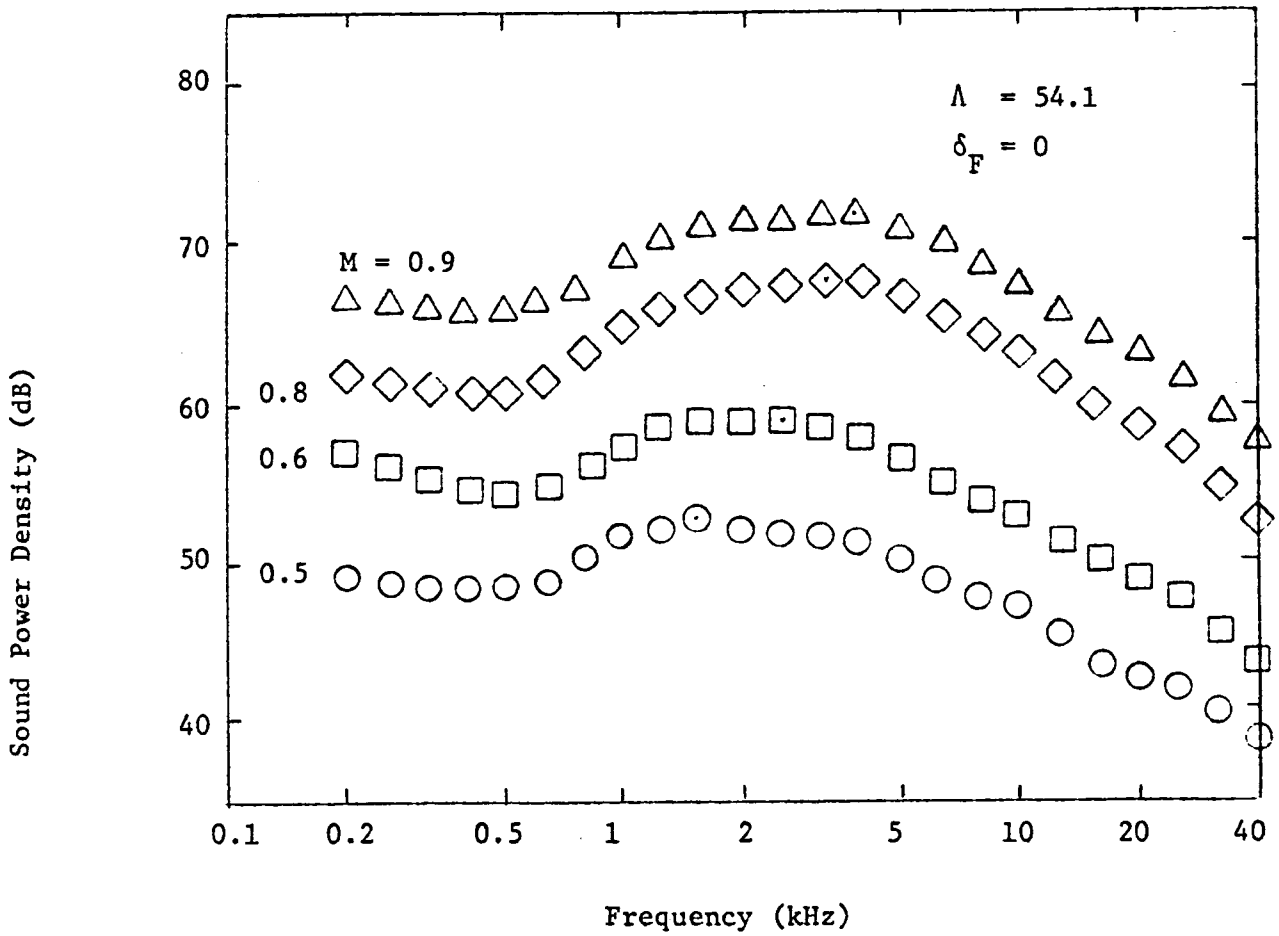


Figure 4.30. Power density spectra of slot jet and flaps at different jet exit Mach numbers.

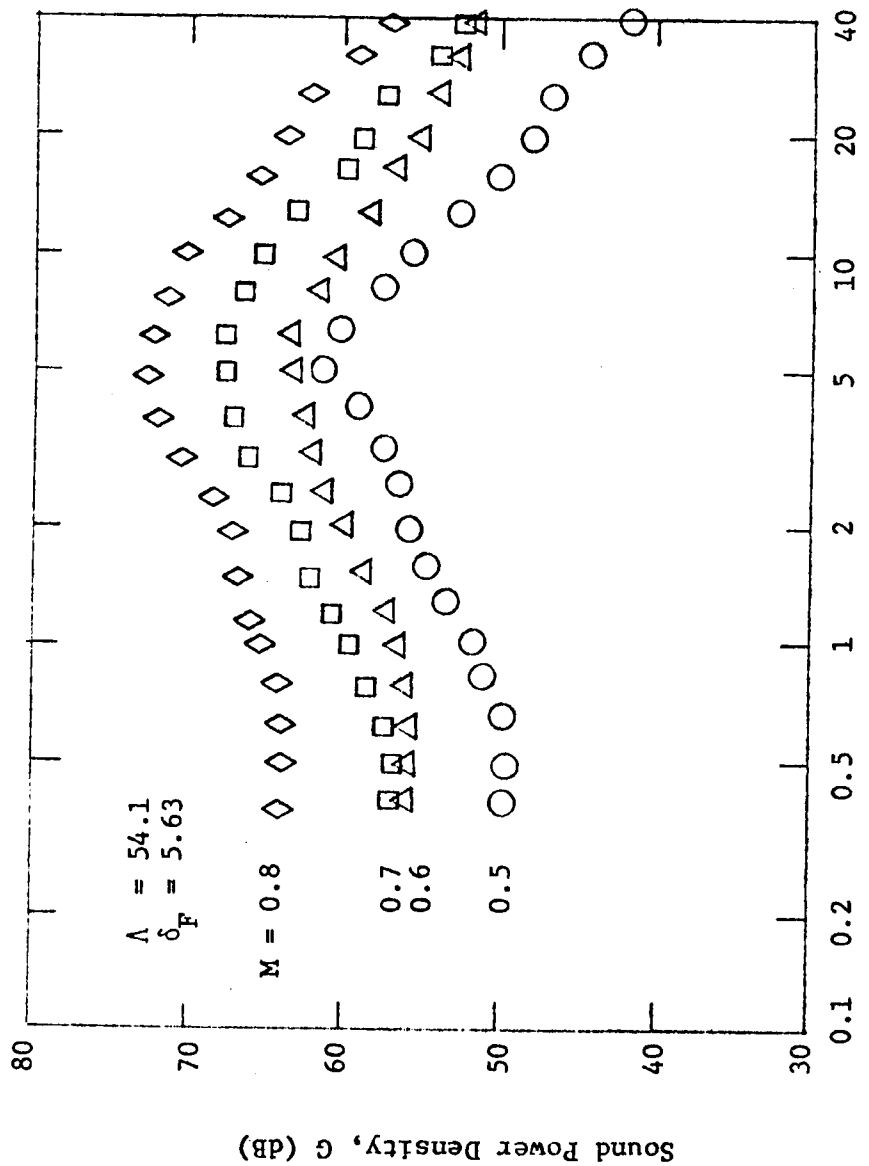


Figure 4.30. continued

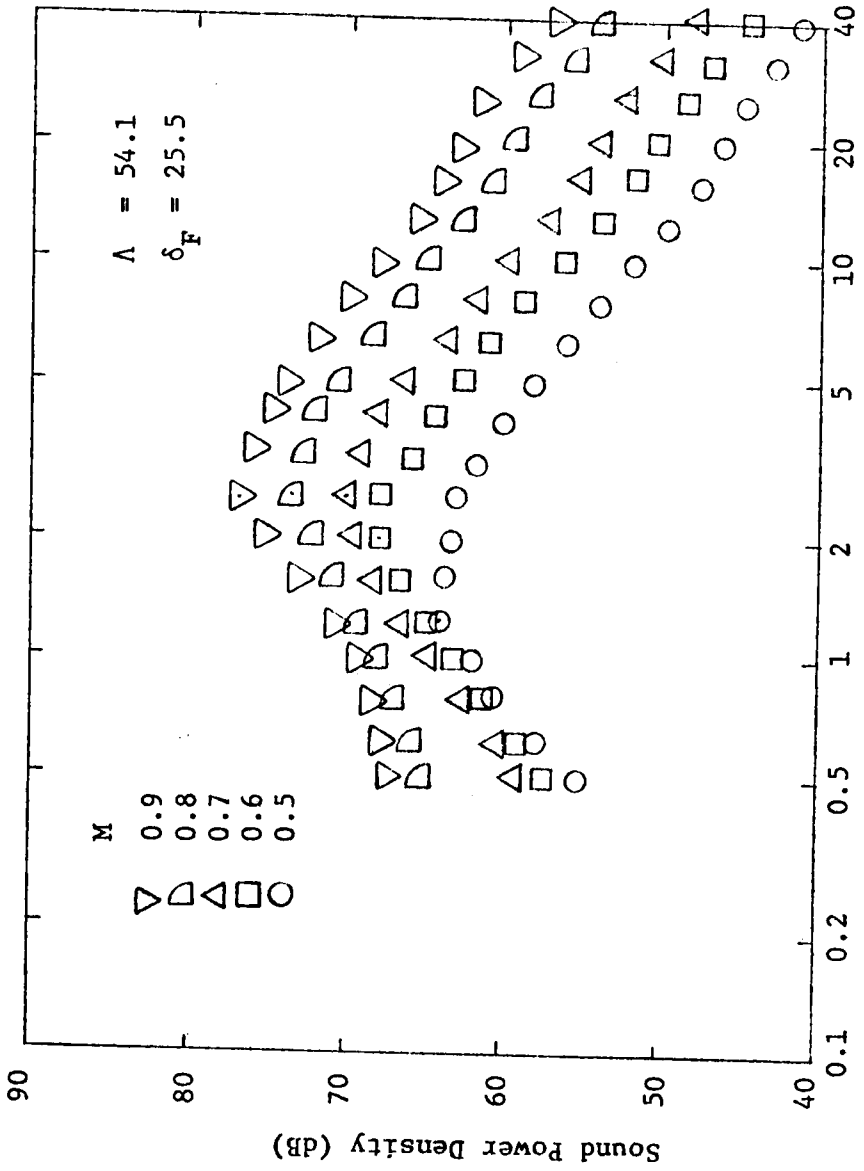


Figure 4.30. continued.

higher frequencies than at lower frequencies. The spectral decay rates at higher frequencies are clearly the same at all Mach numbers.

Figure 4.31 shows the sound power spectral density of jet flap with $\delta_F = 7.12$ at M = 0.9 and for different flap deflection angles. The obvious effect of flap deflection is to eliminate the discrete frequency component and cause reduction of spectral density in the mid frequency range.

C. DISCUSSION OF RESULTS

The free field and reverberant field acoustic measurements presented in sections A and B will be analyzed in this section on the basis of known theoretical results. A formal theory dealing with the influence of solid boundaries upon aerodynamic sound was first developed by Curle [26]. He showed that the sound field due to unsteady flow contiguous to a solid boundary is exactly that which would be generated in a hypothetical unbounded medium at rest acted upon by a volume distribution of quadrupoles (T_{ij}) throughout the region external to the solid bodies and a surface distribution of dipoles (P_i) acting at the surfaces of the solid bodies. The strength of the equivalent dipoles was related to the forces exerted on the fluid by the surfaces. Dimensional analysis indicated that if the body is compact

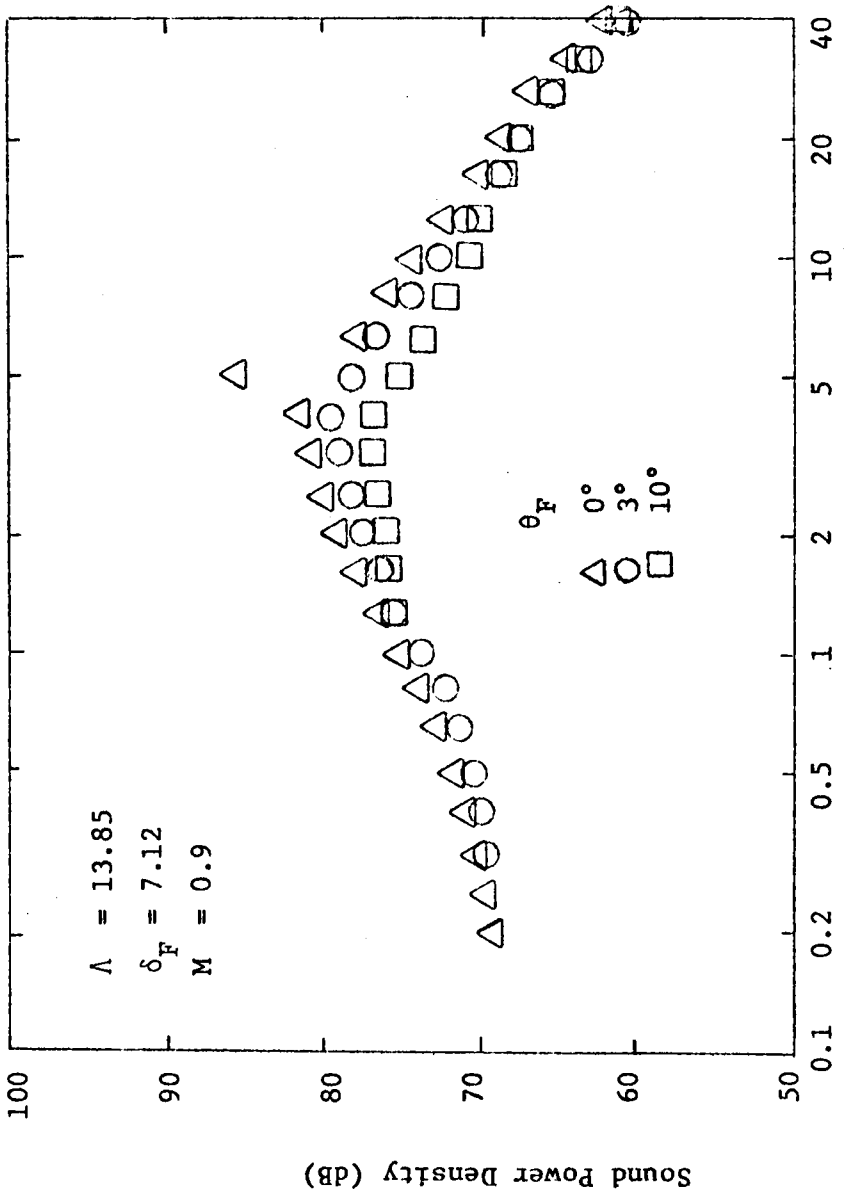


Figure 4.31. Power density spectra for deflected flaps.

and hard with linear dimensions small compared to a typical wavelength, the intensity of "surface noise" varies as the sixth power of a typical flow velocity (U). Making use of the well-established concept that sources become increasingly less efficient at high order, Curle deduced that the equivalent dipole sources would overshadow any hydrodynamic quadrupoles at low flow velocities. These results have been confirmed experimentally by several investigations (e.g. Etkin et al [27]) on the phenomenon of Aeolian tones.

It was Powell [28] who pointed out that while the fluctuating pressures exerted upon a rigid boundary by a contiguous unsteady flow generate sound like a distribution of dipoles, all such dipole effects cancel out in the case of the boundary being plane. In a later publication Powell [29] showed, by using the image principle, that the pressures exerted on a plane rigid boundary are simply reflections of the quadrupole generators of the flow itself. Due to the passive acoustic reflector role of the infinite rigid plane surface, the noise from the boundary layer on such a surface should be expected to vary as the eighth power of velocity as predicted by Lighthill [15] for free turbulence noise.

Powell recognized that in the case of the sound-generating flow extending far enough to envelop the surface edges, the acoustic reflection property of the

surface does not hold in the edge region which may then give rise to sound generation as from pressure dipoles. He suggested the term "edge noise" for this type of noise generation. Ffowcs Williams [30] evaluated Curle's pressure dipole integral for the case of turbulent flow over a finite, rigid, flat plate radiating sound to a point so far away that the plate appears small to establish the near-vanishing strength of the dipole field for sufficiently large surfaces first noted by Powell. His estimates, however, suggest that surfaces have to be very large in order for the dipole distribution to vanish and for the surface to assume the role of an acoustic reflector. Thus surfaces of practical interest are likely to be more than just acoustic reflectors, with a noise generating edge region.

The problem of sound generation due to turbulent flow past an edge has since been solved by Ffowcs Williams and Hall [8]. By posing the problem as that of determining the sound field generated from known quadrupole sources near a rigid half plane, in the framework of Lighthill's theory, they arrived at two important results. First, the sound output (in a plane normal to the edge of the half plane) of eddies which are well within a wavelength of the edge of the half plane (i.e. for $2k\,\bar{r}_o << 1$) is increased by the factor $1/(k\,\bar{r}_o)^3$ where k is the acoustic wavenumber and $\bar{r}_o$ is the distance of the center

of the eddy from the edge. For eddies that are far from the edge no significant sound amplification is produced. Dimensional reasoning that assumed the turbulence frequency to vary directly as the flow velocity and inversely as the eddy diameter then led to the result that the intensity of the scattered field increases in proportion to the fifth power of the fluid velocity (U), thus making it more powerful than Curle's surface dipole field. Secondly, the scattered field has a distinctive directivity given by $\cos^2(\theta'/2) \sin \phi'$ where θ' and ϕ' are defined in Figure 4.32.

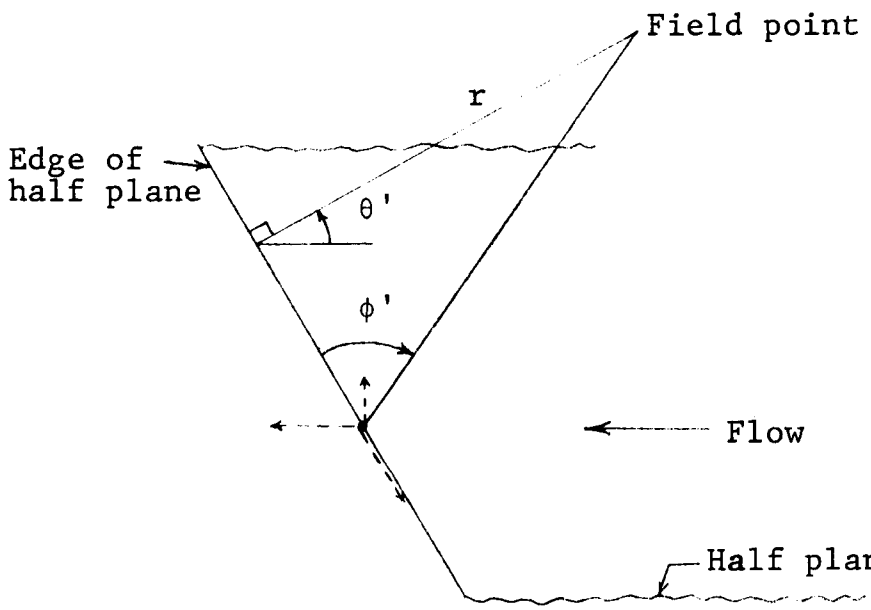


Figure 4.32. Edge geometry of Ffowcs Williams and Hall [8] and Hayden [31].

Hayden [31] took the view point that the convection of wall jet pressure fluctuations past the trailing edge results in the imparting of momentum fluctuations to the fluid at the edge and these fluctuations can appropriately be modeled as simple dipole sound sources along the edge. The edge then acts as a partial baffle causing the dipoles to radiate according to $\cos^2(\theta'/2)\sin^2\phi'$. Directivity patterns in the flyover plane are identically predicted by Hayden's and Ffowcs Williams and Hall's theories. However, the dipole modeling of Hayden predicts a U^6 variation for the diffracted sound field (again assuming the pressure flucutations frequency to be directly proportional to flow velocity and inversely proportional to streamwise correlation length).

Chase [32] has also determined the spectrum and intensity of the radiated pressure generated from turbulent flow by diffraction at the edge of a rigid half plane. Explicit consideration of the Lighthill sources was, however, circumvented by using a model turbulent pressure spectrum. The formulation thus relates the spectrum of sound radiation to the local wavenumber-frequency spectrum of pressure near the edge. The intensity of radiated sound was found to vary as the fifth power of a typical velocity.

It has thus been recognized that surface generated sound depends on the compactness of the surface as well as the source field. If ℓ and u are the length and velocity scales of the turbulent flow and b is the typical surface dimension, then compactness of surface and flow require $b << \ell/m$ and $m << 1$ where $m = u/a_o$ is the turbulence Mach number and $\ell/m = a_o/(u/\ell)$ equals the acoustic wavelength. With both these conditions satisfied and a non-zero total force on the surface, the surface is equivalent to a single dipole, producing an intensity greater than that from a single turbulent eddy by a factor of order $1/m^2$ as predicted by Curle. This result does not hold when any one of the conditions is not satisfied. When the surface is non-compact, no general result can be drawn from the formal solution of Curle. Contributions to his surface integral may add constructively or destructively. The case of an infinite plane surface is one in which where is destructive interference resulting in a sound field of the same order as that due to free turbulence, as shown by Powell. On the other hand, edge noise from a semi-infinite plane has been shown by Ffowcs Williams and Hall to enhance the sound one order of magnitude more than Curle's original estimate. Non-compact surfaces are characterized by local regions where the relevant length and velocity scales are set by other quantities than those of the turbulence, thus violating

the premises of Curle's dimensional analysis and generating sound fields with dependence on flow parameters different from that for the classical dipole. It should also be recognized that sources, though compact when stationary, become essentially non-compact at high convection speeds.

The effect of non-compactness of the surface on the radiated sound field directivity is of equal interest. The directional factor, $\cos \theta'/2$, in the expression for the density fluctuations of the sound field scattered from the edge of a semi-infinite plane makes it clear that the half plane is not equivalent to any compact multipole since multipole radiation would permit only $\cos m\theta$ or $\sin m\theta$ type of variation. This factor shows the peak scattered field to occur at $\theta' = 0$ i.e. on the half plate itself, with zero scattered field on the extension ($\theta' = \pi$) of the half plane.

The theoretical sound radiation directivity and the flow velocity dependence of intensity will be used to analyze the measurements of the present investigation. However, before proceeding to the analysis, enumeration of the major fluid dynamic characteristics of jet flap as modeled by the plane two-dimensional wall jet is in order. Measurements of Schrecker and Maus [34] in the flow field of jet flaps similar to the ones used here are useful in characterizing the fluid dynamics

of such configurations. General features of the flow field are shown in Figure 4.33. The jet upon exit from the nozzle mixes with the ambient air near the upper edge of the jet resulting in a mixing region (called the primary mixing region). On the flap side of the jet a boundary layer grows, bounding a region of potential flow between the primary mixing region and the boundary layer. This region is generally referred to as the jet potential core. Growth of the primary mixing region and the boundary layer further downstream causes narrowing down of the potential core and eventually leads to its extinction when the two shear layers merge. Another shear layer develops on the flap side of the jet at the flap trailing edge. This region will be referred to as the secondary mixing region.

Results from measurements of Schrecker and Maus [33] that are of interest for the present investigation are given in the following. First, the mean velocity profiles, the turbulence intensity profiles and the turbulence spectra in the primary mixing region of jet flaps (δ_F = 5.6, 9, 15.4) are nearly identical to those in the mixing region of the slot jet without the flap. Thus the addition of a flap to the slot jet does not change the fluid dynamics of the primary mixing region so that the contribution to the far field of the sound radiated from the primary mixing region should practically be the same for the jet flaps

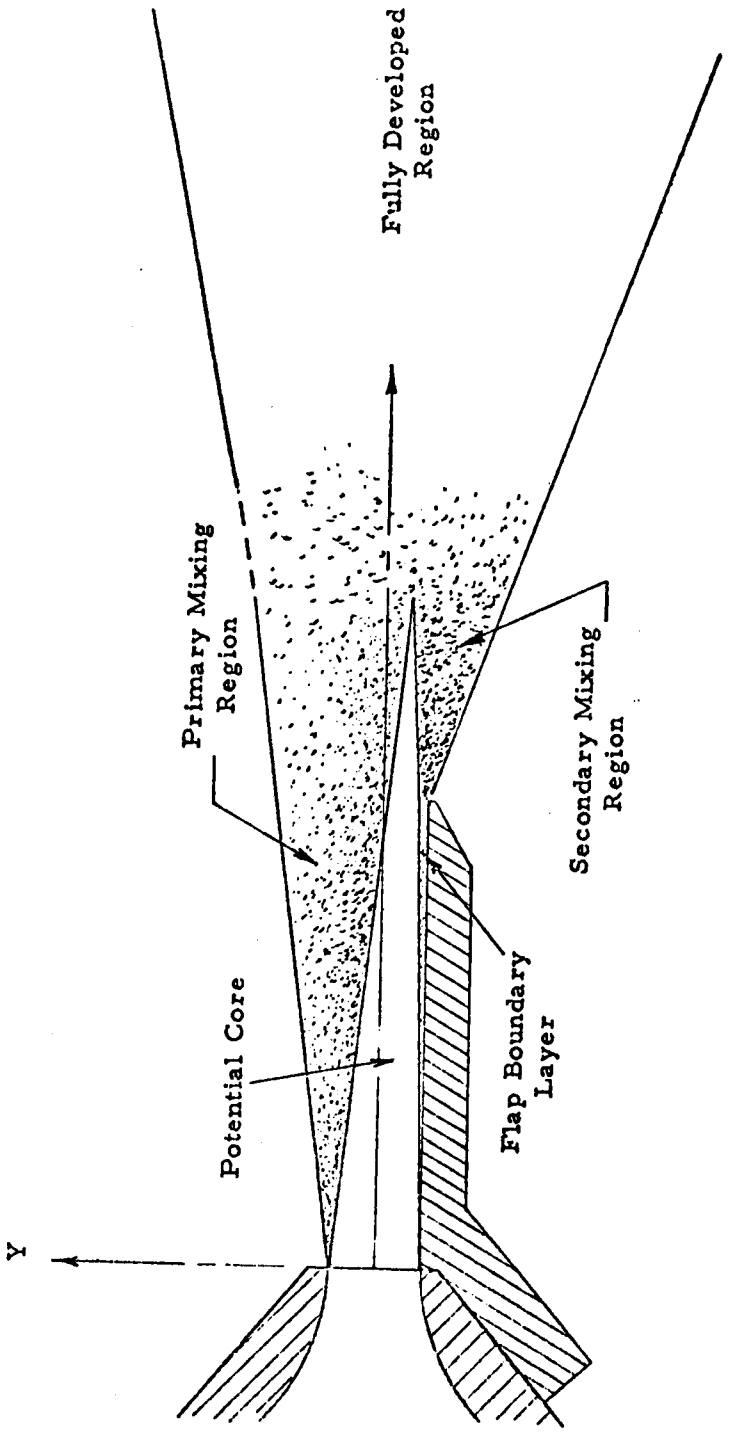
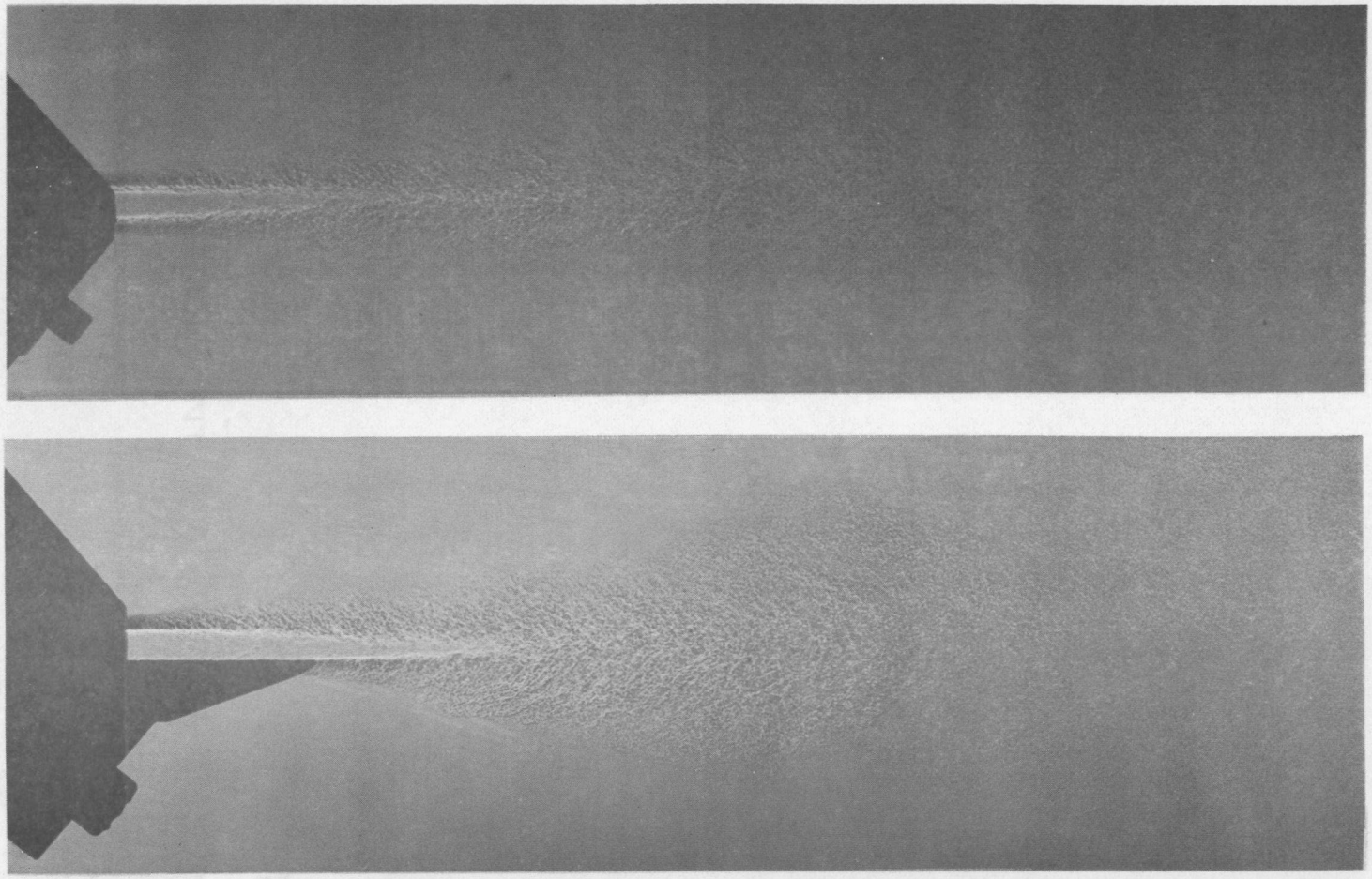


Figure 4.33. Slot nozzle with flap flow field nomenclature.

and the slot jet. Secondly, in the secondary mixing region aft of the flap trailing edge the measured maximum turbulence intensity levels exceed the corresponding maxima in the primary mixing region for about ten nozzle heights downstream of the trailing edge. This difference decreases with increasing flap length. Finally, the absolute maximum turbulence intensity level occurs in the secondary mixing region and immediately downstream of the flap trailing edge for the two flaps with δ_F = 5.6 and 9.9. For the longer flap (δ_F = 15.4) the absolute maximum occurs about 4 to 5 nozzle heights downstream of the trailing edge. The peak turbulence intensity in general decreases with increasing flap length. It should be noted that these are the results of measurements using a hot wire anemometer with the jet exhausting at a Mach number of 0.35. Presence of high turbulence intensity levels in the secondary mixing region and the weak influence of flap on the fluid dynamics of the primary mixing region has, however, been found at a higher jet Mach number (M = 0.7) in recent detailed measurements by Becker [34] on a jet flap with δ_F = 10.
Sample measurements with a hot film probe during the course of the present investigation also indicated the presence of high intensity turbulence in the secondary mixing region at M = 0.9.

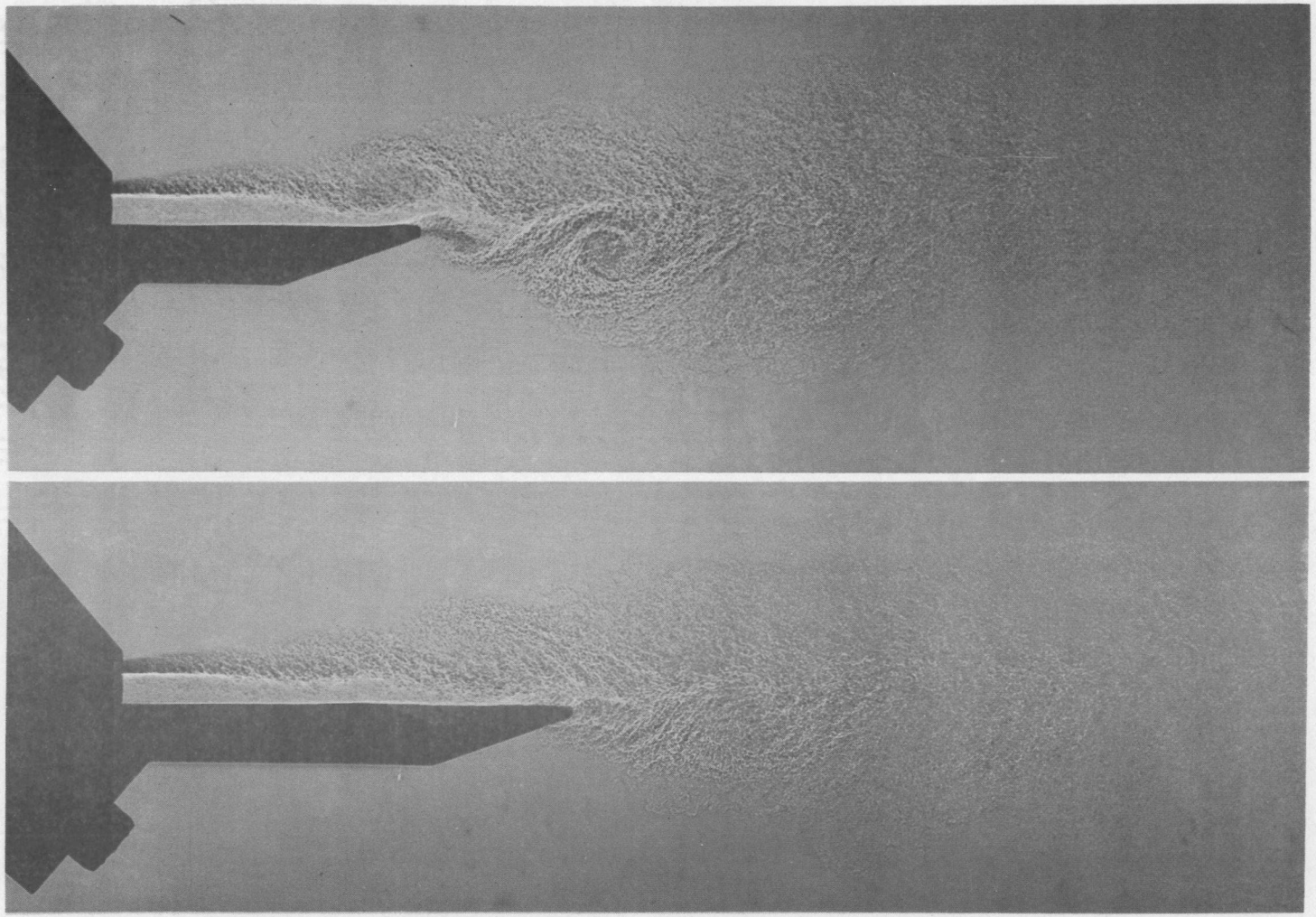
Although detailed probing of the flow field was not done in the present investigation to obtain quantitative turbulence characteristics at high jet exit velocities, visualization of the flow by means of spark shadowgraphs and high speed movies did reveal some features of the flow field. The set up for flow visualization has been described in Chapter 2 and shadowgraphs of various jet flaps with the 27 aspect ratio slot jet exhausting at a Mach number of 0.9 are given in Figure 4.34. It is observed that the slot jet has similar mixing regions on either side of the low turbulence potential core which extends downstream to about 8 nozzle heights. Beyond the potential core the mixing regions merge and the jet becomes fully turbulent. For the jet flap with $\delta_F = 3.96$, however, the jet can mix with the ambient air only on one side and this results in the extension of the potential core beyond that for the slot jet alone. The potential core is now approximately 10 nozzle heights long. The boundary layer on the flap is not visible but the presence of the secondary mixing region downstream of the flap trailing edge is very clear. In this case the flap is shorter than the jet potential core (and the latter is terminated by the merging of the primary and secondary mixing regions). The secondary mixing region is seen to grow (in width) at a rate faster than the primary mixing region starting at the nozzle exit. It should



$\delta_F = 0$

$\delta_F = 3.96$

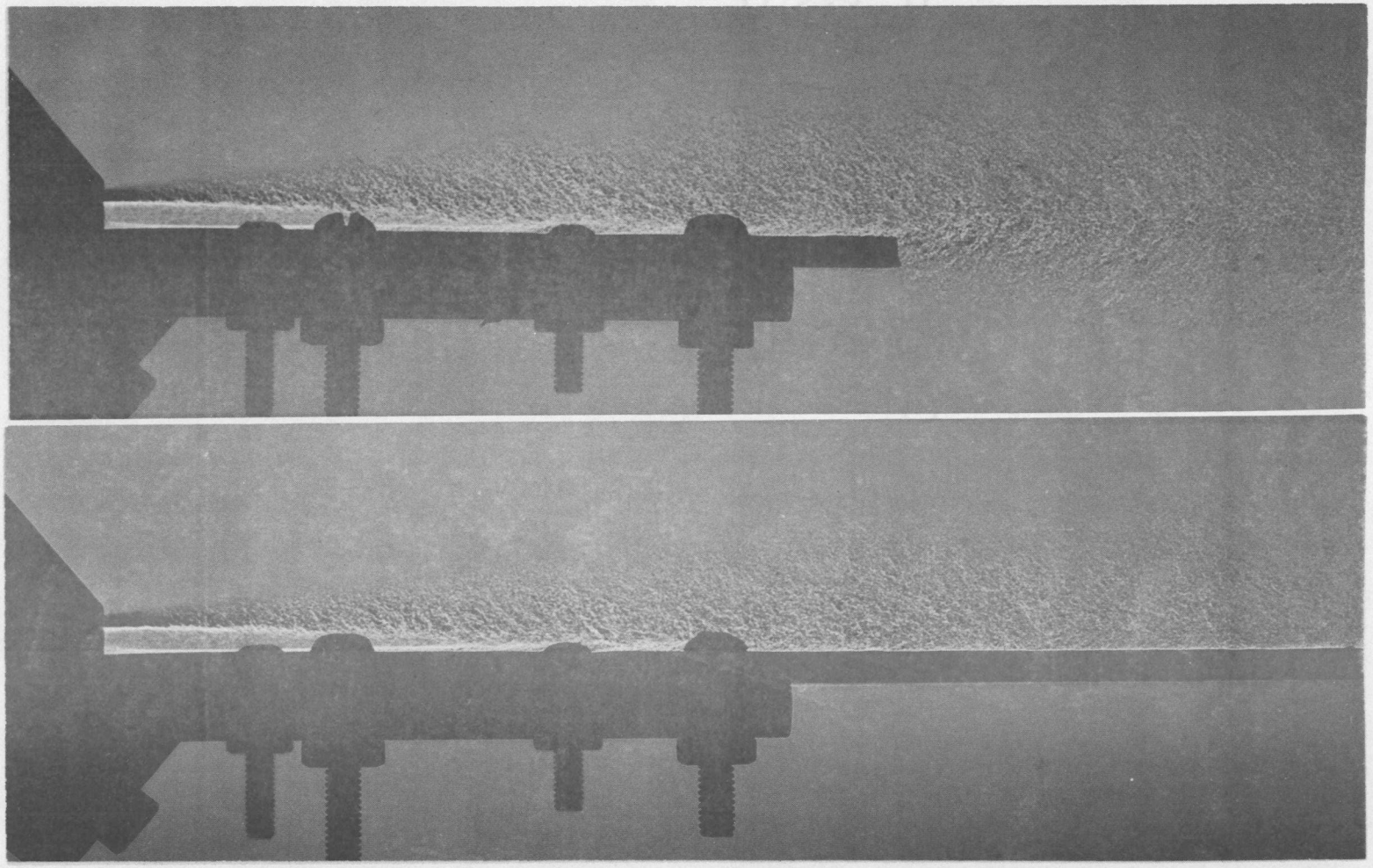
Figure 4.34. Spark shadowgraphs of jet flaps on the 27 aspect ratio slot jet at M = 0.9.



δ_F = 6.83

δ_F = 9.90

Figure 4.34. continued.



$\delta_F = 18$

$\delta_F = 36$

Figure 4.34. continued.

be noted that the structures of the primary mixing regions in the jet flap and the slot jet without flap cases are very similar. When the flap length is increased to $\delta_F = 6.83$ the flow field is considerably changed. Large scale flow oscillations are seen in both the secondary and primary mixing regions. The vortical structures in the secondary mixing region originate at the flap trailing edge and have clockwise vorticity with axes seemingly perpendicular to the direction of jet flow and parallel to the flap edge. In the primary mixing region these structures have counterclockwise rotation and are clearly visible only downstream of about four nozzle heights. The secondary mixing region again has a faster spread and at any axial location downstream of the trailing edge the total jet width is greater than that for a jet from a slot nozzle without flap. These features, though not as clear, can be seen with some imagination in the case of jet flap with $\delta_F = 9.9$. The potential core extends slightly beyond the trailing edge for $\delta_F = 6.83$ but terminates on the flap very close to the trailing edge for $\delta_F = 9.9$.

Increasing the flap length to $\delta_F = 18$ eliminates the striking features of the flow field mentioned in the previous paragraph. The potential core terminates on the flap well upstream of the trailing edge. Large scale oscillations are totally absent in both the primary and

secondary mixing regions. The flow leaving the flap trailing edge seems totally turbulent. Again the primary mixing region seems to have a structure similar to that in the jet without the flap. These features are maintained when the flap length is further increased to $\delta_F = 36$. The screw heads seen in the last two shadowgraphs are only shadows of the screws at the side edges of the plate and are completely out of the flow.

With the jet exhausting at a high Mach number and with the flap exerting little influence on the fluid dynamics of the primary mixing region, whence comes a greater portion of jet noise, some acoustic characteristics of the slot jet without the flap are likely to be found in the data of jet flaps also. Undoubtedly, the directivity, the spectra, the velocity dependence of sound power are all affected by the flap. It is, however, the changes in the characteristics relative to those of the slot jet alone that will be useful in speculating about the source regions since the theories reviewed earlier in the chapter evaluate only the "surface or edge generated noise" part of the total noise.

Referring first to the OASPL directivities in the flyover plane (Figures 4.1, 4.6, 4.7, 4.8, 4.11 and 4.12, pages 44, 55, 56, 58, 63 and 64 respectively) the general effect of flap has been to increase the OASPLs in the plane, the increases being largest in $\theta = +90°$ direction

and lowest at smaller angles to the jet axis. The $\cos^2(\theta'/2)$ directivity factor of Ffowcs Williams and Hall's [8] edge amplified field or Hayden's diffracted dipole [31] will produce the same effect on the far field radiation. With the exception of jet flaps with flap lengths in the range of $\delta_F \approx 10$, the increase in OASPLs relative to those of the slot jet is higher when the jet is exhausting at M = 0.7 than when M = 0.9. U^5 or U^6 dependence of trailing edge noise would obviously have greater effect on jet noise (which varies as U^8) at lower jet Mach numbers. An important observation in these figures is the relatively higher convective amplification for slot jets and jet flaps at M = 0.9 compared to that at M = 0.7. This is so in spite of the larger diffracted field contribution in $\theta = 90°$ direction at M = 0.7. Source convection effects thus clearly exist in jet flap acoustic characteristics.

The spectral character of the sound field due to the edge amplification effect will depend on the frequency of the turbulence at the trailing edge. The latter being dependent on the local flow velocity and correlation length will generally be higher for flaps terminating in or near the potential core regime than for longer flaps. A comparison (Figure 4.13, page 67) of the sound pressure spectra for jet flaps of various flap lengths in $\theta = 90°$ direction, where the edge noise has

considerable radiation, shows this effect. Flap lengths of $\delta_F < 15$ have increased sound levels in the normal direction due to greater contribution from the high frequency components whereas for longer flaps, $\delta_F < 15$, this is due to increased low frequency radiation. That edge amplification is present for very long flaps also is suggested by Figure 4.18 (page 77) where the low frequency components are seen to be considerably increased in the normal direction.

If edge noise, which has theoretically been shown to be symmetric, is the only significant contribution of the jet flap then the non-symmetric flow geometry of such a configuration would be expected to generate non-symmetric OASPL directivities with lower levels in the flap side far-field. Measured directivities indicate that this is true only for long flaps (δ_F approximately greater than 30). Flaps with $\delta_F < 30$, contrary to one's expectations, radiated more sound (about 2 dB) in $\theta < 50°$ sector below the flap than above it. This characteristic is believed to be related to the secondary mixing region downstream of the flap trailing edge. As mentioned earlier measurements in the secondary mixing regions of flaps of moderate lengths have indicated the presence of high turbulence intensities. A major portion of the noise generated in this region radiates on the flap underside. This was observed by Becker [34]

by cross-correlating the signal from a hot wire in the secondary mixing region of a jet flap (δ_F = 10) with the pressure signals from microphones at θ = +45° and -45° in the far-field. For flaps of moderate length the local maximum velocity (which remains constant through the potential core regime) is fairly high at the trailing edge and the flap surface boundary layer thickness is small there. This results in a large velocity gradient making the edge a region of high vorticity. For longer flaps, however, the local maximum velocity, which decays rapidly after the termination of the potential core, is not as large at the trailing edge and the boundary layer is thicker so that the velocity gradient is comparatively lower. Thus the secondary mixing region, into which the flap surface boundary layer is fed, is likely to be less intense for long flaps. This in turn might reduce noise generation in the secondary mixing region thereby leaving the jet noise and edge noise as the major noise sources. The frequency of the noise generated in the secondary mixing region being dependent on the local velocity and correlation length can be expected to be higher for short flaps than for long flaps. Comparison of sound pressure spectra at θ = +30° and θ = -30° showed the higher levels in -30° direction to be due to high frequencies, f > 5000 Hz, (Figures 4.5 and 4.15, pages 52 and 72 respectively) for flaps with δ_F < 15 but due

to lower frequencies, 1000 Hz < f < 8000 Hz for longer flaps (Figure 4.10, page 61). This again suggests the secondary mixing region to be an important noise source for flaps of moderate lengths.

The non-symmetry of OASPL directivities for jet flaps with $\delta_F < 30$ is pronounced only at smaller angles to jet axis. Convective effects being dominant at these angles the cause of non-symmetry can be considered to be due to a convecting source. Jet noise sources convecting in the primary mixing region and known to produce symmetric radiation would, due to the effect of the flap, if any, have only reduced radiation below the flap. This then leaves the secondary mixing region as the only other convecting source.

The above mentioned situation reverses to the expected situation for $\delta_F > 30$. OASPLs on the flap underside are lower than the OASPLs above these flaps. The non-symmetry of the OASPL directivity is again greatest in the sector $\theta < 50°$, (Figure 4.12, page 64). The lower noise levels on the flap underside are, however, for all long flaps, due to mid and high frequency components (Figure 4.15, page 72). This indicates that the effect is that of shielding by the flap of high frequency radiation from sources in the primary mixing region. In the absence of the flap these sources radiate symmetrically with a considerable convective amplification in $\theta = \pm 30°$

directions. The long flap prevents their radiation below the flap. Consequently the directivity polar on the flap underside is circular, as if generated from a simple point source. The fact is that the far-field below the flap is blind (or is it deaf?) to the source convection above the flap. This effect becomes clear upon examining the spectra of the sound radiated by the longest flap, $\delta_F = 132$ (Figure 4.19, page 80). Sound radiated in $\theta = -30°$, $-60°$ and $-90°$ directions is seen to be identical in spectral content and level which is smoothly decaying at higher frequencies. The sound radiated in any direction, θ, above the flap differs from the corresponding radiation in $-\theta$ direction below the flap only in the high frequency. At lower frequencies the corresponding spectra are identical thus producing an abrupt change in the decaying portion of the spectrum.

It is important to observe in Figure 4.16 (page 75) that the effect of increasing flap length for $\delta_F > 51$ is to decrease the OASPL only below the flap with little change. This would lead one to assume that the sound power output of the jet flap would decrease with increasing flap length. However, considering the fact that the maximum OASPL above the flap remains unchanged with flap length (in fact it increases slightly) and that the difference between the maximum OASPLs above and below the flap is about 5 dB at $\delta_F = 51$ and keeps increasing with flap

length, the overall sound power which is the integrated effect of the sound radiated in all directions will be dominated by the maximum OASPL above the flap and thus will not change appreciably for increases in flap length above $\delta_F > 51$. The overall sound power of the jet flap with $\delta_F = 51$ operating at a jet Mach number of 0.9 can, in fact, be seen in Figure 4.29 (page 107) to be equal to the sound power of the slot jet without the flap. Increased flap length would thus produce changes in the directional radiation characteristics without any change in the sound power output.

Since $\theta' = \pi$ in the sideline (XY) plane, the $\cos^2(\theta'/2)$ directivity factor for the scattered intensity predicts zero edge amplification effect in this plane. Neither can there be any radiation in this plane due to pressure dipoles. Neglecting viscous stresses, only quadrupoles can be expected to contribute to sideline radiation. Measurements (Figure 4.22, page 88), however, have shown increased in the OASPLs in XY plane due to the addition of a flap to the slot jet. Sound pressure levels in the sideline plane were generally above the slot jet levels for jet flaps with moderate lengths ($\delta_F < 20$ approximately). For a given slot jet the maximum sound levels in both the XZ and XY planes occurred at the same δ_F (around 10), although the OASPL increase in XY plane was considerably lower than the OASPL

increase in XZ plane. Furthermore the OASPL increases in the XY plane were greater in the convective lobe than in the normal directions. Based on the above arguments it is easy to attribute the increased OASPL in XY plane due to the noise generated in the secondary mixing region which was expected to be intense for moderate flap lengths.

Interestingly, jet flaps with $\delta_F > 20$ have lower sound levels in XY plane compared to those of the slot jet without the flap. This is because at the sideline plane observation points the jet flaps with long flaps appear like a half jet with only one mixing region which is the source of noise for radiation in these directions.

As a result of the edge amplification and reduced noise levels in the sideline direction, the spectral characteristics of the noise radiated in the sideline plane relative to that radiated in the flyover plane are different for the slot jet and the jet flap. Thus for the slot jet (Figure 3.4, page 31) the reduced levels in the sideline plane are due to high frequency reduction in all directions whereas for the jet flap with $\delta_F = 51$ (Figure 4.24) the reduction in the sideline plane is from low and mid frequencies in the 90° direction and from high frequencies in the 30° direction.

Arguments justifying the measured OASPL directional characteristics of jet flaps in the sideline and flyover

planes can be used to explain the OASPL directivities in the nozzle exit (YZ) plane (Figure 4.25, page 97). The major features of these measurements are the clear presence of edge noise in the normal directions for all flap lengths, maximum levels through the plane for δ_F around 10, increased sideline radiation for $\delta_F < 15$ and reduced sideline radiation for $\delta_F > 15$ and generally larger increases in the normal directions than in the sideline directions.

The acoustical compactness of the flap surface is determined by the acoustic wavelength corresponding to the peak frequency of the sound radiated from the mixing region of the slot jet. The sound radiated in $\theta = 90°$ direction by slot jets used in the present investigation peaks around 8 kHz. This corresponds to an acoustic wavelength of about 4 cm. The flap lengths on the jet flaps varied from 2.03 cm to 47.6 cm so that the flap surfaces, with the exception perhaps of the shortest flap, cannot be considered to be compact. Results of Curle's analysis [26] are thus not likely to apply directly. Directional characteristics of the jet flap have already been seen to be different from that of the compact surface dipole. Sound intensity variation with jet velocity for jet flaps can also be expected to be different from that of the classical dipole. Referring back to Figure 4.29 (page 107) it is noted that although the sound output variation with

jet velocity for jet flaps depends on the flap length, most flaps have a near sixth power variation. This sound output, however, includes the contribution of the jet noise also. The sixth power variation is thus no confirmation of Curle's or Hayden's dipole sources. More likely it is a combination of the jet noise contribution that varies as U^8 and the field scattered from the flap trailing edge which according to Ffowcs Williams and Hall [8] varies as U^5 Interestingly the shortest flap ($\delta_F = 5.63$) which was suspected to be compact has sound power output varying as nearly the seventh power of jet velocity. A combination of two fields - one varying as U^8 and the other as U^6 (as for a compact surface) could lead to a U^7 variation of the total sound output. Reference to the OASPL directivities in the flyover plane (Figure 4.11 and 4.12, pages 63 and 64 respectively) further shows that the increase in OASPL of slot jet due to the flap is nearly the same in $\theta = +90°$ and $\theta = +30°$ directions as opposed to the typical edge noise field which has larger sound levels in $\theta = \pm 90°$ directions. OASPL directivities in YZ plane (Figure 4.25, page 97) indicate increases (although small) in the sideline directions thus suggesting the presence of secondary mixing region noise.

The only attempt to predict the sound output of the jet flap configuration as a function of the flap length has been that of Hayden's [31]. Based on the diffracted

dipole model the sound power output of a jet flap was found to vary as $U_m^6 \delta w_c$ where U_m is the maximum velocity, δ the boundary layer thickness and w_c the wetted span, all at the trailing edge. Measured variations of each of these parameters with flap length upon substitution in the above formula showed the sound power to increase by 3 dB with doubling of flap length in the potential core regime (i.e. $\delta_F < 10$) and to decay by 3 dB per doubling of flap length in the regime $\delta_F > 10$. Unfortunately the fact that the sound power output of a jet flap configuration is maximum when the flap length is nearly equal to the potential core length was not stressed. However, the recognition of different variations of the overall sound power in the two regimes $\delta_F < 10$ and $\delta_F > 10$ agrees with the findings of the present investigation (Figure 4.27, page 101) and constitutes an important contribution to jet flap acoustics. Present measurements do not agree quantitatively with the predictions of Hayden [31] for first, the fluid dynamic parameters may not vary as used in the prediction and second, the jet velocity dependence of the surface generated sound might be different.

Hayden's approach tends to suggest that in the potential core regime since the maximum velocity is invariant, the increase in overall sound power with flap length is due to the increasing boundary layer thickness at

the trailing edge whereas for $\delta_F > 10$ the maximum velocity decays rapidly with δ_F and becomes the dominating term in $U_m^6 \delta w_c$ so that the reduction in overall sound power with increasing flap length is due to the reduced velocity at the trailing edge. Measurements of the present investigation indicate that short flaps with the trailing edge well before the potential core termination behave as compact surfaces and thus augment the slot jet noise by dipole sources. For jet flaps of moderate lengths, the flap surface is non-compact and edge amplification occurs. Edge amplification being acoustically more efficient (by one order) than the compact dipole causes further noise increase. For all longer flaps edge amplification continues to be a dominant mechanism. However, it is only for flaps with $\delta_F \gtrsim 10$ that the edge field can reinforce the jet noise field in its peak frequency band and this causes the OASPL increase to be maximum for flaps in the said length range. Edge amplification for longer flaps occurs only at lower frequencies. Furthermore increased flap length results in reduced intensity of turbulence in the secondary mixing region and a consequent reduction of sound generation in that region leaving only one mixing region as a major noise source. This is the cause of the reduction in the sound output of jet flaps for $\delta_F > 10$.

The situation at high jet Mach numbers as seen in the present measurements is different. The overall sound power of jet flap increases very rapidly with flap length in the potential core regime and decays for $\delta_F > 10$, again rapidly. For very long flaps ($\delta_F > 25$) only, the sound power variation with flap length is similar to that at low jet Mach numbers. The different behaviour at high jet Mach numbers ($M \geq 0.7$) is due to the presence of a phenomenon not observed at lower Mach numbers. It is the tone generation phenomenon of jet flaps with $\delta_F \gtrsim 10$ that is being referred to here. Comments regarding the cause of these tones will be deferred to the next chapter.

CHAPTER 5

PRESSURE CORRELATIONS AND TONE CHARACTERISTICS

Information based on far-field measurements regarding the location of prominant noise sources can only be spectulative. An increasingly popular technique for obtaining definitive information about the sources is the causality cross-correlation technique developed by Siddon [35] which uses the fact that there is a cause and effect relationship between the flow fluctuations and the far-field sound. Furthermore it takes some finite time for the flow fluctuations to manifest as sound in the far-field. Thus the cross-correlation between the far-field radiated sound and the source fluctuation variable should give some information about the source. Application of this technique to surface generated noise has also been described by Siddon [36]. Starting with Curle's solution he shows that the strength of surface generated sound can be determined by measuring the pressure fluctuations at various points on the surface and cross-correlating them with the far-field pressure. Details of the analysis are presented in the Appendix.

The causality cross-correlation technique was used in the present investigation to locate the major noise generating regions in the jet flap flow field. Since

the point of interest was to determine the effect of the flap on the acoustic characteristics of the slot jet the fluctuating pressure on the flap surface was correlated with the far-field sound. This was done as described in Chapter 2 for the jet flap with $\delta_F = 18$ at a jet exhaust Mach number of 0.9. The surface pressure fluctuations were monitored at three locations by flush mounted 0.64 cm microphone. The three locations were chosen so that one is within the potential core, one at the core termination and one near flap trailing edge, the latter two having been suggested by the observation that the far-field acoustic characteristics of jet flaps depend on the location of the flap trailing edge relative to the termination of the jet potential core. Autocorrelations of the surface pressure and the far-field sound were also obtained to normalize the cross-correlations. It should be noted that all the correlation plots included here are as obtained at the correlator "output" and plotted on a XY plotter. Efficient utilization of the correlator required different input attenuations for different input signals and this varied the vertical scale of the output. Thus no two correlation curves are directly comparable even if they form different parts of the same figure (unless explicitly indicated). Amplitudes of interest are recorded in the figures.

Autocorrelations of the surface pressure fluctuations measured at three locations on the jet flap with $\delta_F = 18$ are shown in Figure 5.1, the corresponding spectra being given in Figure 5.2. The pressure spectrum from the surface microphone at x/h = 6.3 (under the potential core) is narrow-band with peak frequency in the 6300 Hz one third octave band. The corresponding auto-correlation function is typical of narrow-band random noise. It shows a decaying periodic nature before reaching zero for large delay times. For location near the termination of the potential core, x/h = 9.4, the surface pressure spectrum is only slightly broader than that at x/h = 6.3 but has higher levels at all frequencies. The auto-correlation, likewise, has a shape similar to that at x/h = 6.3 but has a higher value at zero delay time (which is the mean square fluctuation level) and smaller secondary peaks. Pressure fluctuations near the flap trailing edge (x/h = 17.5) are fairly broad-band. This is because the potential core does not exist at this location and the surface pressure field is greatly affected by the broad-band fluctuation in the jet mixing region. The corresponding autocorrelation function is typical of broad-band random noise. The overall fluctuation pressure level, as given by the "linear" on the spectrogram and the autocorrelation function value at zero delay time, is higher near the trailing edge than at both upstream

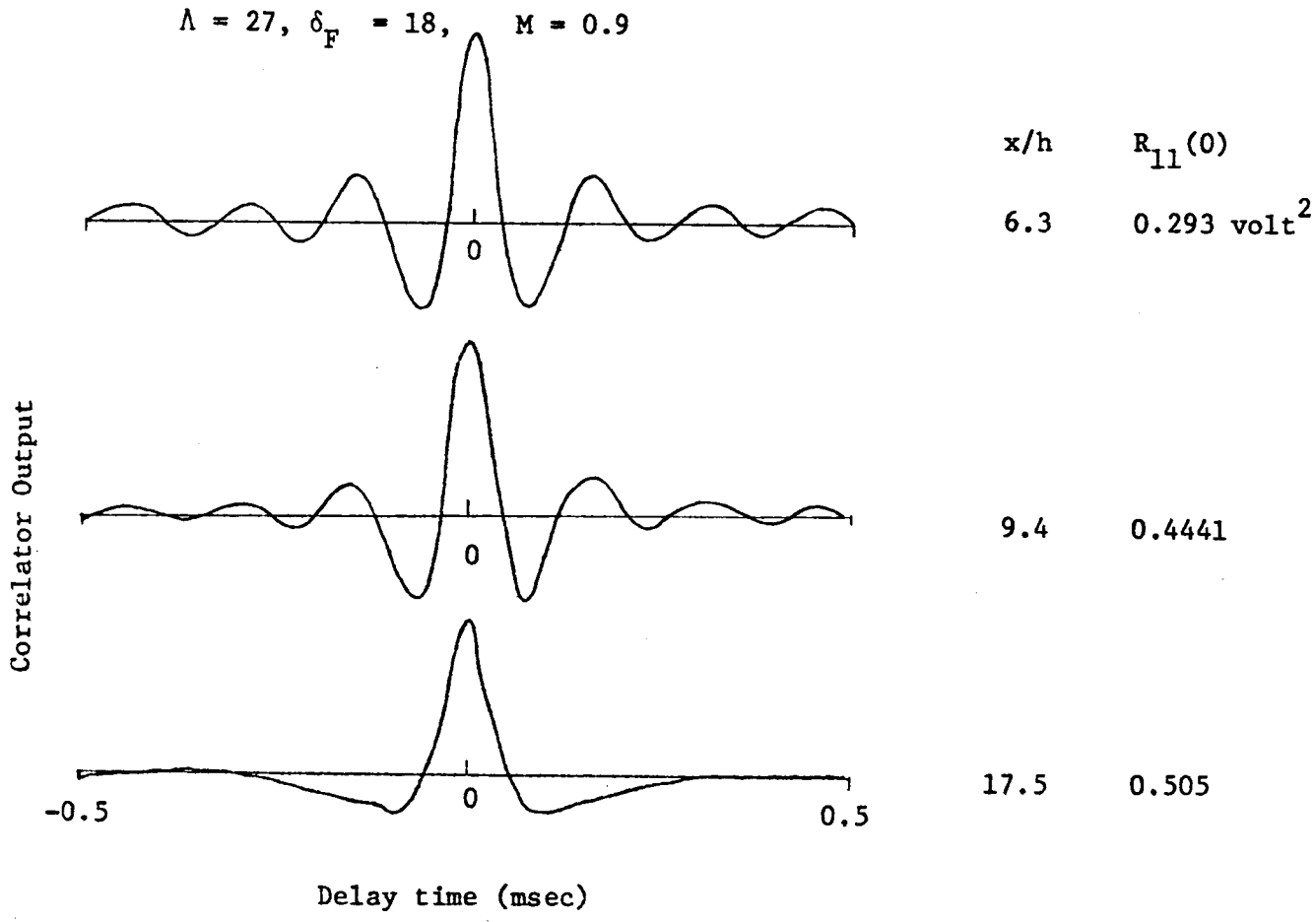


Figure 5.1. Surface pressure autocorrelations for $\delta_F = 18$.

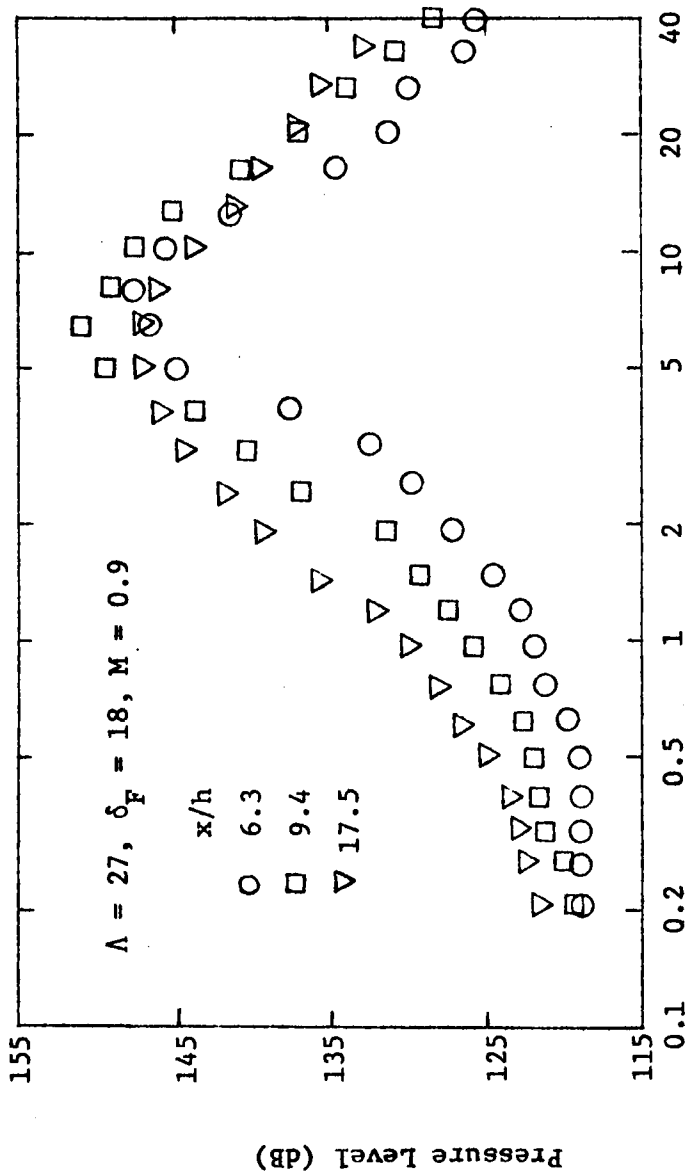


Figure 5.2. Surface pressure spectra for $\delta_F = 18$.

locations. Fluctuations in the peak frequency band are, however, largest near the core termination (x/h = 9.4).

Cross-correlation of the surface pressure fluctuations with the far-field acoustic pressure monitored by a microphone at $\theta = +60°$ in the flyover plane are presented in Figure 5.3. In order to evaluate the far-field acoustic contribution from unit area of flap surface around the surface microphone, the slope of the cross-correlation function at a delay time corresponding to the time required by the pressure signal at the surface to reach the far-field microphone as sound must be determined. It is, however, difficult to exactly determine this acoustic delay time. Siddon [36] has shown that the correlation of the surface pressure with the far-field sound will have an antisymmetric shape centered about the acoustic delay time. Thus the zero crossing time (τ_o) of the cross-correlation function must be an indication of the acoustic delay time. The zero crossing time between the positive and negative peaks of the cross-correlation functions for the jet flap is seen in Figure 5.3 to depend on the surface microphone location. It is least when the surface microphone is closest to the trailing edge. Furthermore the maximum correlation value increases as the surface microphone is moved towards the trailing edge. This suggests the presence of a convecting pressure field that generates

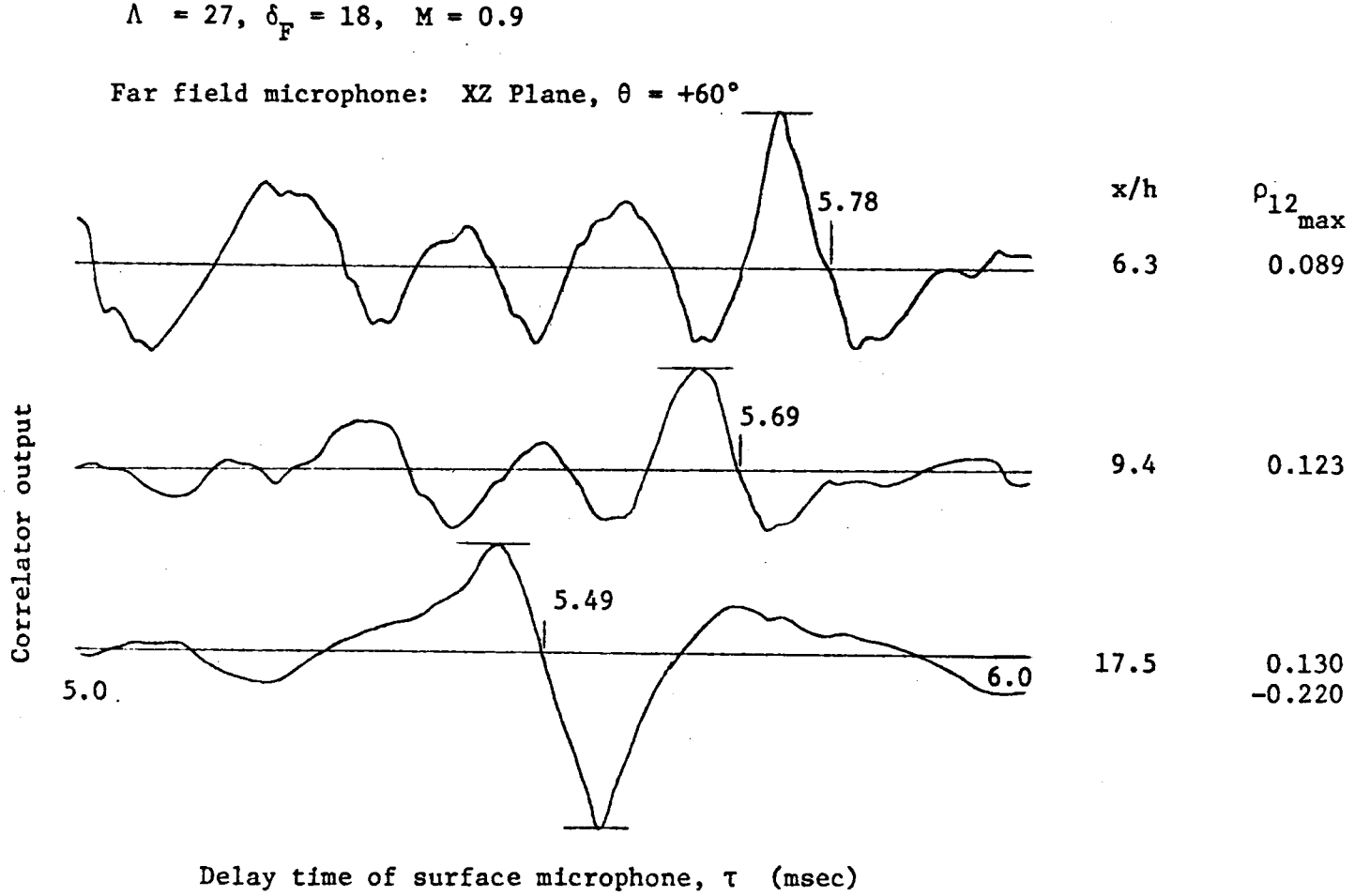


Figure 5.3. Cross-correlations of surface pressures with far-field sound.

noise upon encountering the flap trailing edge. This pressure field is presumably caused by eddies convecting in the jet mixing region.

If U_c represents the eddy convection velocity, x_1 the distance of a surface microphone from the flap trailing edge, r the distance to the far-field microphone from flap trailing edge and a_o, the speed of sound in the ambient medium, the x_1/U_c gives the time for an eddy to convect from a surface microphone location to the flap trailing edge and r/a_o represents the acoustic propagation time from the trailing edge to the far-field. The sum $x_1/U_c + r/a_o$ should equal the delay time (τ_o) of the surface microphone at which the cross-correlation crosses the zero line. Figure 5.4 shows this dependence between the measured zero crossing time and the surface microphone location, $x/\ell_F = 1 - (x_1/\ell_F)$. From the difference in zero crossing times of the surface microphones at x/h = 6.3 and 9.4, the eddy convection velocity can be determined to be 0.6 U where U is the mean jet exit velocity. This velocity increases to 0.7 U after the core termination. It must be mentioned that Davies et al [17] found (from hot wire measurements) the convection velocities in the potential core and in the region of maximum turbulence intensity in the jet mixing region of a round jet to be equal to 0.6 U. This suggests that the fluctuations in the potential core are associated with a field convecting

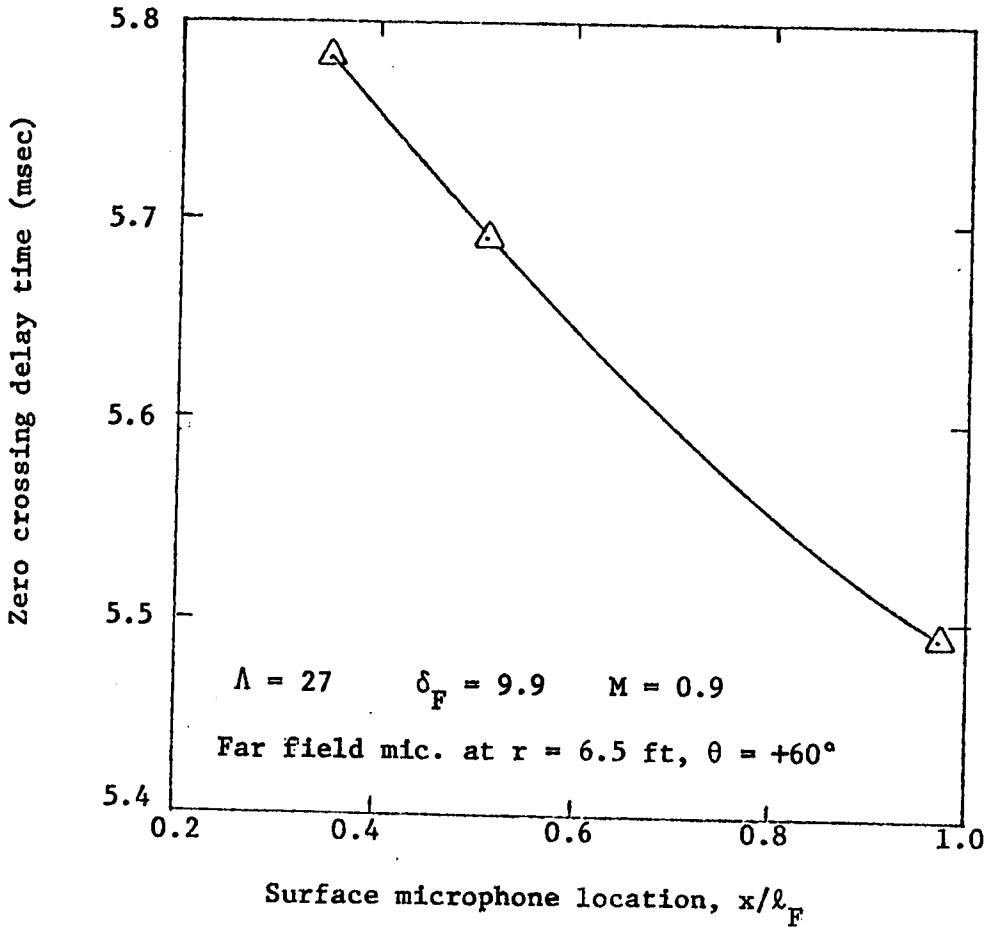


Figure 5.4. Correlation zero crossing delay time variation with surface microphone position.

in the jet mixing layer. It might well be that the fluctuating pressure field on the flap surface is also associated with the field convecting in the primary mixing region. Lau et al [37] have modeled this structure of the jet by an axial array of discrete vortices convecting downstream at U_c = 0.6 U in the region of maximum turbulence intensity. The secondary peaks (that occur, at periodic intervals corresponding to the peak frequency of the turbulence spectrum) in the cross-correlation of the surface pressure at x/h = 6.3 and the far-field sound (Figure 5.3) might be an indication of such a structure in the primary mixing region with each eddy radiating to the far-field directly as well as after interaction with the flap trailing edge. Higher amplitude of the last peak would then indicate that the edge noise field is stronger. The "surface dipole strengths" for the locations x/h = 6.3, 9.4 and 17.5 were determined by Siddon's formula (using the slope of the cross-correlations at zero crossing near the absolute peak) to be in the proportions 0.36 : 0.94 : 1.00. This again suggests the trailing edge region to be an important source of noise.

Cross-correlations of surface pressure and far field sound both filtered in their peak frequency band (which is the one third octave band with center frequency of 6300 Hz) are shown in Figure 5.5. It is interesting to note that the peak correlation value is maximum when the surface

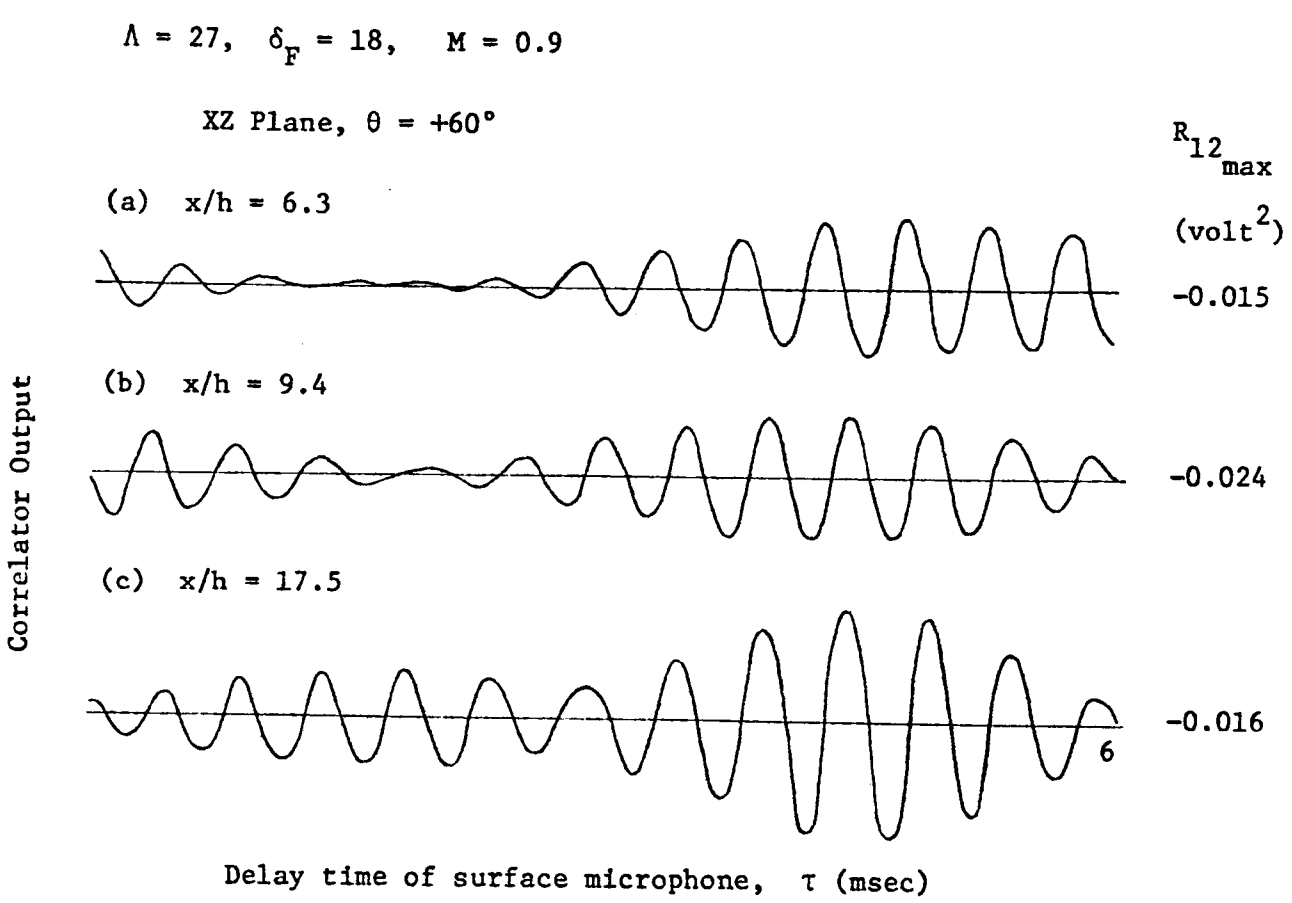


Figure 5.5. Cross-correlation of surface pressures with far field sound in 6300 Hz one-third octave band.

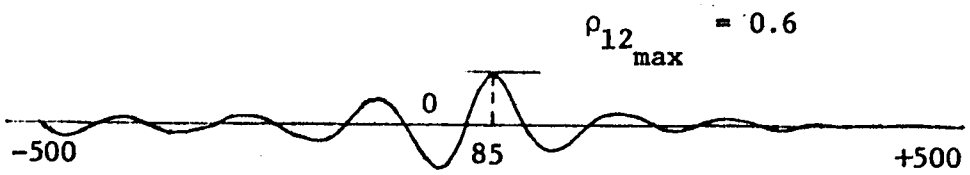
microphone is near potential core termination (x/h = 9.4) on the flap surface as opposed to the trailing edge position for the unfiltered correlations. Recall that the flap surface pressure spectra (Figure 5.2) showed the pressure fluctuations in the 6300 Hz one third octave band to be maximum near the potential core termination.

Cross-correlation of pressure fluctuations measured by two surface mounted microphones is a popular technique in turbulent boundary layer research (e.g. Willmarth [38]). This method was used here to obtain the convection velocity of the fluctuating pressure field on the flap surface. Correlations of the surface pressure at x/h = 6.3 with that at x/h = 9.4 are presented in Figure 5.6 for both broad-band and 6300 Hz one third octave band filtered signals. High coherence of the pressure field is evident from the high value of the maximum normalized correlation coefficient. The correlations have a positive maximum when the upstream microphone is delayed by 85 μsec which corresponds to a convection velocity of U_c = 0.61 U. Recall that the convection velocity obtained from cross-correlations of surface pressures with the far-field pressure was 0.6 U. This good agreement supports the idea that the convecting pressure pattern generates considerable sound by interaction with the flap trailing edge. This is the edge noise phenomenon which was used to explain the far-field acoustic measurements in Chapter 4. The presence of

Microphone A: x/h = 6.3, Microphone B: x/h = 9.4

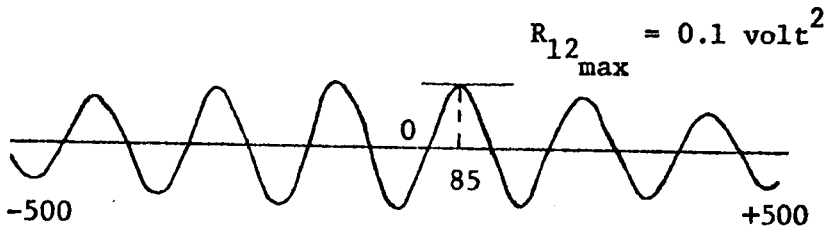
Λ = 27, δ_F = 18, M = 0.9

(a) Broad Band



Delay time of microphone A, τ (sec)

(b) Filtered: 1/3 octave 6300 Hz Band



Delay time of microphone A, τ (μsec)

Figure 5.6. Cross-correlations between flap surface pressures.

the secondary mixing region noise was not explicitly verified here. However, as stated earlier, such phenomenon has been documented in literature. In fact a new school of thought by Tam and Reddy [39] considers this as the dominating noise source for upper surface blown flap systems. It is contended here that for a jet blown flap all the mechanisms, namely, jet noise, edge noise, secondary mixing noise and scrubbing noise co-exist with the dominant mechanism being determined by the flap length relative to the nozzle size.

Pressure correlations, which provided some evidence of the edge effect in the jet flap with $\delta_F = 18$, produced no information on the cause of tone for the jet flap with $\delta_F = 9.9$ as shown below. The surface pressure spectra at x/h = 6.3 and 9.4 for the jet flap with $\delta_F = 9.9$ and the jet exhausting at M = 0.9 are shown in Figure 5.7. Both are narrow band with a very intense component in the 6300 Hz one third octave band. This is the frequency of the tone in the far field. The high levels of the surface pressure spectra could be due to the overriding influence of the sound. It can be noticed in Figure 5.8 that the surface pressure spectra at a fixed location, x/h = 6.3, are nearly identical except in the 6300 Hz one third octave band for the three flaps with $\delta_F = 6.83$, 9.9 and 18. Correlations (both auto and cross) of the fluctuating pressure field with a dominant "discrete"

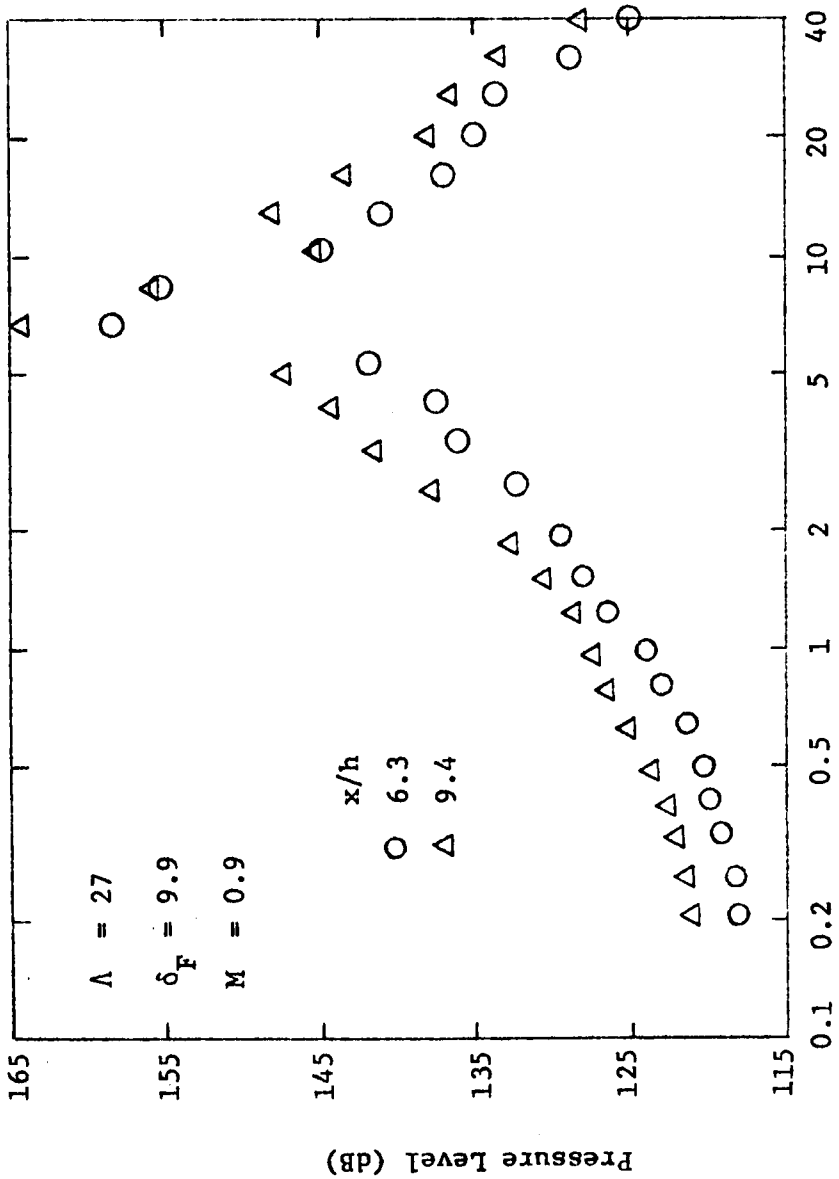


Figure 5.7. Surface pressure spectra for $\delta_F = 9.9$.

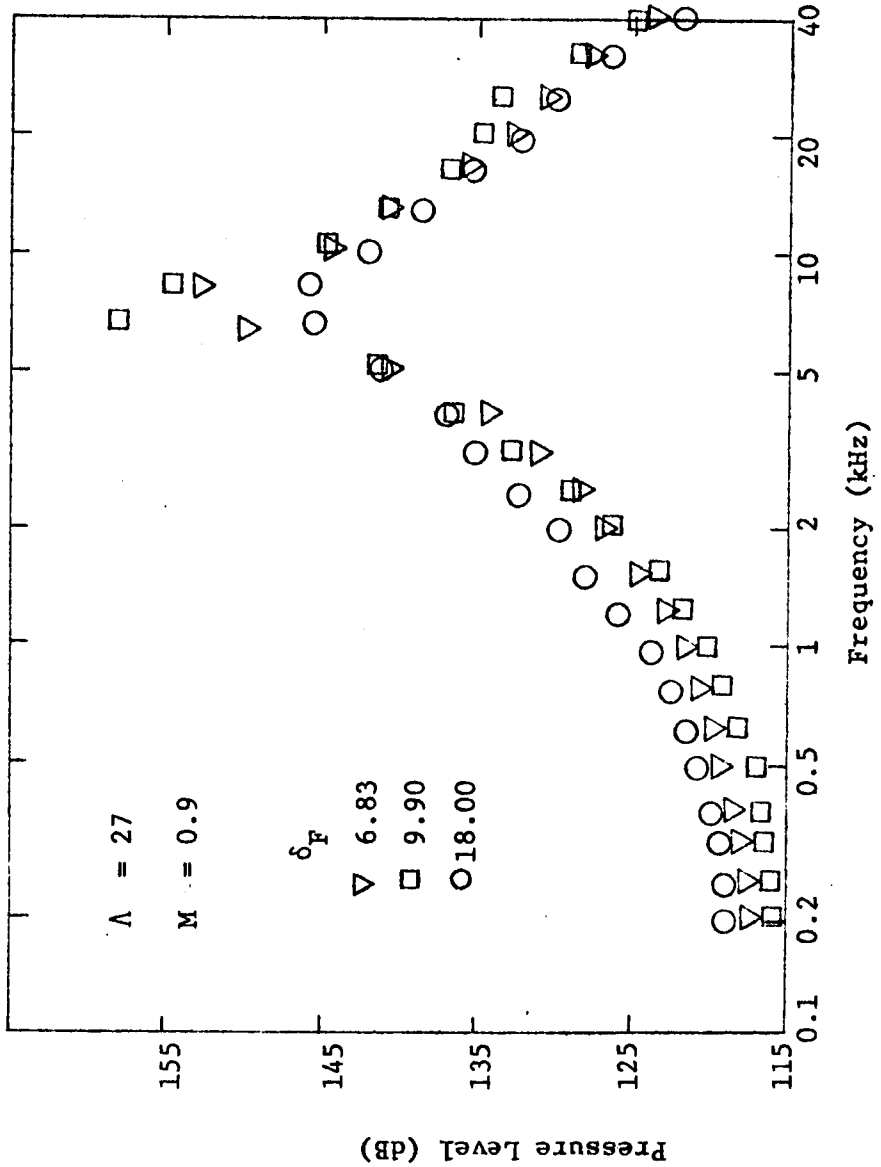
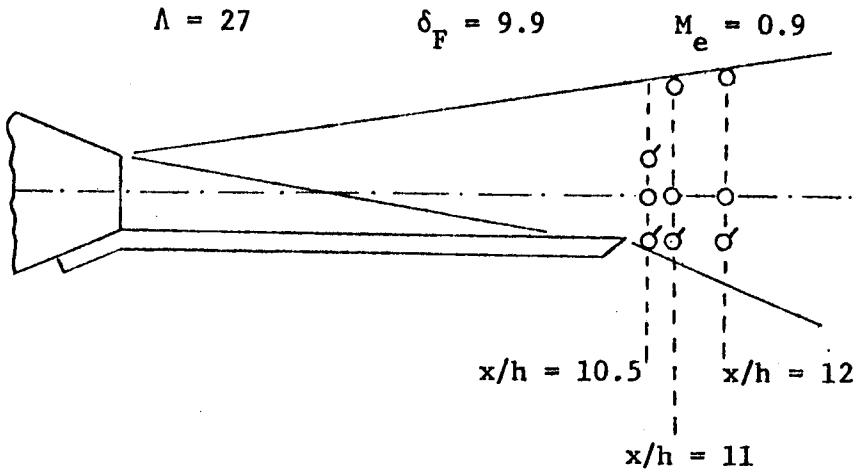


Figure 5.8. Surface pressure spectra at x/h = 6.3.

frequency (or narrow band) component yielded perfectly periodic functions thus losing the meaning of the delay time. Since no useful information could be derived out of these correlations they are not presented here.

Probing of the flow with a hot film anemometer near the vicinity of the flap trailing edge (Figure 5.9) for the jet flap, of flap length $\delta_F = 9.9$, at M = 0.9 showed the velocity fluctuations at certain locations to be very periodic. The periodicity in the turbulence was observed by recording the turbulence spectrum and the autocorrelation from the hot film signal. As indicated in Figure 5.9 the velocity fluctuations were highly periodic at stations in the secondary mixing region in line with the flap surface. The frequency of these fluctuations coincided with the tone frequency (6300 Hz one third octave band). The first harmonic (12,500 Hz one third octave band) was usually present too, but had a lower intensity. This is illustrated in Figure 5.10 which depicts the spectrum of turbulence in the secondary mixing region and one slot height downstream of the flap trailing edge. For locations along the jet centerline the turbulence spectra were generally broad-band with a small bulge in the 6300 Hz one third octave band. Turbulence spectra with the hot film at the edge of the primary mixing region had no indication of periodic fluctuations. However, the periodicity was strongly observed at the



ơ Velocity autocorrelation periodic at these points

O Velocity autocorrelation non-periodic

Figure 5.9. Geometry for hot wire measurements.

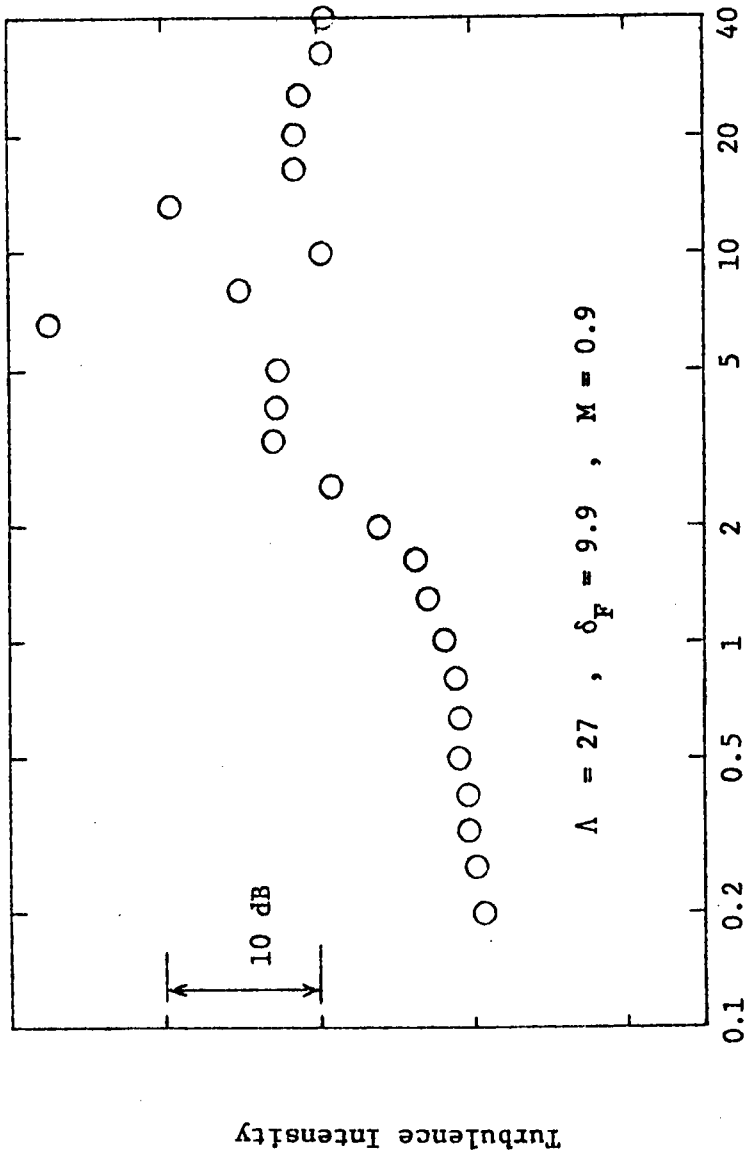


Figure 5.10. Turbulence spectrum in the secondary mixing region - one slot height downstream of flap trailing edge.

location along the centerline of the primary mixing region. In view of the shadowgraphic observations of Figure 4.34 (page 125) the measured turbulence characteristics are not surprising. Presented in Figure 5.11 are the sound power density spectra of jet flaps whose shadowgraphs are given in Figure 4.34. Simultaneous examination of these spectra and the corresponding shadowgraphs immediately reveal the fact that vortical structures in the secondary and primary mixing regions are present only for jet flaps that generated intense tones. Turbulence measurements further confirm the flow instabilities in the secondary mixing region.

Additional information on the flow field of the jet flap with $\delta_F = 9.9$ was obtained by means of a high speed shadowgraphic movie as described in Chapter 2. It was filmed at an average speed of 3000 frames per second. The movie clearly showed lateral oscillations of the potential core near the flap trailing edge. Vortex shedding in the secondary mixing region was, however, not clearly evident. It thus appears that the instability of the jet or the vortex shedding or both are the cause of the tone.

To further investigate the phenomenon simple experiments were designed in which the flow structure in the secondary mixing region or in the primary mixing region could be separately altered by some modification to the jet flap configuration. Two simple ways by which the flow

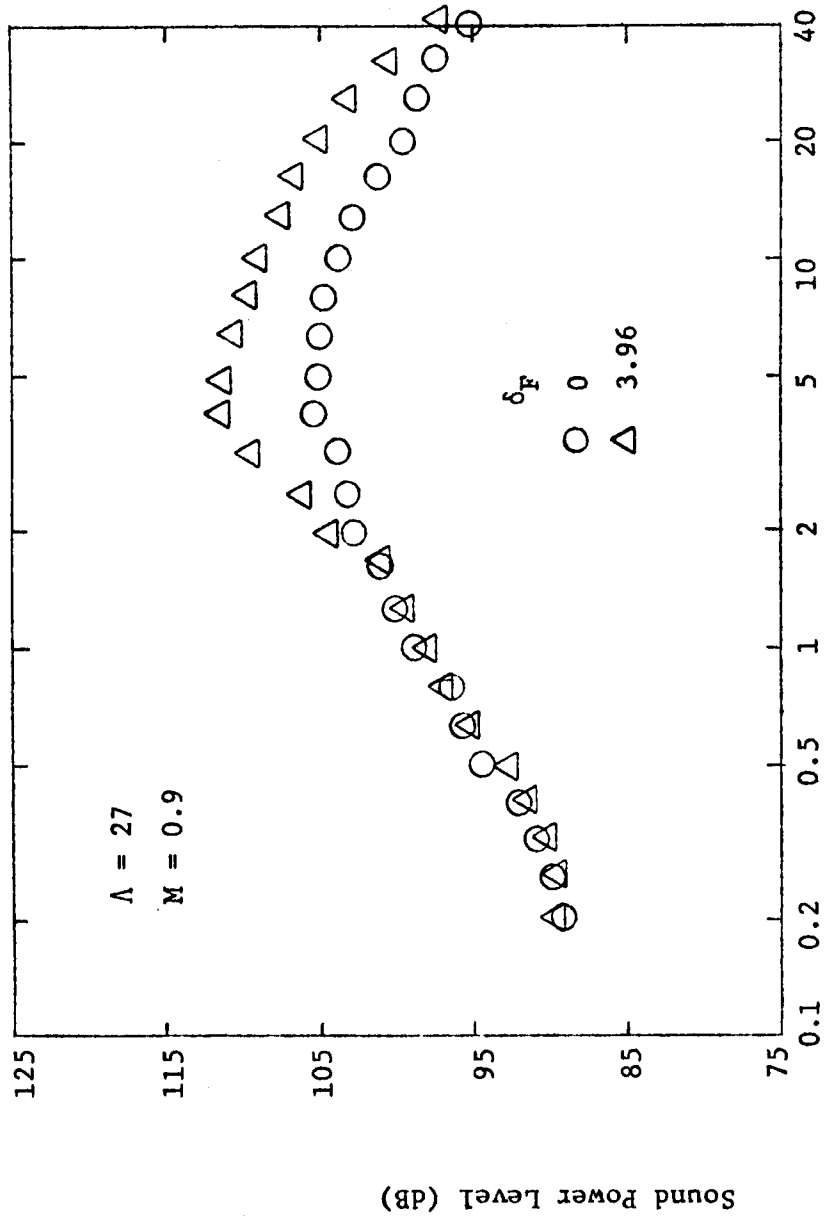


Figure 5.11. Sound power spectra corresponding to the shadowgraphs of Figure 4.34 (page 125).

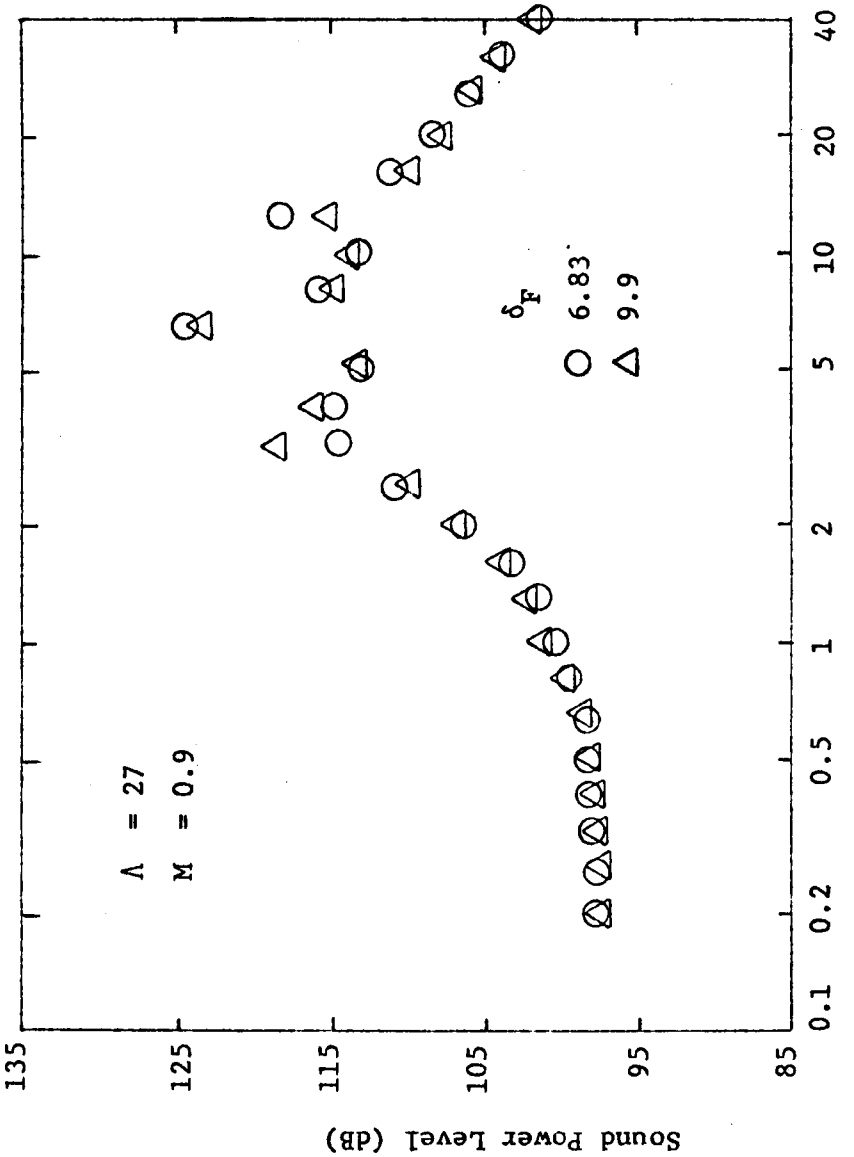


Figure 5.11. continued.

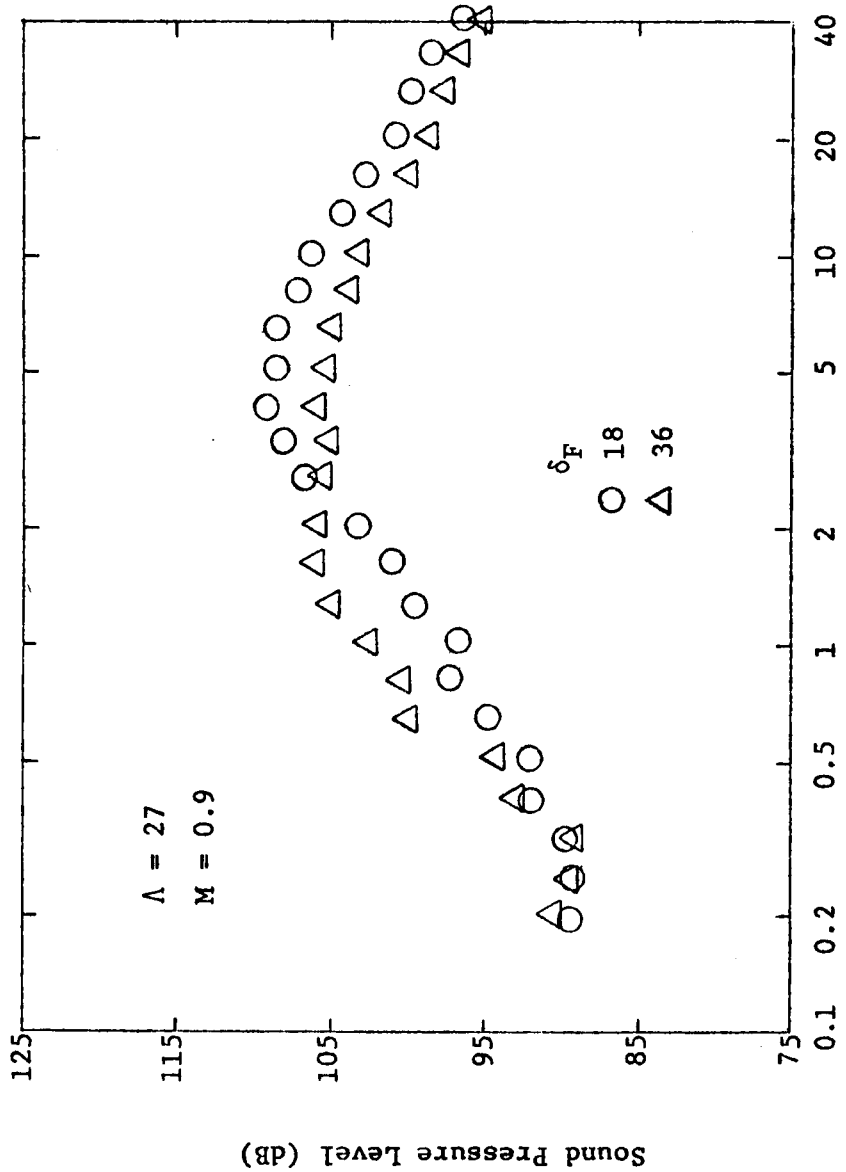


Figure 5.11. continued.

structure in the primary mixing region could be modified are by inserting a trip wire or nail tip into the jet at nozzle upper lip and by roughening a portion of the nozzle upper contour (on the flow side). Analogous to these two ways are the insertion of a trip wire or nail tip into the flow at the flap trailing edge and the roughening of a portion of the flap surface near its trailing edge that would change the structure of the secondary mixing region. These simple modifications were tried on the jet flap with $\delta_F = 9.9$ with interesting results.

It is clear from Figures 5.12 and 5.13 that while roughening a portion of the flap surface near its trailing edge or introduction of a nail tip into the flow at the trailing edge did not affect the tone or acoustic output of the jet flap, roughening the nozzle upper contour or insertion of a trip wire into the flow at the nozzle upper lip totally eliminated the tone and resulted in a considerable decrease in the total sound power output. The trip wire experiments were conducted in the free field while the roughened nozzle and roughened flap experiments were conducted in the reverberation room. In Figure 5.12 it can be noted that when the tone is eliminated by the trip wire the surface pressure fluctuations also reduce considerably. Shadowgraphs were obtained for the roughened nozzle contour experiment to visualize the effect on the flow structure. Figure 5.14 shows the shadowgraphs for the

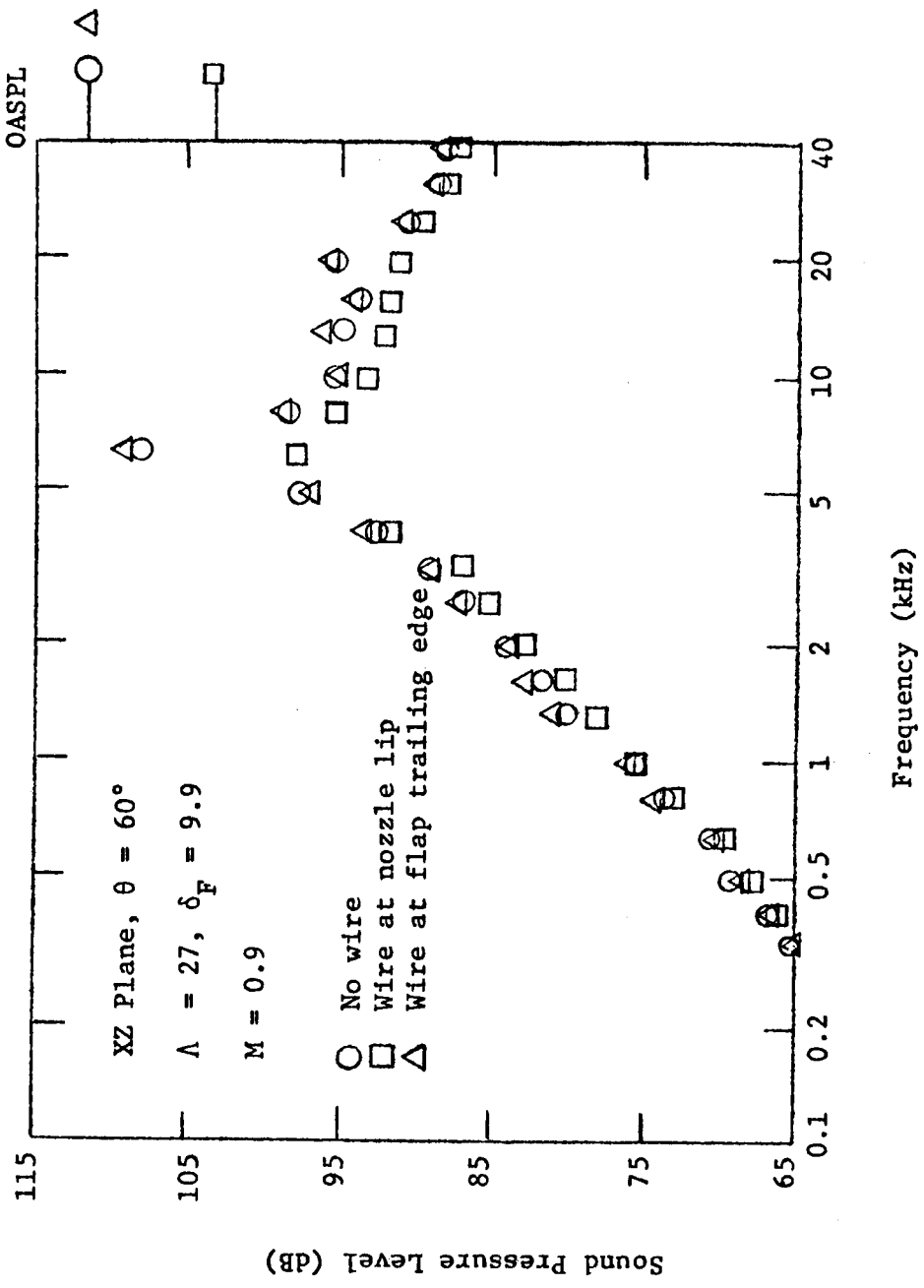


Figure 5.12. Tone alleviation by trip wire.

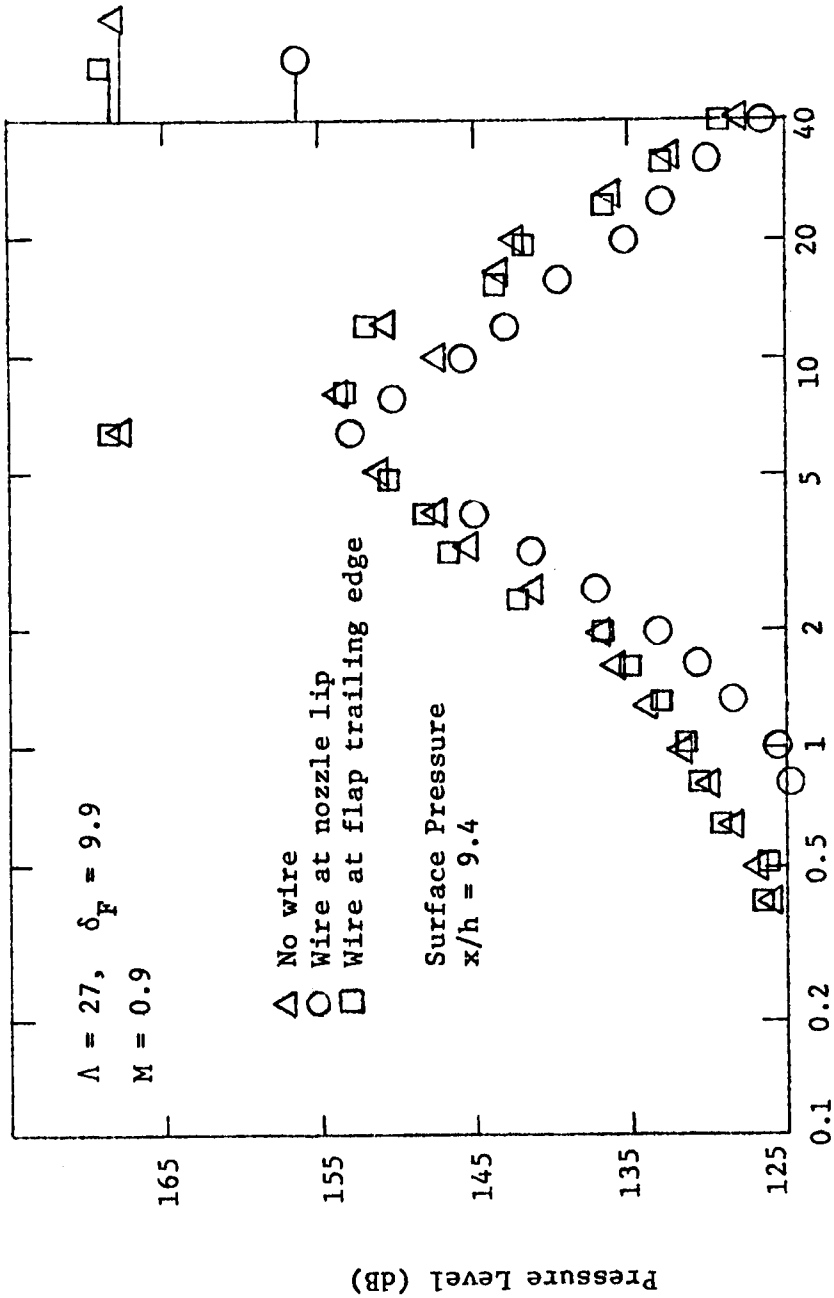


Figure 5.12. continued.

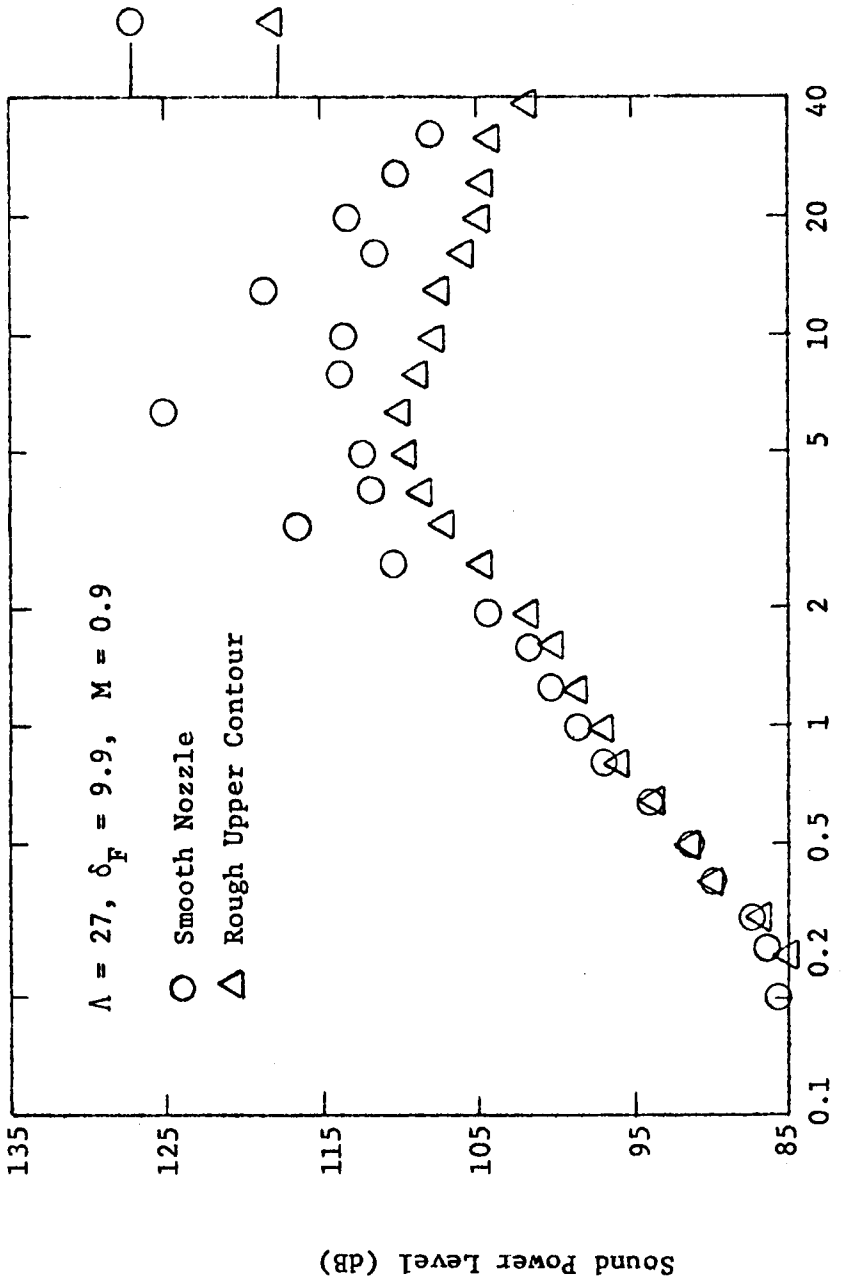


Figure 5.13. Tone alleviation with roughening.

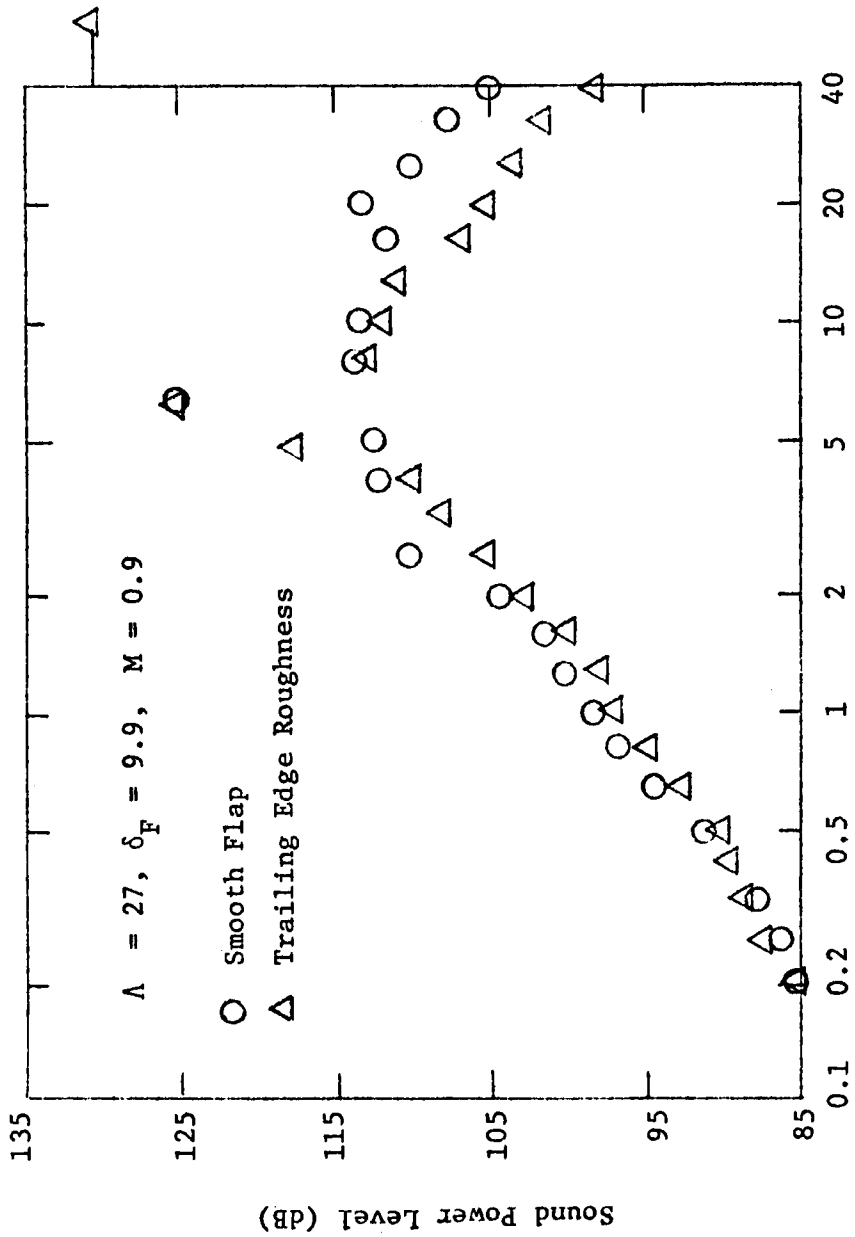


Figure 5.13. continued.

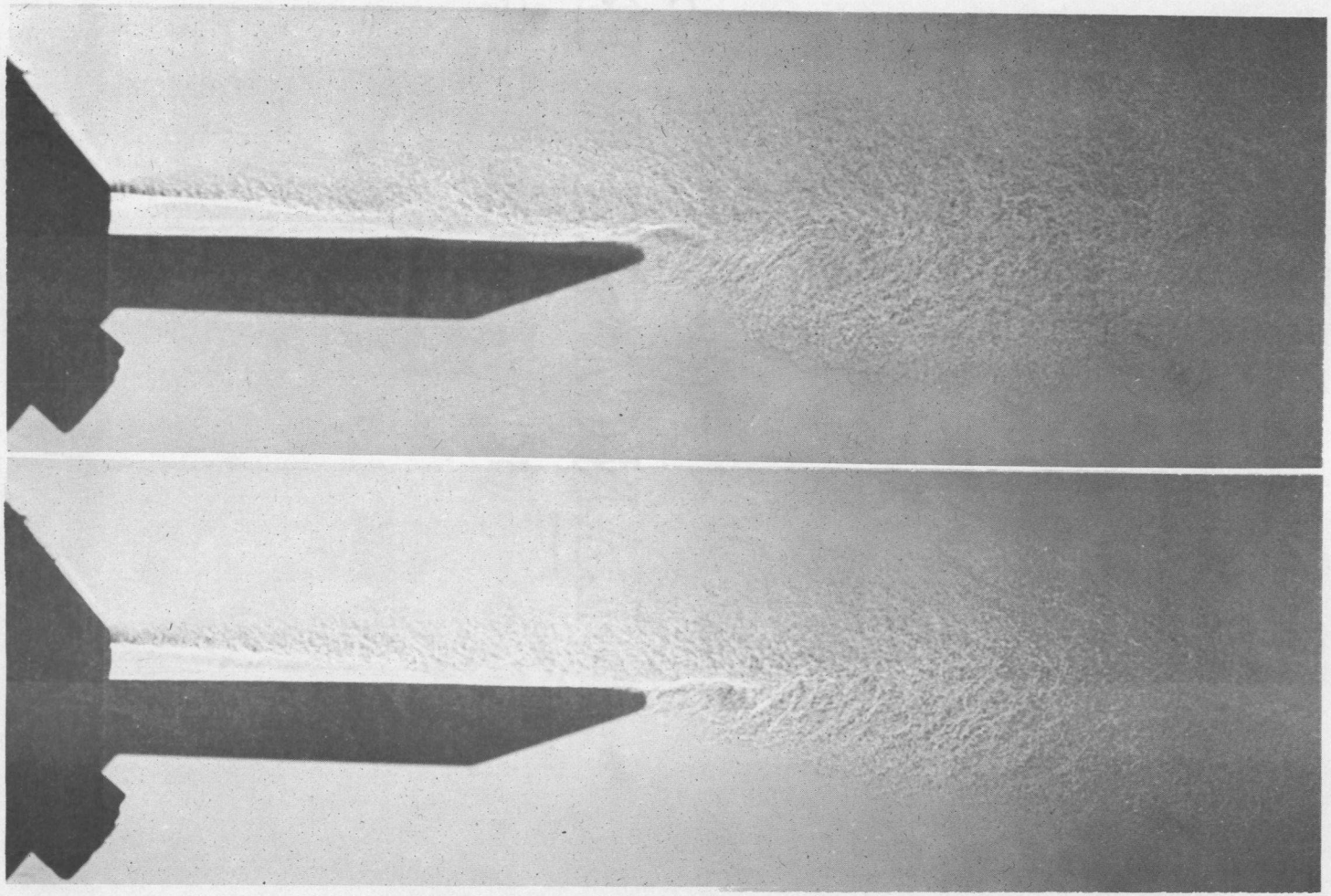


Figure 5.14. Shadowgraphs of the δ_F = 9.9 jet flap at M = 0.9.

jet flap δ_F = 9.9 at M = 0.9. In the top picture the nozzle contour is smooth and corresponds to the configuration that generates tone. The presence of vortex shedding from the trailing edge and large scale vortical structures in the primary mixing region engulfing fluid from the potential core are evident. In contrast, when the nozzle upper contour is roughened (bottom picture) the large scale structures are totally absent and the potential core is clearly seen to terminate on the flap surface. The secondary mixing region still seems to have intense turbulence. It is appropriate to mention here that although not clearly visible in the top shadowgraph of Figure 5.14, the jet mixing layer above the flap becomes turbulent only about half a nozzle height downstream of the nozzle exit. This was observed by taking shadowgraphs in which the flap surface was mirrored and the spark light shone across it (rather than along it) to obtain a picture of the flow over the entire flap span. Unfortunately this picture is not of reproducible quality and is therefore not included here.

These experiments and shadowgraphs thus suggest that the structure or instability of the flow above the flap surface, observed as a flapping potential core in the high speed movie, is reponsible for the tone. The trip wire or roughness on the contour has the effect of introducing artificial turbulence that might help

to stabilize the jet. There are indications that the instability is acoustically excited. For example, it was possible, by simply holding a plate above the nozzle so that acoustic waves are reflected back to the nozzle exit, to trigger the instability even in the case of the jet flap with roughened nozzle. This can be seen by comparing the shadowgraph of Figure 5.15 with bottom shadowgraph of Figure 5.14. The oscillating nature of the potential core is evident in Figure 5.15. With this acoustic triggering of instability, the tone was reproduced. It must be mentioned that when the reflecting plate was so held as to direct the reflected sound further downstream of the nozzle exit the instability was not triggered. In the absence of a reflector plate, the instability must be triggered by the sound generated by the jet flap and incident on the nozzle exit. Herein is the reason why this phenomena is observed for certain flap lengths only. It was shown in Chapter 4 that the edge amplification noise is an important part of the noise generated by jet flaps. Edge noise further has a directivity factor given by $\cos^2 (\theta'/2)$ where $\theta' = 0$ is the upstream direction. This factor produces a pattern with maximum radiation from the flap trailing edge in the direction of the nozzle. It is this part of the edge noise that triggers the instability. For short flaps the instability does not occur becasue the edge noise is not a dominating source. For long flaps,

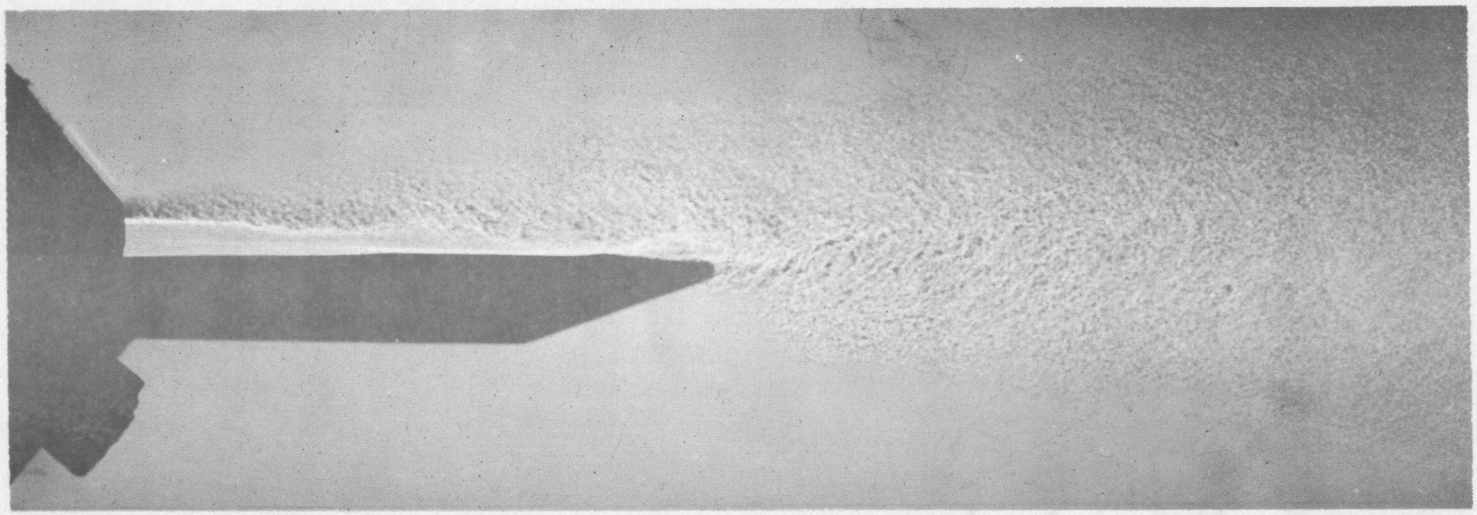


Figure 5.15. Shadowgraphs of the δ_F = 9.9 jet flap with rough nozzle and acoustic excitation by a reflector plate.

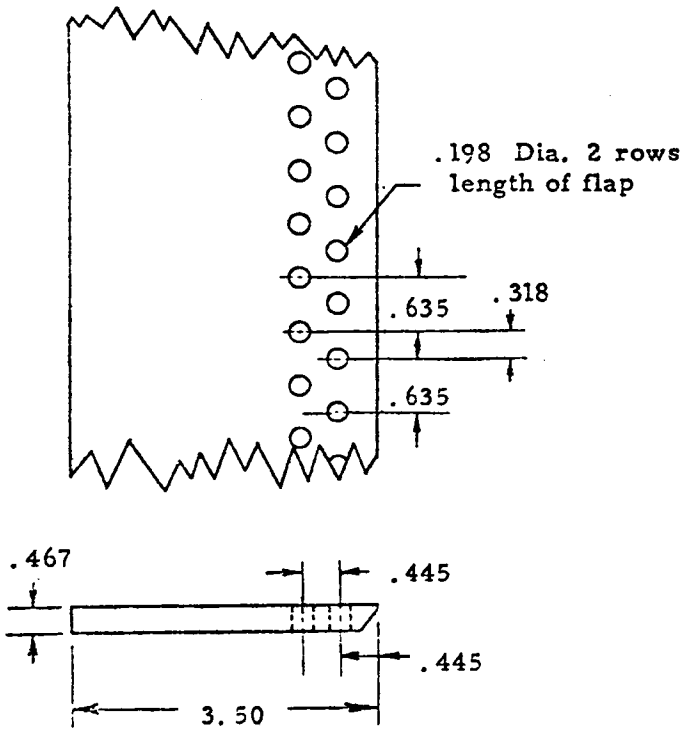
the flap surface provides a stabilizing effect. Furthermore for long flaps the noise field scattered from the edge has a frequency lower than the peak frequency of the fluctuating jet field so that efficient triggering may not occur. It is only for flap lengths of moderate length that the sound scattered from the edge can reinforce the flow fluctuations around their peak frequency. Since the peak frequency of the flow fluctuations is determined by the nozzle height, the flap length for which efficient reinforcement can occur at this frequency will also be governed by the nozzle height. In this connection it should be noted that tones were produced only when the flap length was round 7 to 10 nozzle heights and that the tone frequency scaled inversely with the nozzle height.

Thus the tone phenomenon has been identified as due to jet instability that is acoustically triggered. The triggering is achieved by sound scattered from the trailing edge in the direction of the nozzle. A way of eliminating this tone is to eliminate the exciting energy which amounts to reducing the edge noise. Making the flap short and compact is a possible solution, but may not be practical. Another possibility is creating a continuous transition from "existence of the wall" to "absence of wall" by a porous construction of the flap surface near the trailing edge region, thus reducing the edge effect. This was successfully tried on the jet flap with $\delta_F = 6.83$.

As shown in Figure 5.16 when two rows of holes were drilled near the trailing edge, the tone was totally eliminated and a broad-band reduction was obtained. Similar effect should be expected by having acoustically lined surface at the trailing edge.

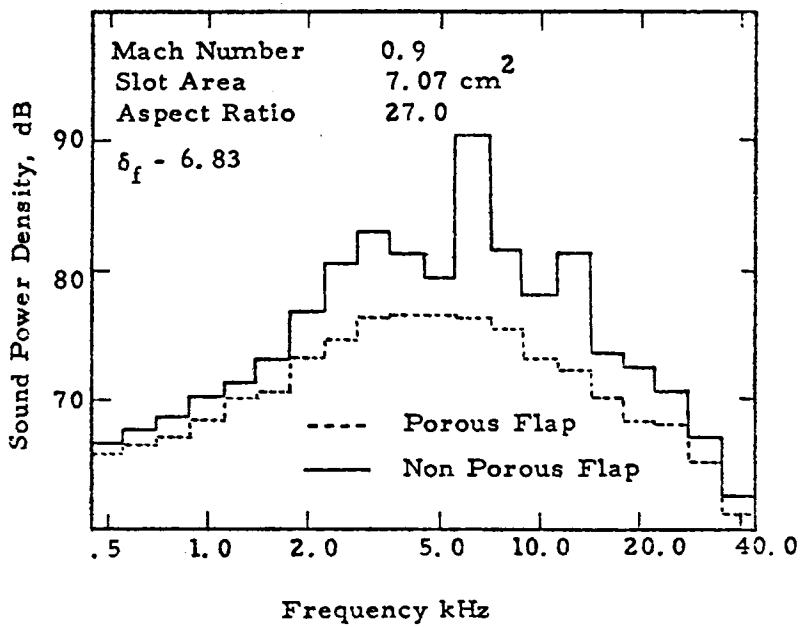
It should be noted that at M = 0.9 for the jet flap with δ_F = 9.9 vortices are shed into the secondary mixing region from the flap trailing edge. If the shedding frequency is equal to the tone frequency it gives a Strouhal number based on nozzle height (fh/U) equal to 0.11 and that based on flap length ($f\ell_F/U$) equal to 1.11. Karman vortex shedding is, however, known to occur at Strouhal number equal to 0.2 based on the body lateral dimension. Thus the vortices in the secondary mixing region are not thought to be directly responsible for the tone. The vortices themselves might be a by product of jet instability.

The jet instability mechanism of the tone phenomenon also explains the observed directivity of Figure 4.25 (page 97). Flapping of the potential core represents a periodically fluctuating force on the flap surface and thus a dipole type noise source with maximum noise radiation in directions normal to the flap surface above and below it and no radiation in the plane of the flap surface.



(dimensions in centimeters)

a) Porous Flap Geometry



b) Spectra Comparison

Figure 5.16. Porous flap geometry and spectral comparison with non-porous flap.

The double lobed directivities measured in the normal (XZ) plane (Figures 4.8 and 4.12, pages 58 and 64 respectively) are hard to explain. OASPL directivities were also measured with the jet flap rotated by 180 degrees so that the flap was above the nozzle. Both the measurements consistently gave a double lobed pattern on the underside of the flap. Furthermore the double lobed directivity found on the δ_F = 9.9 jet flap was just found to rotate when the flap was deflected. It should, however, be noted that the tone was unsteady and the sound level in the far field fluctuated by as much as ±3 dB about the mean value (Figure 5.17).

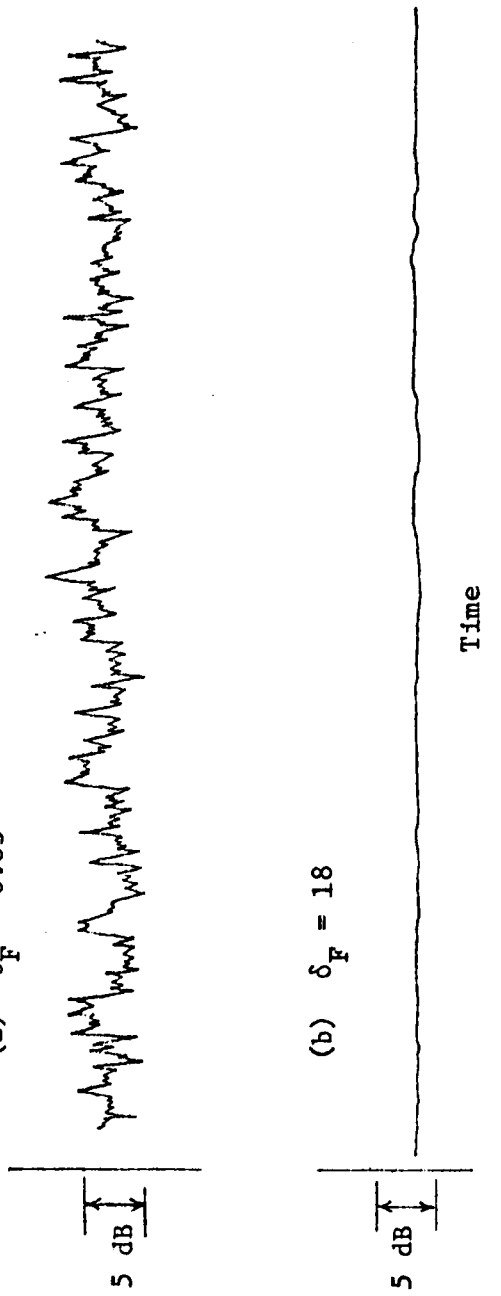


Figure 5.17. Unsteady nature of the tone.

CHAPTER 6

SUMMARY AND CONCLUSIONS

Acoustic characteristics of upper surface blown flaps were investigated experimentally. The blown flap was modeled by a slot nozzle exhausting over a plane flap and measurements were made in the free field and in a reverberation room. Flap length, flap deflection angle, nozzle aspect ratio and jet exit Mach number were among the parameters that were varied. Shadowgraphic stills and movies were obtained for flow visualization and limited turbulence measurements were made using hot film anemometry. Flap surface pressure fluctuations were spectrum analyzed and cross correlated with the far field sound. Results of the investigation are summarized in the following.

The sound power output of a slot jet is less than that of an equivalent area circular jet exhausting at the same mean velocity. This difference increases with increase in the aspect ratio of the slot jet but seems to be reaching an asymptotic value of 3 dB. Sound power of both circular and slot jets vary nearly as the eighth power of jet exit velocity. The sideline plane of the slot jet is quieter than the flyover plane because of a reduction in high frequency components.

The sound output of jet flaps strongly depends on the nondimensional flap length (= flap length/slot height). It increases rapidly above the sound output of the slot jet with increasing flap length, reaches a maximum value for a flap with δ_F around 7 to 10 and decreases slowly with further increase in flap length. Measured OASPL directivities, sound pressure spectra and sound power data have been explained on the basis of jet noise, edge noise, secondary mixing region noise and scrubbing noise.

Short flaps ($\delta_F \leq 5$) behave like compact surfaces and the pressure fluctuations on the flap surface due to the scrubbing of the flow over it tend to introduce dipole type noise sources. The secondary mixing region that develops aft of the flap trailing edge has high turbulence intensity and is also a region of acoustic emission. The U^8 variation of the quadrupole fields of the primary and secondary mixing regions combining with the U^6 variation of the dipole field due to fluctuating pressures on the compact flap surface leads to a near seventh power variation with jet exit velocity of the sound power output.

When the flap length is increased above $\delta_F = 5$, the flap surface becomes non-compact and edge effects become important. The secondary mixing region is still a strong source region. The edge noise field being more efficient than the compact dipole field, the sound output increases above that of the short flap. The U^8 variations

of the sound generated by the quadrupole type sources in the two shear layers combined with the U^5 dependence of the edge amplified field cause a near sixth power variation of the total sound output. In agreement with the theoretical predictions of Ffowcs Williams and Hall [8] the OASPL increases in the flyover plane (θ = -90° to +90°) due to the flap are greatest in $\theta = \pm 90°$ directions and least in directions closer to the jet axis. The preferred radiation characteristic of the secondary mixing region noise, in addition, produces higher sound levels in θ = -30° directions compared to the levels in θ = +30° direction.

Increase in flap length beyond $\delta_F = 10$ results in a decrease in the total sound output of the jet flap system. Due to the rapid reduction in the maximum local velocity beyond the termination of the potential core ($x/h \gtrsim 10$) and the growth of the flap surface boundary layer, the vorticity at the flap trailing edge is reduced for long flaps. This retards the turbulence production in the secondary mixing region resulting in a reduction of the noise generated in that region. The decay in the maximum velocity at the trailing edge is thus the cause of the reduction in the sound output of jet flaps with $\delta_F > 10$. The edge noise still continues to be a major noise source so that the OASPL directivities of the jet flap and the corresponding slot jet are farther apart in

$\theta = \pm 90°$ directions than in directions closer to the jet axis. With reduction in sound generation in the secondary mixing region, which has preferred radiation in directions below the flap, and due to the ability of longer flaps to shield the high frequency radiation below the flap from sources in the primary mixing region the characteristic relation

$$OASPL)_{\theta = -30°} > OASPL)_{\theta = +30°}$$

observed for moderate flap lengths (δ_F = 5 to 25) reverses to

$$OASPL)_{\theta = -30°} < OASPL)_{\theta = +30°}$$

for long flaps ($\delta_F > 25$). Reduction of the source strength in the secondary mixing region results in sound levels below those of the slot jet in the sideline plane where only the quadrupole type sources in the primary and secondary shear layers radiate.

At high jet exit Mach numbers flaps with trailing edge near the potential core termination generate high intensity tones causing considerable increase in the total sound output of these flaps. Spark shadowgraphs of the flow field of the tone-generating jet flaps show the presence of vortical structures in the secondary and primary mixing regions. The structure in the primary mixing region was identified from shadowgraphic high speed movies as due to flapping instability of the jet potential core above the flap surface. The tone is eliminated when the structure

in the primary mixing region is altered by means of a trip wire held near the nozzle upper lip or by roughening a portion of the nozzle upper contour. The tone can, however, be re-introduced by reflecting acoustic waves back to the nozzle exit by means of a reflector plate. The edge noise field which has maximum radiation in the upstream direction can provide the excitation in the absence of a reflector plate. The tone is thus thought to be due to the jet instability triggered by the edge noise field. It can, therefore, be eliminated by reducing edge effects through edge modifications like porous trailing edge region.

Measurements in the free and reverberant fields of jet flaps have thus shown that the edge amplification, as predicted Ffowcs Williams and Hall [8], is an important noise mechanism in the sound generated by finite length flaps and can act to excite instability in the jet to produce high intensity tones. Among the other noise mechanisms, the secondary mixing region noise contribution is important for flaps of moderate lengths (δ_F = 5 to 25) and it takes longer flaps to shield the sound radiation from the primary mixing region in directions below the flap.

LIST OF REFERENCES

LIST OF REFERENCES

1. Dorsch, R. G., E. A. Krejsa and W. A. Olsen. "Blown Flap Noise Research," American Institute of Aeronautics and Astronautics Paper 71-745, 1971.

2. Gibson, J. S. "The Ultimate Noise Barrier - Far Field Radiated Aerodynamic Noise," Inter-Noise '72 Proceedings, M. J. Crocker, editor. Institute of Noise Control Engineers, 1972, Pp. 332-337.

3. Maglieri, D. J., and H. H. Hubbard. "Preliminary Measurements of the Noise Characteristics of Some Jet Augmented Flap Configurations," National Aeronautics and Space Administration Memorandum 12-4-58L, 1959.

4. Coles, W. D. "Jet Engine Exhaust Noise from Slot Nozzles," National Aeronautics and Space Administration Technical Note D-60, 1959.

5. Grosche, F. R. "Zur Schallerzengung durch einen turbulenten Luftstrahl uber einen endlich grossen eben Platte," Mitteilungen aus dem Max-Planck-Institut fur Stromungsforschung und der Aerodynamischen Versuchsanstalt, Selbstverlag Max-Planck-Institut fur Stromungsforschung und Aerodynamische Versuchsanstalt, Gottingen, No. 45, 1969.

6. Hayden, R. E. "Sound Generation by Turbulent Wall Jet Flow over a Trailing Edge," M. S. Thesis, Purdue University, 1969.

7. Schrecker, G. O. "Noise Characteristics of Jet Flap Type Exhaust Flows," Ph.D Dissertation, University of Tennessee, Knoxville, 1973.

8. Ffowcs Williams, J. E., and L. H. Hall. "Aerodynamic Sound Generation by Turbulent Flow in the Vicinity of a Scattering Half Plane," Journal of Fluid Mechanics, Volume 40, 1970, Pp. 657-670.

9. Patterson, G. T., and M. C. Joshi. "Aeroacoustic Characteristics of Slot Nozzles Without and With Attached Flaps," Section 5, Report No. FAA-RD-75-163-II, 1975.

10. Patterson, G. T., M. C. Joshi, and J. R. Maus. "Experimental Investigation of the Aeroacoustic Characteristics of Model Slot Nozzles with Straight Flaps," American Institute of Aeronautics and Astronautics Paper 75-471, 1975.

11. Dunnill, W. A. "Aeroacoustic Facilities of the University of Tennessee Space Institute," Section 2, Report No. FAA-RD-75-163-I, 1975.

12. Borchers, I. U. "Noise and Flow Characteristics of Linear Arrays of Circular Jets and Ejector Flow Systems," Ph.D Dissertation, University of Tennessee, Knoxville, 1976.

13. Kinsler, L. E., and A. R. Frey. Fundamentals of Acoustics. New York: John Wiley and Sons, Inc., 1962.

14. Smith, B. J. Acoustics. Bristol: Longman, 1971

15. Lighthill, M. J. "On Sound Generated Aerodynamically, I. General Theory," Proceedings of the Royal Society, A211, 1952, Pp. 564-587.

16. Ffowcs Williams, J. E. "The Noise from Turbulence Convected at High Speed," Philosophical Transactions of the Royal Society, A255, 1963, Pp. 469-503.

17. Davies, P. O. A. L., M. J. Fisher, and M. J. Barratt. "The Characteristics of the Turbulence in the Mixing Region of a Round Jet," Journal of Fluid Mechanics, Volume 15, 1963, Pp. 337-367.

18. Lush, P. A. "Measurements of Subsonic Jet Noise and Comparison with Theory," Journal of Fluid Mechanics, Volume 46, 1971, Pp. 477-500.

19. Crighton, D. G. "Instability of an Elliptic Jet," Journal of Fluid Mechanics, Volume 59, 1973, Pp. 665-672.

20. Balsa, T. F. "Fluid Shielding of Low Frequency Convected Sources by Arbitrary Jets," Journal of Fluid Mechanics, Volume 70, 1975, Pp. 17-36.

21. Mani, R. "The Influence of Jet Flow on Jet Noise. Part 1. The Noise of Unheated Jets," Journal of Fluid Mechanics, Volume 73, 1976, Pp. 753-778.

22. Ribner, H. S. "The Generation of Sound by Turbulent Jets," Advances in Applied Mechanics, Volume 8, New York: Academic Press, 1964, Pp. 103-182.

23. Coles, W. D. "Jet Engine Exhaust Noise from Slot Nozzles," National Aeronautics and Space Administration Technical Note D-60, 1959.

24. Lighthill, M. J. "Jet Noise," AIAA Journal, Volume 1, 1963, Pp. 1507-1517.

25. Kouts, C. A., and J. C. Yu. "Far Noise Field of a Two Dimensional Subsonic Jet," AIAA Journal, Volume 13, 1975, Pp. 1031-1035.

26. Curle, N. "The Influence of Solid Boundaries Upon Aerodynamic Sound," Proceedings of the Royal Society, A231, 1955, Pp. 505-514.

27. Etkin, B., G. K. Korbacher, and R. T. Keefe. "Acoustic Radiation from a Stationary Cylinder in Fluid Stream (Aeolian Tones)," Journal of Acoustical Society of America, Volume 29, 1957, Pp. 30-36.

28. Powell, A. "Thoughts on Boundary Layer Noise," Aeronautical Research Council Report ARC 16727, F. M. 2061, 1954.

29. Powell, A. "Aerodynamic Noise and the Plane Boundary," Journal of Acoustical Society of America, Volume 32, 1960, Pp. 982-990.

30. Ffowcs Williams, J. E. "Thoughts on the Problem of Aerodynamic Noise Sources near Solid Boundaries," AGARD Report 459, 1963.

31. Hayden, R. E. "Noise from Interaction of Flow with Rigid Surfaces: A Review of Current Status of Prediction Techniques," National Aeronautics and Space Administration CR-2126, 1972.

32. Chase, D. M. "Sound Radiated by Turbulent Flow Off a Rigid Half Plane as Obtained from a Wavevector Spectrum of Hydrodynamic Pressure," Journal of Acoustical Society of America, Volume 52, 1972, Pp. 1011-1023.

33. Schrecker, G. O., and J. R. Maus,"Noise Characteristics of Jet Flap Type Exhaust Flows," National Aeronautics and Space Administration CR-2342, 1974.

34. Becker, R. S. "Acpustic Source Location in a Jet Blown Flap Using a Cross-Correlation Technique," Ph.D Dissertation, University of Tennessee, Knoxville, March 1977.

35. Siddon, T. E. "Noise Source Diagnostics Using Causality Correlation," AGARD CP-131, 1973, Pp. 7-1 to 7-13.

36. Siddon, T. E. "Surface Dipole Strength by Cross-Correlation Method," Journal of Acoustical Society of America, Volume 53, 1973, Pp. 619-633.

37. Lau, J. C., M. J. Fisher, and H. V. Fuchs. "The Intrinsic Structure of Turbulent Jets," Journal of Sound and Vibrations, Volume 22, 1972, Pp. 379-406.

38. Willmarth, W. W. "Space-Time Correlation Measurements of the Fluctuating Wall Pressure in a Turbulent Boundary Layer," Journal of Aerospace Sciences, Volume 25, 1958, Pp. 335-336.

39. Tam, C. K. W., and N. N. Reddy. "Sound Generated in the Vicinity of Trailing Edge of Upper Surface Blown Flap," American Institute of Aeronautics and Astronautics Paper 76-503, 1976.

APPENDIX

APPENDIX

THE "CAUSALITY" CORRELATION TECHNIQUE IN THE LIGHTHILL - CURLE FORMULATION

The continuity and Reynolds form of the momentum equations are

$$\frac{\partial \rho}{\partial t} + \frac{\partial}{\partial x_i} (\rho u_i) = 0 \tag{1}$$

$$\frac{\partial}{\partial t} (\rho u_i) + \frac{\partial}{\partial x_j} (\rho u_i u_j + p_{ij}) = 0 \tag{2}$$

where $p_{ij} = p\delta_{ij} + \mu \left\{ - \frac{\partial u_i}{\partial x_j} - \frac{\partial u_i}{\partial x_i} + \frac{2}{3} \left(\frac{\partial u_k}{\partial x_k}\right) \delta_{ij} \right\}$

is the compressive stress tensor, ρ the density and u_i the velocity in the x_i direction. Rewriting (2),

$$\frac{\partial}{\partial t} (\rho u_i) + a_o^2 \frac{\partial \rho}{\partial x_i} = - \frac{\partial}{\partial x_j} (\rho u_i u_j + p_{ij}) + a_o^2 \frac{\partial \rho}{\partial x_i}$$

$$= - \frac{\partial}{\partial x_j} (\rho u_i u_j + p_{ij} - a_o^2 \rho \delta_{ij})$$

$$= - \frac{\partial (T_{ij})}{\partial x_j} \tag{3}$$

where $T_{ij} = \rho u_i u_j + p_{ij} - a_o^2 \rho \delta_{ij}$, a_o being the ambient speed of sound. Eliminating ρu_i between (1) and (3)

$$\frac{\partial^2 \rho}{\partial t^2} - a_o^2 \frac{\partial^2 \rho}{\partial x_i \partial x_i} = \frac{\partial^2 T_{ij}}{\partial x_i \partial x_j}$$

or (4)

$$\frac{\partial^2 \rho}{\partial t^2} - a_o^2 \nabla^2 \rho = \frac{\partial^2 T_{ij}}{\partial x_i \partial x_j}$$

This is the non-homogeneous wave equation that forms the basis of Lighthill's analogy. Since the homogeneous equation corresponding to (4)

$$\text{i.e., } \frac{\partial^2 \rho}{\partial t^2} - a_o^2 \nabla^2 \rho = 0$$

governs linear acoustics in a uniform medium at rest, the sound generated by a turbulent flow can be considered to be equivalent to the sound generated in a uniform medium at rest under the action of fluctuating applied sources of strength

$$\frac{\partial^2 T_{ij}}{\partial x_i \partial x_j} .$$

When solid rigid boundaries are present in the flow the acoustic radiation from the flow field is given by the following solution of (4) due to Curle [26].

$$a_o^2 \rho' (\bar{x},t) = \frac{1}{4\pi a_o^2} \frac{\partial^2}{\partial x_i \partial x_j} \int_V \frac{1}{r} [T_{ij}] \, dV (\bar{y})$$

$$- \frac{1}{4\pi a_o^2} \frac{\partial}{\partial x_i} \int_S \frac{1}{r} \left[p_i\right] dS (\bar{y}) \quad (5)$$

where $\rho' = \rho - \rho_o$ and p_i is the force per unit area exerted on the fluid by the solid boundaries and may comprise both shear and normal stresses. The square brackets [. . .] denote evaluate at the reatrded time $\hat{t} = t - r/a_o$. V is the volume occupied by the flow and S is the surface in the flow. In the geometric and acoustic far fields (r >> typical body dimension and r >> typical acoutic wavelength) the spatial divergences become time derivatives and $r = |\bar{x} - \bar{y}| \approx x$. (5) can then be simplified to

$$p (\bar{x},t) \simeq \frac{x_i x_j}{4\pi x^3 a^2_o} \int_V \left[\frac{\partial^2 T_{ij}}{\partial t^2}\right] dV$$

$$+ \frac{x_i}{4\pi x^2 a_o} \int_S \left[\frac{\partial}{\partial t} p_i\right] dS$$

Considering only the surface contribution to the radiated sound

$$p\ (\bar{x},t) \simeq \frac{x_i}{4\pi x^2 a_o} \int_S \left[\frac{\partial p_i}{\partial t}\right] \quad dS\ (\bar{y})$$

For cases where the shear stress component is small compared with the local surface pressure fluctuations p_s (normal stress) a relation between the radiation pressure and the fluctuating surface pressure can be obtained for a plane surface:

$$p\ (x,t) \simeq \frac{\cos\theta}{4\pi x a_o} \int_S \left[\frac{\partial p_s}{\partial t}\right] \quad dS\ (\bar{y}) \qquad (6)$$

where θ is the angle between the outward normal of the surface and the field point direction. Multiplying both sides of Equation (4) by the radiation pressure at a new time t' and averaging,

$$\overline{p(t)\ p\ (t')} \simeq \frac{\cos\theta}{4\pi a_o c} \int_S \overline{\frac{\partial p_s}{\partial t}\ (\bar{y},\hat{t})\ p\ (\bar{x},t')} \quad dS\ (\bar{y})$$

If p and p_s are stationary variables and $\tau = t' - t$ then,

$$\overline{pp}\ (\tau) \simeq \frac{-\cos\theta}{4\pi a_o c} \int_S \left[\frac{\partial}{\partial\tau}\ \overline{p_s p}\ (\tau)\right]_{\tau + \frac{r}{a_o}} \quad dS\ (\bar{y})$$

(7)

The mean square acoustic pressure can be obtained by setting $\tau = 0$

$$\therefore \quad \overline{p^2}\,(\bar{x}) \simeq \frac{-\cos\theta}{4\pi a_o c} \int_S \left[\frac{\partial}{\partial \tau}\ \overline{p_s p}\,(\tau)\right]_{\tau = \frac{r}{a_o}} dS\,(\bar{y})$$

or

$$\frac{d\overline{p^2}}{dS} \simeq \frac{-\cos\theta}{4\pi a_o} \left[\frac{\partial}{\partial \tau}\ \overline{p_s p}\,(\tau)\right]_{\tau = \frac{r}{a_o}} \tag{8}$$

This is the result obtained by Siddon [36]. Equation (8) says that the fraction of $\overline{p^2}$ associated with unit surface area at a point where p_s is measured can be obtained from the slope of the cross correlation function at the appropriate value of retarded time.

VITA

Mahendrakumar C. Joshi was born on October 29, 1948 in Madras, India. He received the Bachelor of Science degree in Mathematics from the University of Madras in April 1967. The following June he enrolled at the Madras Institute of Technology and received the Bachelor of Science degree in Aeronautical Engineering in April 1970. In July 1970, he entered the graduate school of the Indian Institute of Technology, Madras and was awarded the degree of Master of Technology with a major in Aeronautical Engineering in August 1972. In the fall of 1972 he accepted a research assistantship at the University of Tennessee Space Institute and began study toward the degree of Doctor of Philosophy in Mechanical Engineering. He received this degree in March 1977.

The author is a member of Sigma Xi, Phi Kappa Phi and the American Institute for Aeronautics and Astronautics.